The epigenetic regulator Mll1 is required for Wnt-driven intestinal tumorigenesis and cancer stemness

DISSERTATION

zur Erlangung des akademischen Grades

Doctor rerum naturalium

(Dr. rer. nat.)

eingereicht an der

Lebenswissenschaftlichen Fakultät der Humboldt-Universität zu Berlin

von

Johanna Grinat, M.Sc.

Präsidentin der Humboldt-Universität zu Berlin

Prof. Dr.-Ing. Dr. Sabine Kunst

Dekan der Lebenswissenschaftlichen Fakultät

Prof. Dr. Bernhard Grimm

Gutachter/innen

1. Prof. Dr. Walter Birchmeier
2. Prof. Dr. Ana Pombo
3. Prof. Dr. Ann Ehrenhofer-Murray

Tag der mündlichen Prüfung: 29.09.2020

Für meine Eltern.

There is a duality in recognising what an incredible disease it is
– in terms of its origin, that it emerges out of a normal cell.
It's a reminder of what a wonderful thing a normal cell is.
In a very cold, scientific sense,
I think a cancer cell is a kind of biological marvel.

Siddhartha Mukherjee

Die vorliegende Arbeit wurde unter der Anleitung von Dr. Julian Heuberger und Prof. Dr. Walter Birchmeier am Max-Delbrück-Centrum für Molekulare Medizin (MDC) in Berlin-Buch angefertigt.

Zusammenfassung

Genetisch bedingte Veränderungen im Wnt-Signalweg sind in der Tumorigenese des Darms von zentraler Bedeutung. Mutationen des Wnt-Effektormoleküls β-Catenin in den adulten Stammzellen des Darmepithels führen zu unkontrollierter Proliferation und Expansion der Darmstammzellen und initiieren die Tumorentstehung. Auch in fortgeschrittenen Darmtumoren unterstützt die Wnt-Signalgebung maßgeblich das Tumorwachstum und den Erhalt von Tumorstammzellen. Nach erfolgreicher chemotherapeutischer Behandlung treten oftmals Tumorrezidive auf, für deren Entstehung therapieresistente Tumorstammzellen verantwortlich gemacht werden. Trotz intensiver Forschung und Entwicklung fehlen in der Darmkrebstherapie nach wie vor Behandlungsansätze zur gezielten Therapie der Tumorstammzellen. Ziel dieser Dissertation ist es, unser Verständnis der molekularen Regulationsmechanismen in Kolonkarzinomen zu erweitern und dadurch die zukünftige Entwicklung rationaler Behandlungsstrategien für Darmkrebspatienten zu fördern. Mittels humaner Kolonkarzinomzellen, 3D-Organoidkulturen und genetischem Maus-Tumormodell wurde in der vorliegenden Arbeit die Bedeutung der Histonmethyltransferase Mll1 in der epigenetischen Regulation humaner und muriner Darmkrebsstammzellen und -tumore identifiziert. Ich konnte zeigen, dass humane Kolonkarzinome eine erhöhte Mll1-Expression aufweisen, die mit dem Level an nukleärem β-Catenin korreliert. Im adulten Darmepithel ist Mll1 insbesondere in den Lgr5-positiven intestinalen Stammzellen exprimiert und maßgeblich an der Wnt/β-Catenin-induzierten Stammzellexpansion sowie der Tumorentstehung beteiligt. Der konditionelle Verlust von Mll1 im murinen Darmkrebsmodell verhindert die β-Catenin-induzierte Tumorigenese. Mll1 unterstützt die Selbsterneuerungsfähigkeit und Proliferation der Tumorstammzellen, indem es die Expression von essentiellen Stammzellgenen wie dem Wnt-abhängigen Stammzellmarker *Lgr5* aufrechterhält und ihre Repression durch Polycomb-vermittelte H3K27 Tri-methylierung verhindert. Mll1 fördert zudem die Expression der Transkriptionsfaktoren Gata4/6, die zum Erhalt der Stammzellfunktion beitragen. Der Verlust von Mll1 verringert progressiv die Selbsterneuerungsfähigkeit der Tumorstammzellen und induziert eine Mapk-vermittelte Differenzierung. Meine Ergebnisse zeigen, dass Mll1 als epigenetischer Regulator der Tumorstammzellen maßgeblich an der Wnt/β-Catenin-induzierten Tumorigenese des Darmepithels beteiligt ist. Eine Inhibition der Mll1-Funktion in der Darmkrebstherapie kann eine gezielte Eliminierung der Tumorstammzellen ermöglichen, wodurch sowohl das fortschreitende Tumorwachstum unterbunden als auch die Bildung von Rezidiven verhindert werden kann.

Abstract

Genetic mutations inducing aberrant activity of Wnt signalling are causative for intestinal tumorigenesis. Mutations of the Wnt effector molecule β-catenin in adult stem cells of the intestinal epithelium drive uncontrolled proliferation, expand the stem cell pool and initiate tumor formation. In advanced tumors, aberrant Wnt signalling promotes tumor growth and maintains cancer stem cells. The cancer stem cells are highly resistant to conventional chemotherapy and frequently initiate tumor relapse after completion of treatment. Despite extensive research, we are still lacking efficient therapies for colon cancer that specifically eliminate the cancer stem cells. This dissertation aims to expand our knowledge on molecular gene regulatory mechanisms in colon cancer cells to promote the identification and future development of rational therapies for colon cancer patients. Studying human colon carcinoma cells, intestinal organoid cultures and the *in vivo* tumorigenesis in a mouse tumor model, I identified the histone methyltransferase Mll1 as an epigenetic regulator in human and mouse intestinal cancer stem cells and tumors. I demonstrate that human colon carcinomas with nuclear β-catenin exhibit high levels of Mll1. In the adult intestinal epithelium of mice, Mll1 is highly expressed in the $Lgr5^{+}$ stem cells and is a prerequisite for the oncogenic Wnt/β-catenin-mediated stem cell expansion and tumorigenesis. Conditional knockout of Mll1 in an intestinal mouse tumor model prevents the β-catenin-driven intestinal tumorigenesis. Knockdown of Mll1 impairs the self-renewal and proliferation of colon cancer sphere cultures and halts tumor growth in xenografts. Mechanistically, Mll1 sustains the expression of specific intestinal stem cell genes including the Wnt/β-catenin target gene *Lgr5* by antagonizing gene silencing through polycomb repressive complex 2 (PRC2)-mediated H3K27 tri-methylation. Mll1 further promotes the expression of Gata4/6 transcription factors to maintain stem cell identity. Mll1-deficient colon cancer cells progressively lose their stemness and differentiate in a Mapk-dependent manner. Taken together, my data demonstrate that Mll1 is essential for the Wnt/β-catenin-induced intestinal tumorigenesis and cancer stemness. Interfering with Mll1 function can efficiently eliminate colon cancer stem cells, and has potential as a rational therapy for colon cancer.

1 Introduction

Cancer is a genetic disease causing uncontrolled growth of mammalian cells. It is a major cause of morbidity and mortality in humans. Colon cancer ranks the third most common cause of cancer-related deaths in the western world[1]. Recent years have seen great progress in the early detection and surgical removal of benign intestinal polyps, which has strongly improved colon cancer prevention. The overall 5-year survival rate of patients with late-stage colon cancer is only 10%, however, due to high rates of post-intervention recurrence and the lack of targeted therapies[1]. Colon cancer arises from intestinal epithelial cells as a consequence of cumulative genetic mutations. Loss-of-function mutations in the tumor suppressor gene *APC* (*adenomatous polyposis coli*) and gain-of-function mutations in the proto-oncogene *β-catenin* (*CTNNB1*) deregulate Wnt signalling and initiate the adenoma-carcinoma sequence of intestinal tumorigenesis[2] (Figure 1.1). The aberrant Wnt activity expands mutant intestinal epithelial cells, giving rise to dysplastic crypts. Subsequent mutations in *KRAS*, *SMAD4* and *p53* sequentially drive tumor progression from benign polyps and adenomas to aggressive carcinomas, eventually followed by metastasis[2].

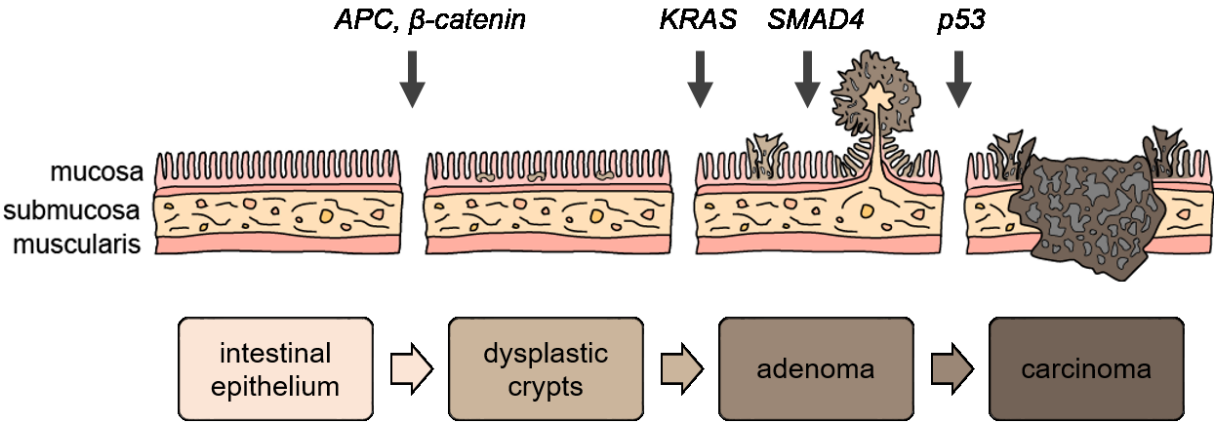

Figure 1.1: The adenoma-carcinoma sequence in colon cancer.
The Vogelstein model describes intestinal tumorigenesis as a stepwise accumulation of genetic mutations, which sequentially transforms the intestinal epithelium (mucosa) into adenomas and carcinomas. Malignant carcinomas invade the submucosa and subjacent muscle layer (muscularis) of the intestinal wall, eventually spreading to distant organs and forming metastases.

The malignancy of colon carcinomas is assessed using the American Joint Cancer Committee tumor/node/metastasis (TNM) staging system which classifies cancer based on the size and invasiveness of the primary tumor (T0/Tis-T4), the extent of spread to nearby lymph nodes (N0-N2) and the presence or absence of distant metastasis (M0-M1). Stage T0/Tis describes carcinomas *in situ*, meaning the tumor is confined to the intestinal mucosa. Stage T1 tumors invade the submucosa, stage T2 tumors the underlying muscle layer. Stage T3 tumors extend to the serosa and tumors classified as stage T4 have spread to adjacent organs.

Single-cell sequencing and cancer genome studies have revealed a mutational heterogeneity in advanced tumors that cannot be reached by sequential acquisition of several driver mutations[3]. The mutational heterogeneity causes a high variability in the growth and progression of benign adenomatous intestinal polyps[4]. Only 5% of polyps progress to malignant carcinomas, thus questioning the strict linear adenoma-carcinoma sequence proposed by the Vogelstein model. Genetic mutations in *APC*, *KRAS*, *SMAD4* and *p53* are recurrently found in colon cancers, though, and are critical for intestinal tumor growth and progression[5, 6]. The malignant growth destroys tissue architecture and impairs organ function. Colon carcinomas frequently metastasize to the liver and lung. These distant metastases are a major cause of mortality from colon cancer[7].

Therapies for advanced-stage colon cancer patients (T3-T4) mostly rely on non-specific radiation and chemotherapy. Chemotherapeutic agents are cytostatics that kill proliferating cells by blocking DNA synthesis or inhibiting nucleic acid metabolism. As tumor cells show a high proliferation rate[8], they are hit by chemotherapy. Due to their non-targeted mechanism of action, however, radiation and chemotherapy do not only destroy tumor cells but also severely harm healthy proliferative tissue. Targeted therapeutic approaches exploit the addiction of cancer cells to oncogenic signalling and metabolic processes[9]. A targeted therapy aims to specifically eliminate tumor cells, while minimizing collateral damage. To date, only few targeted therapies for colon cancer are approved for use in the clinic. As cancer cells hijack the same signalling circuits that control the growth of normal epithelial cells, it is difficult to safely eliminate colon cancer cells without damaging healthy epithelium. Our ability to specifically target cancer cells will critically rely on understanding the differences between normal and cancer cells. The knowledge of the intestinal epithelium, its cell types, signalling and gene regulatory networks is key to understand how oncogenic mutations change the identity of intestinal epithelial cells and transform them into tumor-initiating cancer cells.

1.1 The intestinal epithelium.

The inner surface of the mammalian gastrointestinal tract is covered by a mono-layered epithelium that is specialized on nutrient uptake and digestion. In the small intestine, the epithelium is organized in crypt and villi structures (Figure 1.2a). Protruding long into the intestinal lumen, the villi magnify the absorptive surface area for efficient nutrient uptake. Multiple epithelial invaginations located at the base of each villus, the crypts of Lieberkühn, form the niches for the adult intestinal stem cells that constantly renew the epithelium[10]. In the colon, the epithelium does not possess villi but has a flat surface interspersed by crypts (Figure 1.2b). Along the longitudinal length of the gastrointestinal tract, i.e. from the duodenal, jejunal and ileal parts of the small intestine to the colon, the epithelium shows a gradual decrease in the activity of Wnt signalling and the abundance of stem cells. Distinct levels of Wnt over-activation are required in the individual segments to reach a tumor-initiating threshold,

the 'just-right' level of Wnt activity[11, 12]. The stabilization of β-catenin in the intestinal epithelium of mice efficiently transforms epithelial cells in the small intestine, while colonic lesions are rare or absent[11]. In contrast, human gastrointestinal tumors mostly occur in the colon and rectum; a discrepancy that is attributed to variations in the physiological Wnt levels and stem cell numbers between humans and mice[11].

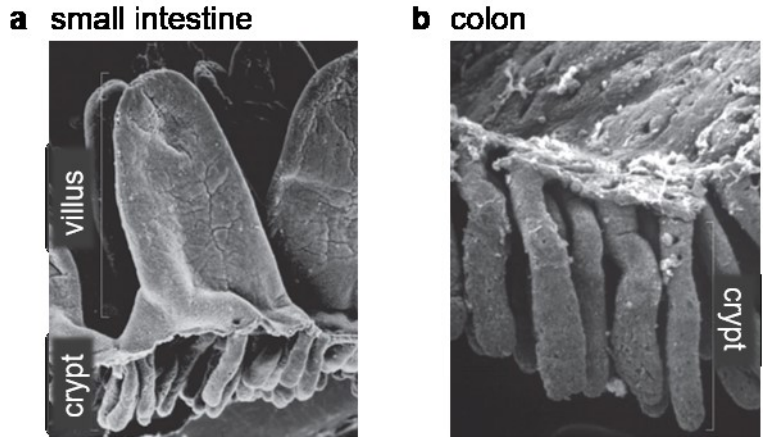

Figure 1.2: Structure of the small intestinal and colon epithelium.
Scanning electron micrographs of the small intestinal epithelium **(a)**. Multiple crypts are located at the base of each villus. The epithelium in the colon **(b)** has a flat surface interspersed with crypts, modified from Barker (2014)[13].

1.1.1 Lgr5$^+$ intestinal stem cells maintain the epithelium.

The intestinal epithelium is a highly proliferative tissue with a fast turnover time of 4-5 days[13]. Actively proliferating stem cells maintain the epithelium. Located at the base of the crypts, the stem cells are well protected from damage by harmful toxins and pathogens in the gut. Due to their column-shaped appearance the stem cells were initially described as crypt base columnar (CBC) cells[14]. CBC cells express the leucine-rich repeat-containing G-protein coupled receptor 5 (Lgr5/Gpr49), a 7-transmembrane receptor for R-spondins, which has emerged as a powerful marker for adult intestinal stem cells[15]. Each crypt contains about six stem cells that divide approximately once every 24h and give rise to all cell types of the epithelium[15]. The maintenance and self-renewal of the intestinal stem cells critically depend on active Wnt signalling[16]. Interfering with canonical Wnt signalling severely impairs intestinal crypt homeostasis. Genetic deletion of the Wnt effectors Tcf4 or β-catenin in the intestinal epithelium inhibits cell proliferation and causes loss of stem cells[16, 17].

1.1.2 Canonical Wnt signalling sustains adult intestinal stem cells.

The Wnt signalling pathway plays crucial roles in embryogenesis and adult tissue homeostasis and is highly conserved in multicellular organisms[18]. In canonical Wnt signalling, secreted Wnt ligands bind to LRP/Frizzled receptor complexes at the cell surface and trigger a signalling cascade that stabilizes β-catenin (Figure 1.3).

In the absence of a Wnt stimulus (Wnt OFF), β-catenin is retained in a destruction complex composed of adenomatous polyposis coli (APC), the Ser/Thr kinases glycogen synthase kinase 3β (GSK3β) and casein kinase Iα (CKI), and Axin/conductin[19-22]. CKI and GSK3β sequentially phosphorylate serine and threonine residues in the N-terminus of β-catenin, marking β-catenin for ubiquitination and degradation by the ubiquitin-proteasome system[21, 23].

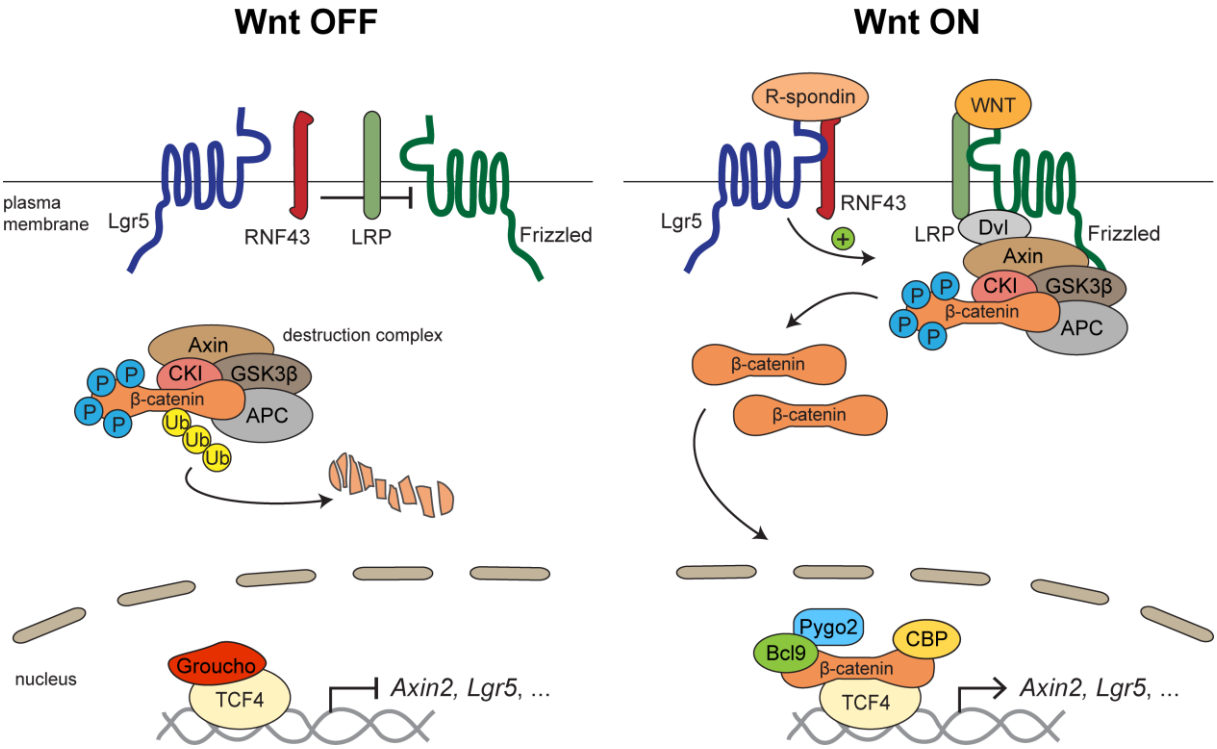

Figure 1.3: Canonical Wnt signalling in intestinal stem cells.
Left: In the absence of Wnt ligands, β-catenin is degraded by the destruction complex and the Wnt target genes are silenced in a Groucho-dependent manner. Right: Wnt ligand binding to LRP/Frizzled receptors inactivates the destruction complex. β-catenin accumulates and translocates to the nucleus, activating the expression of Wnt target genes. In intestinal stem cells, R-spondin binding to Lgr5 receptors potentiates Wnt signalling.

LRP/Frizzled receptor activation by Wnt ligands (Wnt ON) sequesters and inactivates the destruction complex in a Dishevelled (Dvl)-dependent manner, and suppresses β-catenin ubiquitination[24, 25]. Free cytosolic and *de novo* synthesized β-catenin cannot be marked for degradation, accumulates and translocates to the nucleus. Once in the nucleus, β-catenin interacts with T-cell factor/lymphoid enhancer factor-1 (Tcf/Lef1) transcription factors to drive target gene expression[26]. In the intestinal epithelium, the major nuclear effector of Wnt signalling is the Tcf isoform 4 (Tcf4)[27]. Tcf transcription factors occupy their DNA target sites

also in the absence of a Wnt signal, but by then form a complex with co-repressor proteins of the Groucho/Tle (transducin-like enhancer of split) family, which keep the target genes silenced[28]. Upon Tcf interaction with β-catenin, co-repressors are inactivated and co-activators like the CREB-binding protein (CBP)/p300, Pygo2 and Bcl9/Bcl9-like activate the expression of β-catenin/Tcf target genes such as *Axin2* [29-33].

Wnt signalling in intestinal stem cells activates the expression of the stem cell gene *Lgr5* which encodes a receptor for R-spondins[34] (Figure 1.3). R-spondin binding to Lgr5 potentiates the cellular Wnt signalling response by stimulating an association of Lgr5 with the Frizzled/LRP receptor complex[35]. R-spondin binding further induces an interaction of Lgr5 with the stem cell-specific transmembrane E3 ubiquitin ligases RNF43 (ring finger protein 43) and ZNRF3 (zinc and ring finger 3), which ubiquitinate Frizzled receptors and target them for endocytosis and degradation[36, 37]. The interaction with Lgr5 stimulates RNF43/ZNRF3 internalization and membrane clearance, and thus enhances Wnt signalling by increasing the membrane level of Frizzled receptors[37]. The potentiation of Wnt activity by R-spondins is critical for stem cell self-renewal[38]. Wnt ligands by themselves are insufficient to sustain the self-renewal of $Lgr5^+$ intestinal stem cells, but are essential to the intestinal stem cells in that they stimulate the expression of *Lgr5* and hence render the cells responsive to R-spondins[38]. In the absence of Wnt ligands, R-spondins fail to induce canonical Wnt signalling, the stem cells lose their self-renewal capacity and differentiate[38].

A tight control of Wnt signalling by Bmp and Notch is critical for stem cell maintenance.

Deregulation of Wnt signalling perturbs intestinal homeostasis, promotes stem cell differentiation and initiates intestinal tumorigenesis[39]. A tightly controlled level of Wnt signalling is therefore critical for stem cell maintenance. Bmp and Notch signals crosstalk with Wnt signalling to adequately balance the Wnt activity in the intestinal crypts[40, 41]. Bmp signalling restricts stemness and proliferation by repressing the expression of stem cell genes and Wnt signalling[40, 42]. Mesenchymal cells surrounding the crypts produce Bmp antagonists such as Noggin and Gremlin to ensure proper balancing of Wnt and Bmp signalling for stem cell maintenance but prevent Bmp-mediated terminal differentiation[40, 43]. Stem cell maintenance further depends on active Notch signalling[44]. Inhibition of Notch signalling increases the Wnt activity at the crypt base and enforces secretory cell differentiation of intestinal stem cells[41].

1.1.3 Signalling circuits specify the structure and function of the intestinal epithelium.

Lgr5$^+$ intestinal stem cells give rise to highly proliferative transit-amplifying (TA) progenitor cells, which are located above the stem cells in the crypt. TA cells undergo 4-5 cell divisions within a remarkably short time frame of 12h[45]. Moving upwards towards the crypt-villus junction, the TA cells differentiate into absorptive enterocytes and secretory cells, including Paneth cells, mucus-secreting goblet cells, hormone-producing enteroendocrine cells and tuft cells[10] (Figure 1.4a). Except for the Paneth cells, the differentiated cells constantly migrate up the villi. Once they reach the villus tip, the epithelial cells are shed into the intestinal lumen and undergo anoikis, a form of apoptosis induced by the loss of attachment to the extracellular matrix. Paneth cells escape the crypt-villus movement and migrate down into the crypt, where they intersperse the Lgr5$^+$ stem cells and persist for 6-8 weeks[46, 47] (Figure 1.4a). The Paneth cells secrete antimicrobial peptides such as defensins and lysozyme and provide Wnt ligands and other growth factors for stem cell maintenance[48]. The downward migratory path of the Paneth cells is guided by a counter-gradient of ephrin receptor B3 (EphB3) and its ligand ephrin-B[46]. Paneth cells express high levels of the receptor EphB3 and are repulsed by the differentiated cells of the villus that highly express ephrin-B ligands[46]. The Paneth cells are a major source of the Wnt ligand Wnt3a and the Notch ligands Dll1 and Dll4 in the crypt stem cell niche[48]. Mesenchymal cells surrounding the crypts also secrete Wnt ligands and R-spondins, which are sufficient to maintain the stem cells in the absence of Paneth cells[49-51].

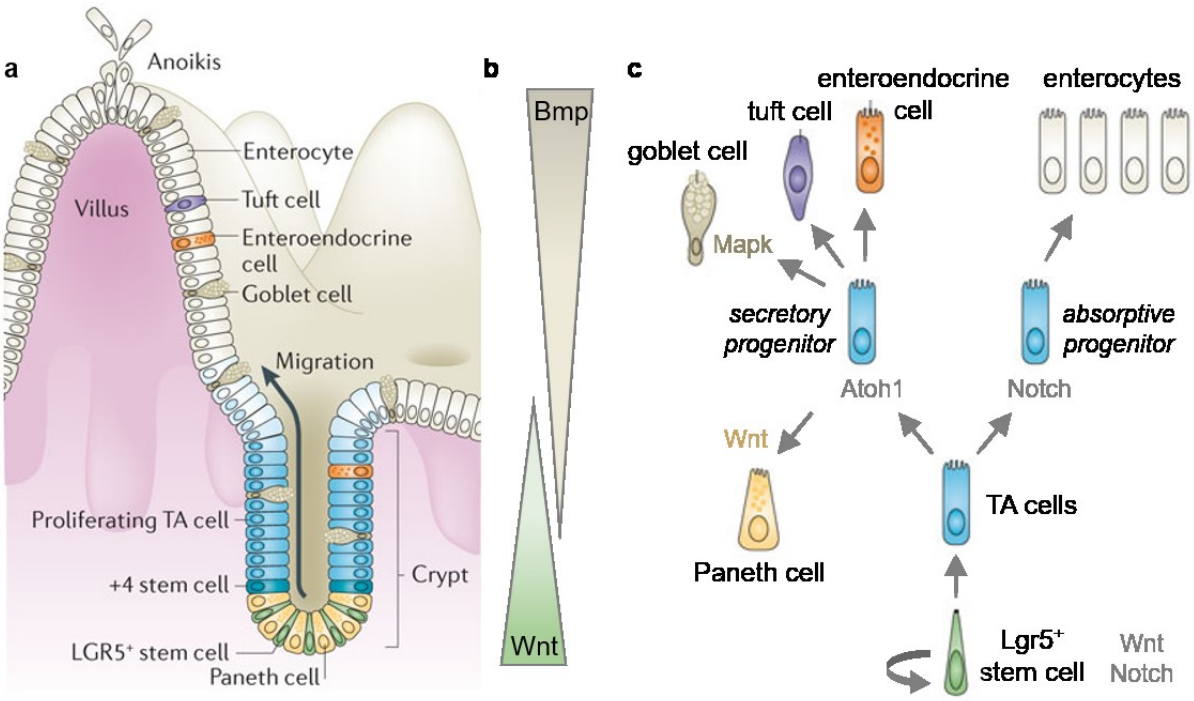

Figure 1.4: The crypt-villus axis and signalling circuits in intestinal epithelial differentiation.
a) The intestinal crypt-villus axis, adapted from Barker (2014)[13]. Lgr5$^+$ intestinal stem cells give rise to transit-amplifying (TA) progenitor cells that proliferate and differentiate into all cell types of the epithelium. **b)** Opposing gradients of Wnt and Bmp signalling organize the epithelium in proliferative

crypt and differentiated villus compartments. **c)** Cell type specification in the intestinal epithelium is guided by a network of signalling systems, modified from Barker (2014)[13]. Wnt and Notch signalling maintain Lgr5$^+$ intestinal stem cells at the crypt base. The stem cells self-renew and give rise to TA cells which are specified towards the secretory or absorptive lineage depending on the activity of Notch signalling. Absorptive progenitor cells differentiate into enterocytes. Secretory progenitors express Atoh1 and differentiate into Paneth, goblet, enteroendocrine or tuft cells.

Inverse gradients of Wnt and Bmp signalling shape the crypt-villus axis.

Opposing gradients of Wnt and Bmp signalling organize the intestinal epithelium in proliferative crypt and differentiated villus compartments (Figure 1.4b). High concentrations of Wnt ligands at the base of the intestinal crypt ensure high Wnt activity in the stem cell niche[52]. The abundance of Wnt receptors presented on the cell surface and progressive dilution of receptor-bound Wnt ligands through cell division establish a Wnt gradient from the crypt base to the villus[53]. Wnt signalling is low in the villus, where high concentrations of Bmp ligands secreted by intra-villus mesenchymal cells stimulate Bmp signalling and promote cell differentiation[54].

Absorptive versus secretory lineage specification by Notch and Atoh1.

A tightly regulated network of signalling pathways guides cellular differentiation in the intestinal epithelium (Figure 1.4c). The first lineage decision takes place in the proliferative TA zone. TA cells are specified towards absorptive or secretory progenitor cells depending on the activity of Notch signalling and the expression of Atoh1. TA cells with high Notch activity express the transcription factor *Hes1* and are prone to differentiate into absorptive enterocytes[55]. Hes1 prohibits secretory differentiation by repressing *Atoh1* (also known as *Math1* in mouse, *Hath1* in humans), a transcription factor critical for secretory lineage specification[55, 56]. Low Notch activity in TA cells and the consequent absence of Hes1 allow for *Atoh1* production, specifying the cells towards the secretory lineage[56] (Figure 1.5). Genetic ablation of the Notch transcription factor Rbp-j disables *Hes1* expression and converts intestinal epithelial crypt cells in secretory goblet cells[57]. Vice versa, the ablation of Atoh1 converts secretory cells into absorptive enterocytes[58].

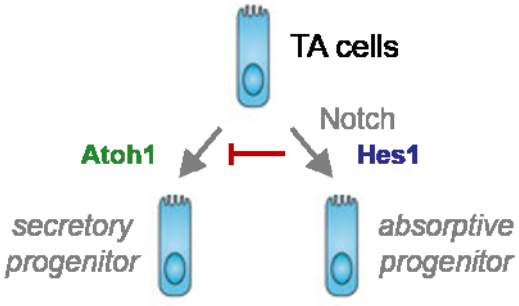

Figure 1.5: Notch/Hes1 and Atoh1 control the absorptive versus secretory fate in TA cells. Absorptive specification depends on Notch-induced expression of the transcription factor Hes1. TA cells with low Notch activity express the transcription factor Atoh1 and differentiate towards the secretory lineage, modified from Barker (2014)[13].

Hes transcription factors suppress the expression of Cdk inhibitors and boost the proliferation of absorptive lineage progenitors[59]. In contrast, secretory progenitor cells exit the cell cycle and stop proliferating, which lets absorptive enterocytes outnumber secretory cells by far[60].

Wnt and Mapk signalling specify Paneth and goblet cell differentiation of secretory progenitor cells.

Atoh1$^+$ secretory progenitor cells differentiate into the diverse cell types of the secretory lineage. The transcription factor Gfi1 acts downstream of Atoh1 to select Paneth/goblet cell fates versus the enteroendocrine fate[61] (Figure 1.6a). Downstream of Atoh1 and Gfi1, the ETS transcription factor Spdef further directs secretory progenitor maturation in goblet and Paneth cells[62, 63]. Deletion of *Spdef* in the mouse intestine leads to an accumulation of immature secretory progenitor cells[62].

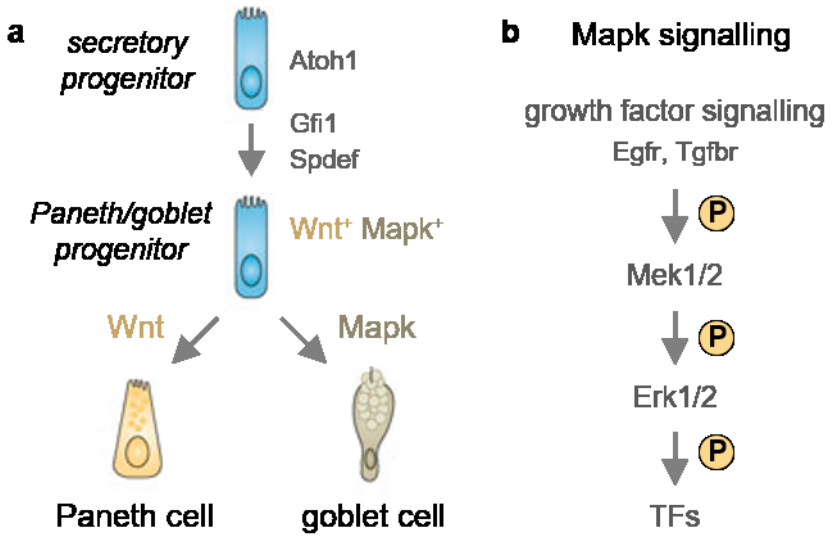

Figure 1.6: Specification of Paneth and goblet cells by Wnt and Mapk signalling.
a) Secretory progenitor maturation towards Paneth and goblet cells is specified by Wnt and Mapk signalling, modified from Barker (2014)[13], Heuberger et al. (2014)[64]. **b)** Scheme of the Mapk signalling cascade. Growth factor signalling via epidermal growth factor receptor (Egfr) or transforming growth factor beta receptor (Tgfbr) induces phosphorylation (P) and activation of the protein kinase Mek1/2. Mek1/2 activates Erk1/2 kinases which phosphorylate transcription factors (TFs) to activate gene expression.

High Wnt activity in secretory progenitor cells promotes the differentiation of Paneth cells[65] (Figure 1.6a). Paneth cells are absent in Tcf4-deficient mice[65]. High Wnt activity blocks goblet cell differentiation, as goblet cells are absent in Apc-mutant intestine[66]. Mitogen-activated protein kinase (Mapk) signalling impedes the Wnt-induced maturation of Paneth cells and shifts the differentiation of common Paneth-goblet progenitors towards a goblet cell fate[64] (Figure 1.6a, b).

1.1.4 Cell type plasticity in the intestinal epithelium.

The intestinal epithelium possesses a remarkable plasticity and a high regenerative capacity[67]. Upon injury to the stem cell niche or experimental ablation of Lgr5$^+$ intestinal stem cells, these stem cells are rapidly replaced by committed progenitor cells that de-differentiate and adopt a stem-like identity. Non-cycling secretory progenitors located at the "+4" position directly above the Paneth cells re-enter the cell cycle and convert into actively cycling Lgr5$^+$ cells upon crypt damage; these progenitor cells are also known as label-retaining Bmi1$^+$ quiescent stem cells[68, 69]. Atoh1$^+$ secretory progenitor cells revert to functional Lgr5$^+$ stem cells both upon injury and at homeostasis[70, 71]. Highly proliferative alkaline phosphatase (Alpi$^+$) enterocyte precursors in the upper crypt can also generate proliferating stem cells and Paneth-like cells after targeted ablation of Lgr5$^+$ stem cells[72]. A "point-of-no-return" defining the loss of de-differentiation capability of terminally differentiated intestinal epithelial cells has not been clearly determined. Even fully differentiated Paneth cells can gain multipotency and stem-like features to regenerate the epithelium upon Lgr5$^+$ stem cell loss[73]. In contrast, Alpi$^+$ enterocytes which have exited the crypt for longer than three days stop proliferating and lose the de-differentiation capacity of the Alpi$^+$ cells in the upper crypt[72]. The plasticity of intestinal epithelial cells thus appears to depend on a certain proximity to the crypt and its growth factor-rich environment, which imposes stemness on intestinal progenitor cells. Moreover, a cell-intrinsic permissive state is a prerequisite for cellular plasticity and de-differentiation, as Notch1$^+$ absorptive progenitor cells lack regenerative capacity despite their proximity to the crypt stem cell niche[70].

1.1.5 Intestinal organoids - a tool to study epithelial stem cell biology.

Single Lgr5$^+$ intestinal stem cells cultured *in vitro* in a basal lamina-like gelatinous matrix can self-organize into three-dimensional organoids, also called "mini-guts" [74]. Intestinal organoid formation and growth critically depend on a specialized serum-free growth medium supplemented with the Wnt amplifier R-spondin1, the Bmp antagonist Noggin and epidermal growth factor (EGF) that mimic the *in vivo* stem cell niche. Intestinal organoids preserve the cellular complexity of the intestinal epithelium: crypt-like domains comprising stem cells and a TA compartment project outward and bud from a hollow roundish structure of differentiated epithelial cells organized in villus domains. Goblet and Paneth cells secrete towards the lumen of the organoid, whereto also dead cells are shed. The lack of innervation, blood vessels, immune cells and a proper *in vivo* microenvironment are limitations to the organoid technology. Closely recapitulating the *in vivo* epithelium and selecting for a purely epithelial culture, though, intestinal organoids have emerged as a valuable system to study epithelial stem cell biology, dissect signalling pathways in organ development and disease, and to investigate the impact of genetic mutations on epithelial homeostasis[75]. Patient-derived tumor organoids are of great value to predict drug response *in vitro*[76].

1.2 Wnt signalling and adult intestinal stem cells in colon cancer.

1.2.1 Deregulation of Wnt signalling in intestinal stem cells initiates colon cancer.

Deregulated Wnt signalling is a hallmark of colon cancer. 85% of all sporadic and hereditary colon cancers show mutations in APC that disrupt its ability to induce the degradation of β-catenin[2]. The remaining 15% of colon cancers with wild-type *APC* frequently show point mutations in *CTNNB1* that alter the serine/threonine residues in the N-terminal domain of β-catenin and render it insensitive to GSK3β-mediated phosphorylation, ubiquitination and proteasomal degradation[77]. Loss of APC and expression of a stabilized form of β-catenin both lead to deregulated nuclear accumulation of β-catenin and aberrant activation of Wnt target genes, inducing crypt hyperplasia and adenoma formation in mice[66, 78]. Over-activation of Wnt signalling in Lgr5$^+$ intestinal stem cells induces adenoma formation, whereas deregulation of Wnt signalling in differentiated intestinal epithelial cells is insufficient to initiate tumorigenesis[79]. This led to the 'bottom-up' model of intestinal tumorigenesis in which stem cells at the crypt base are hit by an oncogenic mutation and initiate tumorigenesis[80]. Contrary to the 'bottom-up' hypothesis, very early adenomatous polyps are frequently observed at the top of colon crypts without any contact to the stem cell niche. A 'top-down model of adenoma morphogenesis' therefore challenges the bottom-up hypothesis[81]. In accordance with a top-down model, inflammation-activated NF-κB signalling promotes Wnt-driven tumor formation from differentiated Lgr5-negative epithelial cells[82]. The NF-κB activity potently enhances Wnt signalling to induce a crypt-progenitor phenotype. The *de novo* crypt-like structures evert from the villus epithelium and form a niche, enforcing a stem-like state on epithelial villus cells and restoring the expression of Lgr5$^+$ stem cell genes[82]. Accordingly, the deregulation of Wnt signalling can initiate tumorigenesis also in a non-stem cell population but requires additional stimuli such as inflammation-induced NF-κB signalling. Both the bottom-up and the top-down intestinal tumorigenesis depend on the emergence of stem-like cells that initiate intestinal transformation in a Wnt-driven manner.

1.2.2 Wnt-dependent cancer stem cells maintain intestinal tumors.

Deregulation of Wnt signalling does not only initiate intestinal tumorigenesis, but high Wnt activity is continuously required for the proliferation and growth of intestinal tumors[83]. Restoring Apc function in advanced-stage Apc-deficient intestinal tumors induces differentiation of the tumor cells and re-establishes intestinal homeostasis in spite of additional oncogenic mutations in *Kras* and *p53* [84]. Even though mutations in APC or β-catenin are expected to uniformly activate Wnt signalling, intestinal tumors exhibit strikingly heterogeneous levels of Wnt activity[85]. Lineage tracing in Apc-mutant tumors revealed that intestinal tumors consist of a heterogeneous population of cells in various differentiation states and retain a cell type hierarchy which is reminiscent of the intestinal epithelium[86]. A small fraction of tumor cells has

a particularly high tumorigenic potential and fuels tumor growth. These cancer cells resemble adult tissue stem cells in that they self-renew and give rise to differentiated non-stem tumor cells, and are therefore called 'cancer stem cells' [87]. Tumor cells with high Wnt signalling have turned out to be functional cancer stem cells, whereas tumor cells with low Wnt activity are rather differentiated[88]. High Wnt activity is thus crucial for the formation and maintenance of colon cancer stem cells.

The gene expression programme of intestinal cancer stem cells is highly reminiscent of the transcriptional profile in Lgr5$^+$ intestinal stem cells, while non-stem cancer cells resemble TA and differentiated epithelial cells[86, 89]. Human colon adenomas show a strong expansion of Lgr5-expressing stem-like cells[90]. Genetic ablation of Lgr5$^+$ cancer stem cells through diphtheria toxin halts colon cancer growth, highlighting the relevance of these stem cells for tumorigenesis[91]. High Wnt signalling promotes colon cancer stemness by directly inducing the expression of stem cell genes like ***Lgr5*** [15], ***Ascl2*** (Achaete-scute complex-like 2)[92] and ***Cd44*** [93]. In addition, colon cancer stem cells express Wnt-independent stem cell genes such as ***Igfbp4*** (insulin-like growth factor-binding protein 4), ***Smoc2*** (secreted modular calcium-binding matricellular protein-2) and ***Olfm4*** (*Olfactomedin-4*)[89], implying that an interplay of Wnt signalling and Wnt-independent regulatory mechanisms defines colon cancer stemness. *Smoc2* expression is activated by the L1CAM-ezrin-NF-κB signalling pathway[94], *Olfm4* expression is regulated by Notch signalling[95]. A recent study has proposed a Wnt-dependent activation of *Olfm4* [96]. However, Olfm4 is absent in Wnt-driven adenomas, in which high Wnt activity represses Notch signalling[92]. The expression of stem cell genes has been shown to predict disease relapse in colon cancer patients: high expression of Lgr5$^+$ stem cell genes characterizes aggressive and metastasized colon cancer and associates with a high risk of tumor recurrence[89].

1.2.3 Targeting cancer stem cells to prevent colon cancer relapse.

Therapeutic interventions in cancer are often ineffective due to cancer stem cells that escape chemotherapy, initiate relapse and metastatic dissemination[97]. Chemotherapy might initially cause tumor shrinkage because the bulk of proliferating tumor cells is effectively killed. It often fails, however, to induce complete tumor regression as highly tumorigenic cancer stem cells survive chemotherapy and re-establish the tumor (Figure 1.7). Relapsing tumors are often more aggressive than the initial tumors, as they are highly enriched for cancer stem cells[98]. It is believed that targeted therapeutic elimination of cancer stem cells will greatly enhance treatment efficacy. Cancer stem cell-targeting therapies are not yet available in the clinic, though, and we are still in search of adequate molecular targets and potent therapeutic agents. Recent studies have revealed a so far unacknowledged plasticity of intestinal tumors. Differentiated colon cancer cells can revert into fully active Lgr5$^+$ colon cancer stem cells and re-grow the tumor after Lgr5$^+$ cell-eliminating therapy[91, 99]. In preclinical models, the

reprogramming of differentiated cancer cells and subsequent tumor regrowth were successfully prevented by combining the depletion of Lgr5^{+} cancer stem cells with conventional chemotherapy[99]. An efficient tumor therapy hence needs to succeed in both the elimination of cancer stem cells and the depletion of the differentiated but plastic tumor bulk.

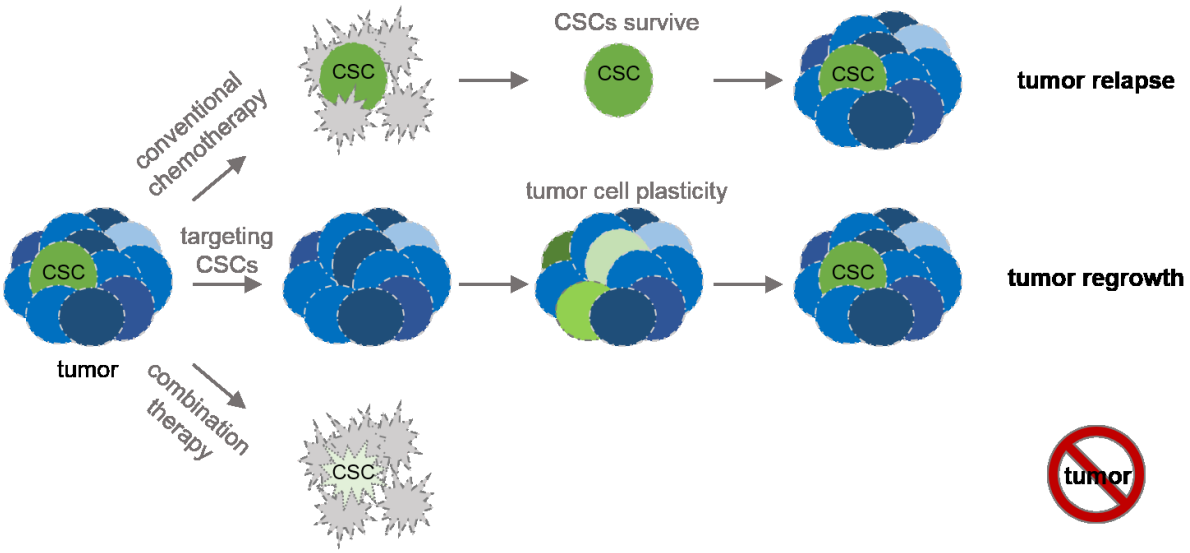

Figure 1.7: The concept of targeting cancer stem cells.
Conventional chemotherapy depletes the tumor bulk, but cancer stem cells (CSCs) remain and initiate relapse. CSC-targeting therapies eliminate CSCs, but fail to prevent de-differentiation of non-stem tumor cells that replenish CSCs and fuel tumor regrowth. A combination therapy of conventional chemotherapy and targeting of CSCs promises to efficiently halt tumor growth.

Given the strong Wnt-dependency of intestinal cancer stem cells and tumors, therapeutic targeting of the Wnt pathway has emerged as a rational treatment for colon cancer. The restoration of Apc function in Apc-deficient colon cancer in mice promotes tumor cell differentiation and re-establishes homeostatic tissue function[84], highlighting the therapeutic potential of targeting aberrant Wnt signalling. In recent years, small molecules which target the Wnt pathway have been developed. The small-molecule inhibitor LF3 disrupts the interaction of Tcf4 with β-catenin and blocks β-catenin/Tcf4-driven Wnt target gene activation[100]. ICG-001 interferes with the interaction of β-catenin and CBP, inhibiting the transactivation activity of the β-catenin/Tcf4 complex[101]. Therapeutic interference with β-catenin activity in colon cancer cells shows strong anti-tumorigenic effects in preclinical studies[100, 101]. Clinical trials for the ICG-001-derivative PRI-724 are underway, but thus far we are lacking a clinically approved drug to target oncogenic Wnt signalling in colon cancer with mutations in APC or β-catenin. A major concern in direct targeting of the Wnt pathway is the critical requirement of Wnt activity for the maintenance and self-renewal of adult intestinal stem cells[102]. A targeted therapy for colon cancer requires the identification of therapeutic targets that discriminate cancer cells from normal epithelial cells.

Epigenetic regulators have emerged as crucial players in tumorigenesis. Their abnormal

activities in cancer cells alter cell-specific gene expression and contribute to tumor progression[103]. Due to their dynamic and reversible nature, epigenetic modifications represent promising targets for cancer therapy. In recent years, several small-molecule inhibitors targeting chromatin-modifying enzymes have been developed that show efficacy in resetting the cancer epigenome in various tumor entities in preclinical studies[103].

1.3 The epigenetic regulation of gene expression.

1.3.1 Chromatin and epigenetics.

All cells of a given organism carry identical genetic information, but are capable of adopting various phenotypes to build different tissues with distinct functions. In the early 1940s, Conrad Waddington introduced the term ‘epigenetics’, meaning ‘in addition to changes in genetic sequence’, to describe the phenomenon of heritable phenotypic divergence without changes to the DNA sequence[104]. In eukaryotic cells, the genetic material is organized in complex structures of DNA-protein interactions, the so-called chromatin (Figure 1.8). 147bp of DNA wrap around histone octamers of the core histone proteins H2A, H2B, H3 and H4 to form a nucleosome. The linker histone H1 ensures stability of nucleosomal histone-DNA particles[105].

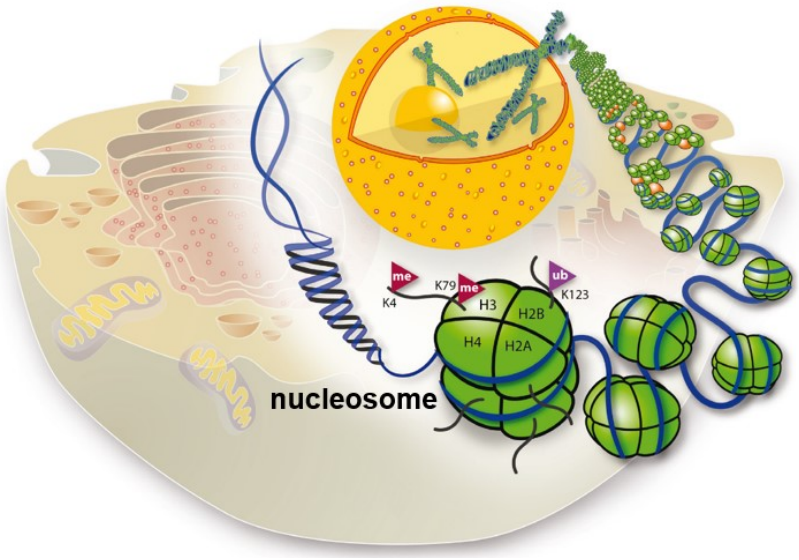

Figure 1.8: Chromatin structure.
Modified from Shilatifard (2012)[105].

Thinking of the DNA in its unfolded state, the nucleosomes appear like ‘beads on a string’, threaded in a regular distance from each other. Histone-histone as well as histone-DNA interactions alter the packing density of the nucleosomes. Eukaryotic nuclei compart into euchromatic “open” regions with loose chromatin packaging and areas with densely packed nucleosomes and a “closed” chromatin structure, the heterochromatin. Heterochromatic areas remain condensed throughout the cell-cycle interphase and contain mostly silenced genes. The open chromatin structure of euchromatic regions confers DNA accessibility and allows for

active gene expression. Hence, epigenetic regulation determines which genes are active and which ones are silenced, and thereby establishes cell identity.

1.3.2 Epigenetic regulation translates cell signalling into gene expression.

Cellular signalling pathways converge in epigenetic regulation to translate intrinsic and extrinsic signals into appropriate lineage-specific gene expression profiles. The number of signalling pathways and signal transducers is limited. To achieve the cellular and phenotypic diversity required to build a functional organism, signalling pathways induce different sets of target genes in distinct cells, rather than instructing a universal gene expression programme[106]. In the intestinal epithelium, Wnt/β-catenin signalling maintains stem cells and drives the proliferation of progenitor cells but also promotes the differentiation of Paneth cells. Distinct sets of activated Wnt/β-catenin target genes underlie these diverse functions: the β-catenin/Tcf4-regulated genes *c-Myc*, *Cd44* and *cyclin D1* are expressed in the proliferative cells of the transit-amplifying compartment, while *Mmp7* and *EphB3* define terminally differentiated Paneth cells[107]. In intestinal stem cells, Wnt signalling induces the expression of stem cell genes such as *Lgr5*, *Ascl2* and *Znrf3* [15, 107]. The regulatory mechanisms underlying these differential lineage-specific target gene responses to Wnt signalling are largely unknown. Cell type-specific β-catenin/Tcf occupancy at target sites would be an obvious explanation for differential Wnt responses, but this concept turned out to be oversimplified: upon activation of Wnt signalling, Tcf/Lef and β-catenin occupy all Wnt target sites regardless of whether the corresponding genes will become expressed in the particular cell or not[108]. The recruitment of β-catenin to target genes does not imply transcriptional activation, β-catenin binding has proven necessary but not sufficient for gene activation[106]. Consequently, regulatory mechanisms apart from β-catenin/Tcf occupancy must determine the lineage-specific activation of Wnt target genes. The histone acetyltransferases CBP and p300 associate with β-catenin in a mutually exclusive manner to activate transcription, inducing fundamentally different transcriptional responses[29]. While CBP/β-catenin complexes activate the expression of genes promoting cell proliferation, p300/β-catenin complexes induce cell differentiation[109]. Epigenetic regulation thus emerges as a determinant of the differential tissue- and cell type-specific expression of Wnt target genes. Various kinds of epigenetic modifications can modulate chromatin structure and gene expression in a cell type-specific manner, among these DNA methylation, chromatin remodelling, long non-coding RNAs and histone modifications.

1.3.3 Epigenetic regulation by histone modifications.

The N-terminal tails of the histone proteins protrude from the nucleosomes and are extensively decorated with posttranslational modifications[110]. These histone modifications directly influence gene activity by altering nucleosome density and chromatin condensation at promoter and enhancer regions. They also offer docking sites for proteins implicated in diverse biological processes. Histone modifications are highly dynamic and reversible, constantly translating developmental and environmental cues into changes in gene activity. Epigenetic modifications and the chromatin structure determine which genes are active and which ones are silenced, thus defining the cellular transcriptome and enabling the emergence of different cell types from an identical genetic code. Various types of histone modifications have been identified, among others histone methylation, acetylation, phosphorylation and ubiquitination that act in concert with transcription factors and co-regulatory proteins to regulate gene expression[110]. Certain types of histone modifications are associated with active gene expression, e.g. the tri-methylation of histone H3 at lysine K4 (H3K4me3) and the acetylation of histone H3 lysine residues, while others repress gene activity, e.g. the tri-methylation of histone H3 at lysine K27 (H3K27me3)[111]. There is evidence for a crosstalk of distinct histone marks, with some modifications acting sequentially or in combination and others being mutually exclusive. This yields a 'histone code' that is 'written', 'read' and 'erased' by histone-modifying proteins and dictates chromatin structure and gene regulation[112]. The 'readers' of histone modifications are equipped with specialized domains: PHD fingers, WD40-repeat domains, chromodomains and Tudor domains recognize methyl marks, bromodomains read acetylations[110]. Once bound to a particular histone mark, the 'readers' recruit transcriptional co-activators or co-repressors, chromatin-remodelling enzymes, transcription factors and components of the RNA polymerase II (RNA pol II) basal transcription machinery to translate histone modifications in gene activity. The language of histone modifications has turned out to be highly complex and we have only started learning how to understand this complexity.

1.3.4 Histone lysine methylation.

Histone methylation occurs on lysine and arginine residues of histone N-terminal tails, mainly of histones H3 and H4. Histone lysine methyltransferases catalyse the transfer of a methyl group (-CH_3) from the methyl group donor *S*-adenosyl-methionine (SAM) to the ε-amino group of lysine residues (Figure 1.9). Several lysine residues in the histone H3 and H4 tails have been identified, which can all be mono-, di- and tri-methylated: histone H3 is methylated at the lysine residues K4, K9, K27, K36 and K79, histone H4 methylation takes place at lysine K20[110]. Depending on the position of the methylated residue on the histone tail, histone lysine methylation induces either gene activation or repression.

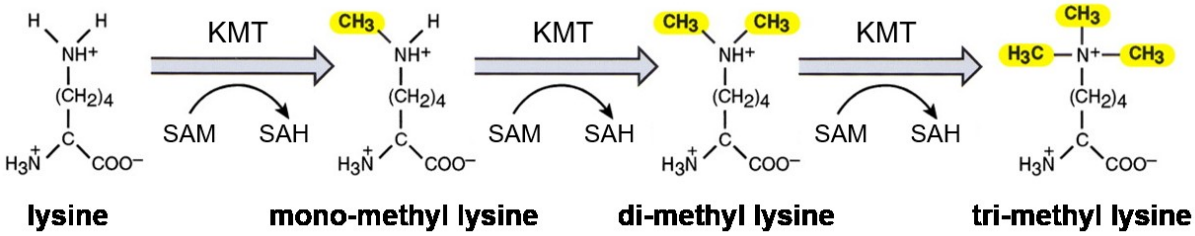

Figure 1.9: Catalysis of histone lysine methylation.
Histone lysine methyltransferases (KMTs) catalyse the transfer of a methyl group (-CH_3) from *S*-adenosyl-methionine (SAM) to the ε-amino group of lysine residues. SAM thereby converts to *S*-adenosyl homocysteine (SAH). Modified from Zhang and Reinberg (2001)[113].

The methylation of histone lysine residues is catalysed by histone lysine methyltransferases (KMTs). All but one of these methyltransferases contain a 130-amino acid catalytic SET domain. This enzymatic domain has first been described as a conserved sequence in the three *Drosophila* methyltransferases suppressor of variegation 3-9 (**S**u(var)3-9), enhancer of zeste (**E**(z)) and trithorax (**T**rx)[114]. The non-SET domain lysine methyltransferase Dot1l (disruptor of telomeric silencing-1-like) is the only known lysine methyltransferase that does not possess a SET domain; it methylates lysine K79 within the globular domain of histone H3[115]. Specialized histone lysine demethylases (KDMs) erase lysine methylation marks and render histone lysine methylation a reversible and dynamic histone mark[116].

1.3.5 H3K4 tri-methylation marks active genes.

Methylation of histone H3 at lysine 4 (H3K4) is found in euchromatic regions of active gene expression. Di-methylated H3K4 (H3K4me2) appears broadly associated with transcribed regions[117], and mono-methylated H3K4 (H3K4me1) is mostly found at active enhancer regions of the genome[118]. The tri-methylation of H3K4 (H3K4me3) is commonly associated with an open chromatin structure and gene activation. A PHD finger of the NURF chromatin-remodelling complex binds H3K4me3 marks, coupling H3K4 tri-methylation to the opening of the chromatin structure[119]. The basal transcription factor TFIID recognizes H3K4me3 via a PHD finger in its TAF3 subunit, which facilitates RNA pol II recruitment to transcription start sites and transcription initiation[120]. H3K4me3 marks are closely linked to actively transcribed genes and tend to occur as defined sharp peaks at the transcription start site, suggesting a direct and essential role in activating transcription[121]. However, experimental evidence for a global instructive role of H3K4me3 in the activation of transcription is lacking. Genome-wide loss of H3K4me3 has only minimal effect on global transcription rates and gene activation[122]. That is why the H3K4me3 mark has been proposed to rather associate than instruct transcription[123]. Recent studies indeed reported a functional role of H3K4 methylation in maintaining lineage-specific gene expression and stabilizing transcription[124, 125]. In any case, the strong positive correlation of H3K4me3, transcription rates and RNA pol II occupancy renders H3K4me3 a marker for active genes.

1.3.6 H3K4 methyltransferases of the Set1/Mll family.

H3K4 methyltransferases were originally identified in the yeast *Saccharomyces cerevisiae*. The yeast Set1 enzyme associates in a large multi-protein complex, the 'complex of proteins associated with Set1' (COMPASS), to catalyse the mono-, di- and tri-methylation of H3K4[126]. While Set1 is the only H3K4 methyltransferase in yeast, the fruit fly *Drosophila melanogaster* possesses three related enzymes (dSet1, trithorax (Trx) and trithorax-related (Trr))[127]. Mammals express six Set1-related H3K4 methyltransferases, the members of the Mll (mixed lineage leukemia)/Kmt2 (histone lysine N-methyltransferase 2) family[105] (Figure 1.10). **Mll1** (Kmt2a) and **Mll2** (Kmt2b) are the mammalian orthologues of *Drosophila* trithorax (Trx) which preferentially di- and tri-methylate H3K4 at promoter regions[105]. They account for about 50% of all Mll complexes and are the most abundant Mll methyltransferases in mammalian cells[128]. Mll1 and Mll2 proteins are present in roughly equal amounts[128]. **Mll3** (Kmt2c) and **Mll4** (Kmt2d) are the mammalian orthologues of *Drosophila* trithorax-related (Trr) which mono-methylate H3K4 at enhancer regions[129]. **Setd1a** (Kmt2f) and **Setd1b** (Kmt2g) are responsible for the bulk of H3K4 tri-methylation at gene promoters[130, 131]. Setd1a is more abundant than Setd1b, accounting for ~25% and ~7% of all Mll proteins, respectively[128]. The paralogues Mll1/Mll2, Ml3/Mll4 and Setd1a/Setd1b have each arisen from chromosomal duplication in mammalian evolution[132].

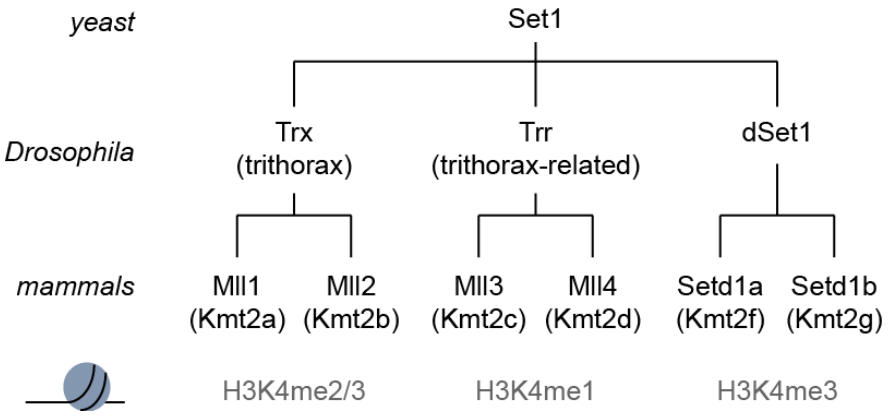

Figure 1.10: The Set1/Mll family of H3K4 methyltransferases.
Yeast Set1 mono-, di- and tri-methylates H3K4. *Drosophila* possesses three enzymes with distinct methylation activities. Mammals comprise six Set1-related H3K4 methyltransferases with distinct H3K4 methylation preferences.

The six methyltransferases of the mammalian Mll family exert non-redundant functions. Despite similar domain structures and interaction partners, even the two paralogues in each subgroup are non-redundant and exhibit largely non-overlapping subnuclear distributions[132]. Similar to yeast Set1, the mammalian Mll family members reside in multi-protein complexes[105]. A common core complex composed of the WD40-repeat containing protein 5 (**W**dr5), retinoblastoma-binding protein 5 (**R**bbp5), Ash2-like (**A**sh2l) and **D**py30, termed WRAD,

assembles around the SET domains and strongly enhances the otherwise weak H3K4 methylation activities of the Mll enzymes[133].

1.3.7 H3K4 methylation by Set1/Mll antagonizes H3K27 methylation and gene silencing by Polycomb group proteins.

H3K4 methylation established by Set1/Mll methyltransferases of the Trithorax Group (TrxG) counteract the repressive tri-methylation of histone H3 at lysine K27 (H3K27me3) catalysed by Polycomb Group (PcG) proteins[134]. PcG proteins exist in two major complexes with distinct enzymatic properties, the polycomb repressive complexes 1 and 2 (PRC1 and PRC2)[135]. PRC2 complexes comprise the H3K27 methyltransferases Ezh1 and Ezh2, PRC1 complexes contain the E3 ubiquitin ligases Ring1a and Ring1b which ubiquitinate H2A at lysine K119 (H2AK119ub). H3K27me3 marks established by PRC2 are recognized by PRC1 complexes that can subsequently catalyse H2A ubiquitination and instruct chromatin compaction to silence gene transcription[136]. The antagonism of TrxG and PcG proteins defines H3K4 and H3K27 methylation at lineage-specific genes to establish and maintain cell type-specific gene expression patterns and cell identity[134]. By bookmarking lineage-specific genes, TrxG and PcG proteins constitute a 'cellular memory' which allows cells to keep their identity and remember it through cell divisions[137]. The biological functions of the TrxG-PcG antagonism in adult mammalian tissues are diverse and depend on the cellular context: in adult stem cells, the counteracting activities of TrxG and PcG proteins define stem cell identity by sustaining the expression of stem cell genes and repressing differentiation-associated genes[138]. Upon differentiation, the TrxG-PcG antagonism is crucial to fine-tune cell type specification by ensuring lineage-specific gene expression and supressing alternate cell fates[138].

1.3.8 Histone methyltransferases in cancer.

The dynamic nature of the epigenome poses a risk for misregulation. Aberrations in histone modifications and mutations in chromatin-modifying enzymes are recurrently found in cancer[103]. In colon cancer, high levels of H3K4me3 are associated with a poor prognosis[139]. Methyltransferases of the Trithorax and Polycomb groups regulate cell identity. Their deregulated activities alter cellular gene expression profiles and drive tumorigenesis[134]. Polycomb PRC1 complexes have been implicated in Wnt-driven intestinal tumorigenesis[140]. The H3K4 methyltransferase Setd1a has been linked to the regulation of distinct Wnt/β-catenin target genes in colon cancer cells[141]. Tumor-promoting functions have also been reported for the histone methyltransferase Mll2[142, 143]. The family member Mll1 has not yet been studied in colon cancer. Genomic translocations of the *Mll1* gene at 11q23 fuse ~1400 amino acids of the Mll1 N-terminus in frame to a variety of different translocation partners and drive aggressive human leukemia[144]. To date, over 70 different oncogenic MLL fusion proteins have been identified, among these fusions to ENL, AF9, AF4, ELL and AF10[144]. The enzymatic SET

domain is invariably deleted in MLL fusion proteins and is replaced by the activity and function of the particular fusion partner. MLL fusion proteins aberrantly activate transcription, often by recruiting the H3K79 methyltransferase Dot1l and the transcription elongation factors Cdk9 and cyclinT1, also known as pTEFb[144]. MLL-rearranged leukemia commonly preserves at least one wild-type *Mll1* allele with an intact SET domain. Recent data suggest that leukemogenesis in fact requires the wild-type allele of *Mll1* [145], although there is controversy on the need of wild-type Mll1 and instead Mll2 has been attributed a major role in sustaining MLL-rearranged leukemia[146]. Given the central role of Mll1 in leukemogenesis, there is great interest in designing small-molecule inhibitors which target Mll1 function. The Menin inhibitor 2 (MI-2) inhibits the interaction of Mll1/Mll2 with Menin (Men1, multiple endocrine neoplasia-1), an essential oncogenic co-factor of MLL fusion proteins in leukemia[147]. Targeting the Menin-MLL interaction inhibits proliferation and induces differentiation of MLL leukemia cells in preclinical models[147]. The WRAD complex subunit Wdr5 is part of all Mll complexes, but only the integrity and methyltransferase activity of the Mll1 complex strongly depend on the interaction with Wdr5. Targeting the Mll1-Wdr5 interaction with the small molecules MM-401 and OICR-9429 specifically interferes with the methyltransferase function of wild-type Mll1 and succeeds in inhibiting MLL leukemia cell growth[148, 149].

1.3.9 The histone methyltransferase Mll1.

The histone methyltransferase Mll1 is a large 3969-amino acid protein with multiple domains. At its N-terminus, Mll1 comprises three DNA-binding AT hooks and a cysteine-rich CxxC zinc-finger domain through which Mll1 binds to non-methylated CpG islands and protects these sites from DNA methylation[150] (Figure 1.11). PHD finger motifs, a PHD-flanking acetyl-lysine binding bromodomain and a transactivation domain (TAD) are followed by a WDR5 interaction (Win) motif and the C-terminal catalytic SET domain[151]. The mature Mll1 protein is proteolytically cleaved by taspase-1 (threonine aspartase-1)[152]. The cleaved N-terminal (N320) and C-terminal (C180) fragments re-associate via their FYRN/C domains and form a stable $Mll1^{N320/C180}$ heterodimer[153]. Post-cleavage association ensures Mll1 protein stability and correct nuclear localization[153].

Multiple interaction partners strongly enhance the methyltransferase activity of Mll1. The WRAD complex composed of Wdr5, Rbbp5, Ash2l and Dpy30 directly associates with the C-terminal SET domain and is essential for enzymatic activity[154]. The Mll1 N-terminus forms a tri-molecular complex with the scaffold protein Menin and the lens epithelium-derived growth factor Ledgf, which assists in recruitment to chromatin target sites[155, 156]. Menin co-regulates a subset of Mll1-controlled genes, especially *homeobox* (*Hox*) targets and the cyclin-dependent kinase inhibitors $p27^{Kip1}$ and $p18^{Ink4c}$ [157, 158]. However, not all Mll1 target genes depend on the co-regulation by Menin[157]. Mll1 also interacts with the histone acetyltransferase MOF (Kat8) which acetylates H4 at K16 (H4K16ac) and coordinates with Mll1 activity to induce

transcription[159]. The Mll1 transactivation domain (TAD) associates with the CREB-binding protein (CBP)[160]. Through CBP, Mll1 interacts with the β-catenin/TCF4 complex[161, 162].

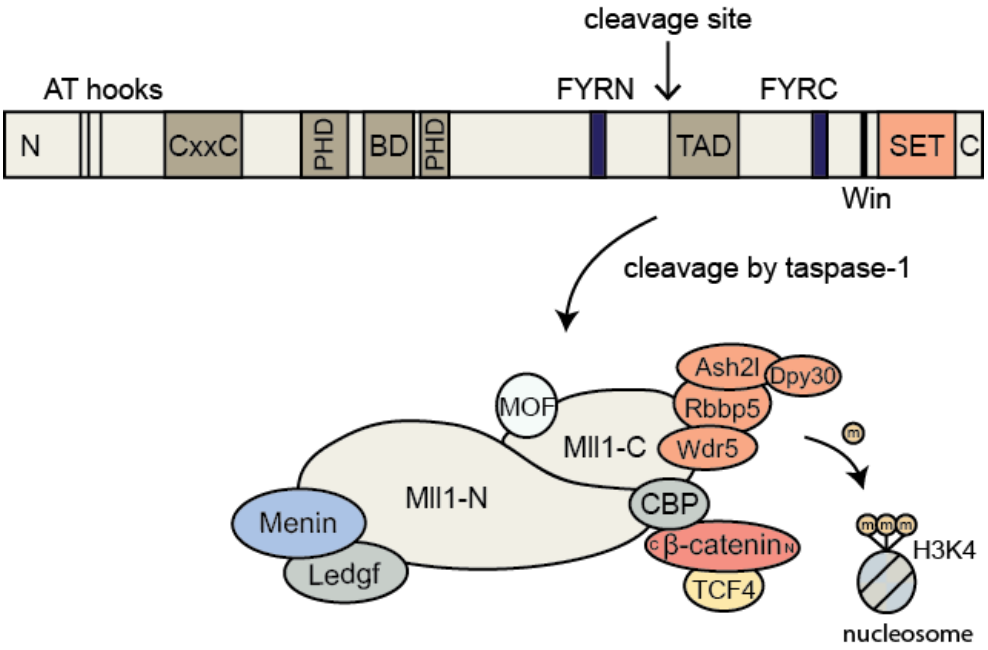

Figure 1.11: Mll1 protein structure and interaction partners.
Full-length Mll1 (upper part) is cleaved by taspase-1. The N- and C-terminal cleavage fragments assemble in a multi-protein complex (lower part). CxxC cysteine-rich zinc finger domain, PHD plant homeodomain, BD bromodomain, TAD transactivation domain, Win WDR5 interaction motif, FYRN/C FY-rich domain N-terminal/C-terminal.

Mll1-induced H3K4me3 proceeds transcription initiation and is required for the binding of the RNA pol II basal transcription machinery[163]. The intrinsic DNA- and CpG island-binding motifs of Mll1 and its interaction partners direct Mll1 binding to specific target sites. The long non-coding RNA *HOTTIP* also recruits the Mll1 complex to distinct chromatin sites[164]. Loss of Mll1 does not affect global H3K4 tri-methylation levels and leads to strikingly few changes in gene expression[163]. Less than 5% of promoter H3K4me3 marks are actually dependent on Mll1[163]. At these specific sites, however, Mll1 strongly affects H3K4 methylation and gene expression. Mll1 thus acts in a highly specific way to control the expression of distinct target genes that are crucial for development and tissue homeostasis.

1.3.10 Mll1 in development, tissue homeostasis and disease.

The deficiency for Mll1 is lethal between embryonic day E10.5 and E13.5[165, 166]. Mice with heterozygous deletion of Mll1 are viable but show developmental defects in the patterning of the axial skeleton and in hematopoiesis[165]. Mll1 maintains the expression of *Hox* genes, which specify body segmentation in development, particularly *Hoxa7* and *Hoxa9* [167]. The misregulation of these *Hox* genes is causative for the skeletal transformations and hematopoietic abnormalities of Mll1-deficient mice[167, 168]. In humans, deleterious *de novo*

mutations in one *MLL1* allele cause a rare genetic disorder known as the Wiedemann-Steiner syndrome (WSS)[169]. WSS patients exhibit a MLL1 haploinsufficiency that causes multiple congenital anomalies, e.g. a short stature due to delayed skeletal maturation, intellectual disability and distinctive facial appearance[169].

Mll1 is crucial for fetal and adult hematopoiesis[170, 171]. Definitive hematopoiesis at E10.5 critically depends on Mll1[172]. In the adult, Mll1 maintains hematopoietic stem and progenitor cells[171]. Hematopoietic stem cells (HSCs) lacking Mll1 fail to self-renew[170, 171]. Quiescent HSCs deficient for Mll1 show ectopic cell cycle entry, which rapidly causes HSC exhaustion and depletes the entire stem cell pool, resulting in fatal bone marrow failure[170, 171]. To sustain hematopoiesis, Mll1 regulates *Hox* genes and self-renewal factors in a manner both dependent and independent of its co-factor Menin[157]. The methyltransferase activity of Mll1 is dispensable for hematopoiesis, but Mll1-dependent recruitment of the histone acetyltransferase MOF is essential for the maintenance of HSC target gene expression[173]. Hematopoietic progenitor cells show a reduced proliferation upon ablation of Mll1, while committed lymphoid and myeloid cells no longer require Mll1 and are unaffected by Mll1 ablation[171]. Apart from its prominent role in the hematopoietic system, Mll1 has been implicated in the regulation of stem cell self-renewal and cell fate specification in other adult tissues. It is essential for neurogenesis from postnatal neural stem cells in the subventricular zone[174]. Mll1-deficient neural stem cells efficiently generate glial progenitors but fail to induce neuronal differentiation[174]. Mll1 contributes to the *de novo* transcriptional activation of the myogenic regulatory factor *Myf5* after asymmetric division of muscle satellite cells by controlling the expression of the transcription factor Pax7[175, 176]. The Mll1-induced expression of *Pax7* is essential for proliferation and self-renewal of activated muscle satellite stem cells and for skeletal muscle regeneration[176]. Satellite stem cells deficient for Mll1 fail to self-renew and differentiate, causing a progressive depletion of the satellite stem cell pool[176].

Somatic mutations of Mll1 are found in various tumor entities[177]. 78% of somatic Mll1 mutations have been reported to be missense mutations that cause gain-of-function phenotypes[177]. The missense mutations R3864C and R3841W are located in the Mll1 SET domain and increase the catalytic activity of Mll1 independent of the regulatory WRAD complex[177]. Even if not mutated, Mll1 and its methyltransferase activity might be exploited by oncogenic signalling to promote tumorigenesis, as has been demonstrated for Wnt-driven salivary gland and head and neck cancers[162, 178]. Interaction with oncogenic β-catenin also implicates Mll1 in cervical carcinoma progression[179]. Wild-type Mll1 has further been linked to glioblastoma stem cell maintenance[180], cervical cancer[181] and melanoma cell growth[182]. Gain-of-function mutants of p53 upregulate the expression of *Mll1*, *Mll4* and the histone acetyltransferase *Moz* to promote tumorigenesis[183]. Mll1 further acts as a co-activator of the androgen receptor signalling complex in prostate cancer[184].

As exemplified for Mll1, oncogenic signalling in cancer cells can exploit epigenetic regulators to fuel tumor growth[132]. Similar to the concept of 'oncogene addiction' [9], which describes the addiction of cancer cells to the presence of a certain oncogene, the viability of cancer cells can strictly depend on the hijacked epigenetic mechanism[103]. Such cancer cells will be highly sensitive to appropriate epigenetic inhibitors[103]. By playing on the addiction to certain oncogenes and epigenetic modifiers in cancer therapy we might be able to specifically eliminate cancer cells, while minimizing detrimental effects on normal tissue function.

2 Aim of the study

Colon cancer is a major cause of cancer death worldwide. Treatment successes are moderate and rational therapies are desperately needed. Current therapies are often ineffective due to cancer stem cells, which can resist conventional chemotherapy and initiate tumor relapse and metastasis. Oncogenic signalling in cancer cells frequently exploits epigenetic mechanisms to fuel tumor growth. The tumorigenicity of the cancer cells then critically relies on cancer-specific epigenetic changes. A comprehensive understanding of the epigenetic changes in cancer is expected to have high therapeutic potential. Epigenetic therapies hold great promise to inhibit tumor growth and cancer cell plasticity by resetting the cancer epigenome. The reversible nature of histone modifications makes chromatin modifiers attractive targets for therapeutic manipulation. The present study aims to understand the role of epigenetic regulation by the histone methyltransferase Mll1 in Wnt-driven colon cancer to promote the identification of potential therapeutic targets and the future development of rational treatment. Previous work in our lab has implicated non-mutant Mll1 in Wnt-driven salivary gland and head and neck tumorigenesis. So far, a role for Mll1 in intestinal tumorigenesis and colon cancer stemness has not been determined. Given the high Wnt activity in colon cancer cells and in particular in colon cancer stem cells, we postulated a crucial role of Mll1 in Wnt-driven colon cancer. The understanding of Mll1 function in Wnt-activated colon cancer cells will establish novel strategies for future targeted therapies, which will be of great benefit for colon cancer patients.

3 Results

3.1 Mll1 expression is upregulated in Wnt-high human colon carcinomas.

To assess the expression of the histone methyltransferase MLL1 in colon carcinomas, biopsies from colon cancer patients were analysed by immunohistochemistry. Human colon carcinomas showed substantial MLL1 expression: weak to moderate and strong MLL1 staining intensities were observed at all tumor stages (T0-T4) (Figure 3.1a, upper left panel, stainings of tumor stages T1-T4 in Supplementary Figure 1a, left panel, page 114). The majority of tumors exhibited moderate to strong MLL1 expression (Figure 3.1b), which was associated with high levels of nuclear β-catenin, indicating high activity of Wnt signalling (Figure 3.1a, c, Supplementary Figure 1, page 114): at all tumor stages, carcinomas with strong expression of MLL1 exhibited high levels of nuclear β-catenin. Vice versa, carcinomas with weak MLL1 expression had predominantly low levels of nuclear β-catenin. Accordingly, MLL1 expression is upregulated in Wnt-high human colon carcinomas.

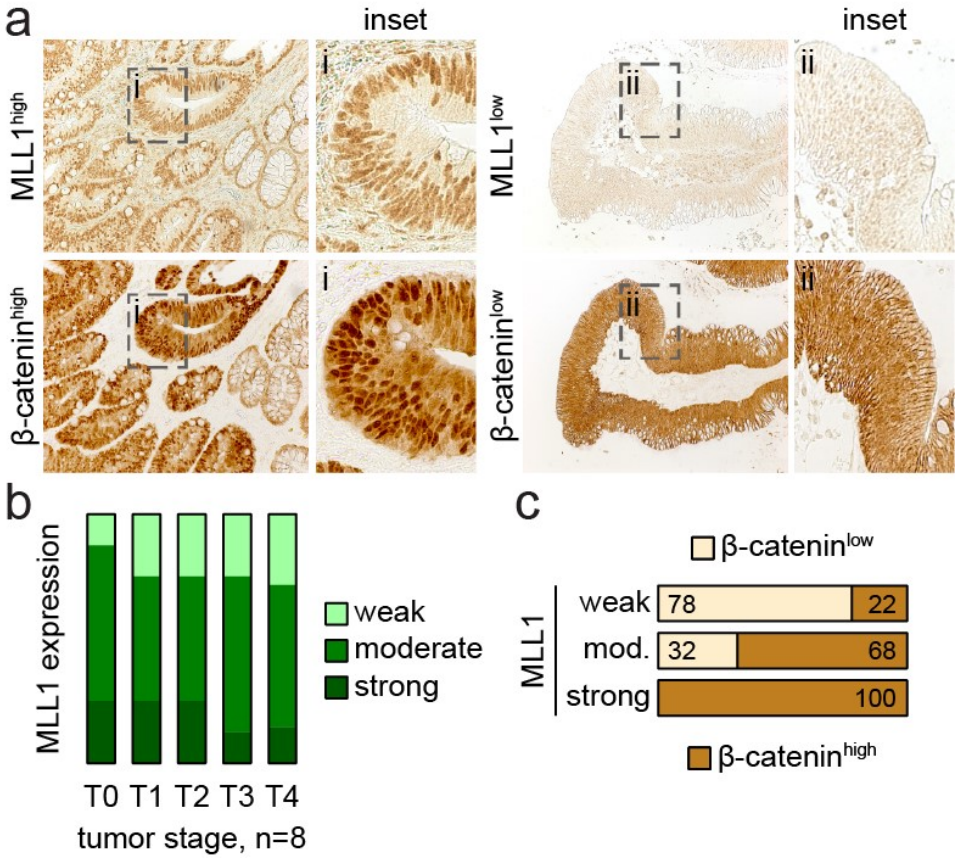

Figure 3.1: High Mll1 expression correlates with high nuclear β-catenin in human colon carcinomas.

a) Immunohistochemistry for MLL1 (upper panels) and β-catenin (lower panels) on naïve colon cancer patient biopsies, tumor stage T0, with high expression (left) and low expression (right) of MLL1 and β-catenin, magnifications in insets i and ii. Biopsy sections were kindly provided by Michael Vieth, Pathology Klinikum Bayreuth. Immunohistochemistry staining was performed by Julian Heuberger, MDC. Staining specificity was verified as described in section 5.9, page 90 and Supplementary Figure

2, page 115. **b)** Quantification of MLL1 stainings scored as weak, moderate and strong in human colon carcinomas: tumor stages T0-T4, n=8 each. **c)** Quantification of nuclear β-catenin staining scored as low and high in tumors with weak, moderate and strong expression of MLL1 across all stages, n=39.

3.2 Lgr5$^+$ intestinal stem cells highly express Mll1 in a Wnt-dependent manner.

Lgr5$^+$ intestinal stem cells have been identified as the cells-of-origin in colon cancer[79]. High Wnt activity in the intestinal crypts sustains Lgr5$^+$ stem cells that constantly produce secretory and absorptive progenitors. These progenitor cells migrate out of the Wnt-high niche and differentiate once they reach the villus compartment enriched for differentiation-inducing factors such as Bmp4[10, 185] (scheme in Figure 3.2a). We used immunofluorescence to examine the expression of Mll1 along the intestinal crypt-villus axis of mice. Mll1 expression is high at the base of the crypt and in the proliferating cells of the transit-amplifying (TA) zone, and is gradually lost towards the differentiated villus compartment (Figure 3.2b). We observed highest expression of Mll1 in the stem cells which were identified by the Lgr5-EGFP-IRES-Cre^{ERT2} reporter[15] (Figure 3.2c, white arrows). The differentiated Paneth cells in the crypt, which were distinguished from adjacent stem cells by immunofluorescence for Mmp7[186], exhibited low levels of Mll1 expression (Figure 3.2c, lower panel, white asterisks). Quantitative immunofluorescence confirmed strongest expression of Mll1 in Lgr5$^+$ stem cells, which gradually decreased in the TA cells, Paneth cells and enterocytes (Figure 3.2d).

The high expression of Mll1 in the Wnt-high crypt compartment and particularly in Lgr5$^+$ stem cells suggested that Mll1 is crucial for stemness and is lost upon differentiation. We addressed the role of the inverse Wnt/Bmp gradients, which define the crypt stem cell niches and the differentiated villus compartments of the intestinal epithelium, in regulating the expression of *Mll1*. We used intestinal organoids which depend on a defined culture medium containing the essential growth factors EGF, Noggin and R-spondin1 that mimic the crypt stem cell niche[74] (compare 1.1.5, page 11). Modulating stem cell niche properties in organoid culture through removal of the Bmp antagonist Noggin and administration of Bmp4 led to a reduction of the expression of *Mll1*, accompanied by a repression of the stem cell gene *Lgr5* in a concentration-dependent manner (Figure 3.2e). The activation of Bmp signalling and the triggering of differentiation were confirmed by increased expression of *Id2* [187] (Figure 3.2e). Stimulating Wnt activity by adding the Wnt ligand Wnt3a increased the expression of *Mll1* (Figure 3.2e). Wnt3a treatment also increased the expression of the Wnt-regulated stem cell gene *Lgr5* [15] and the classical Wnt target *Axin2* [33] (Figure 3.2e). Our data reveal that the opposing Wnt/Bmp gradients restrict Mll1 expression to the Wnt-activated crypt cells.

Crypt-villus fractionations of mouse small intestinal epithelia confirmed the strong expression of *Mll1* in the crypts (Figure 3.2f). The crypt enrichment was proven by high expression of *Lgr5*. Like Mll1, the Mll family members Mll2-4, Setd1a and Setd1b also exhibited a higher expression in the crypts compared to villi (Figure 3.2f). In accordance, we observed a crypt-villus gradient for H3K4 tri-methylation (H3K4me3), the active chromatin mark established by

enzymes of the Mll family (Figure 3.2g). A similar distribution of Mll1 and H3K4me3 was observed in the epithelium of the mouse colon (Figure 3.2h).

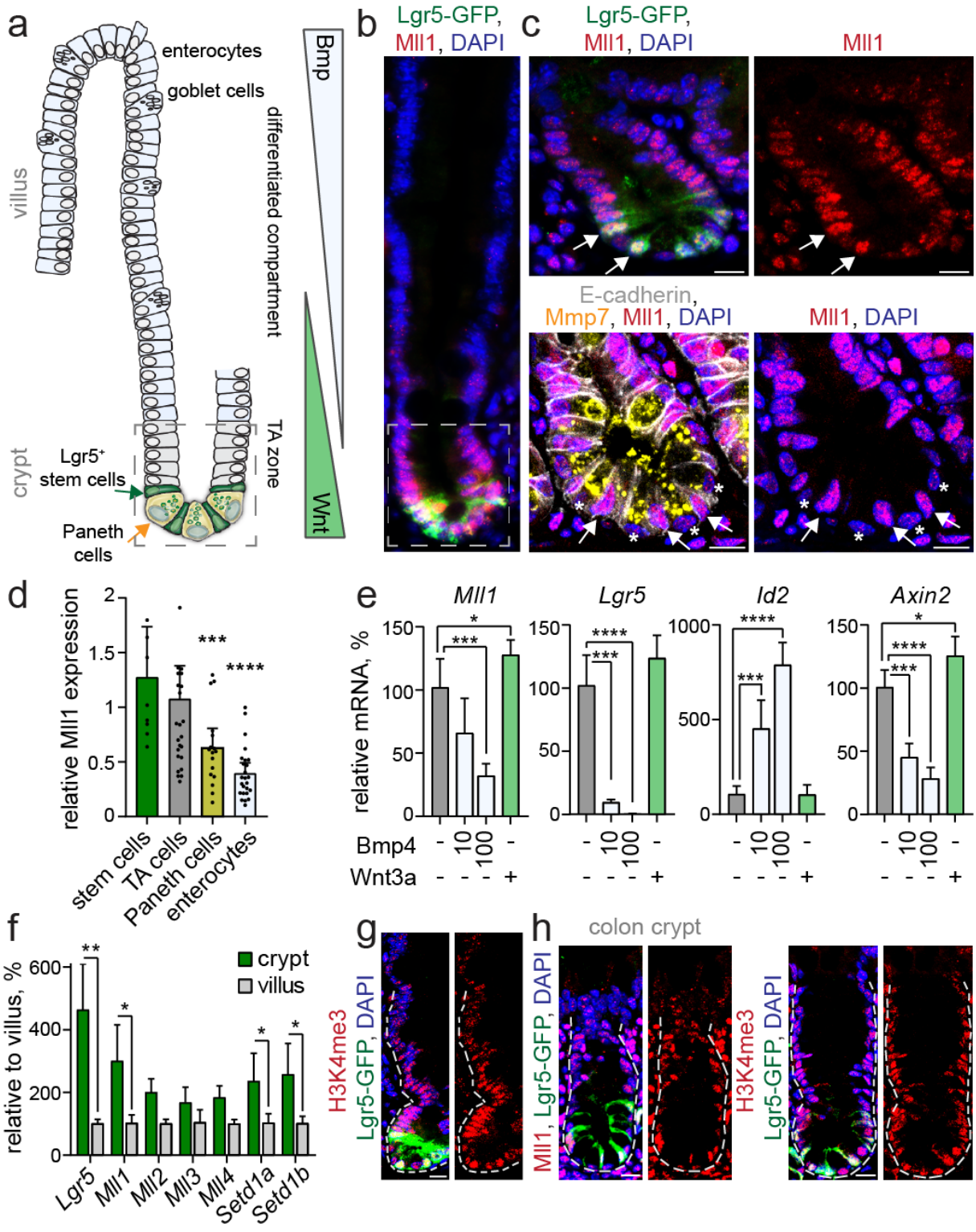

Figure 3.2: High Mll1 expression in Lgr5⁺ stem cells and Wnt-activated crypt cells of the mouse intestinal epithelium.

a) Scheme of the murine small intestinal crypt-villus axis. In the lower crypt, Lgr5⁺ stem cells (green) intersperse between Paneth cells (yellow). Stem cells produce progeny that proliferate and differentiate in the transit-amplifying (TA) zone (grey). Terminally differentiated cells (e.g. enterocytes and goblet

cells, light blue) move into the villus. Opposing gradients of Wnt and Bmp signalling specify proliferation and differentiation along the crypt-villus axis. **b)** Immunofluorescence staining for Mll1 (red) on the small intestine of Lgr5-GFP mice reveals a gradual decrease in Mll1 expression from crypt to villus. Stem cells marked by Lgr5-GFP (green), nuclei in blue (DAPI). **c)** Magnification of the crypt region; upper panel, white arrows mark stem cells with high Mll1 expression (red); lower panel, asterisks mark Paneth cells stained by Mmp7 (yellow) with low Mll1 expression. E-cadherin (white) stains cell borders. Nuclei in blue (DAPI), scale bars 10µm. **d)** Quantification of the Mll1 staining intensity in nuclei of crypt and villus cells, normalized to the mean Mll1 expression in TA cells located just above the stem cell niche (up to relative +8 position), quantified from independent stainings of 5 mice, Mann-Whitney test for significance relative to stem cells. **e)** *Mll1*, *Lgr5*, *Id2* and *Axin2* mRNA expression in intestinal organoids treated with 10ng/ml and 100ng/ml Bmp4 and 0.66µg/ml recombinant Wnt3a for 24h, n=5, unpaired t test. **f)** mRNA expression of *Lgr5*, *Mll1* and Mll family members in intestinal crypts relative to villi fractions, n=4, unpaired t test. **g)** H3K4me3 (red) and Lgr5-GFP (green) staining on the small intestine, nuclei in blue (DAPI), scale bar 20µm. **h)** Immunofluorescence for Mll1 or H3K4me3 (red) and Lgr5-GFP (green) in colon crypts of Lgr5-GFP mice, nuclei in blue (DAPI), scale bars 20µm.

Given the particularly strong expression of Mll1 in the stem cells of the mouse intestine (see Figure 3.2, page 28), we investigated the effect of Mll1 ablation on the viability and self-renewal of the $Lgr5^+$ intestinal stem cells. To ablate Mll1 specifically in the $Lgr5^+$ stem cells, we crossed Lgr5-EGFP-IRES-Cre^{ERT2} mice with $Mll1^{flox}$ mice[188]. Mutagenesis was induced by intraperitoneal injections of tamoxifen in Lgr5-EGFP-IRES-Cre^{ERT2}; $Mll1^{flox/+}$ and Lgr5-EGFP-IRES-Cre^{ERT2}; $Mll1^{flox/flox}$ mice (referred to as $Mll1^{+/-}$ and $Mll1^{-/-}$, respectively). $Lgr5^+$ cells, in which the *Lgr5* promoter is active, express eGFP and a tamoxifen-inducible Cre recombinase that allows for conditional mutagenesis[15]. The Cre activity deletes the floxed exon 2 of the *Mll1* locus, introducing a premature stop codon and causing loss of Mll1 protein expression[188] (compare Materials and Methods, Figure 5.1a, page 84). A crossed-in LacZ reporter allele[189] allowed us to trace recombined cells and their progeny. Conditional mutagenesis using the *Lgr5-Cre^{ERT2}* caused a mosaic of recombined $LacZ^+$ and non-recombined (wild-type) crypts (Figure 3.3a, upper panel). The insertion of the *EGFP-IRES-Cre^{ERT2}* cassette into the first exon of the *Lgr5* locus abolishes Lgr5 protein production. As the homozygous ablation of Lgr5 is neonatally lethal, only mice which are heterozygous for the *Lgr5-GFP-IRES-Cre^{ERT2}* allele are viable[15, 190]. Selective silencing of the *Lgr5-GFP-IRES-Cre^{ERT2}* knock-in allele has been reported, producing a mosaic of *Lgr5-EGFP-IRES-Cre^{ERT2}* expression[191]. Consequently, a substantial portion of $Lgr5^+$ intestinal stem cells produces neither GFP nor the Lgr5-Cre^{ERT2} and escapes mutagenesis.

LacZ lineage tracing revealed that mutant $Mll1^{-/-}$ stem cells produced $LacZ^+$ progeny up to 20 days after the induction of mutagenesis. From 20 days onwards, $LacZ^+$ $Mll1^{-/-}$ crypts were progressively lost and replaced by non-recombined crypts (Figure 3.3a lower panels, quantification on the right), but a substantial number of $Mll1^{-/-}$ crypts persisted beyond 50 days after the induction of mutagenesis, as assessed by immunohistochemistry staining for Mll1 (Figure 3.3b). The number of $Mll1^{-/-}$ crypts decreased from initial 30-40% mutant crypts at 10-20 days down to 25-30% at 50 days after induction (Figure 3.3b, quantification on the right).

The Mll1$^{-/-}$ mice did not show any abnormalities. Until 50 days after induction the intestinal epithelium remained intact and overall organ function was not visibly impeded, as non-recombined stem cells functionally replaced Mll1$^{-/-}$ crypts and preserved the intestinal homeostasis. The functional replacement of mutant crypts by fission of non-recombined crypts had previously been described in the intestine of mice with conditional knockout of the stem cell gene *Ascl2* [92]. Our data indicate that, under normal homeostatic conditions, the loss of Mll1 causes a mild phenotype, with a slow reduction of mutant stem cells over time.

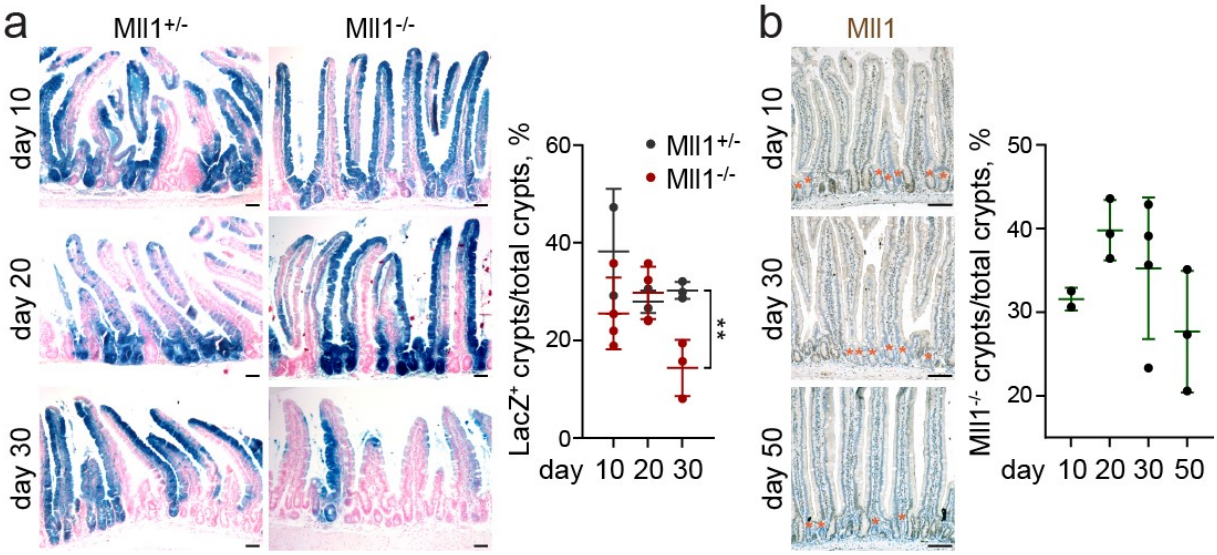

Figure 3.3: A functional role of Mll1 in intestinal stem cells.
a) Lineage tracing: sections of LacZ (blue) whole-mount stainings of intestines of Lgr5-EGFP-IRES-Cre^{ERT2}; Rosa-LacZ; Mll1$^{flox/+}$ and Lgr5-EGFP-IRES-Cre^{ERT2}; Rosa-LacZ; Mll1$^{flox/flox}$ mice (referred to as Mll1$^{+/-}$ and Mll1$^{-/-}$, respectively) at days 10 (n=2 Mll1$^{+/-}$, n=4 Mll1$^{-/-}$), 20 (n=3 Mll1$^{+/-}$, n=5 Mll1$^{-/-}$) and 30 (n=2 Mll1$^{+/-}$, n=3 Mll1$^{-/-}$) after Cre induction. Nuclear fast red counter-staining, scale bars 50µm. Quantification of LacZ^{+} crypts per total crypts on the right, dot plot with mean and standard deviation, unpaired t test. **b)** Immunohistochemistry for Mll1 on sections of Mll1$^{-/-}$ intestines at days 10 (n=2), 20 (n=3), 30 (n=4) and 50 (n=3) after induction, nuclei counter-stained with hematoxylin, scale bars 100µm. Orange asterisks mark Mll1$^{-/-}$ crypts. Quantification of Mll1$^{-/-}$ crypts per total crypts on the right, dot plot with mean and standard deviation.

3.3 The β-catenin^{GOF}-induced intestinal tumorigenesis depends on Mll1.

The tight correlation of Mll1 and nuclear β-catenin in human colon cancer specimens (see Figure 3.1, page 26) and the high expression of Mll1 in the Lgr5^{+} intestinal stem cells, the cells-of-origin in colon cancer[79], suggested a role of Mll1 in Wnt-driven intestinal tumorigenesis. We made use of a Wnt/β-catenin-dependent genetic mouse model of intestinal cancer[78]: Cre-mediated recombination deletes the exon 3 of the *β-catenin* locus (compare Materials and Methods, Figure 5.1b, page 84), which removes the N-terminal phosphorylation sites of β-catenin and impedes its ubiquitin-proteasomal degradation, resulting in a stabilized oncogenic form, β-cat^{GOF}. By intraperitoneal injections of tamoxifen we induced the activation of β-catenin and loss of Mll1 in the Lgr5^{+} stem cells of Lgr5-EGFP-IRES-Cre^{ERT2}; β-cat^{GOF}; Mll1$^{flox/+}$ and Lgr5-EGFP-IRES-Cre^{ERT2}; β-cat^{GOF}; Mll1$^{flox/flox}$ mice (hereafter called β-cat^{GOF}; Mll1$^{+/-}$ and β-cat^{GOF}; Mll1$^{-/-}$ mice). Mice were analysed at different time points up to 100 days after induction.

The intestines of the β-cat^{GOF}; Mll1$^{+/-}$ mice became severely dysplastic within 30 days and developed adenomas which were highly proliferative, as indicated by Ki67 staining, and contained islets with high Mll1 expression (Figure 3.4a, upper panel). Other tissues with Lgr5^{+} stem cells like skin, liver, kidney, and stomach[192-194] appeared normal. The β-cat^{GOF}; Mll1$^{+/-}$ mice were viable up to 40 days after the induction of mutagenesis. In contrast, the homozygous ablation of Mll1 led to normal crypt-villus structures in β-cat^{GOF}; Mll1$^{-/-}$ mice, with proliferation restricted to the crypt regions (Figure 3.4a, lower panel). We observed Mll1-depleted crypts among non-recombined Mll1-expressing crypts (Figure 3.4a, inset in bottom right panel). The homozygous ablation of Mll1 prevented the β-catenin^{GOF}-induced intestinal tumorigenesis, as shown by a Kaplan-Meier plot of tumor incidence (Figure 3.4b). β-cat^{GOF}; Mll1$^{-/-}$ mice did not show any tumors up to 100 days after the induction of mutagenesis.

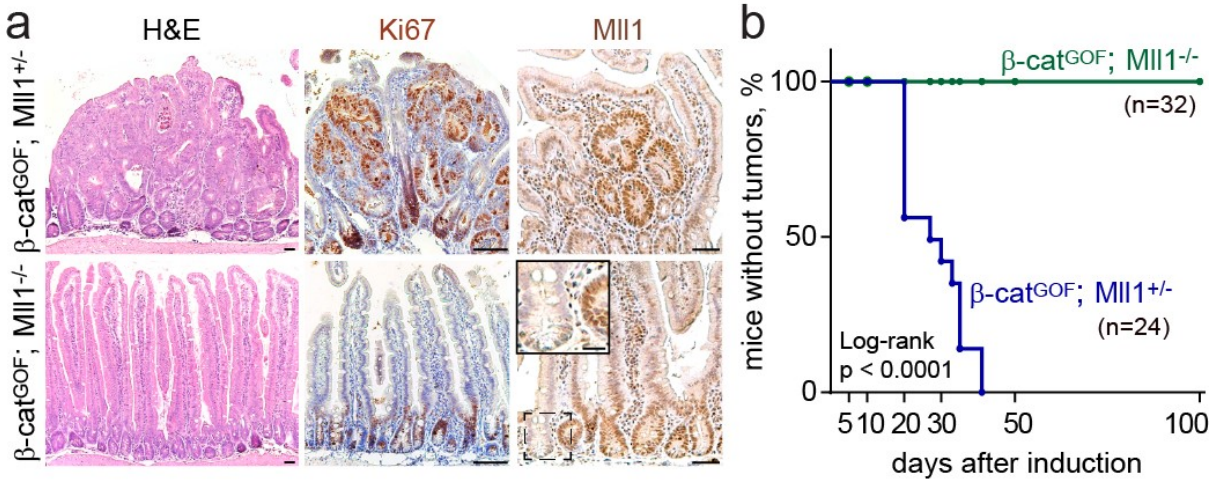

Figure 3.4: β-catenin^{GOF}-induced intestinal tumorigenesis depends on Mll1.
a) Sections of intestines of Lgr5-EGFP-IRES-Cre^{ERT2}; β-cat^{GOF}; Mll1$^{+/-}$ and Lgr5-EGFP-IRES-Cre^{ERT2}; β-cat^{GOF}; Mll1$^{-/-}$ mice, called β-cat^{GOF}; Mll1$^{+/-}$ and β-cat^{GOF}; Mll1$^{-/-}$, at 30 days after induction with

tamoxifen: H&E staining (left), scale bar 50µm; Ki67 staining (middle), nuclei counter-stained with hematoxylin, scale bar 100µm; Mll1 immunohistochemistry (right), scale bar 50µm, with magnification of Mll1 knockout crypt in inset, scale bar 20µm. **b)** Kaplan-Meier plot of tumor incidence in β-cat^{GOF}; Mll1$^{+/-}$ and β-cat^{GOF}; Mll1$^{-/-}$ mice. p<0.0001 Log-rank test, β-cat^{GOF}; Mll1$^{+/-}$ n=24, β-cat^{GOF}; Mll1$^{-/-}$ n=32.

We crossed in a LacZ reporter allele[189] to trace the recombined cells and their progeny. Equal recombination was observed at day 5 after the induction of mutagenesis: about 25% of crypts overall were LacZ^{+} in both β-cat^{GOF}; Mll1$^{+/-}$ and β-cat^{GOF}; Mll1$^{-/-}$ mice (Figure 3.5a, upper panel, quantification in b). Subsequently, the mutant cells in β-cat^{GOF}; Mll1$^{+/-}$ mice expanded at day 10 and had formed LacZ^{+} dysplasias by day 30. In contrast, β-cat^{GOF}; Mll1$^{-/-}$ mice showed a gradual reduction of LacZ^{+} cells down to 10% over time (Figure 3.5a, quantification in b). At 30 days, complete crypts in β-cat^{GOF}; Mll1$^{+/-}$ intestines were LacZ^{+}, whereas the intestines of the β-cat^{GOF}; Mll1$^{-/-}$ mice exhibited crypts with LacZ^{+} long-lived Paneth cells interspersed with non-mutant (LacZ^{-}) stem cells (Figure 3.5c, marked by an arrow). This indicates that Mll1-deficient stem cells had produced LacZ^{+} progeny, were subsequently lost and replaced by non-recombined stem cells. Despite the widespread loss of Mll1-deficient crypts, a substantial number of LacZ^{+} β-cat^{GOF}; Mll1$^{-/-}$ crypts persisted up to 100 days after the induction of mutagenesis.

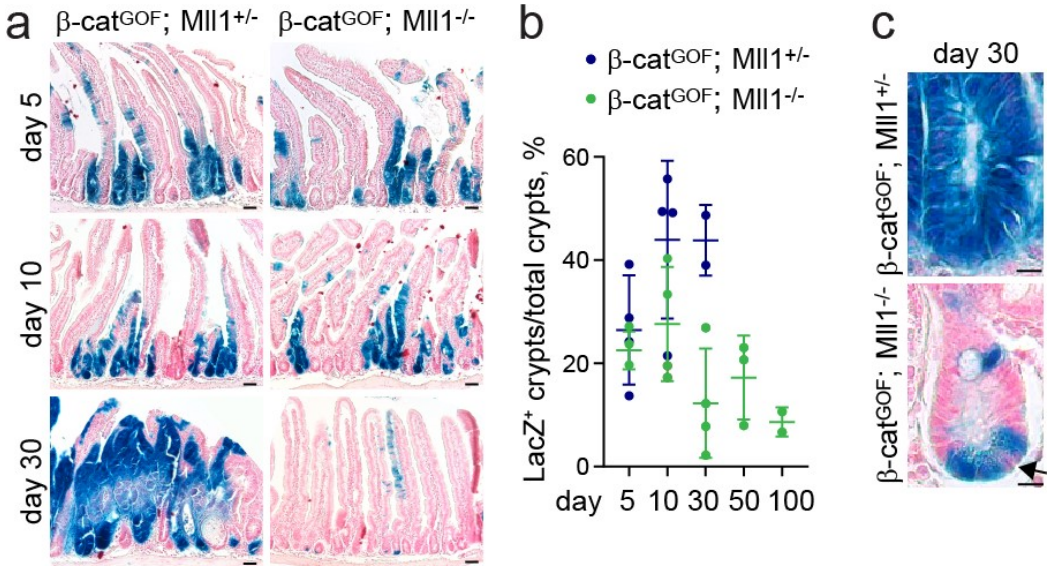

Figure 3.5: Progressive loss of β-catenin^{GOF} stem cells upon ablation of Mll1.
a) Transgenic lineage tracing: a Rosa-LacZ reporter allele was used to trace recombined cells and their progeny. Mutant mouse intestinal cells (blue) at days 5, 10, and 30 after the induction of mutagenesis. Nuclear fast red counter-staining, scale bars 50µm. **b)** Quantification of LacZ^{+} crypts per total crypts in β-cat^{GOF}; Mll1$^{+/-}$ (blue) and β-cat^{GOF}; Mll1$^{-/-}$ mice (green) at days 5 (n=4 β-cat^{GOF}; Mll1$^{+/-}$, n=3 β-cat^{GOF}; Mll1$^{-/-}$), 10 (n=4 β-cat^{GOF}; Mll1$^{+/-}$, n=4 β-cat^{GOF}; Mll1$^{-/-}$), 30 (n=2 β-cat^{GOF}; Mll1$^{+/-}$, n=4 β-cat^{GOF}; Mll1$^{-/-}$), 50 (n=3 β-cat^{GOF}; Mll1$^{-/-}$) and 100 (n=2 β-cat^{GOF}; Mll1$^{-/-}$), dot plot with mean and standard deviation. β-cat^{GOF}; Mll1$^{+/-}$ mice do not survive past 40 days after induction. **c)** Magnification of LacZ^{+} crypts in β-cat^{GOF}; Mll1$^{+/-}$ (upper panel) and β-cat^{GOF}; Mll1$^{-/-}$ mice (lower panel) at day 30 after induction. Arrow marks non-mutated (LacZ^{-}) stem cell adjacent to long-lived mutant (LacZ^{+}) Paneth cells in crypts of Rosa-LacZ; β-cat^{GOF}; Mll1$^{-/-}$ mice. Paneth cells were identified by lysosomal vesicles. Nuclei visualized by nuclear fast red staining, scale bar 20µm.

3.4 Mll1 promotes the β-catenin^{GOF}-driven tumorigenic expansion of intestinal stem cells.

The dysplastic tissue in the β-cat^{GOF}; Mll1$^{+/-}$ intestines showed expansions of Lgr5-GFP^{+} stem cells (Figure 3.6a). The β-cat^{GOF} tumors exhibited an increased expression of the stem cell genes *Lgr5*, *Smoc2* and *Cd44* [195] (Figure 3.6b). The stem cell expansion in β-cat^{GOF} tumorous intestines was associated with an increase in Mll1 protein levels (Figure 3.6c). The β-cat^{GOF} tumorous tissue displayed high levels of nuclear β-catenin (Figure 3.6d). Specifically, tumor cells with high levels of β-catenin, among these also Lgr5-GFP^{+} stem cells, expressed high levels of Mll1 (Figure 3.6e; green arrows mark β-catenin^{high} cells, white arrowheads indicate β-catenin^{low} cells).

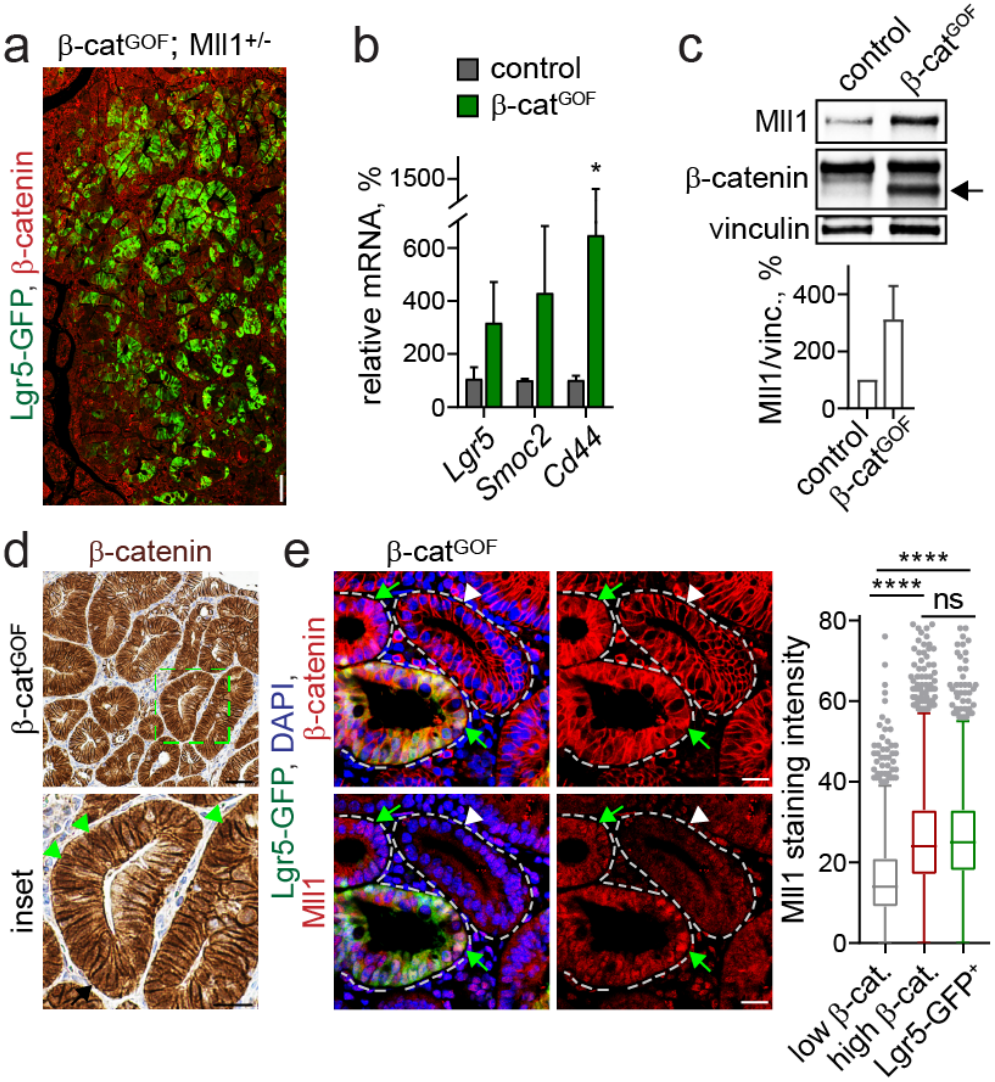

Figure 3.6: β-catenin^{GOF}-induced tumors show expansions of Lgr5^{+} intestinal stem cells.
a) Tile scan of immunostaining for Lgr5-GFP (green) and β-catenin (red) on β-cat^{GOF}; Mll1$^{+/-}$ tumor section, scale bar 100µm. **b)** mRNA expression of the intestinal stem cell markers *Lgr5*, *Smoc2* and *Cd44* in mouse control and β-cat^{GOF} intestines, n=3, unpaired t test. **c)** Western blot for Mll1 and β-catenin in control (n=1) and β-cat^{GOF} intestines (n=2), vinculin as control for equal loading. Quantification below, normalized to vinculin and relative to control. Mutant deltaEx3 β-cat^{GOF} is marked

by an arrow. **d)** Immunohistochemistry for β-catenin on β-cat^{GOF} mouse intestinal tumor section, scale bar 50µm. Magnification of inset below, scale bar 25µm. Arrowheads (green) mark cells with nuclear β-catenin. **e)** Immunostaining for β-catenin (red, upper panel), Mll1 (red, lower panel) and Lgr5-GFP (green) on β-cat^{GOF} mouse intestinal tumor section, scale bars 20µm. Nuclei in blue (DAPI). Green arrows mark β-catenin^{high} cells, white arrowheads mark β-catenin^{low} cells. Right: quantification of Mll1 staining intensity in low β-catenin, high β-catenin and Lgr5-GFP^{+} tumor cells, n=3, Mann-Whitney test.

The heterozygous loss of Mll1 did not affect the β-catenin^{GOF}-driven stem cell expansion (Figure 3.7a, upper panel). The expanding Lgr5-GFP^{+} stem cells in the β-cat^{GOF}; Mll1$^{+/-}$ tumors exhibited nuclear β-catenin (Figure 3.7a, insets a in the upper panel). Remarkably, the homozygous ablation of Mll1 prevented the β-catenin^{GOF}-induced expansion of stem cells (Figure 3.7a, lower panel). Although a large part of mutant crypts was progressively lost from β-cat^{GOF}; Mll1$^{-/-}$ intestines (see Figure 3.5, page 32), we observed normally shaped crypts depleted for Mll1 but with nuclear β-catenin (β-cat^{GOF}) and positive for Lgr5-GFP that persisted up to 100 days after mutagenesis (Figure 3.7a, insets b in the lower panel).

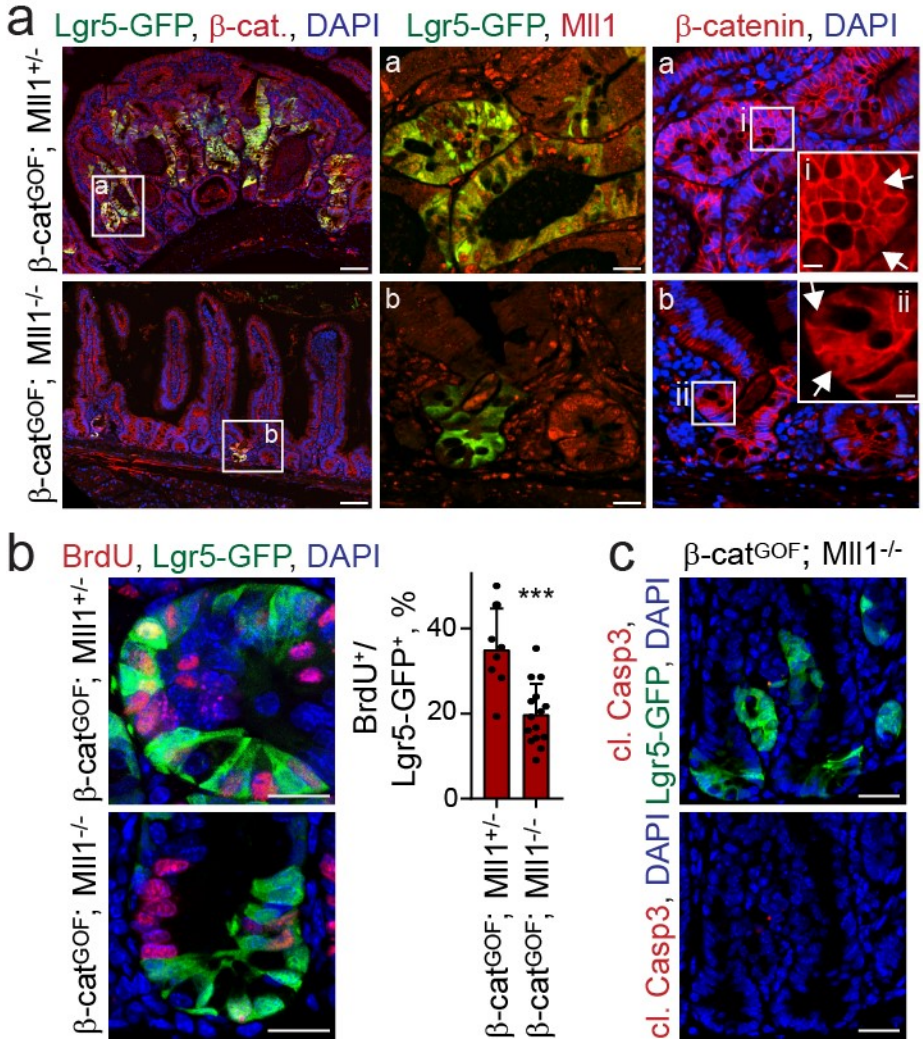

Figure 3.7: Mll1 is a prerequisite for the β-catenin^{GOF}-induced stem cell expansion.
a) Immunofluorescence for Lgr5-GFP stem cells (green) and β-catenin (red) on intestinal sections of β-cat^{GOF}; Mll1$^{+/-}$ and β-cat^{GOF}; Mll1$^{-/-}$ mice at day 30 after induction with tamoxifen, scale bars 100µm.

Insets (a, b) middle: immunostaining for Lgr5-GFP (green) and Mll1 (red), scale bars 20µm. Insets (a, b) right: immunostaining for β-catenin (red) on β-cat^{GOF}; Mll1$^{+/-}$ and β-cat^{GOF}; Mll1$^{-/-}$ intestine, scale bars 20µm. Nuclei in blue (DAPI). Magnifications in insets i and ii, scale bars 10µm, nuclear β-catenin marked by white arrows. **b)** Immunofluorescence for BrdU (red) and Lgr5-GFP (green) in crypts of β-cat^{GOF}; Mll1$^{+/-}$ and β-cat^{GOF}; Mll1$^{-/-}$ mice at day 30 after induction, nuclei in blue (DAPI), scale bars 20µm. BrdU incorporation for 2h before sacrifice. Quantification of BrdU^{+} stem cells relative to total Lgr5-GFP^{+} stem cells on the right, n=5 independent mice, unpaired t test. **c)** Immunostaining for cleaved Caspase-3 (red) and Lgr5-GFP (green) on β-cat^{GOF}; Mll1$^{-/-}$ intestine, nuclei in blue (DAPI), scale bars 20µm.

The Lg5-GFP^{+} cells in persisting β-cat^{GOF}; Mll1$^{-/-}$ crypts exhibited a slightly reduced proliferation, as seen by a decrease in the incorporation of the thymidine analogue BrdU compared to stem cells in β-cat^{GOF}; Mll1$^{+/-}$ crypts (Figure 3.7b). Apoptosis (cleaved Caspase-3) was not detected in the β-cat^{GOF}; Mll1$^{-/-}$ crypts (Figure 3.7c).

3.4.1 The ablation of Mll1 prevents β-catenin^{GOF}-induced stem cell expansion but does not decrease global Wnt activity.

To explore the role of Mll1 in the β-catenin^{GOF}-driven intestinal stem cell expansion, we made use of the organoid system (compare 1.1.5, page 11). Organoids from β-cat^{GOF}, β-cat^{GOF}; Mll1$^{+/-}$ and β-cat^{GOF}; Mll1$^{-/-}$ mice were mutated in culture by administration of tamoxifen. The *in vitro* mutagenesis does not recombine all stem cells and leads to a mixed culture containing recombined and non-recombined organoids. We selected for recombined β-cat^{GOF} organoids by withdrawing the Wnt-stimulating growth factor R-spondin1 from the culture medium. All β-cat^{GOF} organoids grew independently of R-spondin1 (Figure 3.8). Non-recombined control organoids did not survive past day 4 of R-spondin1 withdrawal (Figure 3.8, fourth panel). The ablation of Mll1 did not impair the R-spondin1-independent growth, demonstrating functional β-cat^{GOF} activity in the β-cat^{GOF}; Mll1$^{-/-}$ organoids.

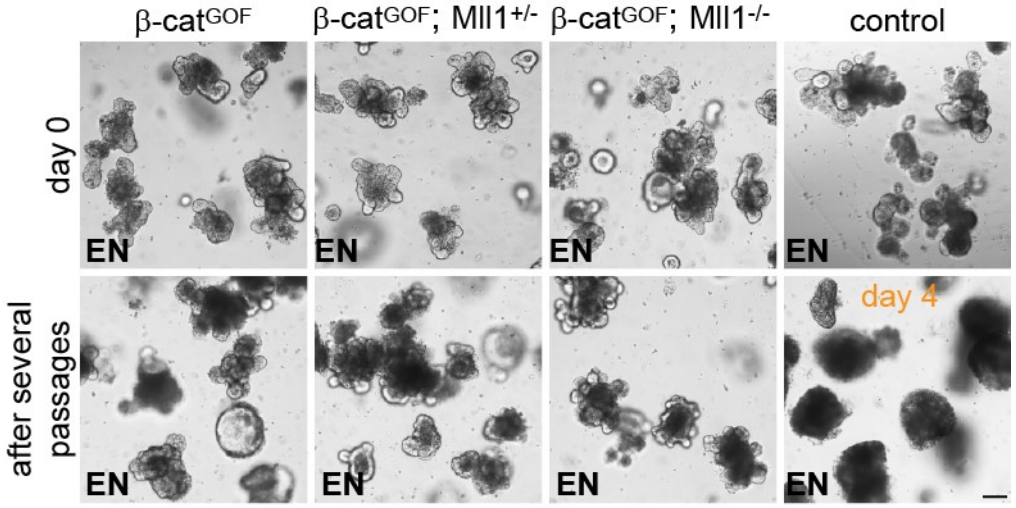

Figure 3.8: R-spondin1 withdrawal selects for β-catenin^{GOF}-mutant organoids.
Brightfield images of tamoxifen-induced Lgr5-GFP-IRES-Cre^{ERT2}; β-cat^{GOF}, Lgr5-GFP-IRES-Cre^{ERT2}; β-cat^{GOF}; Mll1$^{+/-}$ and Lgr5-GFP-IRES-Cre^{ERT2}; β-cat^{GOF}; Mll1$^{-/-}$ intestinal organoids at day 0 and after

4 weeks of R-spondin1-free culture in crypt medium supplemented with EGF and Noggin (EN). Non-induced control organoids do not survive past day 4 in the absence of R-spondin1, scale bar 200µm.

Non-recombined (control) intestinal organoids from Lgr5-EGFP-IRES-Cre^{ERT2} mice recapitulated the Mll1 expression pattern observed in the control (wild-type) intestines (see Figure 3.2, page 28): highest expression is seen in Wnt-dependent Lgr5-GFP^{+} stem cells (Figure 3.9a, b first panel). β-cat^{GOF} induced a strong expansion of Lgr5-GFP^{+} stem cells (Figure 3.9a, b, second panel). This stem cell expansion was maintained in organoids with heterozygous deletion of Mll1, β-cat^{GOF}; Mll1$^{+/-}$ (Figure 3.9a, b, third panel). In contrast, homozygous deletion of Mll1 hampered the β-cat^{GOF}-driven expansion of the stem cell population in β-cat^{GOF}; Mll1$^{-/-}$ organoids (Figure 3.9a, b, fourth panel). Western blotting for Lgr5-GFP confirmed the stem cell expansion phenotype (Figure 3.9c, quantification below).

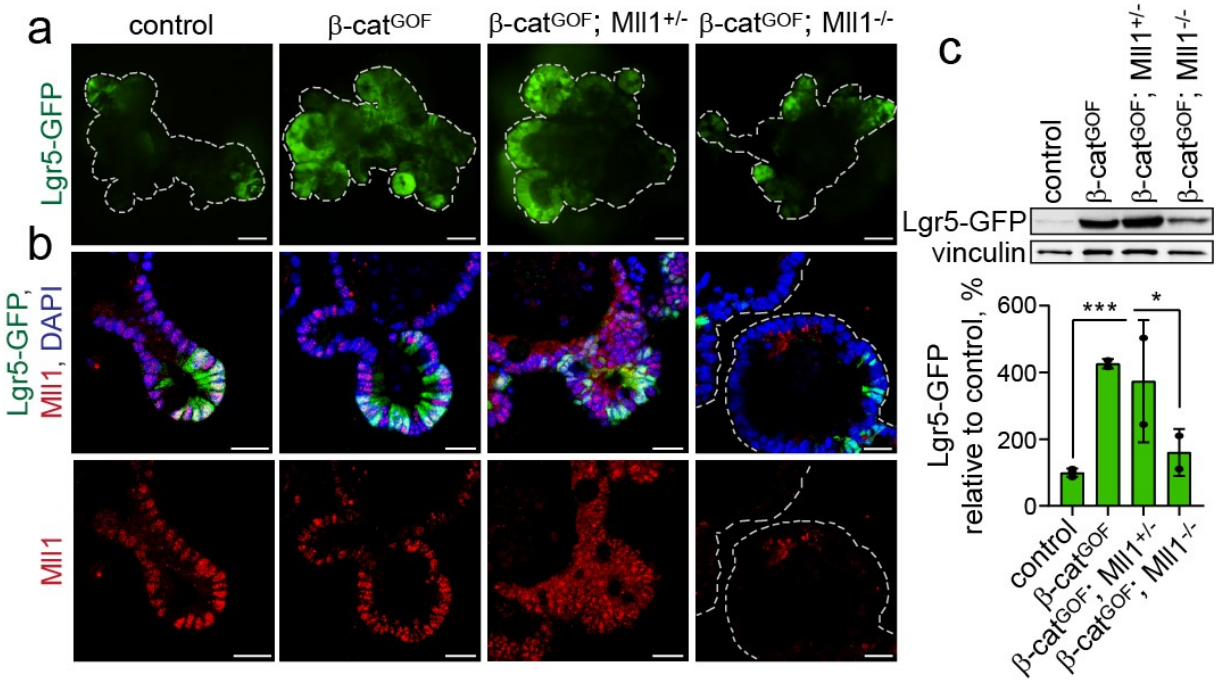

Figure 3.9: Mll1 is essential for the β-catenin^{GOF}-induced stem cell expansion in organoids.
a) Fluorescence live imaging of non-induced (control) and tamoxifen-induced β-cat^{GOF}, β-cat^{GOF}; Mll1$^{+/-}$ and β-cat^{GOF}; Mll1$^{-/-}$ intestinal organoids. Lgr5-GFP (green) marks intestinal stem cells, scale bars 100µm. **b)** Immunofluorescence staining for Lgr5-GFP (green) and Mll1 (red) on sections of organoids of the four genotypes, nuclei in blue (DAPI), scale bars 30µm. **c)** Western blot for Lgr5-GFP in control and tamoxifen-induced β-cat^{GOF}, β-cat^{GOF}; Mll1$^{+/-}$ and β-cat^{GOF}; Mll1$^{-/-}$ organoids, vinculin as control for equal loading. Below: quantification of Lgr5-GFP protein levels in mutant organoids normalized to vinculin and relative to control, n=2, unpaired t test.

We confirmed the heterozygous and homozygous ablation of Mll1 in β-cat^{GOF}; Mll1$^{+/-}$ and β-cat^{GOF}; Mll1$^{-/-}$ organoids, respectively, by RT-PCR analysis of the mutant lines (Figure 3.10a). β-cat^{GOF}; Mll1$^{-/-}$ organoids exhibited a decrease in the expression of the intestinal stem cell genes *Lgr5*, *Smoc2* and *Olfm4* [195], compared to β-cat^{GOF} and β-cat^{GOF}; Mll1$^{+/-}$ organoids (Figure 3.10b). The expression of the Wnt-regulated stem cell gene *Ascl2* [92] and the Wnt target gene *Axin2* [33] was unaffected by the ablation of Mll1 (Figure 3.10b).

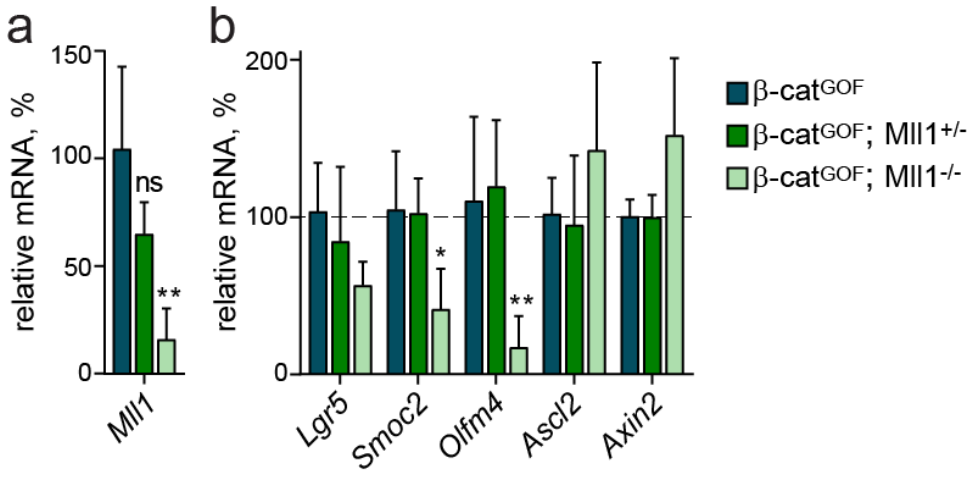

Figure 3.10: The ablation of Mll1 decreases the expression of specific stem cell genes in β-catenin^{GOF} organoids.
mRNA expression of **a)** *Mll1* and **b)** intestinal stem cell genes in β-cat^{GOF}; Mll1$^{+/-}$ and β-cat^{GOF}; Mll1$^{-/-}$ organoids relative to β-cat^{GOF} organoids, n=4, unpaired t test.

The loss of Mll1 slightly reduced the proliferation of Lgr5-GFP^{+} stem cells in β-cat^{GOF}; Mll1$^{-/-}$ organoids compared to β-cat^{GOF}; Mll1$^{+/-}$ organoids, as seen by a decrease in the incorporation of the thymidine analogue EdU (Figure 3.11, white arrows).

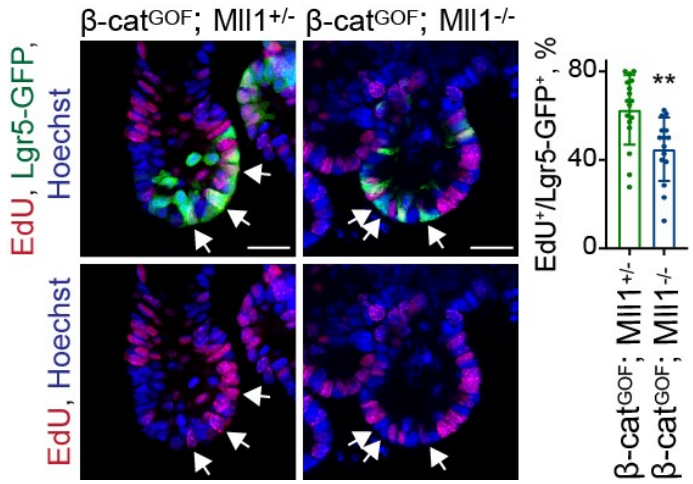

Figure 3.11: The loss of Mll1 decreases the proliferation of stem cells in β-catenin^{GOF} organoids.
Optical section of whole-mount confocal images of EdU incorporation (red) in β-cat^{GOF}; Mll1$^{+/-}$ (left panel) and β-cat^{GOF}; Mll1$^{-/-}$ (right panel) organoid crypt buds. White arrows indicate Lgr5-GFP^{+} stem cells (green), nuclei stained with Hoechst (blue), scale bars 20µm. Quantification of EdU^{+} relative to total Lgr5-GFP^{+} stem cells per crypt on the right, n=11, unpaired t test.

To further investigate the proliferation and self-renewal of the Mll1-deficient cells, β-cat^{GOF}; Mll1$^{-/-}$ organoids were dissociated into single cells and organoid formation was traced upon serial re-plating in crypt medium supplemented with EGF, Noggin and R-spondin1. Single β-cat^{GOF}; Mll1$^{-/-}$ cells expanded into spheroid-shaped organoids, owing to the high Wnt activity induced by β-cat^{GOF} as previously described[196]. β-cat^{GOF}; Mll1$^{-/-}$ cells re-formed organoids over many passages with high efficiency (Figure 3.12a), demonstrating proliferative potential and self-renewal capacity of Mll1-deficient β-cat^{GOF} cells. From the seventh passage on, β-cat^{GOF}; Mll1$^{-/-}$ cells formed less organoids which were smaller and acquired a thick-walled shape (Figure 3.12a, b), indicating differentiation and progressive exhaustion of stemness upon loss of Mll1. Apoptosis was not prominent, but late-passage β-cat^{GOF}; Mll1$^{-/-}$ organoids exhibited a strong expression of the differentiation marker ITF (Figure 3.12c).

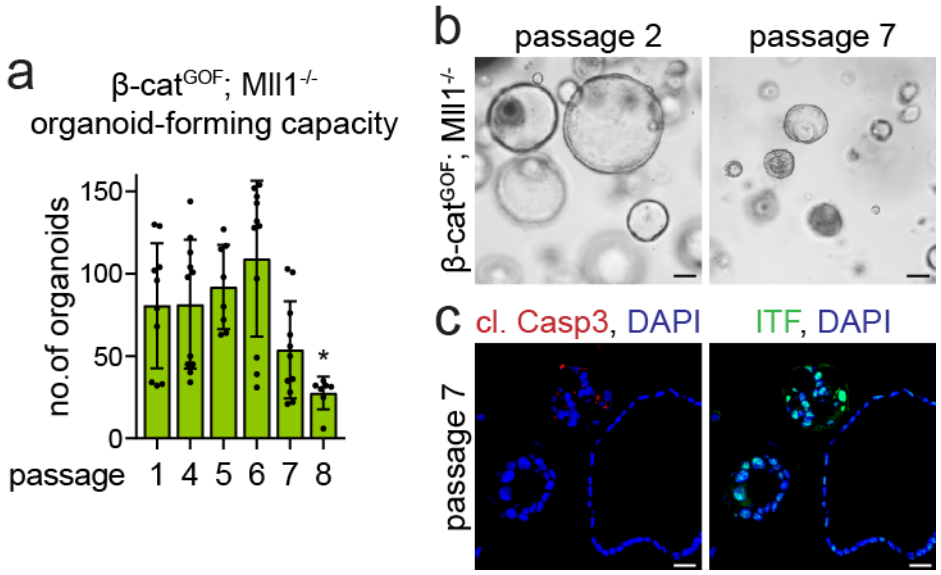

Figure 3.12: Progressive exhaustion of Mll1-deficient β-catenin^{GOF} stem cells.
a) Serial re-plating of β-cat^{GOF}; Mll1$^{-/-}$ intestinal organoids by single cell dissociation. Numbers of organoids counted as triplicates in n=4 independent assays from two organoid lines. Cells were cultured in crypt medium supplemented with EGF, Noggin and R-spondin1. Significance calculated versus passage 1, unpaired t test. **b)** Brightfield images of single cell-derived β-cat^{GOF}; Mll1$^{-/-}$ organoids at passages 2 and 7, scale bars 100µm. **c)** Immunostaining for cleaved Caspase-3 (red) and ITF (green) on sections of single cell-derived β-cat^{GOF}; Mll1$^{-/-}$ organoids at passage 7, scale bars 50µm. Nuclei stained with DAPI (blue).

In summary, these data demonstrate by genetic means that Mll1 is essential for the β-catenin^{GOF}-driven stem cell expansion and tumorigenesis. The loss of Mll1 did not interfere with β-cat^{GOF} function *per se*, as Mll1 knockout crypts exhibited nuclear β-catenin, β-cat^{GOF}; Mll1$^{-/-}$ organoids grew independently of R-spondin1, and the expression of classical Wnt target genes such as *Axin2* was not decreased. Apoptosis was not detected, but the β-cat^{GOF}; Mll1$^{-/-}$ cells progressively lost their self-renewal capacity and differentiated. Accordingly, Mll1 is crucial to maintain the stemness of β-catenin-activated intestinal stem cells.

3.5 Mll1 prevents differentiation of β-catenin^{GOF} intestinal stem cells.

To gain deeper insights into how the ablation of Mll1 prevented the β-catenin^{GOF}-driven intestinal stem cell expansion and tumorigenesis, we applied a high-throughput next-generation sequencing approach and analysed the transcriptome of β-cat^{GOF}; Mll1$^{-/-}$ stem cells. In collaboration with Neha Goveas, Andrea Kranz and Francis Stewart at the Technical University in Dresden (Germany), we isolated the Lgr5-GFP^{+} intestinal stem cells from β-cat^{GOF}; Mll1$^{+/-}$ and β-cat^{GOF}; Mll1$^{-/-}$ mice at 10 days after the induction of mutagenesis using fluorescence-activated cell sorting (FACS) and analysed transcriptomic changes by RNA sequencing. The bioinformatic analysis was performed by Ramon Oliveira Vidal and Sascha Sauer from the Laboratory of Functional Genomics, Scientific Genomics Platforms of the Max Delbrück Center for Molecular Medicine (BIMSB/BIH). The transcriptome analysis revealed that β-cat^{GOF}; Mll1$^{+/-}$ stem cells exhibited a Paneth-like phenotype, which was caused by high Wnt activity due to the β-cat^{GOF} mutation[39]. Immunofluorescence staining of β-cat^{GOF}; Mll1$^{+/-}$ tumor sections and RT-PCR analysis of β-cat^{GOF}-mutant intestines revealed a strong expression of the Paneth cell marker Mmp7[186] (Figure 3.13a).

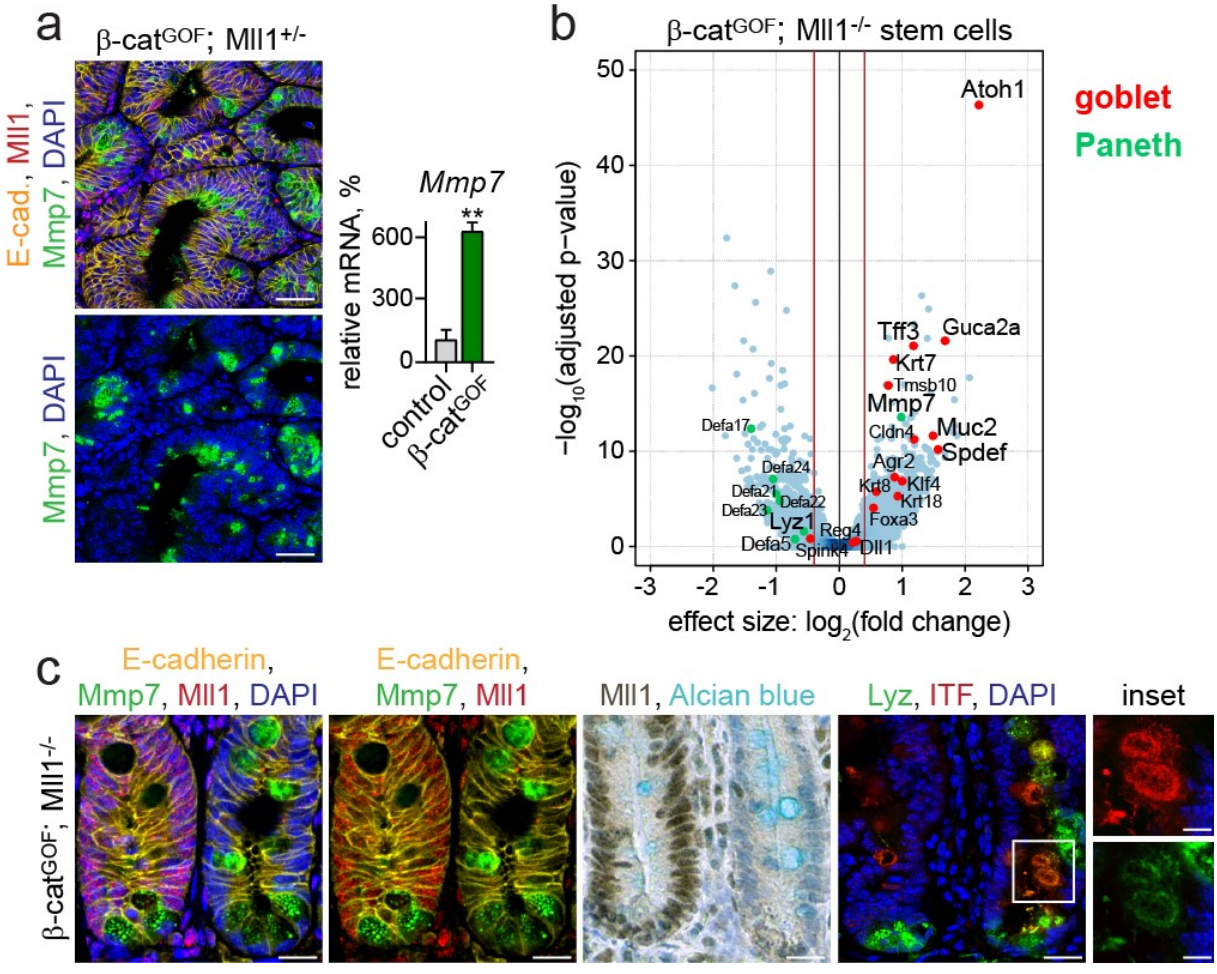

Figure 3.13: The ablation of Mll1 enforces differentiation of β-catenin^{GOF} intestinal stem cells.
a) Left: Immunostaining for Mmp7 (green) and Mll1 (red) on β-cat^{GOF}; Mll1$^{+/-}$ tumor section, scale bar 50µm. Nuclei stained with DAPI (blue), E-cadherin (yellow) stains cell borders. Right: mRNA

expression of *Mmp7* in control and β-cat^{GOF} intestines, n=3, unpaired t test. **b)** Volcano plot of differentially expressed genes in β-cat^{GOF}; Mll1$^{-/-}$ relative to β-cat^{GOF}; Mll1$^{+/-}$ Lgr5-GFP^{+} stem cells isolated from 4 independent mice each, represented as blue dots. Cut-off $\log_2$ fold change ≥ 0.5. Goblet and Paneth cell-specific genes[197] marked in red and green, respectively, and indicated by name. **c)** Immunostainings on sections of adjacent non-recombined (left) and recombined (right) small intestinal crypts in β-cat^{GOF}; Mll1$^{-/-}$ mice, left: for Mmp7 (green) and Mll1 (red), middle: for Mll1 (brown) and Alcian blue; nuclear counter-staining with hematoxylin, right: for Lyz (green) and ITF (red), scale bars 20µm. Insets on the right: magnifications of mutant double-positive cells, scale bars 10µm. Nuclei stained with DAPI (blue), E-cadherin (yellow) stains cell borders.

A volcano plot of the differentially expressed genes in β-cat^{GOF}; Mll1$^{-/-}$ versus β-cat^{GOF}; Mll1$^{+/-}$ stem cells showed both up- and downregulation of genes upon ablation of Mll1 (Figure 3.13b). This included a global increase in the expression of goblet cell-specific genes, among these *Tff3* (*Itf*) and *Muc2* [198]. Downregulated genes included specific markers for Paneth cells, e.g. *Defa5, Defa17*, *Lyz1* [186], indicating that the ablation of Mll1 shifted the Paneth-like identity of β-cat^{GOF} stem cells towards a goblet cell fate. β-cat^{GOF}; Mll1$^{-/-}$ stem cells exhibited a strongly increased expression of *Atoh1*, a transcription factor essential for secretory lineage determination[56], and its target gene *Spdef*, which instructs secretory cell differentiation in Paneth and goblet cells[62, 199] (Figure 3.13b; compare 1.1.3, page 9). The expression of *Hes1*, a Notch-controlled transcription factor that represses *Atoh1* expression[55], was not downregulated in the β-cat^{GOF}; Mll1$^{-/-}$ stem cells. There were also no decreases in other Notch target genes such as *Hes5* and *Hey1* (not shown), which meant that the upregulation of *Atoh1* occurred independently of a global decrease in Notch signalling. The Paneth cell gene *Mmp7* was increased in β-cat^{GOF}; Mll1$^{-/-}$ stem cells, suggesting a priming towards a mixed Paneth-goblet state. Mll1-deficient crypts of β-cat^{GOF}; Mll1$^{-/-}$ mutant mice exhibited large cells which were double-positive for Paneth cell (Mmp7 and Lyz) and goblet cell markers (Alcian blue (mucin) and ITF) (right crypt in Figure 3.13c). Such Paneth-goblet intermediate cells were not observed in adjacent non-recombined Mll1-expressing crypts on the same section (left crypt in Figure 3.13c). Taken together, the stem cell transcriptome revealed that the ablation of Mll1 primed β-cat^{GOF} intestinal stem cells for differentiation and shifted the Wnt-imposed Paneth-like identity towards a goblet cell fate. Thus, Mll1 maintains stemness by restricting differentiation of β-cat^{GOF} intestinal stem cells.

3.5.1 Mll1 regulates Foxa1 and Gata4 transcription factors in β-catenin^{GOF} stem cells.

Apart from the differentiation phenotype, the RNA sequencing of the sorted Lgr5-GFP^{+} stem cells also revealed that β-cat^{GOF}; Mll1$^{-/-}$ stem cells exhibited a decreased expression of several transcription factors and intestinal stem cell genes (Figure 3.14). As illustrated in a volcano plot, Mll1-deficient β-cat^{GOF} stem cells showed a decreased expression of the intestinal stem cell gene *Olfm4*. *Lgr5* and *Smoc2* expression was not significantly altered (Figure 3.14a). The ablation of Mll1 did not affect the expression of the Wnt target gene *Axin2* (Figure 3.14a), as had also been observed in β-cat^{GOF}; Mll1$^{-/-}$ organoids (see Figure 3.10, page 37). In β-cat^{GOF};

Mll1$^{-/-}$ stem cells, the expression of the transcription factors *Foxa1* and *Gata4* was downregulated (Figure 3.14a), the latter of which had previously been proposed as a Mll1 target gene[163]. Immunostaining confirmed a strong reduction of the GATA binding protein 4 (Gata4) in Mll1-deficient crypts compared to non-recombined Mll1-expressing crypts on sections of β-cat^{GOF}; Mll1$^{-/-}$ small intestines (Figure 3.14b).

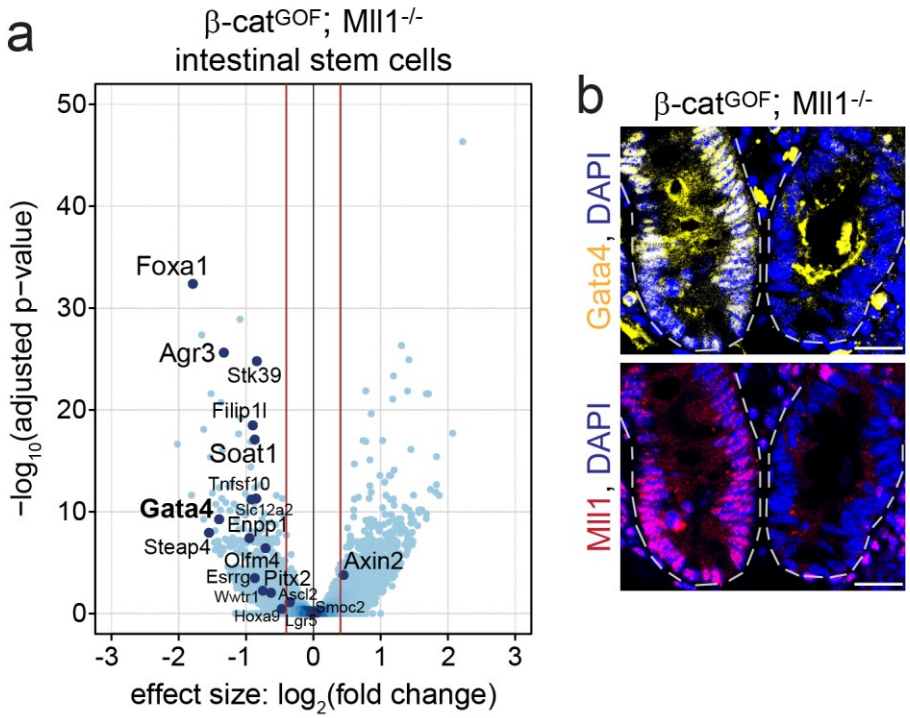

Figure 3.14: Mll1 regulates Foxa1 and Gata4 expression in β-catenin^{GOF} intestinal stem cells.
a) Volcano plot showing differentially expressed stem cell genes and transcription factors in β-cat^{GOF}; Mll1$^{-/-}$ relative to β-cat^{GOF}; Mll1$^{+/-}$ Lgr5-GFP^{+} stem cells isolated from 4 independent mice each, represented as dark blue dots. Cut-off log_2 fold change ≥ 0.5. **b)** Immunostaining for Gata4 (yellow, upper panel) and Mll1 (red, lower panel) on sections of adjacent non-recombined (left) and recombined (right) small intestinal crypts in β-cat^{GOF}; Mll1$^{-/-}$ mice, scale bars 20µm. Nuclei stained with DAPI (blue).

3.6 Inducible shMLL1 colon cancer cell lines - a tool to study MLL1 function.

We aimed to generate a tool to further clarify the molecular role of MLL1 in Wnt-dependent intestinal cancer stem cells. The human colon adenocarcinoma cell lines Ls174T and DLD1 are frequently used in mechanistic studies connected to Wnt signalling. Ls174T cells harbour a β-cat^{GOF} mutation, but are diploid and wild-type for p53 and APC, and are classified as Dukes' type B adenocarcinoma of the colon[200]. DLD1 cells are predominantly diploid, classified as Dukes' type C adenocarcinoma of the colon and harbour APC mutations and a non-functional Ser241Phe mutation in p53 that prevents its DNA binding[200]. Given their high Wnt activity due to β-catenin gain-of-function and APC loss-of-function mutations, the Ls174T and DLD1 cells emerged as suitable cell lines to study the role of MLL1 in Wnt-driven colon cancer. Both cell lines have previously been used to establish the intestinal Wnt signature and exhibit substantial

expression of intestinal stem cell genes[107], thus offering the chance to assess the regulatory role of MLL1 in colon cancer stemness.

Using a CRISPR/Cas9-based approach to delete MLL1, we did not obtain viable cell clones, indicating a strong MLL1 dependency of the colon cancer cells. By lentiviral transduction, we established stable doxycycline-inducible shMLL1 knockdown cell lines, using the pInducer11 system[201]. Transduced cells constitutively express GFP and a reverse Tet repressor (rtTA3) which binds Tet response elements (TRE) only in the presence of doxycycline (Figure 3.15a). Treatment with doxycycline induces the production of dsRed and a miR30-based shRNA against MLL1 (shMLL1). By FACS for GFP and dsRed we isolated 'high responders' with strong shMLL1 induction (Figure 3.15b).

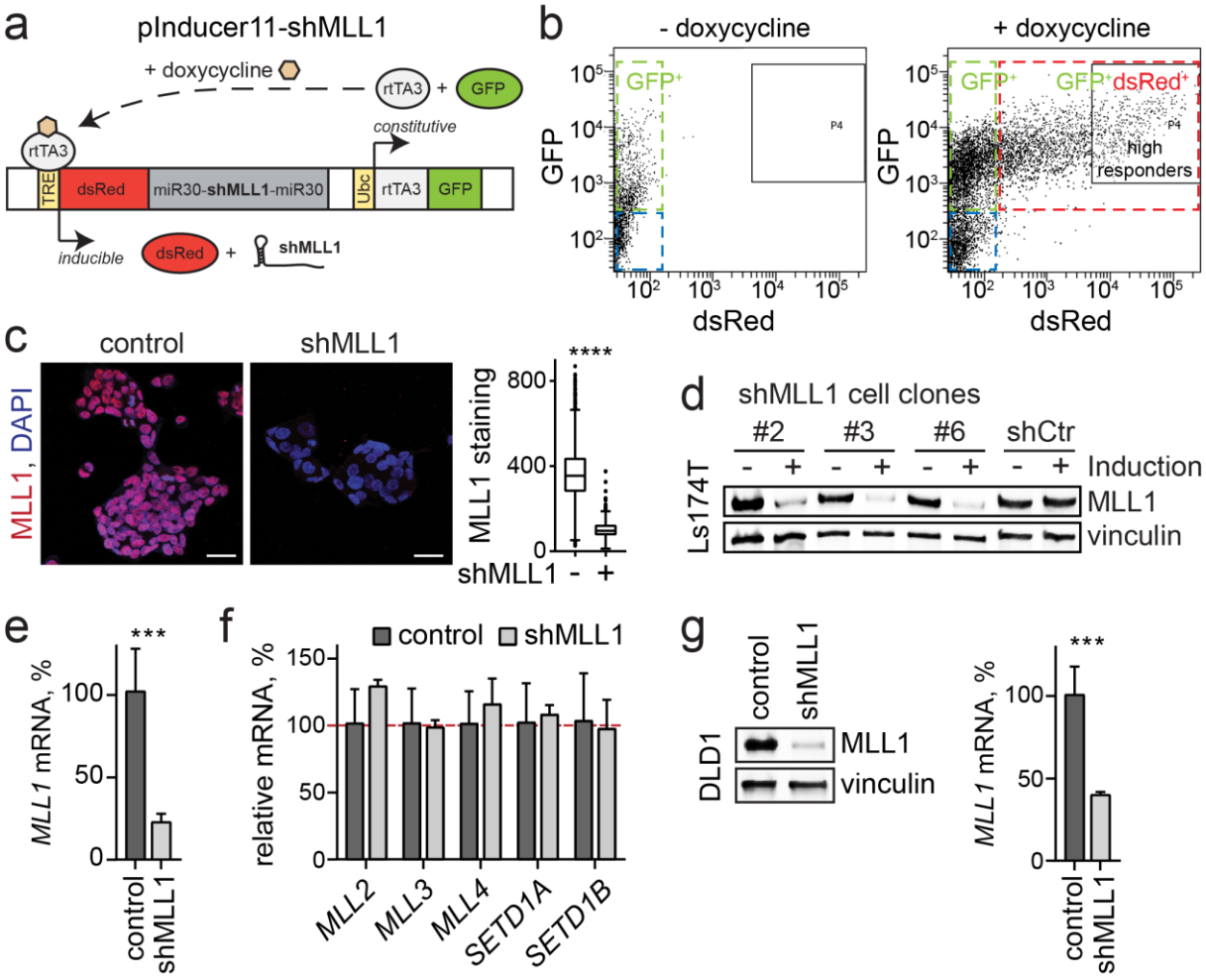

Figure 3.15: Establishment and characterization of inducible shMLL1 human colon cancer cells. **a)** The doxycycline-inducible pInducer11 system. Transduced cells constitutively express GFP and the reverse Tet repressor (rtTA3) that binds Tet response elements (TRE) in the presence of doxycycline, inducing dsRed and shMLL1 production. **b)** Representative FACS plots of Ls174T cells transduced with pInducer11-shMLL1. Transduced cells constitutively express GFP (green dashed box). Blue dashed box contains apoptotic cells and cell debris. Doxycycline treatment induces dsRed expression (right plot, red dashed box). Gate P4 (grey box) contains GFP⁺ dsRed⁺ double-positive cells that represent 'high responders'. **c)** Immunofluorescence for MLL1 (red) on control and 3d doxycycline-induced shMLL1 Ls174T cells. Nuclei in blue (DAPI), scale bars 20µm. Right: quantification of MLL1 staining intensity in

control and three shMLL1 Ls174T cell clones, n=7, Mann-Whitney test. **d)** MLL1 Western blot of three shMLL1 Ls174T cell clones #2, #3, #6 both non-induced and 3d doxycycline-induced, and shCtr cells with shRNA against Renilla luciferase, vinculin as control for equal loading. **e)** *MLL1* mRNA expression in control and shMLL1 Ls174T cell clones, n=4, unpaired t test. **f)** mRNA expression of *MLL* family members in control and shMLL1 Ls174T cells, n=4. **g)** Left: MLL1 Western blot of shMLL1 DLD1 cells both non-induced and 3d doxycycline-induced, vinculin as control for equal loading. Right: *MLL1* mRNA expression in control and shMLL1 DLD1 cells, n=3, unpaired t test.

We identified three shMLL1 Ls174T single cell clones that exhibited an efficient knockdown of MLL1 (Figure 3.15c-e). MLL1 knockdown cells were compared to non-induced cells and to cells transduced with a non-targeted shRNA against Renilla luciferase (shCtr)[202], revealing no difference between non-induced and shCtr cells. The ablation of MLL1 did not significantly alter the expression of the MLL family members *MLL2*, *MLL3*, *MLL4*, *SETD1A* and *SETD1B* (Figure 3.15f). DLD1 cells transduced with shMLL1 were used as a pool of 'high responders' that exhibited a profound knockdown of MLL1 (Figure 3.15g).

3.7 MLL1 is required for initiation and growth of human Ls174T colon cancer xenografts.

To test the role of MLL1 in tumor initiation and growth of human colon cancer, we studied the *in vivo* growth of the human shMLL1 Ls174T colon cancer cells in xenograft assays. Doxycycline-induced shMLL1 and control Ls174T colon cancer cells were subcutaneously engrafted in nude mice. Mice inoculated with shMLL1 cells were administered doxycycline throughout the experiment. Control cells formed large tumors within 28 days (Figure 3.16a). In contrast, the tumor formation by shMLL1 cells was reduced by 75%. The residual shMLL1 Ls174T xenografts showed a substantial reduction of MLL1 protein (Figure 3.16b).

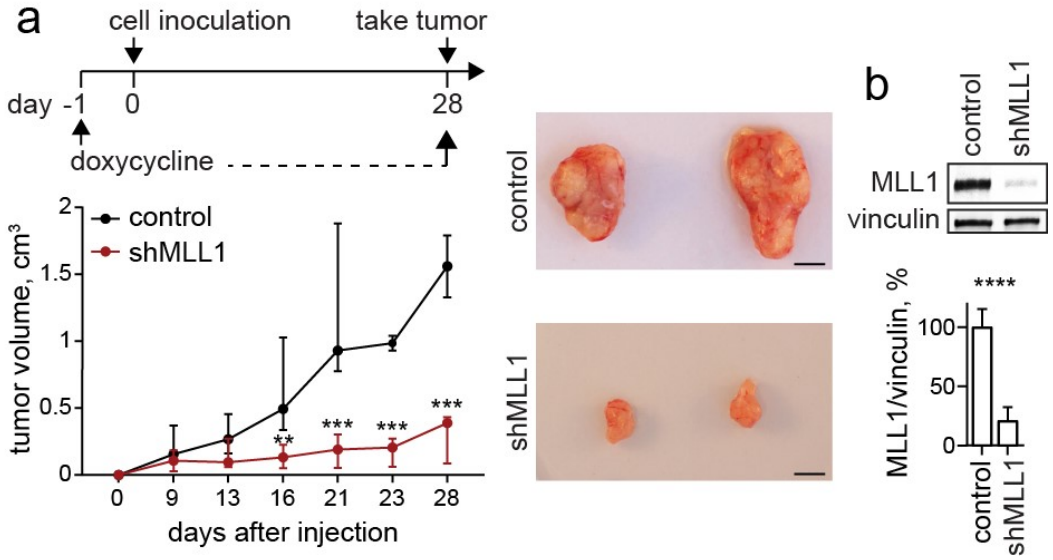

Figure 3.16: MLL1 is required for initiation and growth of human colon cancer xenografts.
a) Xenografts of control and shMLL1 human Ls174T cells in NMRI$^{nu/nu}$ mice. Mice inoculated with shMLL1 cells were administered doxycycline from day -1 throughout the experiment as indicated. Left: tumor growth curves of control (black) and shMLL1 Ls174T cells (red) plotted as median with range,

n=6, unpaired t test. Right: dissected tumors at day 28, scale bars 2cm. **b)** Western blot for MLL1 from control and shMLL1 Ls174T xenografts at day 28, vinculin as control for equal loading. Quantification below, normalized to vinculin and relative to control, n=6 tumors, unpaired t test.

Residual shMLL1 xenografts exhibited reduced levels of H3K4me3 (Figure 3.17a left) and significantly fewer Ki67$^+$ proliferating cells (Figure 3.17a right). The apoptosis marker cleaved Caspase-3 did not increase in shMLL1 xenografts (Figure 3.17b, c). The residual shMLL1 tumors were less densely packed than control tumors, and exhibited an enlarged cell morphology (Figure 3.17d).

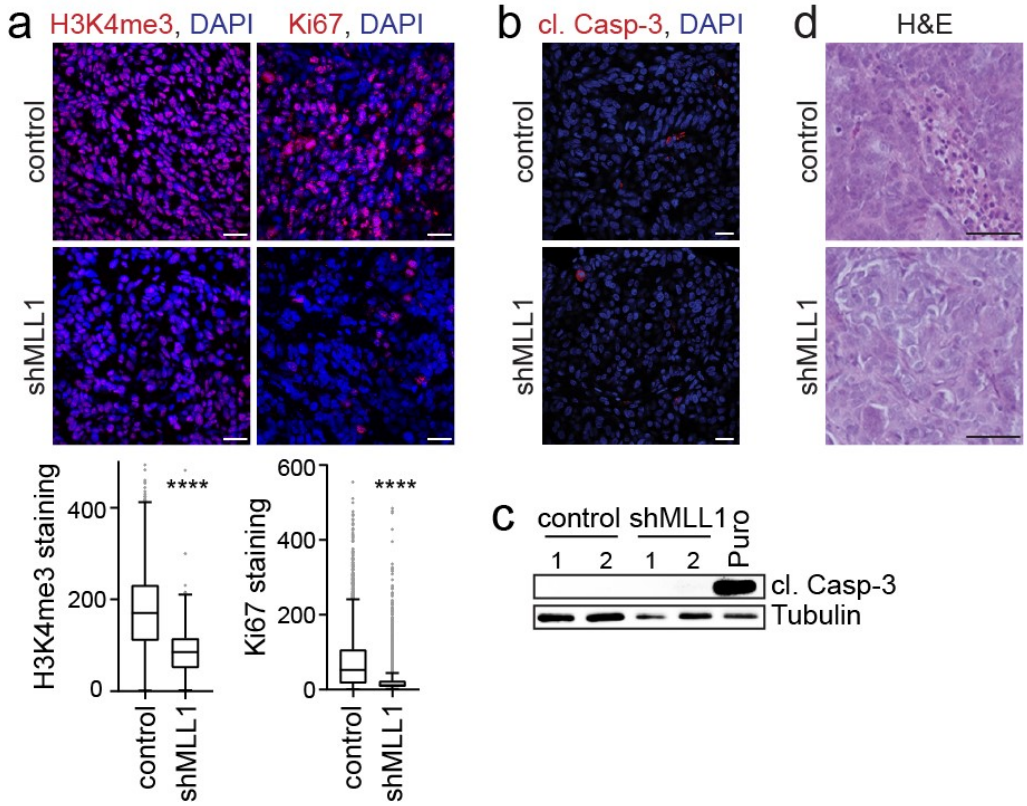

Figure 3.17: Reduced H3K4me3 and proliferation in shMLL1 xenografts.
a) H3K4me3 and Ki67 stainings (red) of control and shMLL1 tumor sections, scale bars 25µm. Nuclei in blue (DAPI). Quantifications below, n=4, Mann-Whitney test. **b)** Immunofluorescence for cleaved Caspase-3 (red) on control and shMLL1 xenograft sections, nuclei in blue (DAPI), scale bars 20µm. **c)** Cleaved Caspase-3 Western blot of two pairs of control and shMLL1 tumors (right), tubulin as control for loading. Puromycin (2µg/ml) treatment for 24h as positive control. **d)** H&E stainings of control and shMLL1 tumor sections, scale bars 50µm.

To address the role of MLL1 in the growth and maintenance of established colon tumors, we performed subcutaneous xenograft assays with the Ls174T cell clones and induced the knockdown of MLL1 after the establishment of the primary tumor, i.e. at day 6 after cell inoculation (Figure 3.18a). Control cells continuously grew and formed large tumors within 20 days (Figure 3.18b). In contrast, the growth of MLL1-depleted tumors was markedly slowed down, indicating a crucial role of MLL1 also in established intestinal tumors. The level of growth reduction strictly depended on the efficiency of MLL1 depletion (Figure 3.18b, c; compare

growth curves and MLL1 protein expression in knockdown tumors Mll1^{med} (green) and Mll1$^{low-1, low-2}$ (blue)). Taken together, the xenograft data show that MLL1 is crucial for tumor formation and growth of human Ls174T colon cancer cells.

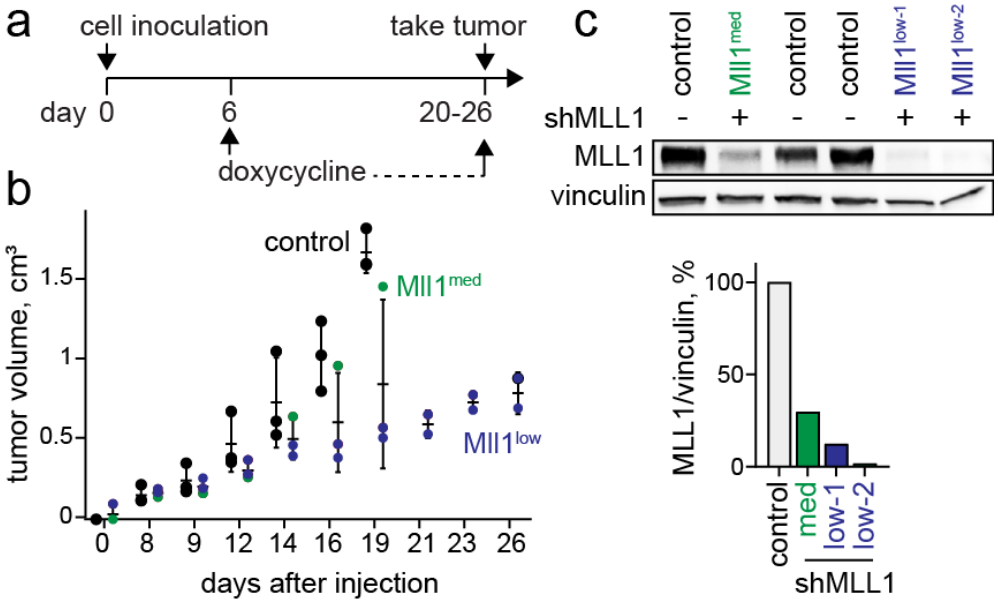

Figure 3.18: MLL1 in tumor maintenance.
a) Xenografts of control and shMLL1 human Ls174T cells in NMRI$^{nu/nu}$ mice. Mice inoculated with shMLL1 cells were administered doxycycline starting from day 6 after cell inoculation as indicated. **b)** Tumor growth curves of control (black dots) and shMLL1 Ls174T cells (green and blue dots), plotted as mean with SD, n=3, unpaired t test. **c)** Western blot for MLL1 from control and shMLL1 xenografts, vinculin as control for equal loading. Quantification below, normalized to vinculin and relative to control.

3.8 MLL1 sustains the stemness of human colon cancer cells.

3.8.1 MLL1 controls the expression of Lgr5⁺ stem cell genes in human colon cancer cells.

To identify the gene expression programme regulated by MLL1 in Wnt-driven colon cancer cells, we investigated transcriptomic changes upon knockdown of MLL1 by RNA sequencing. The knockdown of MLL1 induced a predominant downregulation of gene expression, as illustrated in a heatmap of the three Ls174T single cell clones compared to control cells (Figure 3.19a), demonstrating that MLL1 acts as a transcriptional activator in Wnt-driven colon cancer cells. Comparison of the differentially expressed genes with a signature of Mll1-ablated fibroblasts[163] revealed a downregulation of MLL1 target genes such as *SMOC2* and *ENPP1* (Figure 3.19b), confirming the validity of our knockdown approach. Of note, the human shMLL1 colon cancer cells also showed decreases in the expression of *FOXA1* and *GATA6*, the colon homologue of *GATA4* [203], which we had identified as Mll1-regulated genes in murine β-cat^{GOF}; Mll1$^{-/-}$ intestinal stem cells (see Figure 3.14, page 41). Gene set enrichment analysis (GSEA) revealed that the knockdown of MLL1 interfered with the expression of Lgr5⁺ stem cell signature genes (Figure 3.19c).

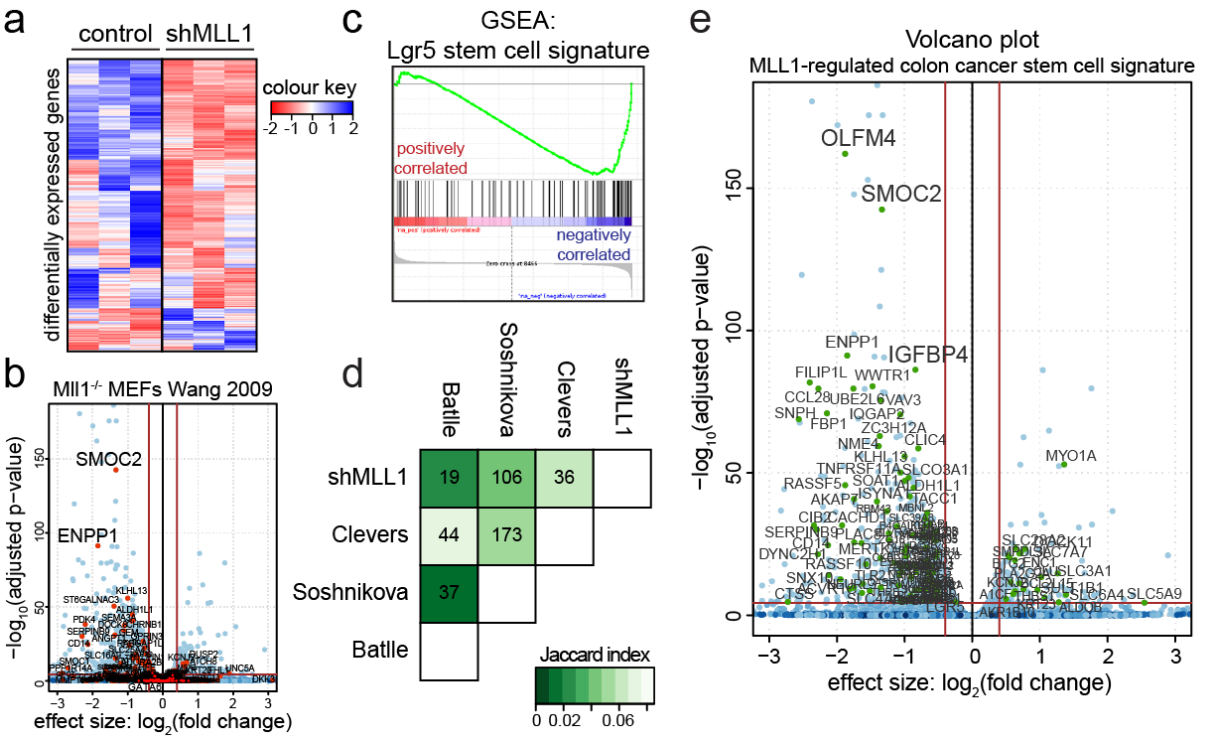

Figure 3.19: MLL1 regulates Lgr5⁺ intestinal stem cell genes.
a) Heatmap of differentially expressed genes in three control versus shMLL1 Ls174T cell clones at 3 days after induction with doxycycline, cut-off $\log_2$ fold change ≥ 0.5, adjusted p-value ≤ 0.05. Bioinformatics performed by Ramon Oliveira Vidal and Sascha Sauer from the Laboratory of Functional Genomics, Scientific Genomics Platforms of the MDC (BIMSB/BIH). **b)** Volcano plot of differentially expressed genes in human shMLL1 Ls174T cells, represented as blue dots. Genes of a mouse embryonic fibroblast (MEF) Mll1$^{-/-}$ signature[163] marked in red and indicated by name. **c)** GSEA analysis

of differentially expressed genes in shMLL1 Ls174T cells reveals negative correlation with a $Lgr5^+$ intestinal stem cell signature[89]; p-value 0.001, NES -1.65, FDR 0.001. **d)** Differentially expressed genes in shMLL1 Ls174T cells compared to intestinal stem cell signatures reported by the groups of Clevers[195], Soshnikova[204] and Batlle[89]. The correlation table indicates the number of common genes, green colour gradations encode the Jaccard index of similarity between the signatures, the lighter the colour the higher the similarity. **e)** Volcano plot of the differentially expressed genes in shMLL1 Ls174T cells overlaid with our MLL1-regulated colon cancer stem cell signature (Supplementary Table 1, page 116), genes of the signature are marked as green dots and indicated by name.

Comparisons of the differentially expressed genes in shMLL1 Ls174T cells with intestinal stem cell signatures reported by the groups of Clevers[195], Soshnikova[204] and Batlle[89] revealed a significant overlap of genes (Figure 3.19d: Clevers 36, Soshnikova 106 and Batlle 19 genes). The correlation table in Figure 3.19d illustrates both the number of overlapping genes and the degree of similarity between the compared stem cell signatures (Jaccard index). A high number of overlapping genes does not necessarily indicate that two signatures are the most similar because of differences in the number of genes comprising each signature: 'Soshnikova and shMLL1' are less similar to each other than 'Clevers and shMLL1', despite the fact that the former pair shares a higher number of overlapping genes. The 'Soshnikova' signature contains many more genes than the 'Clevers' signature. 132 deregulated stem cell genes were compiled to establish a MLL1-regulated colon cancer stem cell signature (Supplementary Table 1, page 116). A volcano plot of the deregulated genes overlaid with this signature showed predominant downregulation of intestinal stem cell genes upon knockdown of MLL1; these included *OLFM4*, *SMOC2*, *IGFBP4* and the Wnt-regulated gene *LGR5* (Figure 3.19e, Supplementary Table 1, page 116).

3.8.2 MLL1 regulates the stemness and self-renewal of human colon cancer cells.

The observed deregulation of stem cell genes in shMLL1 cells suggested a role of MLL1 in sustaining the stemness and self-renewal of colon cancer cells. We therefore assessed the self-renewal capacity of shMLL1 Ls174T and DLD1 cells. MLL1 was essential for the clonal expansion of Ls174T cells in a colony formation assay; shMLL1 cells were unable to expand into cell colonies (Figure 3.20a). Non-adherent sphere culture growth and high re-plating efficiency are characteristic properties of cancer stem cells[87, 162]. Ls174T cells cultured as 3D non-adherent colon cancer spheres expressed the stem cell genes *LGR5*, *SMOC2* and *CD44*, and showed an increased expression of the cancer stem cell marker *CD166* [93] (Figure 3.20b). MLL1 protein levels were strongly increased in the non-adherent, self-renewing sphere cultures of human Ls174T cells compared to adherent cultures (Figure 3.20c).

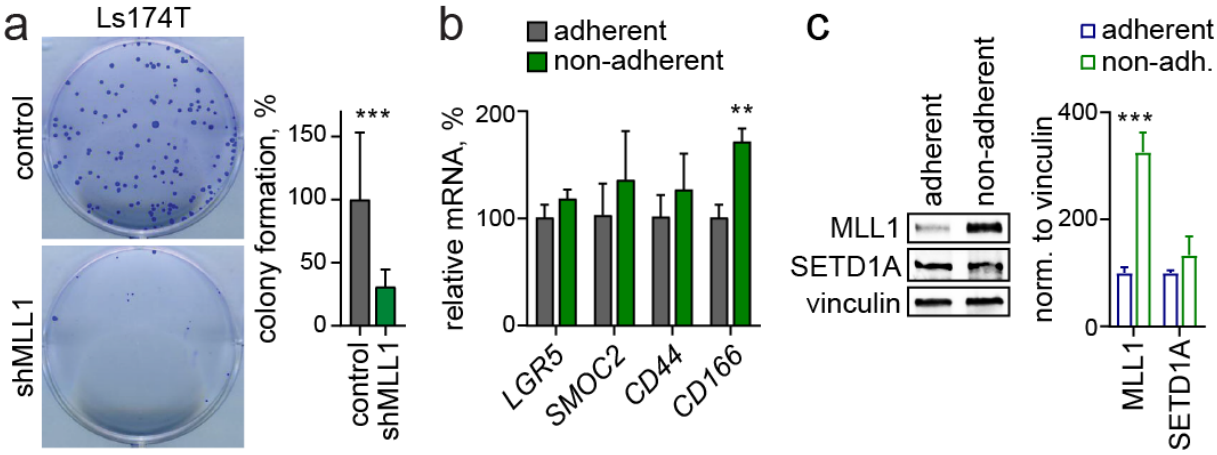

Figure 3.20: MLL1 and the stemness of human colon cancer cells.
a) Crystal violet staining of cell colonies from control and shMLL1 Ls174T cells, quantification on the right, n=6, unpaired t test. **b)** mRNA expression of the stem cell genes *LGR5*, *SMOC2*, *CD44* and the cancer stem cell marker *CD166* in Ls174T cells cultured under adherent and non-adherent conditions. **c)** Western blot for MLL1 and SETD1A in Ls174T cells cultured under adherent and non-adherent conditions, vinculin as control for equal loading. Quantification on the right, normalized to vinculin, n=3, unpaired t test.

The expression of the MLL family member SETD1A was not increased in the non-adherent sphere cultures of Ls174T cells (Figure 3.20c). SETD1A had previously been reported to regulate the expression of several Wnt target genes in colon cancer cells[141]. Given the strong correlation of oncogenic Wnt signalling and MLL1 expression in human colon cancer patient samples and β-cat^{GOF} mouse intestinal tumors (see Figure 3.1, page 26 and Figure 3.6, page 33), we investigated whether MLL1 controlled the expression of reported SETD1A-regulated Wnt target genes. The knockdown of MLL1 did not affect the expression of the SETD1A-regulated Wnt targets *TCF1* and *TCF4* [141] (Figure 3.21), indicating that the two histone methyltransferases MLL1 and SETD1A regulate distinct Wnt target genes in colon cancer cells.

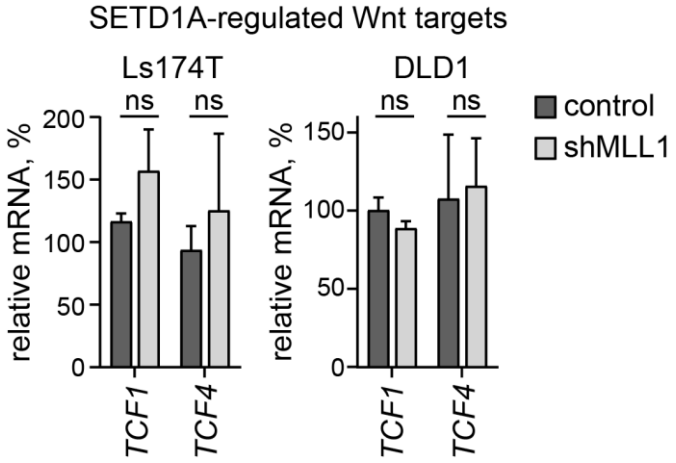

Figure 3.21: MLL1 and SETD1A regulate distinct Wnt target genes in colon cancer cells.
mRNA expression of the SETD1A-regulated Wnt target genes *TCF1* and *TCF4* in control and shMLL1 Ls174T and DLD1 sphere cells, n=4, unpaired t test.

We investigated the effect of MLL1 ablation on the growth of Ls174T and DLD1 colon cancer cells in adherent and non-adherent cultures. Serial re-plating assays revealed that the knockdown of MLL1 did not immediately affect viability and proliferation of Ls174T and DLD1 cells in adherent 2D cultures. A significant growth reduction was detected only after four passages at 10-14 days after shMLL1 induction (Figure 3.22a, b). In contrast to the 2D culture, the knockdown of MLL1 in non-adherent 3D sphere cultures of Ls174T and DLD1 cells had a rapid effect on the growth and self-renewal of the cancer cells. Secondary sphere formation of shMLL1 cells was reduced by 80% in Ls174T and by 60% in DLD1 cells compared to control cells (Figure 3.22c, d).

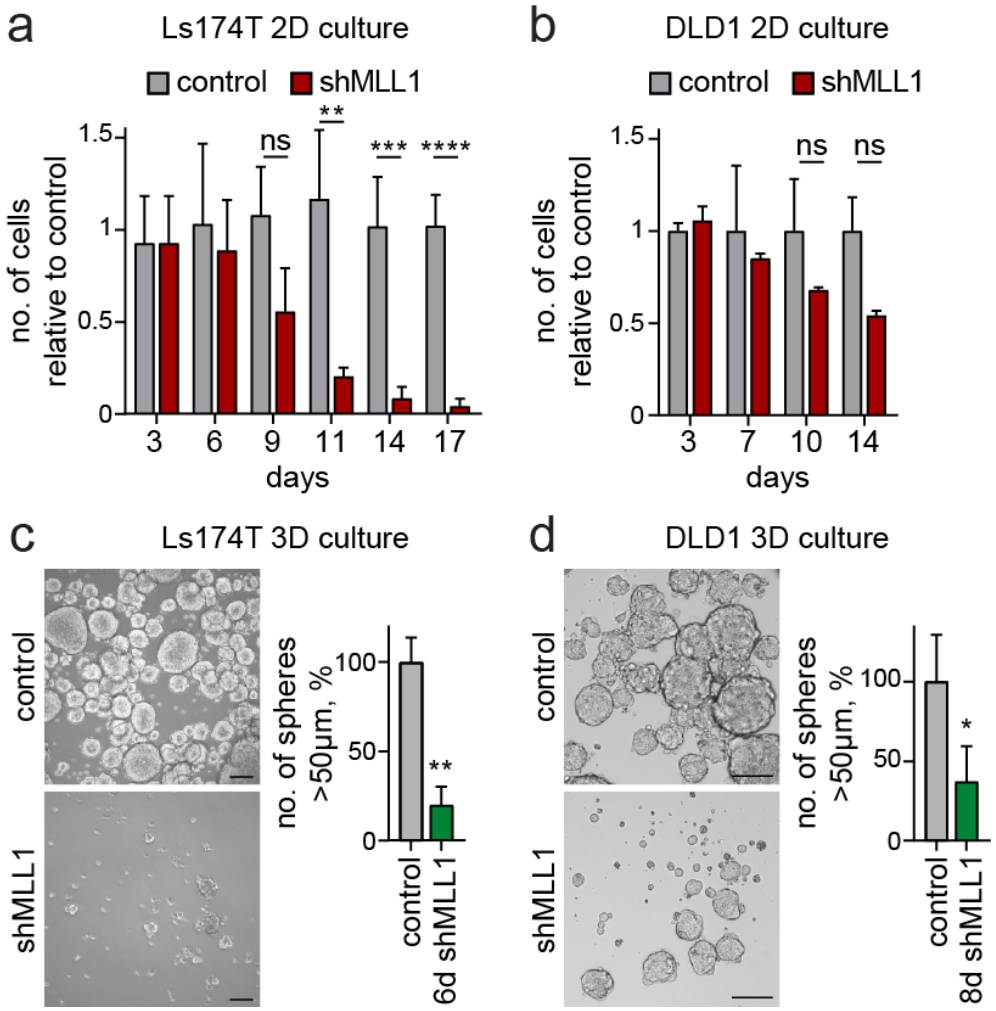

Figure 3.22: MLL1 is crucial for the self-renewal of human colon cancer cells.
Serial re-plating assays: quantification of viable **(a)** shMLL1 Ls174T and **(b)** shMLL1 DLD1 cells cultured under 2D adherent conditions at indicated time points after shMLL1 induction relative to control cells, n=4, unpaired t test. **c)** Brightfield images of control and 6d doxycycline-induced shMLL1 Ls174T secondary spheres, scale bars 100µm. Quantification of spheres >50µm in size on the right, n=3, unpaired t test. **d)** Brightfield images of control and 8d doxycycline-induced shMLL1 DLD1 secondary spheres, scale bars 100µm. Quantification of spheres >50µm in size on the right, n=3, unpaired t test.

Residual spheres exhibited minimal MLL1 expression and reduced proliferation as shown by staining for Ki67 (Figure 3.23a). shMLL1 spheres were negative for the apoptosis marker cleaved Caspase-3 (Figure 3.23a, b).

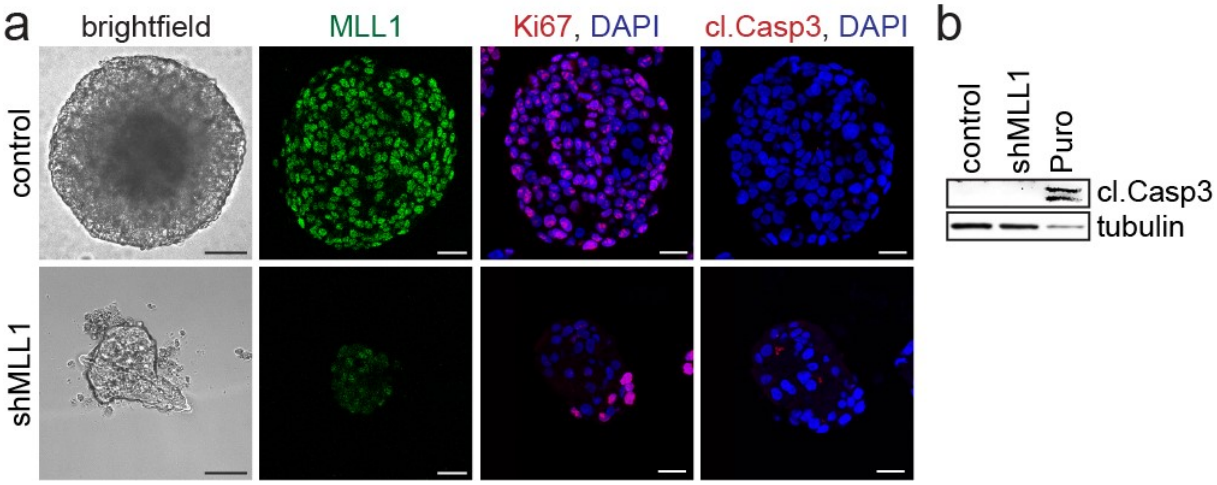

Figure 3.23: MLL1 is required for 3D sphere growth of human colon cancer cells.
a) Brightfield images of control and shMLL1 Ls174T spheres, scale bars 25µm. MLL1 (green), Ki67 (red) and cleaved Caspase-3 (red) stainings in control and shMLL1 Ls174T spheres, scale bars 20µm. DAPI (blue) stains nuclei. **b)** Western blot for cleaved Caspase-3, tubulin as control for loading. Puromycin (2µg/ml) treatment for 24h as positive control for apoptosis.

Our studies in the human colon cancer cell lines Ls174T and DLD1 demonstrate a crucial role of the histone methyltransferase MLL1 in sustaining the stemness of Wnt-activated colon cancer cells. MLL1 was highly expressed in non-adherent sphere cultures and was crucial for the self-renewal of the tumor cells. Our findings in the shMLL1 cells correlated well with the stem cell expansion phenotype that we had observed in Mll1-deficient β-cat^{GOF} mouse intestinal tumors and organoids, approving the Ls174T and DLD1 cells as suitable model systems to investigate the epigenetic mechanism underlying the role of MLL1 in colon cancer stemness.

3.8.3 MLL1 epigenetically sustains the expression of specific stem cell genes.

The ablation of MLL1 in Ls174T cells deregulated the expression of intestinal stem cell genes (see Figure 3.19, page 46). RT-PCR analyses of sphere cultures confirmed the decrease in the expression of the stem cell genes: the expression of *LGR5*, *IGFBP4*, *SMOC2* and *OLFM4* [195] was downregulated upon knockdown of MLL1 (Figure 3.24a). *CD44* and *LRIG1* [195] expression was not significantly decreased. There was no reduction in the expression of the Wnt-regulated genes *ASCL2* [92], *SOX9* [205] and *AXIN2* [33] (Figure 3.24a). The selective regulation of Wnt target genes was likewise observed in DLD1 colon cancer cells (Figure 3.24b): the knockdown of MLL1 decreased the expression of *LGR5* but not *ASCL2* and *AXIN2*. The ablation of MLL1 did not affect the overall activity of Wnt signalling, as shown by a TCF/LEF luciferase reporter assay (TOPflash)[206] in comparison to cells either treated with the Wnt activator CHIR99021[207] or the Wnt inhibitor LF3[100] (Figure 3.24c).

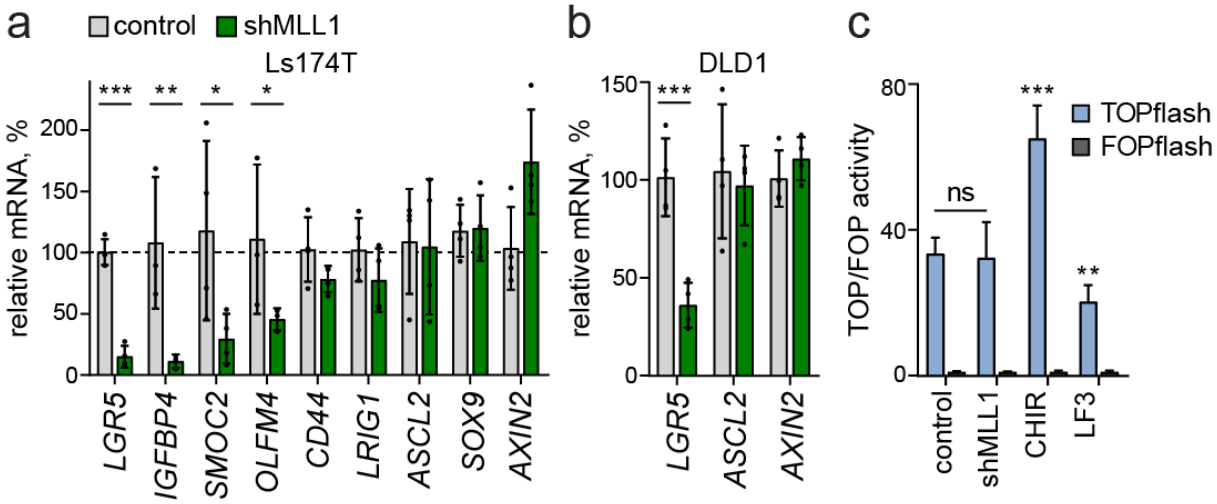

Figure 3.24: The ablation of MLL1 downregulates specific stem cell genes but does not decrease global Wnt activity in colon cancer cells.
a) mRNA expression of intestinal stem cell genes and classical Wnt targets in control and 6d doxycycline-induced shMLL1 Ls174T sphere cells from 3 independent single cell clones, n=4, unpaired t test. **b)** mRNA expression of Wnt-regulated genes in 8d doxycycline-induced control and shMLL1 DLD1 sphere cells, n=4, unpaired t test. **c)** TCF/LEF luciferase reporter assays in control and shMLL1 Ls174T cells treated with doxycycline for 10 days, n=6 of 3 independent experiments, unpaired t test. Wnt-responsive luciferase activity (TOPflash) calculated relative to control (FOPflash). 3µM CHIR99021 and 50µM LF3 added for 24h to stimulate and repress Wnt signalling, respectively, n=3, unpaired t test.

To find out whether the regulated stem cell genes are directly controlled by MLL1 and its H3K4 tri-methyltransferase activity, we performed chromatin immunoprecipitation (ChIP) of the activating and repressive chromatin marks H3K4me3 and H3K27me3. This revealed high H3K4me3 and low H3K27me3 levels at the transcription start sites (TSS) of the MLL1-regulated stem cell genes *LGR5, SMOC2*, *IGFBP4* and *OLFM4*. Ablation of MLL1 shifted the epigenetic state of the stem cell genes from transcriptionally permissive (H3K4me3) to repressed (H3K27me3) (Figure 3.25a). There were no changes in the levels of H3K4me3 and

H3K27me3 at the TSS of *ASCL2* and *AXIN2* (Figure 3.25b), which was in line with the unaffected expression of these Wnt target genes (see Figure 3.24, page 51). ChIP validity was confirmed by H3K4me3 enrichment at the *GAPDH* TSS and its absence at a negative control region (Figure 3.25c). Global levels of H3K4 and H3K27 methylation were not changed (Figure 3.25d), demonstrating a gene-specific function of the histone methyltransferase MLL1.

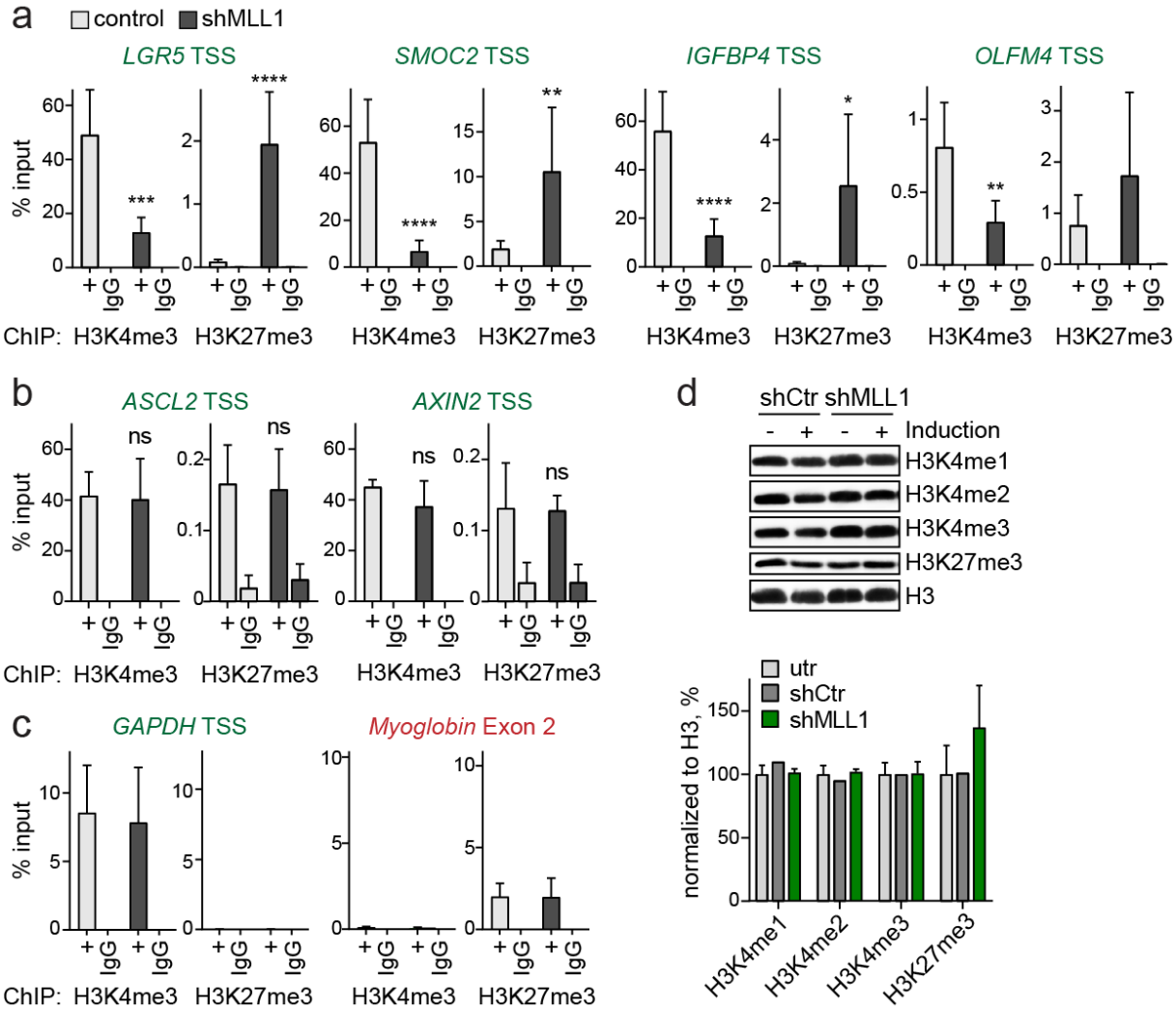

Figure 3.25: The ablation of MLL1 switches H3K4me3 marks to repressive H3K27me3 at specific stem cell genes.
ChIP for H3K4me3 and H3K27me3 at the TSS of **a)** *LGR5*, *SMOC2*, *IGFBP4* and *OLFM4* (n=7) and of **b)** *ASCL2* and *AXIN2* (n=4) in non-induced control (light grey columns) and 11d doxycycline-induced shMLL1 Ls174T cells (black columns), represented as % input. Unpaired t test, significance calculated for control versus shMLL1. **c)** *GAPDH* TSS and *Myoglobin* Exon 2 as positive and negative controls, n=7. **d)** Western blots for global H3K4 and H3K27 methylation in non-induced (utr) and 6d doxycycline-induced shCtr (n=1) and shMLL1 (n=3) cells. Quantification below, normalized to total H3.

We established ChIP for MLL1 and identified MLL1 binding to the promoters of the intestinal stem cell genes *LGR5*, *SMOC2*, *IGFBP4* and *OLFM4* (Figure 3.26a). ChIP specificity was confirmed by MLL1 binding to *MECOM*, a previously reported MLL1 target gene[208], and by comparison to a negative control region (*TAL1*+70[141]). MLL1 binding to the *LGR5* promoter

was also detected in DLD1 colon cancer cells (Figure 3.26b). Strongly reduced binding of MLL1 was observed in shMLL1 cells (Figure 3.26a, b; knockdown control Western blot in Figure 3.26c).

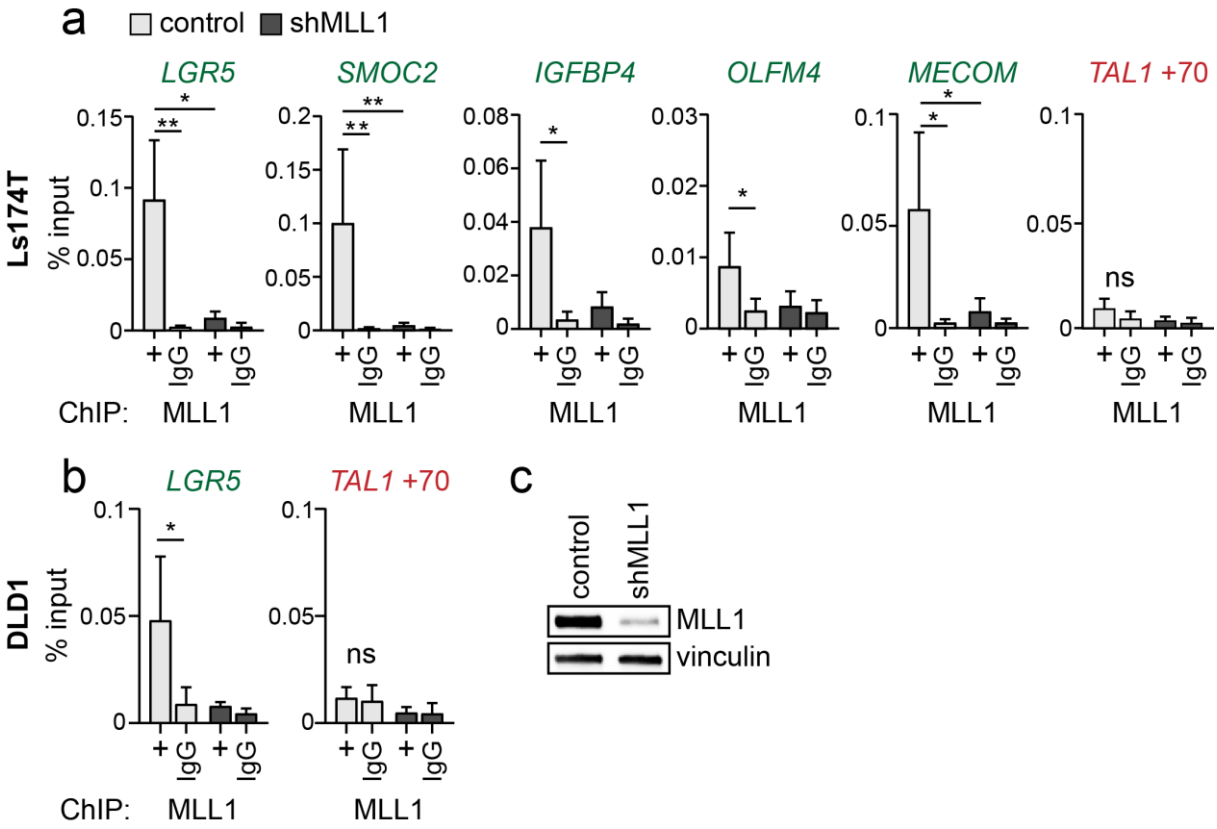

Figure 3.26: MLL1 binds to the promoters of stem cell genes.
a) ChIP for MLL1 in non-induced control (light grey columns) and 6d doxycycline-induced shMLL1 Ls174T cells (black columns), binding at the *LGR5*, *SMOC2*, *IGFBP4* and *OLFM4* promoters, represented as % input, n=6, unpaired t test, significance calculated for control versus shMLL1 and IgG. *MECOM* TSS and +70kb downstream region of the *TAL1* promoter positive and negative controls. **b)** ChIP for MLL1 in non-induced control (light grey columns, n=6) and 8d doxycycline-induced shMLL1 DLD1 cells (black columns, n=3), binding at the *LGR5* promoter, negative control region *TAL1* +70, represented as % input. Unpaired t test, significance calculated for control versus shMLL1 and IgG. **c)** Representative MLL1 knockdown control Western blot from cells used for ChIP analyses.

3.8.4 MLL1 antagonizes PcG-mediated silencing of stem cell genes.

The ablation of MLL1 shifted the epigenetic state of the regulated stem cell genes from transcriptionally permissive (H3K4me3) to repressed (H3K27me3) (see Figure 3.25, page 52). H3K27me3 marks are deposited by the polycomb repressive complex 2 (PRC2)[134] (compare 1.3.7, page 20). To assess an antagonistic control of the stem cell genes by Mll1 and PRC2, we treated MLL1 knockdown cells with the small molecule Gsk126[209], an inhibitor of the catalytic PRC2 subunit Ezh2 (scheme in Figure 3.27a). Gsk126 treatment partially restored the decreased expression of *LGR5*, *SMOC2*, *IGFBP4* and *OLFM4* even in the absence of MLL1 (Figure 3.27b). H3K4me3 marks at the TSS of the stem cell genes were not restored upon Gsk126 treatment (Figure 3.27c), indicating that the re-initiation of *LGR5*,

SMOC2, *IGFBP4* and *OLFM4* expression was independent of MLL1 and its methyltransferase activity. The expression of the MLL1-independent Wnt target genes *ASCL2* and *AXIN2* was unaffected by Gsk126 treatment (Figure 3.27d), and H3K4me3 and H3K27me3 TSS marks were unchanged (Figure 3.27e).

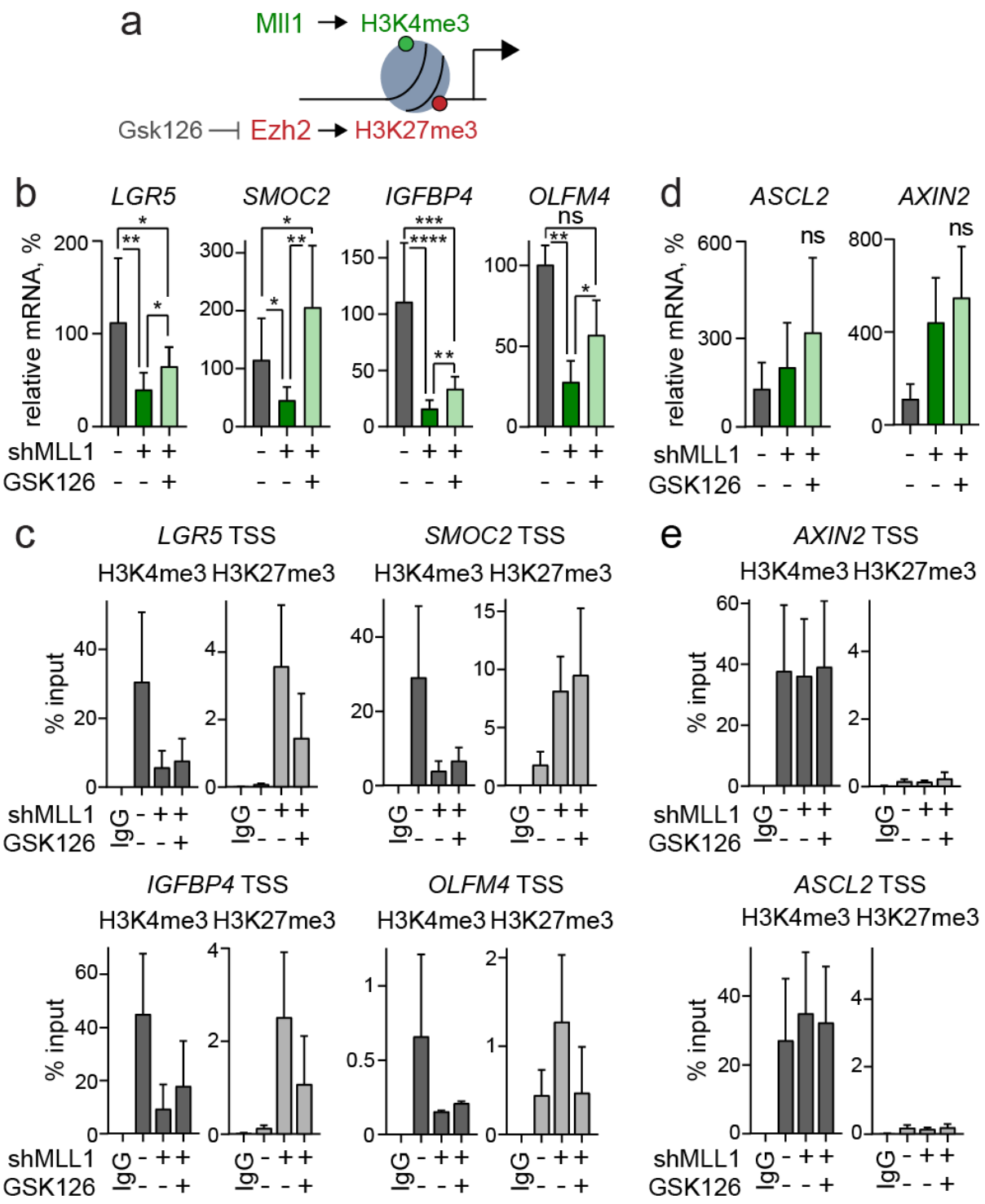

Figure 3.27: MLL1 antagonizes PRC2 to sustain the expression of specific stem cell genes.
a) Scheme: The antagonism of Mll1-dependent H3K4me3 and PRC2-mediated H3K27me3 controls gene expression. The chemical compound Gsk126 inhibits the H3K27 tri-methyltransferase activity of Ezh2 and blocks the PRC2-mediated tri-methylation of H3K27. **b)** mRNA expression of *LGR5*, *SMOC2*,

IGFBP4 and *OLFM4* in control (dark grey), 6d doxycycline-induced shMLL1 Ls174T cells (dark green) and shMLL1 Ls174T cells following 4-day Gsk126 treatment (light green), n=6, unpaired t test. **c)** ChIP for H3K4me3 (dark grey columns) and H3K27me3 (light grey columns) at the TSS of *LGR5*, *SMOC2*, *IGFBP4* and *OLFM4* (n=3) in control, 11d doxycycline-induced shMLL1 Ls174T cells and shMLL1 Ls174T cells following 4-day Gsk126 treatment, represented as % input. **d)** mRNA expression of *ASCL2* and *AXIN2* in control (dark grey), 6d doxycycline-induced shMLL1 Ls174T cells (dark green) and shMLL1 Ls174T cells following 4-day Gsk126 treatment (light green), n=6, unpaired t test. **e)** ChIP for H3K4me3 (dark grey columns) and H3K27me3 (light grey columns) at the TSS of *ASCL2* and *AXIN2* (n=3) in control, 11d doxycycline-induced shMLL1 Ls174T cells and shMLL1 Ls174T cells following 4-day Gsk126 treatment, represented as % input.

These data demonstrate that the intestinal stem cell genes *LGR5*, *SMOC2*, *IGFBP4* and *OLFM4* are antagonistically controlled by MLL1 and the polycomb repressive complex 2 (PRC2). MLL1 counteracts the PcG-mediated silencing of the stem cell genes.

3.8.5 MLL1 is essential for the β-catenin/TCF4-induced expression of *LGR5*.

The expression of the stem cell gene *LGR5* is controlled by Wnt/β-catenin signalling[107]. We asked whether the ablation of MLL1 changed the promoter occupancy of the β-catenin/TCF4 complex. ChIP for TCF4 and β-catenin revealed binding of the β-catenin/TCF4 complex at the *LGR5* promoter (Figure 3.28a, b). There was no change in β-catenin/TCF4 occupancy upon knockdown of MLL1 (Figure 3.28a, b).

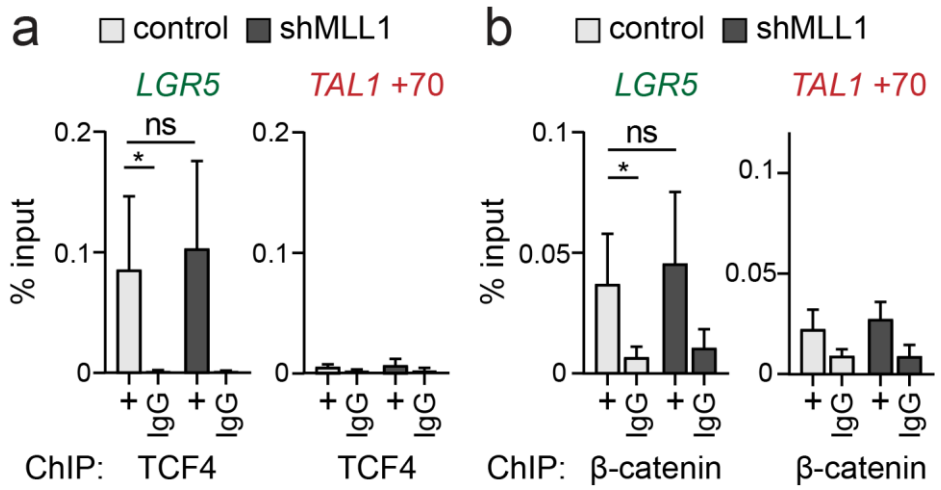

Figure 3.28: β-catenin/TCF4 binding to the *LGR5* promoter in control and shMLL1 Ls174T colon cancer cells.
ChIP for TCF4 **(a)** and β-catenin **(b)** at the *LGR5* promoter in non-induced control (light grey columns) and 6d doxycycline-induced shMLL1 Ls174T cells (black columns), negative control region *TAL1* +70, represented as % input, n=5. Unpaired t test, significance calculated for control versus shMLL1 and IgG.

Taken together, our results show that the histone methyltransferase MLL1 sustains the oncogenic Wnt-driven expression of specific stem cell genes by antagonizing PcG-mediated gene silencing. In the absence of MLL1, PRC2 catalyses the tri-methylation of H3K27me3 and mediates gene repression. In the case of *LGR5*, this occurs regardless of the promoter occupancy of β-catenin/TCF4 (summarized in the schemes in Figure 3.29).

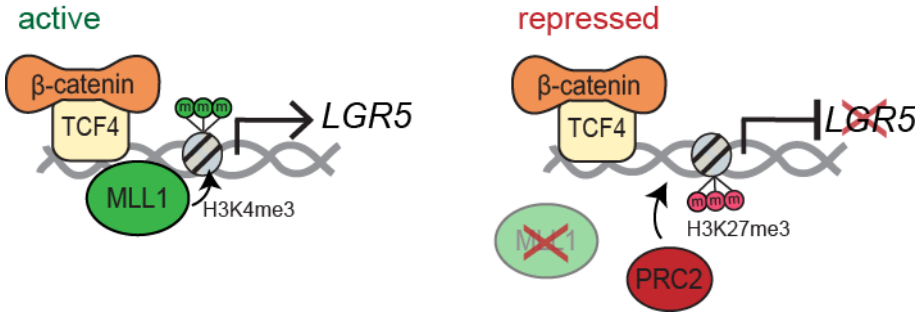

Figure 3.29: Scheme of the antagonistic control of *LGR5* by MLL1 and PRC2.
Scheme of β-catenin/TCF4-MLL1-dependent regulation of *LGR5* in colon cancer cells. MLL1 prevents PRC2-mediated gene silencing to sustain *LGR5* expression. This is associated with the MLL1-dependent H3K4 tri-methylation at the *LGR5* TSS. Right: Ablation of MLL1 results in PRC2-mediated H3K27me3 and silencing of *LGR5* expression.

3.9 MLL1 prevents differentiation of human colon cancer cells.

The shMLL1 Ls174T human xenograft tumors and sphere cells showed enhanced differentiation with an increase in the expression of the Paneth cell genes *DEFA5* and *LYZ* and the goblet cell markers *MUC2* and *ITF* (Figure 3.30a, b), as was also observed in the β-cat^{GOF} mouse tumor model (see Figure 3.13, page 39). Ls174T spheres also increased the expression of the enterocyte differentiation marker cytokeratin *KRT20* [210] upon knockdown of MLL1 (Figure 3.30b on the right). DLD1 sphere cells did not express Paneth cell genes and showed unchanged *MUC2* expression, but upregulated the expression of *ITF* and *KRT20* upon knockdown of MLL1 (Figure 3.30c). Our data suggest that MLL1 maintains human colon cancer cells in a non-differentiated stem-like state. The ablation of MLL1 induces differentiation of xenograft tumors and sphere cultures.

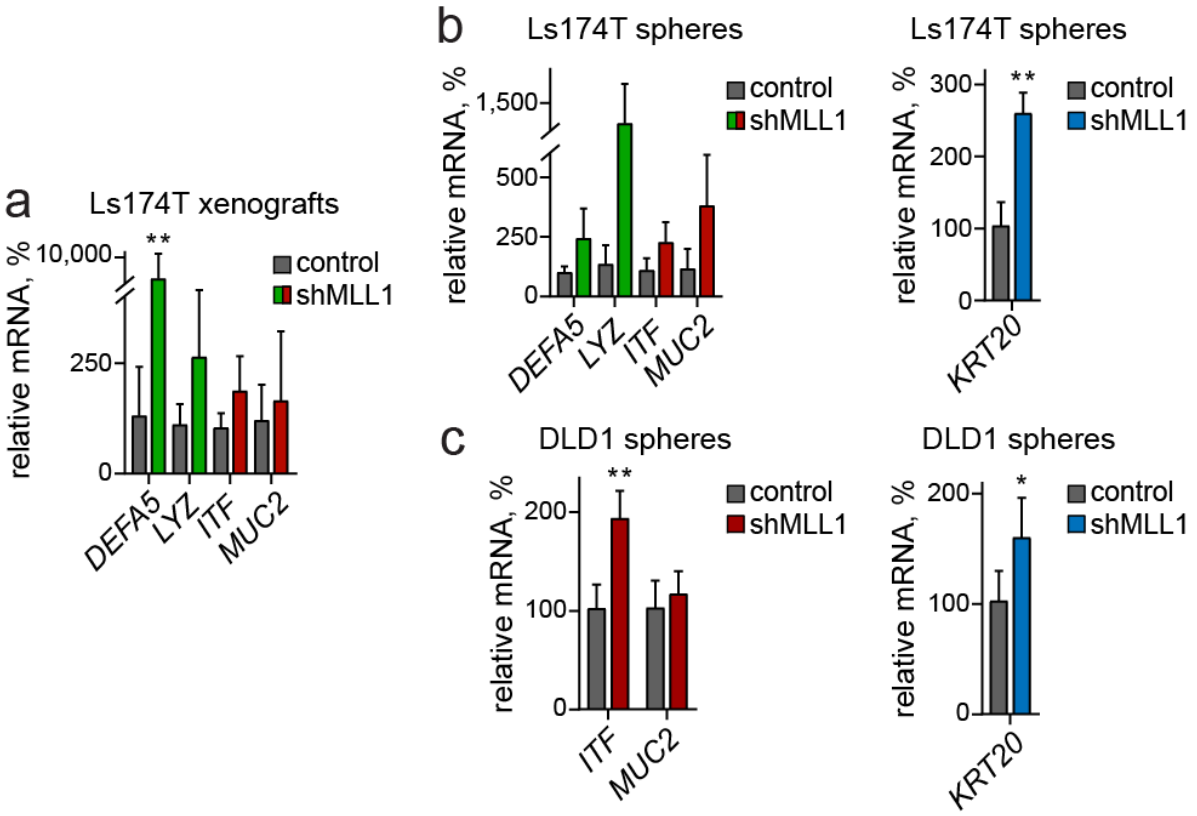

Figure 3.30: The knockdown of MLL1 induces differentiation of human colon cancer cells.
a), **b)** mRNA expression of Paneth cell (green), goblet cell (red) and enterocyte (blue) markers in human shMLL1 Ls174T xenograft tumors (n=4) and sphere cells (n=4) relative to non-induced controls, unpaired t test. **c)** mRNA expression of goblet cell (red) and enterocyte (blue) markers in human shMLL1 DLD1 sphere cells relative to control sphere cells, n=4, unpaired t test.

3.10 Exploring the molecular mechanism of differentiation reveals a Mll1-Gata4/6-Bmp4 axis.

We sought to determine the molecular mechanism underlying the differentiation of Mll1-deficient tumor-propagating cells in β-cat^{GOF}; Mll1$^{-/-}$ intestinal stem cells and organoids and in human colon cancer xenografts and spheres (see Figure 3.13, page 39 and Figure 3.30, page 57). The transcriptome profiling of β-cat^{GOF}; Mll1$^{-/-}$ intestinal stem cells had identified the transcription factor Gata4 as a Mll1-regulated gene in Wnt-activated tumor-initiating cells (see Figure 3.14, page 41). Gata4 expression is restricted to the small intestine[211], mouse and human colon epithelia express the homologue Gata6[203]. Ablation of Gata6 in mouse and human colon cancer cells has been shown to upregulate the expression of the Bmp receptor ligand *Bmp4*, suppressing self-renewal and inducing differentiation of cancer stem cells[203].
We observed a decreased expression of *Gata4* in β-cat^{GOF}; Mll1$^{-/-}$ small intestinal organoids, compared to β-cat^{GOF} and β-cat^{GOF}; Mll1$^{+/-}$ organoids (Figure 3.31a, b). The decreased *Gata4* expression was associated with a strong increase in the expression of *Bmp4* (Figure 3.31b).

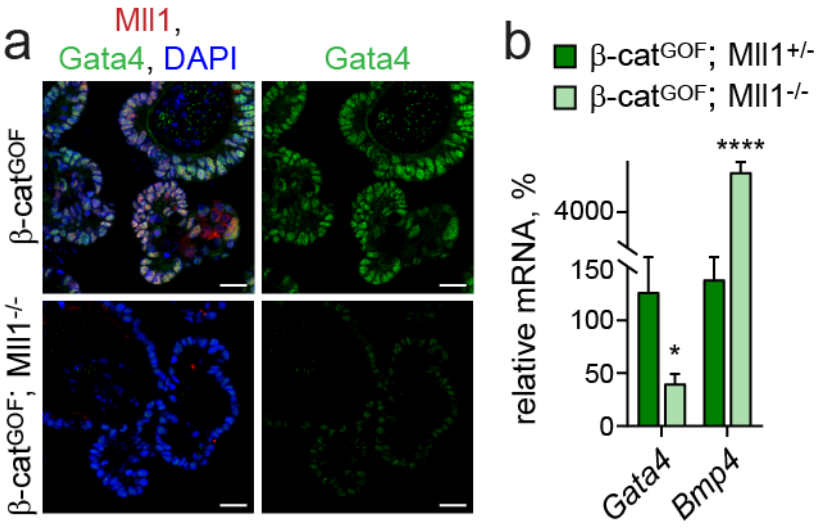

Figure 3.31: The ablation of Mll1 shifts Gata4 and Bmp4 expression in small intestinal organoids. **a)** Immunofluorescence staining for Mll1 (red) and Gata4 (green) on sections of β-cat^{GOF} and β-cat^{GOF}; Mll1$^{-/-}$ organoids. Nuclei in blue (DAPI), scale bars 20µm. **b)** mRNA expression of *Gata4* and *Bmp4* in β-cat^{GOF}; Mll1$^{+/-}$ and β-cat^{GOF}; Mll1$^{-/-}$ organoids, n=3, unpaired t test.

In Ls174T and DLD1 colon cancer sphere cells, the ablation of MLL1 decreased the expression of *GATA6*, while *BMP4* expression increased (Figure 3.32a). *GATA4* expression was not detectable in the colon cancer cells. ChIP revealed MLL1 binding to the *GATA6* promoter (Figure 3.32b). The MLL1 binding was strongly reduced in shMLL1 cells and was absent at a negative control region 70kb downstream of the *TAL1* promoter (Figure 3.32b). Histone methylation at the *GATA6* TSS switched from activating H3K4me3 to repressive H3K27me3 upon knockdown of MLL1 (Figure 3.32c). Immunohistochemistry staining confirmed a strong decrease in GATA6 levels in shMLL1 Ls174T sphere cells (Figure 3.32d). These data suggest that MLL1 acts as an upstream regulator of *GATA6* to prevent a BMP4-induced differentiation of the colon cancer cells.

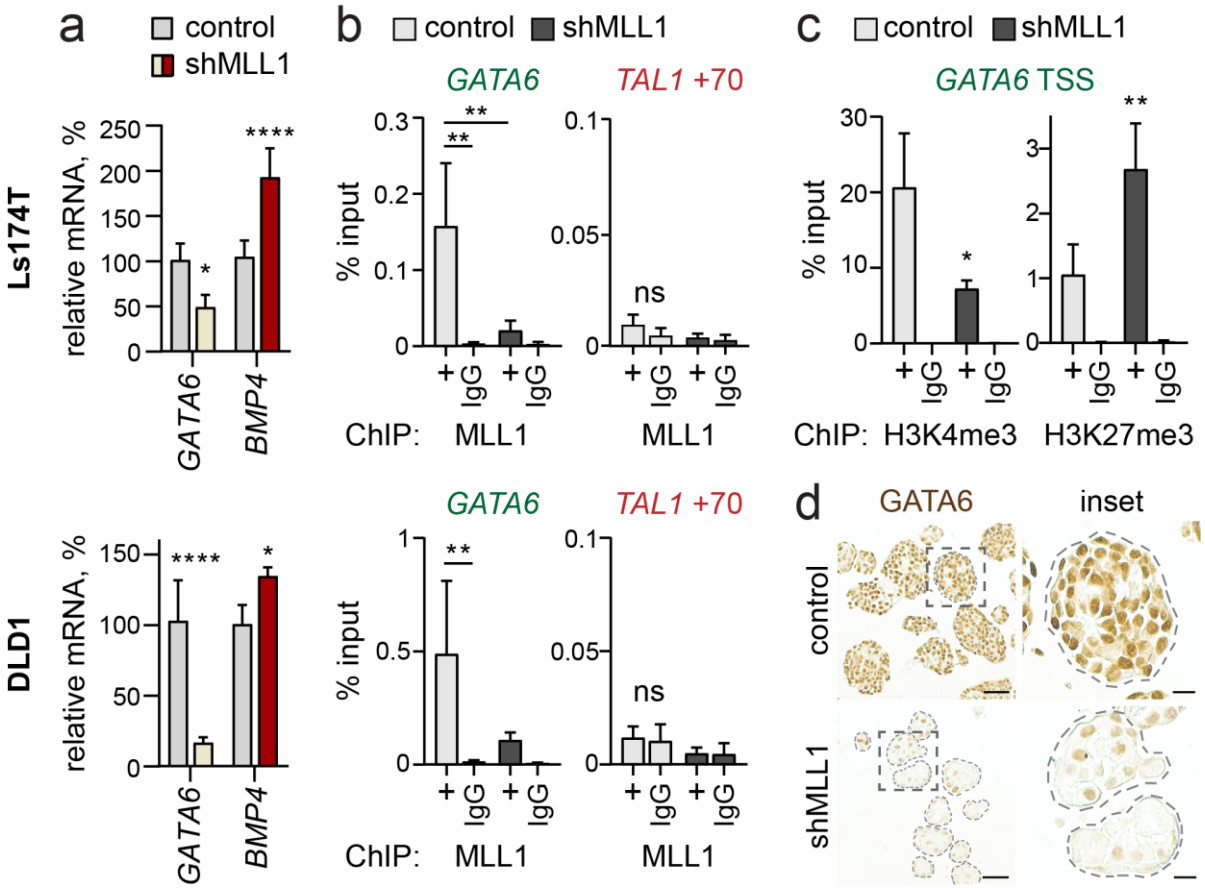

Figure 3.32: MLL1 controls the expression of GATA6 in human colon cancer cells.
a) mRNA expression of *GATA6* (beige) and *BMP4* (red) in control and shMLL1 Ls174T (upper panel) and shMLL1 DLD1 sphere cells (lower panel), n=4, unpaired t test. **b)** ChIP for MLL1 in control (light grey columns) and 6d doxycycline-induced shMLL1 Ls174T cells (black columns; upper panel, n=6) and in control (light grey columns) and 8d doxycycline-induced shMLL1 DLD1 cells (black columns; lower panel, n=4), binding at the *GATA6* promoter, *TAL1* +70kb as negative control region, represented as % input, unpaired t test, significance calculated for control versus shMLL1 and IgG. **c)** ChIP for H3K4me3 and H3K27me3 at the TSS of *GATA6* in control (light grey columns) and 11d doxycycline-induced shMLL1 Ls174T cells (black columns), represented as % input, n=4. **d)** Immunohistochemistry for GATA6 on sections of control and shMLL1 Ls174T spheres, scale bars 50µm, insets 25µm.

Bmp signalling has previously been shown to suppress intestinal stem cell genes and induce differentiation of Lgr5^{+} intestinal stem cells[42]. This has been associated with the expression of the cell cycle inhibitor and differentiation marker *p21*$^{CIP1/WAF1}$ (*Cdkn1a*). The ablation of MLL1 in Ls174T cells strongly increased *p21* expression over time, while *LGR5* expression gradually decreased (Figure 3.33a). This inverse regulation was observed on both mRNA and protein level. The expression of *p21* was also markedly upregulated in shMLL1 Ls174T sphere cells (Figure 3.33b, c). Along with the increased *p21* expression, the MLL1-depleted cells showed a slight decrease in c-MYC protein levels (Figure 3.33d). Increased p21 levels and decreased c-MYC protein levels were also observed in shMLL1 Ls174T xenograft tumors (Figure 3.33e, f). A complementary pattern of c-Myc and p21 has previously been reported in the crypts and villi of the intestinal epithelium[212]. Interference with Wnt/β-catenin signalling by introduction of dnTCF4 in Ls174T cells reduced c-MYC protein levels and released its interaction with MIZ-1 at the *p21* promoter, upregulating *p21* expression and causing secretory and enterocyte differentiation[212].

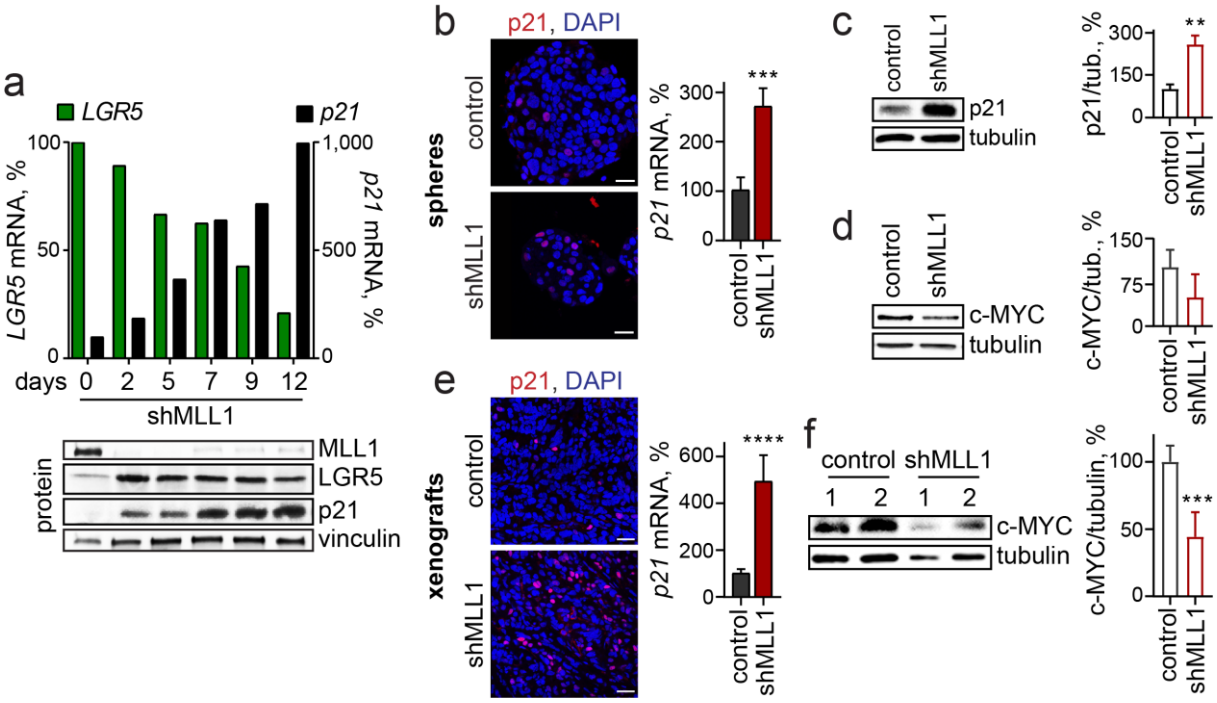

Figure 3.33: shMLL1 Ls174T cells upregulate the cell cycle inhibitor p21.
a) mRNA expression of *LGR5* (green) and *p21* (black) in control and shMLL1 Ls174T cells at indicated time points after shMLL1 induction, n=1. Below: Western blot for MLL1, LGR5 and p21, vinculin as control for equal loading. **b) I**mmunostaining for p21 (red) in control and shMLL1 Ls174T sphere cells. Nuclei in blue (DAPI), scale bars 20µm. Right: *p21* mRNA expression in control and shMLL1 Ls174T sphere cells, n=4, unpaired t test. **c)** Western blot for p21 in control and shMLL1 Ls174T sphere cells, tubulin as control for equal loading. Quantification on the right, normalized to tubulin, n=3, unpaired t test. **d)** Western blot for c-MYC in control and shMLL1 Ls174T sphere cells, tubulin as control for equal loading. Quantification on the right, normalized to tubulin, n=3. **e)** Immunostaining for p21 (red) on control and shMLL1 Ls174T xenograft sections. Nuclei in blue (DAPI), scale bars 20µm. Right: *p21* mRNA expression in control and shMLL1 Ls174T xenografts, n=6, unpaired t test. **f)** Western Blot for c-MYC in two pairs of control and shMLL1 Ls174T xenografts, tubulin as control for equal loading. Quantification on the right, normalized to tubulin, n=6, unpaired t test.

We considered the increased levels of BMP4 causative for the upregulation of *p21* in the shMLL1 Ls174T cells. Treatment of Ls174T colon cancer spheres with BMP4 induced the expression of p21 (Figure 3.34a). Mouse intestinal organoids treated with increasing concentrations of BMP4 under Noggin-free conditions upregulated the expression of the Bmp target gene and differentiation marker *Id2* and of *p21* in a concentration-dependent manner (Figure 3.34b). The Bmp inhibitor Noggin blocks Bmp signal transduction by inhibiting Bmp receptor activation and thus preventing phosphorylation of SMAD signal transducing proteins, the hallmark of active Bmp signalling[213]. Noggin treatment reduced phospho-SMAD1/5/8 levels and effectively decreased the strong *p21* induction in shMLL1 Ls174T cells (Figure 3.34c, quantifications on the right).

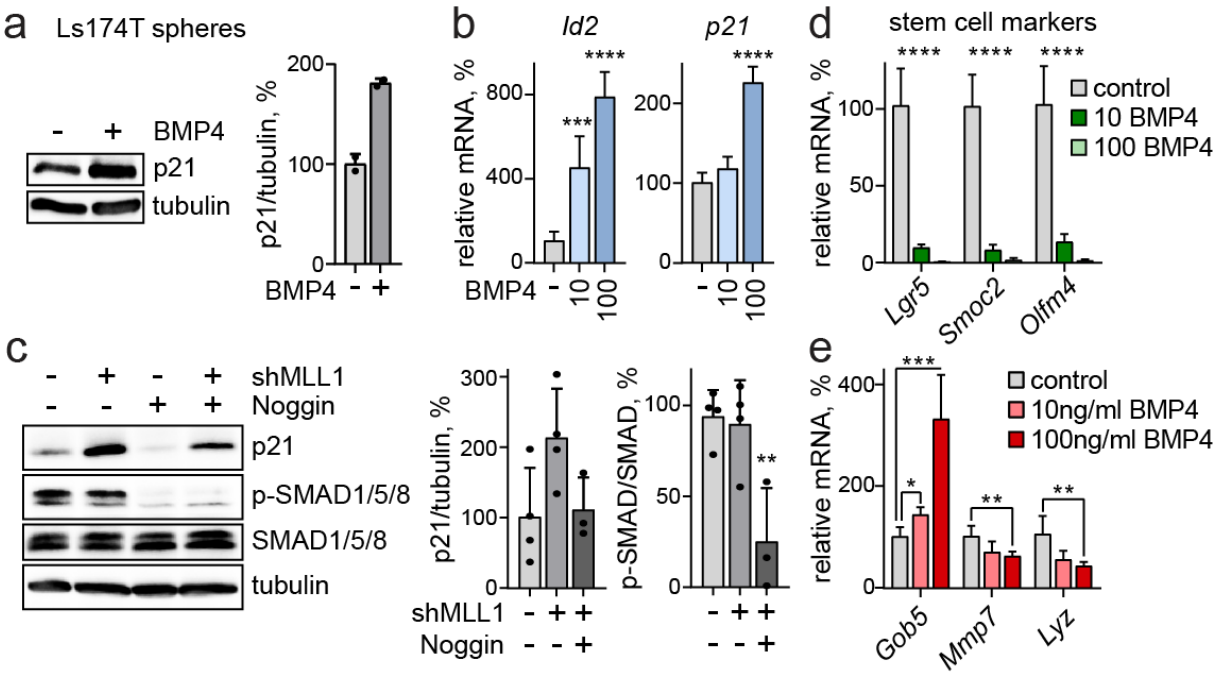

Figure 3.34: BMP4 induces p21 expression and differentiation.
a) Western blot for p21 in control and 48h BMP4-treated Ls174T sphere cells, tubulin as control for equal loading. Quantification on the right, normalized to tubulin, n=2. **b)** *Id2* and *p21* mRNA expression in mouse intestinal organoids treated with 10ng/ml and 100ng/ml of BMP4 for 24h, n=5, unpaired t test. **c)** Western blot for p21, p-SMAD1/5/8 and SMAD1/5/8 in untreated and 48h Noggin-treated control and 7d doxycycline-induced shMLL1 Ls174T sphere cells, tubulin as control for equal loading. Quantifications of p21 and p-SMAD1/5/8 levels normalized to tubulin and SMAD1/5/8, respectively, in control, shMLL1 and Noggin-treated shMLL1 cells on the right, n=4, unpaired t test. **d)** mRNA expression of *Lgr5*, *Smoc2* and *Olfm4* in mouse intestinal organoids treated with 10ng/ml and 100ng/ml of BMP4 for 24h, n=5, unpaired t test. **e)** mRNA expression of *Gob5*, *Mmp7* and *Lyz* in mouse intestinal organoids treated with 10ng/ml and 100ng/ml of BMP4 for 24h, n=5, unpaired t test.

In line with Qi et al. (2017)[42], BMP4-treated intestinal organoids strongly reduced the expression of the stem cell genes *Lgr5*, *Smoc2* and *Olfm4* (Figure 3.34d). BMP4 treatment upregulated the expression of the goblet cell-specific gene *Gob5* [214] but reduced the

expression of the Paneth cell markers *Mmp7* and *Lyz* (Figure 3.34e), promoting differentiation towards a goblet cell fate.

Of note, the knockdown of MLL1 did not increase the levels of phospho-SMAD1/5/8 in the Ls174T cells (Figure 3.34c, first two lanes and quantification on the right), indicating that the increased levels of BMP4 in shMLL1 Ls174T cells induced the expression of *p21* independent of an increased activity of the classical Bmp pathway. As *p21* is a well-established p53 target gene[215], we investigated the role of p53 in inducing *p21* expression in the shMLL1 cells. The p53-mutant DLD1 cells did not show an increased expression of *p21* upon knockdown of MLL1 (Figure 3.35a). In shMLL1 Ls174T sphere cells, total levels of p53 protein did not change compared to control cells, indicating that basal levels of p53 are present but do not increase upon knockdown of MLL1 in Ls174T cells (Figure 3.35b). Binding of p53 to the p53 binding site -2283bp upstream of the *p21* promoter[216] did not increase in shMLL1 Ls174T cells (Figure 3.35c). These data indicate that the induction of *p21* expression in shMLL1 Ls174T cells was not a consequence of p53 activation. Basal levels of p53 seem to be required for *p21* expression, though, as DLD1 cells failed to induce *p21*.

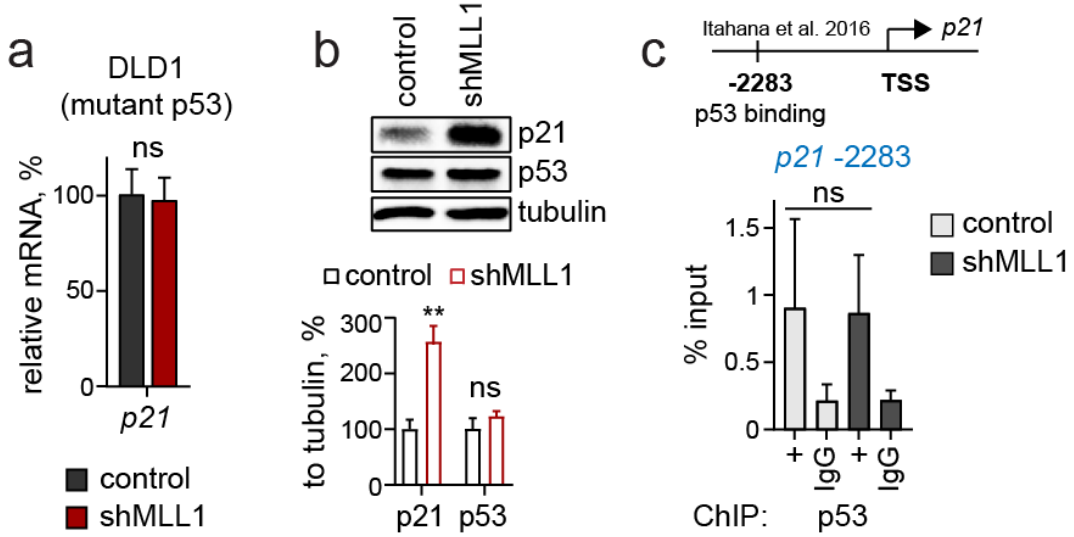

Figure 3.35: The *p21* induction in shMLL1 human colon cancer cells depends on p53.
a) *p21* mRNA expression in control and shMLL1 DLD1 sphere cells, n=4, unpaired t test. **b)** Western blot for p21 and p53 in control and shMLL1 Ls174T sphere cells, tubulin as control for equal loading. Quantification below, normalized to tubulin, n=3, unpaired t test. **c)** ChIP for p53 in control (light grey columns) and 11d doxycycline-induced shMLL1 Ls174T cells (black columns), binding at the p53 binding site -2283bp upstream of the *p21* promoter[216], n=2, represented as % input.

3.10.1 The ablation of MLL1 induces senescence of Ls174T cells.

The upregulation of *p21* has been implicated in cellular senescence, a state of permanent cell cycle arrest that cells might undergo in response to oncogene activation, DNA damage, chromatin perturbation and other stressors[217]. Epigenetic silencing of *Lgr5* has recently been reported to induce a p21-mediated senescence in aging intestinal organoids[218]. Concomitant with an increased expression of the cell cycle inhibitor *p21* (see Figure 3.33, page 60), the

shMLL1 Ls174T cells cultured under 2D adherent conditions showed a gradual decrease in proliferation (Figure 3.36a) and after 11 days in culture exhibited senescence-associated β-galactosidase (SA-β-Gal) activity (Figure 3.36b). Strong SA-β-Gal activity was also observed in shMLL1 Ls174T spheres (Figure 3.36c), along with p21 and the senescence-associated repressive chromatin mark H3K9me3 (Figure 3.36d) and increased DNA damage foci marked by γ-H2A.x (Figure 3.36e)[219]. The increase in *p21* expression coincided with a decreased expression of the senescence-inhibiting factor *RAC3* [220] (Figure 3.36f). Taken together, the knockdown of MLL1 in Ls174T cells caused a decrease in GATA6 and c-MYC protein levels and a concomitant increase in *BMP4* and *p21* expression, inducing differentiation and driving the cancer cells into senescence (see scheme in Figure 3.36g). The p53-mutant DLD1 cells failed to upregulate *p21* expression (see Figure 3.35a, page 62) and did not undergo senescence, yet differentiated in a BMP4-dependent manner upon knockdown of MLL1 (see Figure 3.30, page 57 and Figure 3.32, page 59).

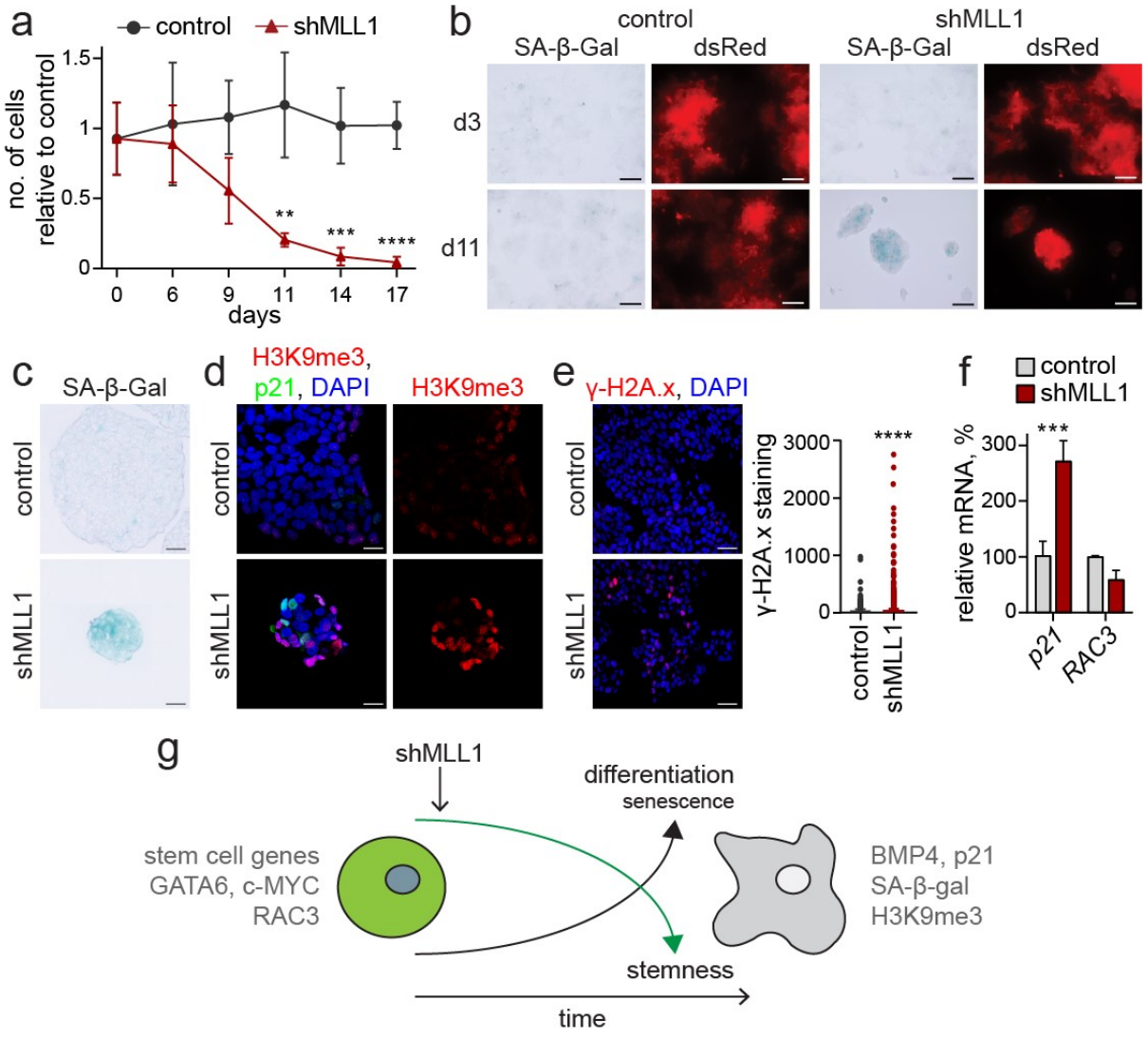

Figure 3.36: shMLL1 Ls174T cells undergo p21-induced cellular senescence.

a) Quantification of viable shMLL1 Ls174T cells cultured under 2D adherent conditions, normalized to control cells at indicated time points after shRNA induction, n=4, unpaired t test. The data are derived from the same experiment as in Figure 3.22 (page 49) and are re-described here to illustrate the gradual decrease in shMLL1 Ls174T cell growth. **b)** Senescence-associated β-galactosidase (SA-β-Gal) staining (blue) of control and shMLL1 Ls174T cells at days 3 and 11 after doxycycline induction. dsRed as reporter of shRNA production, scale bars 100µm. **c)** SA-β-Gal staining (blue) of control and 11d doxycycline-induced shMLL1 Ls174T spheres, scale bars 10µm. **d)** Immunostaining for H3K9me3 (red) and p21 (green) in control and shMLL1 Ls174T spheres, nuclei in blue (DAPI), scale bars 10µm. **e)** Immunostaining for γ-H2A.x (red) in control and shMLL1 Ls174T spheres. Nuclei in blue (DAPI), scale bars 20µm. Quantification on the right, n=12, Mann-Whitney test. **f)** mRNA expression of *p21* (n=4) and *RAC3* (n=2) in control and shMLL1 Ls174T spheres, unpaired t test. **g)** Scheme: The knockdown of MLL1 induces differentiation. Colon cancer stem cells express stem cell genes, GATA6, c-MYC and RAC3. Knockdown of MLL1 reduces their stemness and decreases GATA6 and c-MYC levels, causing upregulation of BMP4 and p21, which mediate differentiation and senescence.

Collectively, the data suggest that Mll1 acts as an upstream regulator of a Gata4/6-Bmp4 axis to sustain the stemness and self-renewal of tumor-propagating intestinal cancer cells. Mll1 promotes *Gata4/6* expression to suppress *Bmp4* and prevent differentiation. The ablation of Mll1 downregulates *Gata4/6*, upregulates the expression of *Bmp4* and enforces differentiation of the cancer stem cells, pushing them to less aggressive fates. In p53-competent cells, the ablation of Mll1 leads to *p21* expression, which may ultimately cause cellular senescence.

3.11 Mll1 controls Wnt and Mapk signalling to specify secretory differentiation.

3.11.1 Mll1 suppresses Mapk signalling and prevents goblet cell differentiation of Wnt-activated cells.

A network of Wnt/β-catenin, Mapk and other signalling pathways guides lineage specification of secretory progenitor cells in the TA zone (compare 1.1.3, page 10). High Wnt signalling in secretory progenitors induces differentiation into Paneth cells and prevents the maturation of goblet cells[64]. The ablation of Mll1 induced differentiation of oncogenic Wnt-activated Lgr5^{+} stem cells and shifted the β-cat^{GOF}/Wnt-imposed Paneth-like identity towards a goblet cell fate, giving rise to double-positive Paneth-goblet cells (see Figure 3.13, page 39). Goblet cell differentiation has been shown to depend on Mapk signalling[64]. Correspondingly, immunohistochemistry staining on sections of β-cat^{GOF}; Mll1$^{+/-}$ and β-cat^{GOF}; Mll1$^{-/-}$ organoids revealed a strong increase in phospho-Erk1/2 levels upon loss of Mll1 (Figure 3.37a, upper panel). Western blotting for phospho-Erk1/2 and phospho-Mek1/2 confirmed an increased activity of the Mapk pathway in β-cat^{GOF}; Mll1$^{-/-}$ organoids compared to β-cat^{GOF}; Mll1$^{+/-}$ organoids (Figure 3.37b). The high Mapk signalling in the β-cat^{GOF}; Mll1$^{-/-}$ organoids correlated with increased numbers of goblet cells and strong mucinous secretion towards the inside of the organoids, as assessed by Alcian blue staining (Figure 3.37a, lower panel, quantification in c). Increased phospho-Erk1/2 levels were also detected in the mutant crypts of β-cat^{GOF}; Mll1$^{-/-}$ mice at 10 days after induction, compared to β-cat^{GOF}; Mll1$^{+/-}$ mice and adjacent non-recombined crypts (Figure 3.37d).

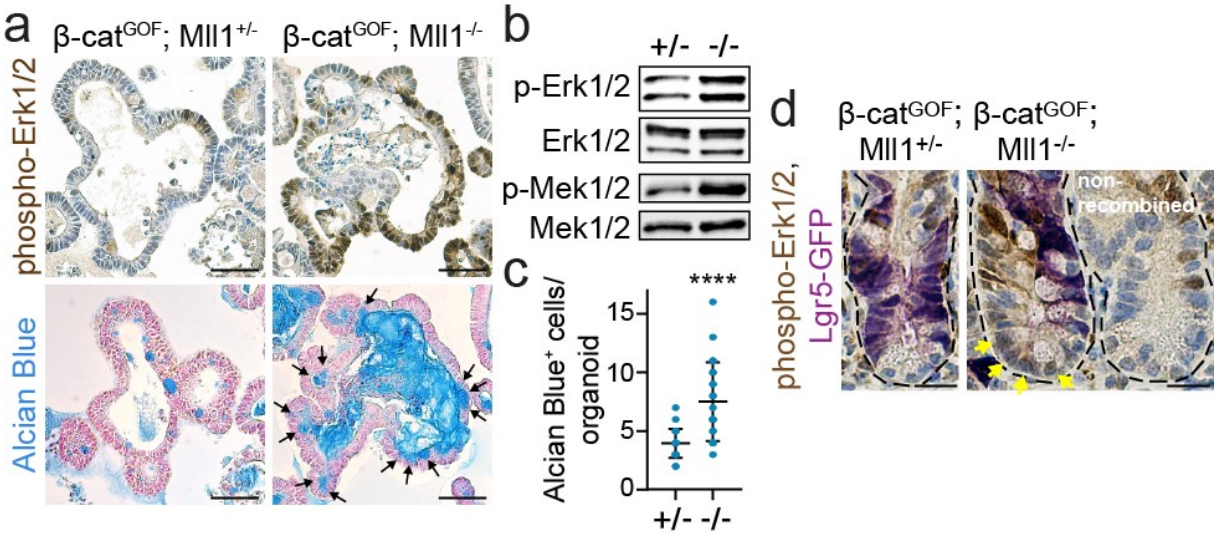

Figure 3.37: The ablation of Mll1 increases Mapk signalling and goblet cell differentiation in β-catenin^{GOF} intestinal organoids and crypts.

a) Immunohistochemistry stainings for phospho-Erk1/2 and Alcian blue stainings on serial sections of β-cat^{GOF}; Mll1$^{+/-}$ and β-cat^{GOF}; Mll1$^{-/-}$ organoids, nuclei counter-stained with hematoxylin and nuclear fast red, scale bars 50µm. Black arrows indicate Alcian blue-positive goblet cells. **b)** Western blot for phospho-Erk1/2 and Erk1/2, phospho-Mek1/2 and Mek1/2 in β-cat^{GOF}; Mll1$^{+/-}$ (+/-) and β-cat^{GOF}; Mll1$^{-/-}$ (-/-) intestinal organoids. **c)** Number of Alcian blue-positive cells in β-cat^{GOF}; Mll1$^{+/-}$ and β-cat^{GOF}; Mll1$^{-/-}$ organoids, quantified from at least 20 organoids, unpaired t test. **d)** Immunohistochemistry staining for

phospho-Erk1/2 and Lgr5-GFP on sections of β-cat^{GOF}; Mll1$^{+/-}$ and β-cat^{GOF}; Mll1$^{-/-}$ intestines at 10 days post-induction compared to adjacent non-recombined crypt, nuclei counter-stained with hematoxylin, scale bars 20µm. Yellow arrows highlight phospho-Erk1/2 in nuclei of β-cat^{GOF}; Mll1$^{-/-}$ crypt cells.

3.11.2 Mll1 controls the Wnt/Mapk-driven differentiation of secretory cells.

We aimed to further examine the role of Mll1 in controlling the Wnt/Mapk-driven differentiation of secretory cells in the intestinal epithelium. To study the role of Mapk, we crossed in the *Mek1DD* allele[221, 222]. Cre-mediated recombination removes a translation stop cassette and activates the expression of a constitutively active gain-of-function variant of *Mek1* (*Mek1DD*) from the *Rosa26* locus (compare Materials and Methods, Figure 5.1d, page 84). We established organoids from the small intestine of Lgr5-EGFP-IRES-Cre^{ERT2}; β-cat^{GOF}; Mek1^{DD}; Mll1$^{flox/+}$ and Lgr5-EGFP-IRES-Cre^{ERT2}; β-cat^{GOF}; Mek1^{DD}; Mll1$^{flox/flox}$ mice (hereafter called β-cat^{GOF}; Mek1^{GOF}; Mll1$^{+/-}$ and β-cat^{GOF}; Mek1^{GOF}; Mll1$^{-/-}$ mice, respectively) and induced the mutagenesis in culture by *in vitro* administration of tamoxifen.

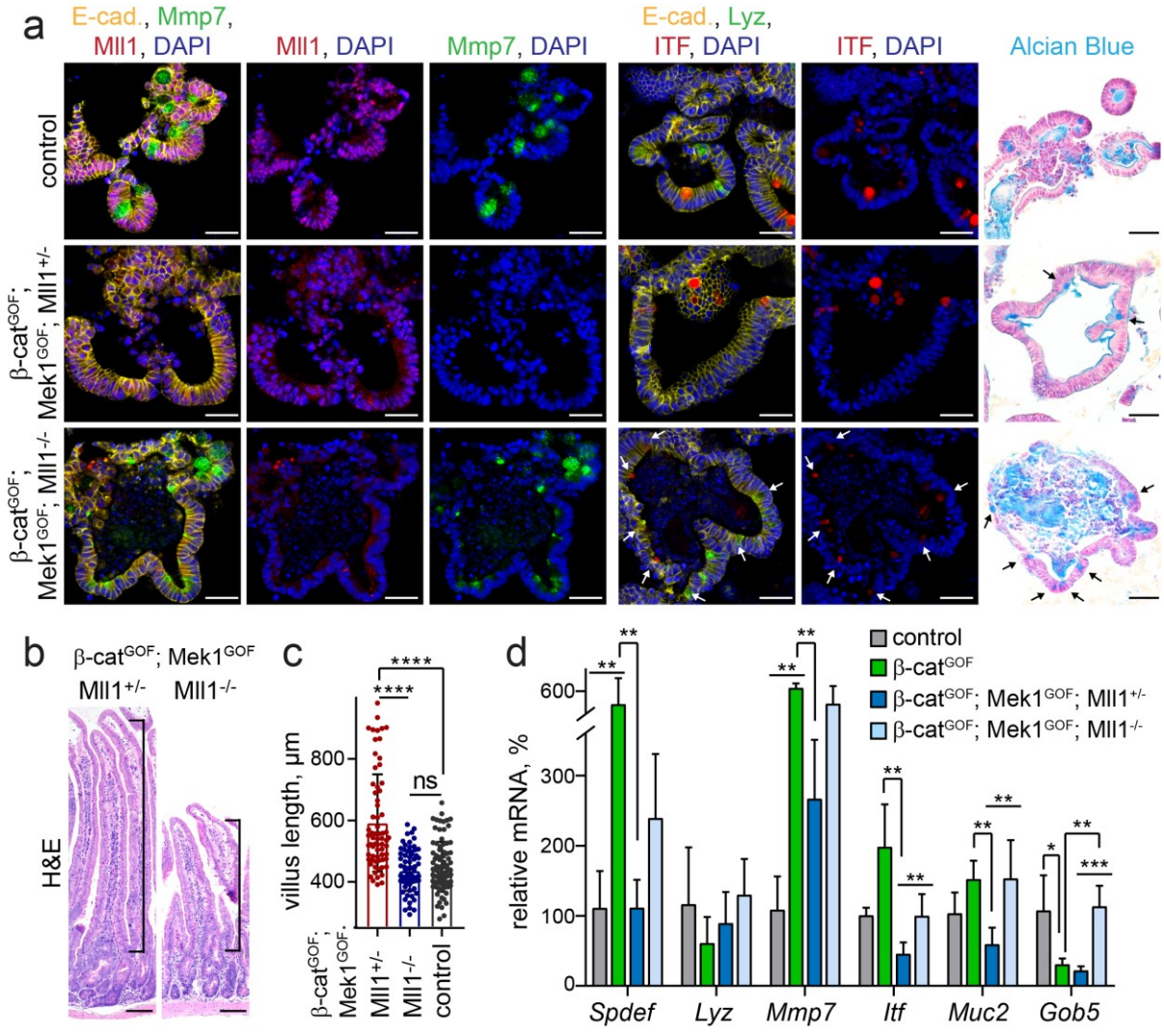

Figure 3.38: Mll1 controls Wnt/Mapk-driven secretory differentiation.
a) Left: immunofluorescence for Mmp7 (green) and Mll1 (red) on sections of non-induced (control) and tamoxifen-induced β-cat^{GOF}; Mek1^{GOF}; Mll1$^{+/-}$ and β-cat^{GOF}; Mek1^{GOF}; Mll1$^{-/-}$ mouse intestinal organoids.

Middle: immunofluorescence staining for Lyz (green) and ITF (red) on sections of organoids of the three genotypes, white arrows indicate cells with weak ITF expression. E-cadherin (yellow) stains cell borders, nuclei in blue (DAPI). Right: Alcian blue staining for goblet cells, nuclear fast red counter-staining, black arrows indicate Alcian blue-positive goblet cells. Scale bars 50µm. **b)** H&E staining on sections of small intestines of β-cat^{GOF}; Mek1^{GOF}; Mll1$^{+/-}$ and β-cat^{GOF}; Mek1^{GOF}; Mll1$^{-/-}$ mice at 20 days after induction with tamoxifen, scale bars 100µm. **c)** Quantification of villus length in β-cat^{GOF}; Mek1^{GOF}; Mll1$^{+/-}$ (n=8) and β-cat^{GOF}; Mek1^{GOF}; Mll1$^{-/-}$ (n=6) mice at 20 days after induction relative to control (wild-type) mice (n=3), at least 10 villi per mouse measured, Mann-Whitney test. **d)** mRNA expression of secretory lineage markers *Spdef*, *Lyz*, *Mmp7*, *Itf*, *Muc2* and *Gob5* in intestines of control (grey, n=3), β-cat^{GOF} (green, n=3), β-cat^{GOF}; Mek1^{GOF}; Mll1$^{+/-}$ (blue, n=5) and β-cat^{GOF}; Mek1^{GOF}; Mll1$^{-/-}$ mice (light blue, n=5) at 20 days after the induction of mutagenesis, unpaired t test.

The simultaneous activation of Wnt and Mapk signalling impaired the maturation of Paneth (Lyz, Mmp7) and goblet cells (Alcian blue) (Figure 3.38a, second panel). Remarkably, Paneth and goblet cells re-appeared in organoids with homozygous ablation of Mll1 (Figure 3.38a, bottom panel). The stabilization of β-catenin and Mek1^{GOF} and the loss of Mll1 were then induced by intraperitoneal injections of tamoxifen in β-cat^{GOF}; Mek1^{GOF}; Mll1$^{+/-}$ and β-cat^{GOF}; Mek1^{GOF}; Mll1$^{-/-}$ mice. The intestines of β-cat^{GOF}; Mek1^{GOF}; Mll1$^{+/-}$ mice became dysplastic and exhibited elongated villi (Figure 3.38b left, quantification in c). The mice did not survive beyond 20 days after the induction of mutagenesis. Homozygous ablation of Mll1 attenuated the β-cat^{GOF}; Mek1^{GOF}-induced hyperplastic phenotype. The villi were of normal (wild-type) length (Figure 3.38b right, quantification in c).

Wnt signalling maintains intestinal stem and progenitor cells and induces differentiation of secretory Paneth cells, while it prevents the maturation of goblet cells[64]. In the intestines of β-cat^{GOF} mice, we observed an increased expression of the Paneth cell marker *Mmp7* and the secretory lineage marker *Spdef*, whereas the goblet cell marker *Gob5* strongly decreased (Figure 3.38d). The expression of *Lyz*, which is specific for mature Paneth cells, was not increased, indicating an immature nature of the Paneth cells. High Mapk signalling impedes differentiation of Paneth cells and shifts secretory cell specification towards a goblet fate[64]. Interestingly, simultaneous activation of Wnt and Mapk signalling in β-cat^{GOF}; Mek1^{GOF}; Mll1$^{+/-}$ mice on the one hand decreased *Mmp7* expression and reverted the β-cat^{GOF}-induced expression of *Spdef* to control levels, and on the other hand reduced the expression of the goblet cell markers *Itf*, *Muc2* and *Gob5* (Figure 3.38d). This indicates that the opposing Wnt and Mapk signalling activities work against each other, disturbing the maturation of both Paneth and goblet cells, as was also observed in the organoids (Figure 3.38a, second panel) and proposed by Heuberger et al. (2014)[64] (compare 1.1.3, page 10). The ablation of Mll1 in β-cat^{GOF}; Mek1^{GOF}; Mll1$^{-/-}$ mice re-established secretory cell differentiation, as demonstrated by upregulation of *Spdef* and the Paneth cell-specific *Mmp7*, and by expression of the goblet cell markers *Itf*, *Muc2* and *Gob5* (Figure 3.38d). This fits our observations in organoids, where both Paneth and goblet cells re-appeared upon ablation of Mll1; the re-appearing cells were largely double-positive for Paneth and goblet cell markers (Figure 3.38a, lower panel). In

summary, these data demonstrate that Mll1 keeps intestinal epithelial cells in an immature state and a decrease in Mll1 expression is necessary to allow for secretory differentiation. Our data further indicate that Mll1 also plays a role in controlling the Wnt/Mapk-driven specification of Paneth and goblet cells. In β-cat^{GOF} crypts, Mll1 suppressed a Mapk-induced goblet cell differentiation. The ablation of Mll1 unleashed Mapk signalling, giving rise to mixed Paneth-goblet cells.

3.11.3 Mll1 promotes the crypt proliferation and restricts the goblet cell differentiation driven by Mapk signalling.

To gain deeper insights into the role of Mll1 in the Mapk-driven goblet cell differentiation, we analysed *Mek1DD* mice with heterozygous and homozygous ablation of Mll1 (compare Materials and Methods, Figure 5.1c, page 84), Lgr5-EGFP-IRES-Cre^{ERT2}; Mek1^{DD}; Mll1$^{flox/+}$ and Lgr5-EGFP-IRES-Cre^{ERT2}; Mek1^{DD}; Mll1$^{flox/flox}$ mice, (hereafter called Mek1^{GOF}; Mll1$^{+/-}$ and Mek1^{GOF}; Mll1$^{-/-}$, respectively) at 10 days after the induction of mutagenesis. Activation of Mapk signalling by Mek1^{GOF} in Mek1^{GOF}; Mll1$^{+/-}$ mice increased the proliferation of crypt cells, as seen through an increase in the incorporation of BrdU in mutant eGFP-positive crypts compared to adjacent non-recombined crypts (Figure 3.39a, upper panel, quantification in b). The eGFP is co-expressed with Mek1^{GOF} from an IRES-EGFP linked to the *Mek1DD* allele[221, 222] and allows to distinguish recombined from non-recombined crypts. Of note, in Lgr5-EGFP-IRES-Cre^{ERT2}; Mek1^{DD} mice the eGFP also identifies Lgr5-GFP^{+} stem cells[15]. High Mapk signalling in the crypts decreased the number of Paneth cells, as shown by immunostaining for the Paneth cell marker Lyz on serial sections of adjacent recombined and non-recombined crypts (Figure 3.39c, upper left). Mmp7 staining revealed the presence of secretory Paneth-like cells further up in the crypts (Figure 3.39c, upper middle). Mek1^{GOF}; Mll1$^{+/-}$ crypts did not show a strong increase in goblet cells, as revealed by ITF and Alcian Blue staining compared to adjacent non-recombined crypts (Figure 3.39c, upper panel, quantification in d).

The homozygous ablation of Mll1 in Mek1^{GOF}; Mll1$^{-/-}$ mice prevented the Mek1^{GOF}-induced hyper-proliferation of crypt cells (Figure 3.39a, lower panel, quantification in b). Proliferation was restricted to the crypt bottom. Mek1^{GOF}; Mll1$^{-/-}$ crypts were filled with secretory cells, which were positive for the Paneth cell marker Mmp7 and exhibited a strong expression of goblet cell markers (ITF, Alcian Blue) (Figure 3.39c, lower panel, quantification in d). The loss of Mll1 did not interfere with the activity of Mapk signalling, as shown by immunohistochemistry for phospho-Erk1/2 in the mutant crypts of Mek1^{GOF}; Mll1$^{-/-}$ mice compared to Mek1^{GOF}; Mll1$^{+/-}$ mice (Figure 3.39c, right panel). Like in Mek1^{GOF}; Mll1$^{+/-}$ crypts, the strong Mapk activity in Mek1^{GOF}; Mll1$^{-/-}$ crypts reduced the number of Paneth cells at the crypt bottom to one (Figure 3.39c, left panel).

These results confirm that high Mapk signalling counteracts the Wnt-induced differentiation of Paneth cells and favours goblet cell differentiation, as had been reported by Heuberger et

al. (2014)[64]. They further reveal that the effect of Mapk signalling depends on the level of Mll1 expression. In the presence of Mll1, Mapk signalling promotes crypt cell proliferation. Loss of Mll1 is required for the Mapk-induced specification of goblet cells. Accordingly, Mll1 restricts the Wnt/Mapk-driven secretory differentiation to sustain stem and progenitor cells in the intestinal epithelium. Mll1-deficient secretory cells in Mek1^{GOF}; Mll1$^{-/-}$ crypts were double-positive for Paneth and goblet cell markers and did not fully mature into goblet cells, despite a strong activity of Mapk signalling. This indicates that Mll1 also plays a role in safe-guarding the Wnt/Mapk-driven differentiation of secretory cells by preserving lineage-specific maturation.

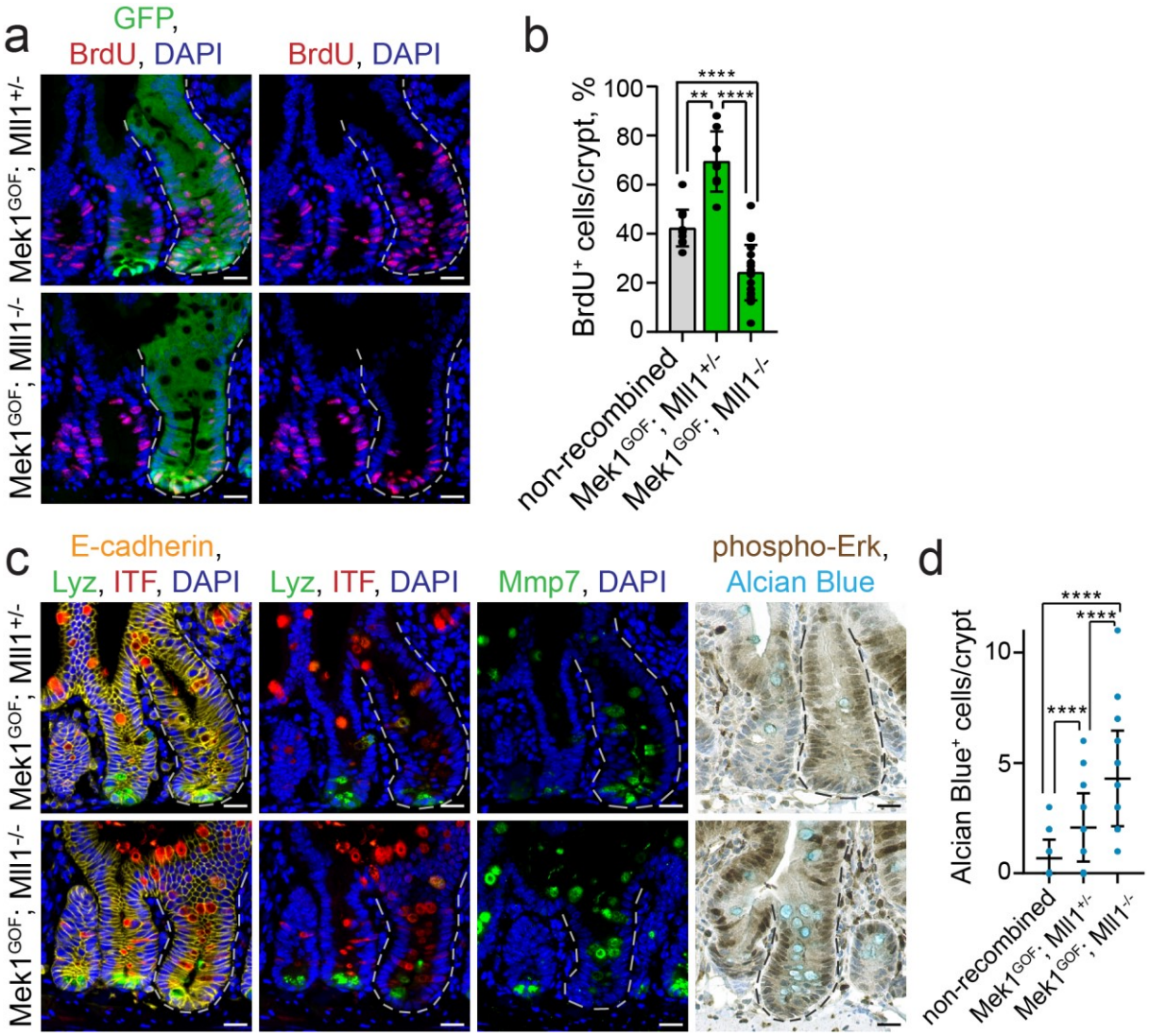

Figure 3.39: Mll1 restricts the Mapk-induced specification of goblet cells.
a) Immunofluorescence for BrdU (red) and GFP (green) in crypts of Mek1^{GOF}; Mll1$^{+/-}$ mice and Mek1^{GOF}; Mll1$^{-/-}$ mice at day 10 after induction, nuclei in blue (DAPI), scale bars 20µm. Recombined crypts are surrounded by dashed lines. BrdU was incorporated for 2h before sacrifice. **b)** Quantification of BrdU^{+} cells per total cells in mutant crypts of Mek1^{GOF}; Mll1$^{+/-}$ mice and Mek1^{GOF}; Mll1$^{-/-}$ mice compared to adjacent non-recombined crypts, n=2 mice each, Mann-Whitney test. **c)** Left: immunofluorescence for Lyz (green) and ITF (red) on sections of Mek1^{GOF}; Mll1$^{+/-}$ and Mek1^{GOF}; Mll1$^{-/-}$ mouse small intestine at 10 days after induction. Middle: immunofluorescence staining for Mmp7 (green) on serial sections. E-cadherin (yellow) stains cell borders, nuclei in blue (DAPI), scale bars 20µm. Recombined crypts

surrounded by dashed lines. Right: immunohistochemistry for phospho-Erk1/2 and Alcian blue staining for goblet cells, nuclei counter-stained with hematoxylin, scale bars 20µm. **d)** Number of Alcian blue-positive cells in Mek1^{GOF}; Mll1$^{+/-}$ and Mek1^{GOF}; Mll1$^{-/-}$ crypts compared to adjacent non-recombined crypts, quantified from at least 20 crypts per mouse, n=3 mice each, Mann-Whitney test.

3.12 Translational approaches: Targeting MLL1 in colon cancer.

We investigated the effect of MLL1 inhibition in Wnt-dependent colon cancer cells and intestinal organoids *in vitro*. Previous research in our lab had demonstrated a direct interaction of MLL1 and β-catenin/TCF4 in Wnt-driven cancer cells[162]. That is why we treated human Ls174T colon cancer cells with inhibitors of the MLL1/β-catenin/TCF4 complex, ICG-001[101], LF3[100] and MI-2[147] (Figure 3.40a). Control cells expanded into cell colonies within 14 days, while inhibition of Wnt signalling with the β-catenin-CBP inhibitor ICG-001 and the β-catenin-TCF4 inhibitor LF3 completely blocked colony formation (Figure 3.40b). Treatment with the Menin-MLL1/2 inhibitor MI-2 was as efficient in preventing colony formation as the treatment with the Wnt inhibitors (Figure 3.40c). MI-2 and ICG-001 treatment impaired Ls174T colon cancer sphere formation in a concentration-dependent manner (Figure 3.40d). MI-2 treatment significantly impaired sphere formation of Ls174T colon cancer cells within 48h (Figure 3.40e).

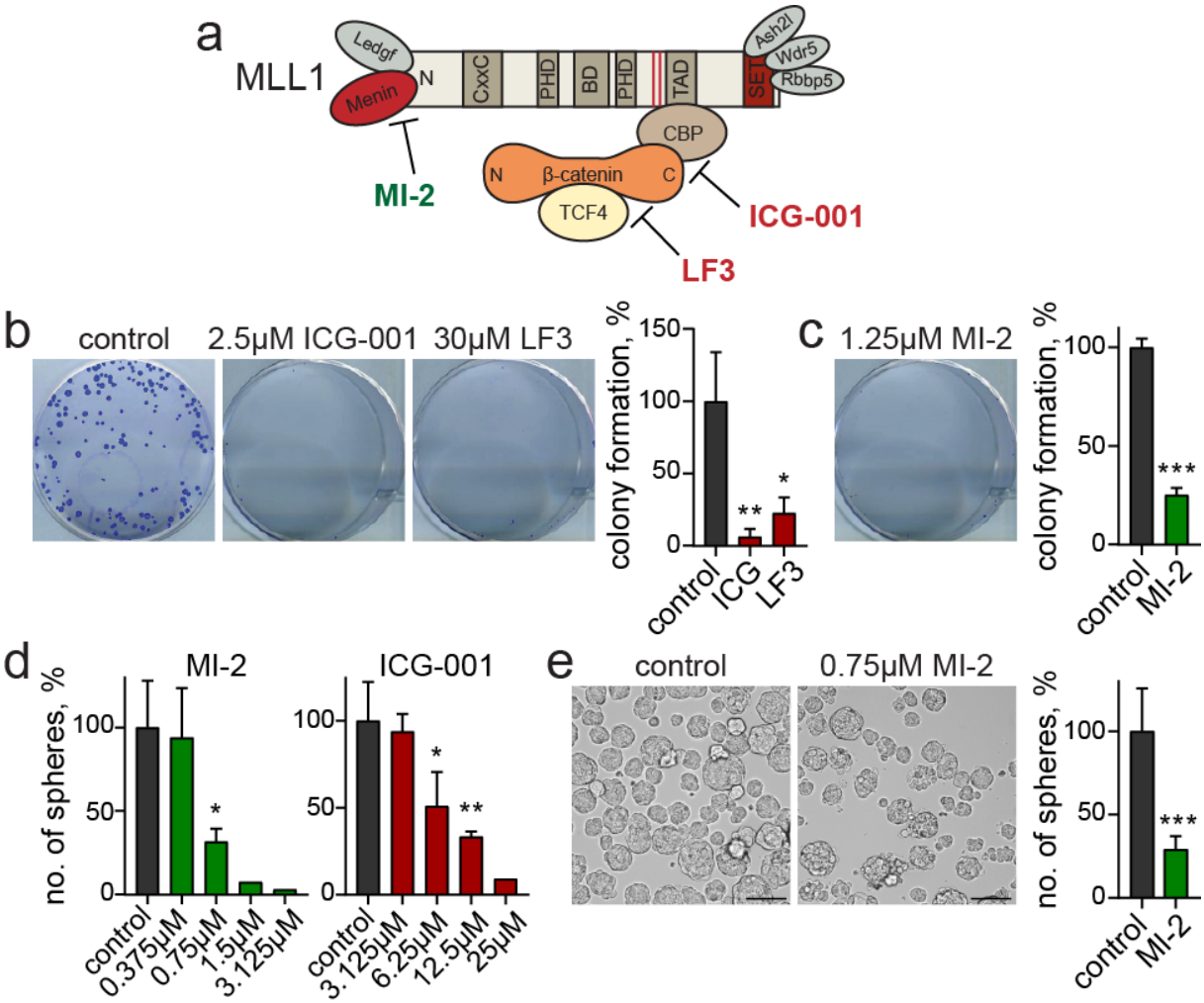

Figure 3.40: Pharmacological interference with the MLL1/β-catenin/TCF4 complex.

a) Scheme: Small molecules interfering with the MLL1-β-catenin/TCF4 complex, the Wnt inhibitors ICG-001 and LF3 and the Menin inhibitor-2 (MI-2). **b)** Colony formation from Ls174T human colon cancer cells treated with 2.5μM ICG-001 or 30μM LF3 for 13 days compared to control cells. Quantification on the right, n=4 from two independent assays, unpaired t test. **c)** Colony formation from Ls174T cells treated with 1.25μM MI-2 for 13 days. Quantification relative to control on the right, n=4 from two independent assays, unpaired t test. **d)** Numbers of Ls174T colon cancer spheres >50μm relative to control after 48h of MI-2 and ICG-001 treatment at indicated concentrations, n=3 from two independent assays, unpaired t test. **e)** Brightfield images of control and 48h MI-2-treated Ls174T spheres, scale bars 75μm. Quantification of spheres >50μm on the right, n=7 from two independent assays, unpaired t test.

Treatment of tamoxifen-induced Lgr5-EGFP-IRES-Cre^{ERT2}; β-cat^{GOF} intestinal organoids with increasing concentrations of MI-2 reduced cell viability and resulted in death of the β-cat^{GOF} organoids within 3-4 days in a concentration-dependent manner (Figure 3.41a). MI-2 treatment did not prevent the β-cat^{GOF}-induced expansion of the Lgr5-GFP^{+} stem cell niches until the death of the organoids at 72h (Figure 3.41b).

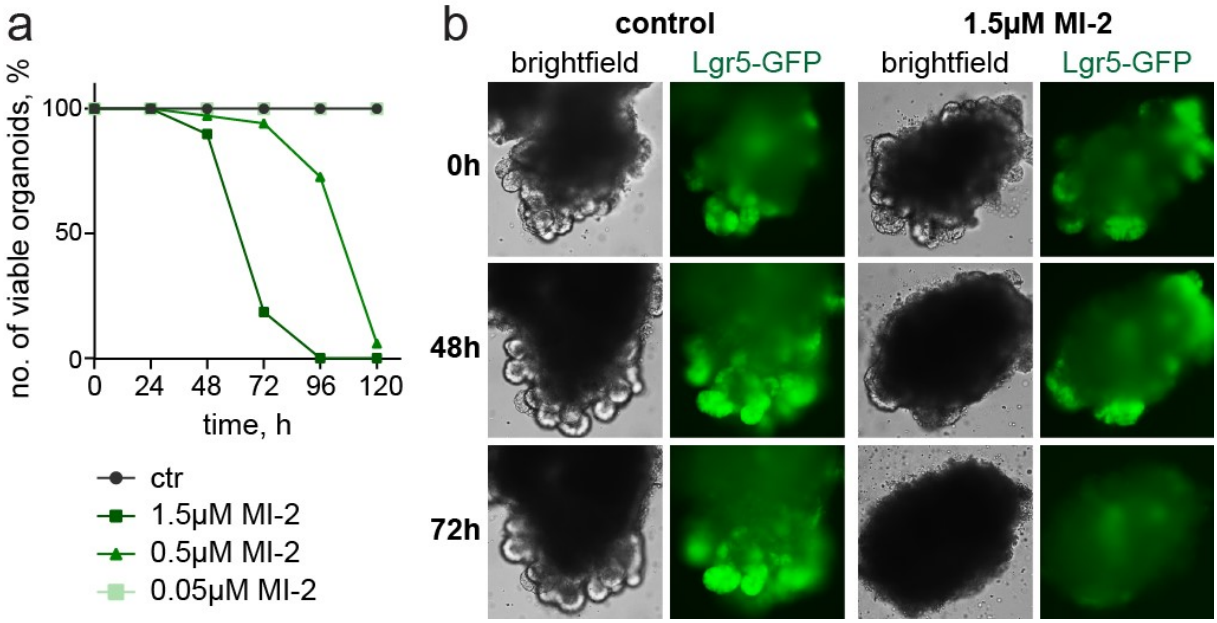

Figure 3.41: MI-2 treatment of β-catenin^{GOF} intestinal organoids.
a) Viability of tamoxifen-induced Lgr5-GFP-IRES-Cre^{ERT2}; β-cat^{GOF} mouse intestinal organoids treated with MI-2 at indicated concentrations, relative to control. **b)** Live imaging of tamoxifen-induced Lgr5-GFP-IRES-Cre^{ERT2}; β-cat^{GOF} control and 1.5μM MI-2-treated organoids at 0h, 48h and 72h. Lgr5-GFP (green) marks intestinal stem cells.

4 Discussion

The work presented in this doctoral thesis identifies the epigenetic modifier Mll1 as an essential regulator in Wnt/β-catenin-driven intestinal tumors. A detailed knowledge of the oncogenic signalling and gene regulatory processes in colon cancer cells is crucial for the future development of rational therapies. Our study demonstrates the critical role of epigenetic regulation in colon cancer growth by dissecting the role of Mll1 in Wnt/β-catenin-induced cancer stemness, which is expected to shape future therapeutic approaches.

About 90% of human colon cancers exhibit mutations in APC or β-catenin which deregulate Wnt signalling and initiate intestinal transformation[77]. The impact of aberrant Wnt signalling on colon cancer growth and progression is well studied. Little is known, however, on the epigenetic regulation of Wnt-induced intestinal tumorigenesis. Recent work has implicated the histone methyltransferase Mll1 in the Wnt/β-catenin-dependent growth of solid tumors of the salivary gland[162, 178], but a proposed role for Mll1 in Wnt-induced cancer stemness remained mechanistically undefined. By conditional genetic ablation in a stem cell-based intestinal mouse tumor model and by RNA interference in self-renewing sphere cultures and xenografts of human colon cancer cells, we now demonstrated a crucial role of Mll1 in Wnt/β-catenin-driven intestinal tumor formation and cancer stemness. We showed that Mll1 promotes the β-catenin^{GOF}-induced expansion of Lgr5^{+} intestinal tumor-initiating cells. Mechanistically, Mll1 does not interfere with the global activity of Wnt signalling, but controls its outcome at the level of gene regulation. Mll1 sustains the expression of stem cell genes in Wnt-activated tumor cells by antagonizing PcG-mediated silencing. We further identified Mll1 as an upstream regulator of Gata4/6 transcription factors that promote stemness of Wnt-mutated cancer cells and counter differentiation. Cancer stem cells were depleted upon loss of Mll1.

4.1 Mll1 is essential for the β-catenin^{GOF}-induced intestinal stem cell expansion and tumorigenesis.

We showed that Mll1 promotes the β-catenin^{GOF}-induced expansion of Lgr5^{+} intestinal stem cells, which initiates tumor formation. Intestinal stem cells at homeostasis divide symmetrically and produce an excess of daughter stem cells that maintain the stem cell pool in the crypts and ensure the continuous production of progenitor cells[223]. The niche space at the crypt base is limited. To compensate for overcrowding, surplus stem cells are randomly expelled from the crypt base and differentiate. The intestinal stem cell pool is thus not long-lived but highly dynamic and subject to constant stochastic replacement, the ‘neutral drift’. These neutral drift kinetics drive polyclonal crypts towards monoclonality within 1-6 months in adult mice[223, 224]. Genetic alterations causing activation of Wnt signalling are gatekeeper mutations in intestinal transformation and major drivers of intestinal tumorigenesis[2]. Aberrant activation of Wnt signalling in a crypt stem cell, e.g. by β-cat^{GOF}, biases the neutral drift kinetics operating in the

stem cell niche[225, 226]. The β-cat^{GOF} mutation confers a selective advantage to the particular stem cell. As a consequence, the mutated stem cell displaces non-mutated stem cells and takes over the crypt. The aberrant Wnt signalling then expands the mutant stem cell niches[227]. Such enlarged mutant crypts are highly prone to multiply by crypt fission, spreading Wnt-mutated stem cells across the epithelium[227]. The tumorigenic stem cells are capable of expanding independently of the crypt-based stem cell niche to initiate tumor formation[79, 86]. The cell-intrinsic molecular features required for the niche-independent growth of β-cat^{GOF}-mutant stem cells remained unclear. Recent years have revealed epigenetic regulation as a critical determinant of adult stem cell function[228]. The polycomb repressive complex PRC1 has been shown to be crucial for adult intestinal stem cell maintenance, intestinal homeostasis and tissue identity[140]. Genetic inactivation of PRC1 in oncogenic Wnt-activated intestinal stem cells has a tumor-preventive effect[140], implying a role of PRC1 in promoting Wnt-driven intestinal tumorigenesis.

We now identified the epigenetic modifier Mll1 as an essential cell-intrinsic determinant of the oncogenic Wnt/β-catenin-driven stem cell expansion. The conditional ablation of Mll1 prevented the β-catenin^{GOF}-induced expansion of Lgr5^{+} stem cells and tumorigenesis in an intestinal mouse tumor model. The knockdown of Mll1 in human colon cancer xenografts impaired tumor formation and growth, and slowed down tumor progression. Thus, the epigenetic regulation by Mll1 is crucial for the initiation and growth of Wnt-driven colon cancer. Mll1-deficient cells did not undergo apoptosis, but exhibited a reduced proliferation, as β-cat^{GOF}; Mll1$^{-/-}$ stem cells in mice and organoids showed a diminished incorporation of the thymidine analogues BrdU and EdU. According to the neutral drift kinetics, a reduced proliferation would exclude Mll1-deficient stem cells from the crypt stem cell pool, thus eliminating the β-cat^{GOF}-mutant tumor-initiating stem cells and preventing tumorigenesis. However, entire crypts rather than individual stem cells were deficient for Mll1 after 5-10 days of induction and the proliferative and self-renewal capacities of β-cat^{GOF}; Mll1$^{-/-}$ cells were only gradually lost. Hence, the β-cat^{GOF}; Mll1$^{-/-}$ stem cells retained their potential to divide, although in a slowed-down manner, persisted in the crypts and generated Mll1-deficient progeny up to 100 days after the induction of mutagenesis. Consequently, the minor reduction in stem cell proliferation upon ablation of Mll1 is unlikely to solely account for the prevention of the β-catenin^{GOF}-driven stem cell expansion. Our studies in organoids confirmed that the loss of Mll1 did not immediately eliminate β-cat^{GOF} stem cells but progressively exhausted their stemness. The ablation of Mll1 did not globally alter oncogenic Wnt signalling, as assessed by a TCF/LEF luciferase reporter assay in shMLL1 human colon cancer cells. Mll1-deficient stem cells in β-cat^{GOF}; Mll1$^{-/-}$ mice exhibited nuclear β-catenin and highly expressed classical Wnt target genes such as *Axin2*. Despite functional β-cat^{GOF} activity, though, the β-cat^{GOF}; Mll1$^{-/-}$ stem cells were unable to expand niche-independently to form tumors, indicating that the

oncogenic Wnt activity *per se* is incapable of promoting cancer stemness but relies on a permissive epigenetic setting. The presence of Mll1 is a prerequisite for the oncogenic Wnt-induced intestinal cancer stemness. Our data propose that Mll1 promotes the β-catenin^{GOF}-induced stem cell expansion and tumorigenesis by directly controlling the expression of key stem cell genes and preventing differentiation of tumor-initiating stem cells.

4.2 Mll1 sustains oncogenic Wnt-induced stem cell gene expression and colon cancer stemness.

Colon cancer cells with a stem-like gene expression profile possess high tumor-initiating potential and self-renewal capacity[89], implying that intestinal stem cell gene products play an instrumental role in tumorigenesis. We discovered that Mll1 sustains the expression of the intestinal stem cell genes *Lgr5*, *Smoc2*, *Igfbp4* and *Olfm4* in oncogenic Wnt-activated cells. Expression of *Lgr5* correlates with the malignant potential of colon cancer cells. Colon tumors with increased *Lgr5* levels are more invasive and aggressive[229]. Wnt/β-catenin signalling is known to directly activate the expression of the stem cell genes *Lgr5*, *Ascl2* and *Cd44* [107]. In addition, the Wnt pathway cross-talks with other signalling pathways such as NF-κB to induce the expression of stem cell genes like *Smoc2* [94]. Thus, Wnt signalling imposes a stem-like identity on colon cancer cells[82]. In accordance, we found that the β-catenin^{GOF}-driven adenomas in β-cat^{GOF} mice exhibited an increased expression of the β-catenin/Tcf4-regulated stem cell gene *Lgr5* as well as the NF-κB-induced *Smoc2*. Our study identified the histone methyltransferase Mll1 as an essential epigenetic regulator of the Wnt-induced colon cancer stemness. Mll1 did not merely regulate Wnt target genes, but controlled the expression of both the β-catenin/Tcf4-dependent *Lgr5* and β-catenin/Tcf4-independent stem cell genes such as *Smoc2*, *Igfbp4* and *Olfm4*. We detected a strong correlation of MLL1 expression with high levels of nuclear β-catenin in human colon carcinomas. Likewise, β-cat^{GOF} tumor cells showed elevated levels of Mll1. Wnt3a treatment increased *Mll1* expression in intestinal organoids, suggesting a Wnt-controlled regulation of *Mll1*. This is consistent with a previous study in Wnt/β-cat^{GOF}; Bmpr1a^{LOF} salivary gland and head and neck cancer that proposed a Wnt-driven upregulation of Mll1 and identified functional Tcf4 binding sites in regulatory regions upstream of the *Mll1* promoter[162]. The ablation of Mll1 hampered the ability of β-cat^{GOF} to confer a stem-like identity and to promote self-renewal of colon cancer cells. Our data demonstrate that the high expression of Mll1 in Wnt-activated tumor cells is essential to promote a stem-like identity and sustain Wnt-induced colon cancer stemness.

4.3 Mll1 antagonizes Polycomb-dependent silencing to sustain the expression of stem cell genes.

We identified Mll1 as an epigenetic regulator of a panel of intestinal stem cell genes. Mll1 knockdown resulted in a switch of the histone methylation marks at the TSS of the stem cell genes *Lgr5, Smoc2, Igfbp4* and *Olfm4* from activating H3K4me3 to repressive H3K27me3. To exert its regulatory functions on chromatin, Mll1 can act through its intrinsic methyltransferase activity, recruitment of acetyltransferases or antagonism of polycomb repressive factors. Mll1 is known to prevent PRC2-mediated H3K27me3 and gene silencing[230]. Our data suggest that the ablation of Mll1 vacated a PRC2 binding site or unleashed PRC2 activity at the *Lgr5, Smoc2, Igfbp4* and *Olfm4* promoters, allowing for PRC2-mediated H3K27 tri-methylation and gene silencing. CpG-dense regions have been identified as the main target sites for Mll1-deposited H3K4 methylation, antagonizing PRC2-dependent H3K27me3 at these sites[230]. In agreement, the intestinal stem cell genes *Lgr5*, *Smoc2* and *Igfbp4* identified here as Mll1 targets possess CpG islands around their TSS. Strikingly, the inhibition of the polycomb H3K27 tri-methyltransferase Ezh2 with Gsk126[209] partially restored the expression of *Lgr5* and the other stem cell genes in Mll1-deficient cells despite the absence of Mll1 and H3K4me3 marks. This implies that Mll1 and its H3K4me3 activity are dispensable for initiating the expression of the stem cell genes but crucial for preventing PRC2-mediated silencing of the *Lgr5* and other stem cell promoters[231]. These observations concord with the opposition between trithorax and Polycomb group proteins in *Drosophila*[232]. Acetylation of H3K27 (H3K27ac) by the histone acetyltransferase CBP has been shown to initiate the expression of PcG-repressed genes upon depletion of H3K27 methylation marks[233]. This might account for the re-activation of *Lgr5*, *Smoc2*, *Igfbp4* and *Olfm4* in Mll1 knockdown cells upon Gsk126 treatment.

The ablation of Mll1 eliminated cancer stemness and prevented Wnt-driven tumor growth. Remarkably, the genetic inactivation of the polycomb complex PRC1 in oncogenic Wnt-activated intestinal stem cells also has a tumor-preventive effect[140]. Further, PRC2 ablation in the mouse intestine causes loss of stem cells and aberrant secretory differentiation by deregulating Wnt signalling and cell proliferation[234]. In the light of our data, this indicates that a fine-tuned balance of active and repressive histone modifications controlled by the Mll1-PcG antagonism is essential for the maintenance of intestinal stem and tumor-initiating cells, a regulatory mechanism of stemness in which Mll1 is crucially involved.

The finding that Mll1 is required as an anti-silencing factor for maintaining and stabilizing stem cell gene expression is consistent with the emerging concept that H3K4 tri-methylation is essential for stabilizing gene expression rather than initiating transcription[124, 125]. A recent study has highlighted the importance of the non-catalytic co-activator functions of TrxG complexes: in pancreas development, the promoter binding of TrxG proteins such as Mll1 is critical for lineage specification, but their H3K4 methyltransferase activity is dispensable for the activation

of lineage-specific genes[235]. The tri-methylation of H3K4 by TrxG complexes proved essential, however, for stabilizing transcriptional activity and maintaining lineage-specific expression patterns[235]. In the postnatal brain, Mll1 maintains the expression of the ventral transcription factor *Nkx2-1* to sustain the regional identity of ventral neural stem cells and distinguish them from dorsal cells[236]. Even transient interference with Mll1 function durably abolishes *Nkx2-1* expression and ventral identity, as Mll1 fails to re-initiate *Nkx2-1* expression[236]. The role of Mll1 in transcriptional maintenance rather than initiation of intestinal stem cell gene expression complies with our observations in organoids and the *in vivo* Lgr5-GFP^{+} stem cell tracing: β-cat^{GOF}; Mll1$^{-/-}$ intestinal stem cells retained their Lgr5-GFP expression and stemness as long as they persisted in the crypt stem cell niche, but were unable to sustain the expression of *Lgr5* and other stem cell genes independent of the niche. Mll1-deficient β-cat^{GOF} stem cells differentiated once they left the stemness-promoting niche environment.

4.4 Mll1-deficient cancer cells lose their stemness and differentiate.

Transcriptome profiling of β-cat^{GOF}; Mll1$^{-/-}$ stem cells identified the transcription factors Foxa1 and Gata4/6 as Mll1-regulated genes in β-cat^{GOF} intestinal stem cells and Wnt-mutated colon cancer cells. Both transcription factors have been implicated in the regulation of stemness: Foxa1 maintains the identity of intestinal stem and progenitor cells in *Drosophila*[237]. High expression of Foxa1 is observed in poorly differentiated colon cancer[238]. The Gata transcription factors Gata4 and Gata6 maintain jejunal-ileal identities in the adult intestine and promote proliferation in intestinal crypts[211, 239]. A recent study has linked Gata6 to the regulation of stemness in Wnt-driven colon cancer[203]. Our data suggest that Mll1 sustains the stemness of Wnt-mutated intestinal stem cells by controlling the expression of stem cell genes and the stemness-promoting transcription factors *Gata4/6*. High levels of Mll1 are essential for Wnt-activated colon cancer cells to sustain a non-differentiated stem-like state.

The transcriptome profiling of β-cat^{GOF}; Mll1$^{-/-}$ stem cells further revealed an increase in the expression of differentiation markers upon ablation of Mll1. The loss of Mll1 also enforced differentiation of human colon cancer cells in sphere cultures and xenograft tumors. Mll1 knockdown colon cancer cells showed a decreased expression of *Gata6* that was associated with an upregulation of *Bmp4*. Gata6 has been reported to compete with β-catenin/Tcf4 for binding to a distal regulatory region of the *Bmp4* locus, sustaining stemness and preventing a Bmp4-induced differentiation of colon cancer cells[203]. Besides Bmp signalling, secretory differentiation in the intestinal epithelium depends on the expression of Atoh1, a transcription factor that instructs secretory lineage specification and promotes a goblet cell differentiation programme[54, 56]. The β-cat^{GOF}; Mll1$^{-/-}$ stem cells exhibited a strongly increased expression of *Atoh1*. Atoh1 has been shown to act as a tumor suppressor in colorectal neoplasia and is frequently silenced in colon cancer cells[240]. Increased Atoh1 levels and goblet cell numbers have been observed in Gata4-deficient intestines[211, 241]. Similar to our observations in β-cat^{GOF};

Mll1$^{-/-}$ stem cells, the ablation of Gata4 increases *Atoh1* levels independent of a decreased expression of *Hes1* and other Notch target genes[241], indicating that Gata4 can directly repress *Atoh1*. Our data support a Gata4-mediated restriction of *Atoh1* expression and goblet cell differentiation. The β-cat^{GOF}; Mll1$^{-/-}$ organoids and crypts exhibited an increased activity of Mapk signalling. The high Mapk activity in β-cat^{GOF}; Mll1$^{-/-}$ cells imposed a goblet cell-like identity on the Wnt-activated stem cells, giving rise to mixed Paneth-goblet cells, as previously suggested by Heuberger et al. (2014)[64]. The Mapk-induced goblet cell differentiation was supported by the increased levels of Atoh1 and Bmp4 in the Mll1-deficient cancer cells. Bmp4 treatment of intestinal organoids induced the expression of goblet cell-specific genes, while it decreased the expression of Paneth cell markers. Taken together, we here identified Mll1 as an upstream epigenetic regulator of the Gata4/6-mediated repression of Bmp4, Atoh1, Mapk signalling and goblet cell differentiation.

Remarkably, the high Wnt activity caused by β-cat^{GOF} imposed a Paneth-like identity on the β-cat^{GOF}; Mll1$^{+/-}$ stem cells. This proposes that the cells-of-origin of intestinal cancer might not be “pure” stem cells but rather stem cells that exhibit Paneth-like properties. We may speculate that a population of tumor-initiating stem cells with a Paneth-like identity intrinsically has all the attributes to expand niche-independently and initiate tumorigenesis. In the crypt stem cell niche, Paneth cells support Lgr5^{+} intestinal stem cells by providing essential niche ligands, growth factors such as Wnt3 and EGF, and metabolic supply[48, 242]. Paneth cells can convert into functional stem cells under regenerative conditions[73]. The priming towards a Paneth fate might thus drive tumor formation by creating a self-supporting system that expands independently of a crypt-based niche. Consistent with the idea of a requirement of a Paneth-like identity for the expansion and tumorigenicity of Wnt-mutated intestinal stem cells, colon cancer cells have been shown to require ligand-dependent Wnt signalling for the maintenance of a stem-like behaviour, even in case of mutations in the downstream Wnt effectors APC or β-catenin[243]. Our data revealed that Mll1 is essential for the Paneth-like behaviour and stemness of the β-cat^{GOF} stem cells. The ablation of Mll1 shifted the Paneth-like identity of the β-cat^{GOF} stem cells to a goblet cell fate in an Atoh1- and Mapk-driven manner. This rendered the β-cat^{GOF}; Mll1$^{-/-}$ stem cells incapable of niche-independent expansion and caused a progressive exhaustion of the Mll1-deficient stem cells which were ultimately lost by differentiation. Correspondingly, high Mapk signalling has previously been shown to exhaust intestinal stem cells by converting them into proliferative TA cells[244]. It is remarkable that the Mll1-deficient Atoh1^{+} stem cells failed to sustain their stemness, since Atoh1^{+} secretory progenitor cells have been attributed a high plasticity that renders the cells capable of acquiring functional stem cell properties and promoting tumorigenesis[70, 71]. Apparently, the loss of Mll1 abolished the cellular plasticity of Atoh1^{+} progenitor cells, as β-cat^{GOF}; Mll1$^{-/-}$ crypts did not expand into tumors.

Taken together, our data show that Wnt-activated intestinal stem cells depend on high levels of Mll1 to sustain stemness, a Paneth cell-like fate and cellular plasticity, which are required for niche-independent growth and tumorigenicity. A role of Mll1 in fine-tuning the specification of Paneth cells while restricting a goblet cell fate contributes to its tumor-promoting function in the intestinal epithelium. Our data do not indicate whether the main function of Mll1 in intestinal cancer stem cells is to sustain stem cell gene expression or to prevent differentiation. The RNA sequencing of isolated $Lgr5^{+}$ stem cells at 10 days after genetic recombination did not identify a decreased expression of the stem cell genes *Lgr5* and *Smoc2* in β-cat^{GOF}; $Mll1^{-/-}$ mutant cells, arguing that the primary function of Mll1 in the β-cat^{GOF} stem cells is to prevent differentiation. This would imply that the Mll1-deficient β-cat^{GOF} stem cells initially activated a goblet cell differentiation programme. The decreased expression of Mll1-controlled stem cell genes occurs timely delayed. In Wnt-activated colon cancer cells, however, we identified Mll1 as a direct regulator of stem cell genes. To further clarify this issue, it will be interesting to investigate whether depletion of the Mll1-regulated stem cell gene products in cancer stem cells would induce *Atoh1* expression, Mapk signalling and differentiation similar to Mll1 ablation. We can conclude that Mll1 sustains the stemness of intestinal cancer cells both by sustaining the expression of stem cell genes and by preventing differentiation. The loss of Mll1 enforces differentiation of tumorigenic β-cat^{GOF}-mutant stem cells, pushing them to less aggressive fates and disabling tumor formation.

4.5 Mll1 is a gene-specific co-regulator of β-catenin/Tcf4.

Our study identified the histone methyltransferase Mll1 as an epigenetic regulator of the Wnt-dependent stem cell gene *Lgr5*. Mll1 had previously been shown to associate with the β-catenin/Tcf4 complex[161, 162]. Our data support a role of Mll1 in the differential regulation of Wnt/β-catenin target genes. Wnt signalling exerts diverse functions in the intestinal epithelium: on the one hand, it maintains intestinal stem cells and drives proliferation of transit-amplifying progenitor cells, on the other hand it guides the maturation and terminal differentiation of Paneth cells[107]. The cellular context critically defines the spectrum of Wnt target genes that become expressed in response to active Wnt signalling[106, 108]. It has been unclear, however, how such differential and cell type-specific Wnt responses are regulated on the molecular level. Our data suggest critical roles for epigenetic modifiers in the selective regulation of Wnt target genes and identify Mll1 as a gene-specific co-regulator of the β-catenin/Tcf4 complex. Mll1 regulated the expression of the stem cell gene *Lgr5*, whereas it did not regulate the expression of the Wnt targets *Axin2*, *Sox9* and *Ascl2*. *Lgr5* expression critically depends on Mll1: in the absence of Mll1, β-catenin binding was not sufficient to sustain *Lgr5* expression.

We showed that Mll1 is crucial for tumorigenesis and confers Wnt-induced cancer stemness. Sphere cultures of human colon cancer cells, which enrich for self-renewing cancer stem cells, showed an increased expression of Mll1 but not its family member Setd1a. In fact, Setd1a had been reported to control Wnt target genes that drive the proliferation and growth of colon cancer cells[141], rather than cancer stemness. Mll1 did not regulate the expression of the Wnt targets *Tcf1* and *Tcf4*, which have been shown to be controlled by the Mll family member Setd1a[141]. These observations indicate non-overlapping functions of the Mll family members Mll1 and Setd1a in Wnt-driven colon cancer. It argues that distinct epigenetic regulatory components of the β-catenin/Tcf4 complex are implicated in the activation of different sets of Wnt target genes. Mll1 and Setd1a appear to be part of distinct co-regulatory complexes that determine a differential Wnt responsiveness of common β-catenin/Tcf4 target genes. Accordingly, the spectrum of activated Wnt target genes in any given cell type might differ depending on which co-regulators are expressed, thus allowing for the diverse and cell type-specific effects of Wnt signalling.

4.6 Mll1 controls adult epithelial stem cells and cell fate choice in the intestine.

Extensive research has established a crucial role of Mll1 in the hematopoietic system[167, 170, 171]. Recent studies have associated Mll1 with adult stem cell function and lineage maturation also in solid tissues such as muscle and neural tissue[174, 176]. Here we detected a so far unknown role of Mll1 in the stem and progenitor cells of the adult intestinal epithelium. Mll1 is highly expressed in the Lgr5^{+} intestinal stem cells and in progenitor cells of the TA zone, and its expression decreases as the cells differentiate. The ablation of Mll1 in the Lgr5^{+} intestinal stem cells resulted in loss of a substantial number of mutated crypts over time. The progressive but not immediate loss of Mll1-deficient intestinal stem cells relates to its role in sustaining rather than conferring intestinal stemness. The gradual loss of Mll1 knockout crypts might be due to progressive exhaustion of the stem cells deficient for Mll1. Exhaustion of Mll1-deficient stem cells has also been reported in the hematopoietic system and for muscle satellite cells[171, 176]. Since similar effects have been observed in different tissues, this suggests a more general function of Mll1 in adult stem cell maintenance. This function might relate to the role of Mll1 in sustaining the expression of transcription factors that maintain stem cell identity, e.g. Pax7 in muscle satellite cells[176], and Gata4/6 in intestinal epithelial stem cells.

We demonstrated that Mll1 is repressed upon differentiation in a Bmp-dependent manner. The stimulation of Bmp signalling by administration of Bmp4 repressed *Axin2* and *Mll1* expression in intestinal organoids, suggesting that the inverse crypt-villus gradients of Wnt and Bmp signalling restrict Mll1 expression to the intestinal crypts. Our data indicate that a decrease in Mll1 protein levels is essential for the differentiation of intestinal epithelial cells. We showed that Mll1 sustains the expression of stem cell genes by antagonizing PRC2-mediated silencing. PRC2 is known to support crypt-villus differentiation by mediating the H3K27me3-dependent silencing of intestinal stem cell genes such as *Lgr5* [231]. In conjunction, these data propose that Mll1 is involved in the maintenance of intestinal stem cell gene expression at homeostasis and needs to be downregulated to enable PRC2/H3K27me3-mediated silencing of intestinal stem cell genes and permit terminal differentiation.

Mll1 controls the Wnt/Mapk-driven specification of secretory progenitor cells.

Our data suggest that Mll1 exerts a dual role in intestinal homeostasis: it sustains intestinal stem cells and needs to be downregulated to enable terminal differentiation, but also plays a role in safeguarding cell fate determination of secretory Paneth and goblet cells driven by the counteracting activities of Wnt and Mapk signalling, respectively. We observed that simultaneous activation of Wnt/β-catenin and Mek1/Mapk signalling abrogated secretory cell maturation in intestinal organoids and imposed an immature precursor state, as had previously been suggested by Heuberger et al. (2014)[64]. While β-cat^{GOF}-induced Wnt activation promoted a Paneth cell fate and prevented Mapk-induced goblet cell differentiation, the ablation of Mll1 in β-cat^{GOF} and in β-cat^{GOF}; Mek1^{GOF} cells led to the re-appearance of goblet cells, largely as

mixed Paneth-goblet entities. This suggests that Mll1 restricts Mapk signalling and goblet cell differentiation in Wnt-high secretory progenitor cells. In Mll1-competent Mek1^{GOF} crypts, Mapk signalling promoted cell proliferation. The ablation of Mll1 shifted the effect of Mapk signalling from pro-proliferative to differentiation-inducing. Mek1^{GOF}; Mll1$^{-/-}$ crypts exhibited increased numbers of goblet cells. The presence of Mll1 thus maintains a proliferative progenitor state and restricts goblet cell differentiation. This closely fits our observation of high levels of Mll1 in TA cells, in which active Mapk signalling promotes cell proliferation[64]. Whether the loss of Mll1 increases Mapk activity or changes the target gene spectrum to allow for goblet cell differentiation remains to be determined. Our data suggest that in the process of differentiation, Wnt-high secretory progenitor cells retain Mll1 expression to restrict a Mapk-induced goblet cell fate and ensure Paneth cell differentiation. Vice versa, Wnt-low secretory progenitors lose Mll1, which causes a Mapk-induced goblet cell differentiation, presumably by decreasing the expression of the Mll1-dependent Gata4/6. The transcription factors Gata4 and Gata6 are required for secretory cell differentiation and lineage maturation in the epithelium of the small intestine and colon[239]. Gata4 is expressed throughout the small intestinal epithelium of the jejunum, but is absent in goblet and enteroendocrine cells[211]. The ablation of Gata4 promotes maturation of goblet cells[239]. Our data suggest a regulatory sequence in the process of cell specification that is controlled by Mll1: reduction of Wnt signalling is followed by decreased expression of Mll1, which results in downregulation of Gata4/6 expression and unleashes an Atoh1- and Mapk-driven goblet cell differentiation. By sustaining the expression of Gata4/6 transcription factors and balancing opposing Wnt and Mapk activities, Mll1 suppresses goblet cell specification of mixed-lineage secretory progenitor cells and promotes the alternate Paneth cell fate. A similar mechanism has been described in the immune system, where Mll1 regulates Gata3 to specify and maintain memory Th_2 cells[245].

The accumulating secretory cells in Mek1^{GOF}; Mll1$^{-/-}$ crypts were double-positive for Paneth and goblet cell markers despite high Mapk activity and absence of Mll1, indicating that Mll1 is essential for preserving the lineage-specific differentiation and cell identity of Paneth and goblet cells. Like Mll1, polycomb PRC2 complexes have been implicated in the maintenance of intestinal stem and progenitor cells: their genetic ablation causes loss of stem cells and aberrant secretory differentiation into mixed Paneth-goblet cells[234, 246]. In the light of our study, this highlights the importance of a proper balance of antagonistic Mll1 and PcG activities for establishing cell specification and maintaining cell identity during secretory differentiation[138]. Our observations illustrate an interplay of epigenetic and signalling cues in the control of cell fate determination in adult tissues. The aberrancies in secretory differentiation could result from changes to the epigenome of the Mll1-deficient progenitor cells, though, rather than be a direct effect on the counteracting activities of Wnt and Mapk signalling. Further dissecting the role of Mll1 in balancing the effects of Wnt and Mapk signalling as well as its interplay with PcG

proteins to control cell fate specification of intestinal secretory progenitors will be a relevant subject for future investigation.

4.7 Mll1 as a rational target for colon cancer therapy.

Recent years have seen limited success in the development of rational treatments for colon cancer. Therapeutic targeting of aberrant Wnt signalling has not yet reached the clinics, but recent preclinical studies in adult mice have indicated that a systemic inhibition of Wnt signalling severely impairs intestinal homeostasis and causes high mortality[51]. An in-depth understanding of the mechanistic differences between physiological and pathological Wnt signalling is therefore crucial and will be key to tumor-specific targeting of the Wnt pathway. Current therapies are often ineffective due to cancer stem cells which escape treatment and the plasticity of non-stem cancer cells that can readily revert into stem-like cells[91, 99]. Combining experimental depletion of $Lgr5^{+}$ cancer stem cells with conventional chemotherapy prevented the reprogramming of differentiated cancer cells into cancer stem cells and led to tumor regression in preclinical studies[99]. As cancer stem cells are highly reminiscent of their normal tissue counterparts, a detailed understanding of the regulatory mechanisms which control stemness, de-differentiation and cellular plasticity of intestinal cancer cells will be required to safely eliminate colon cancer stem cells without affecting intestinal stem cells and tissue homeostasis. To succeed in colon cancer therapy, we therefore need to identify targets that allow for defined interference with the stemness-promoting effects of oncogenic Wnt signalling. Our work is a major step forward in the understanding of the epigenetic regulation of oncogenic Wnt-induced cancer stemness. We show that the epigenetic regulator Mll1 promotes intestinal tumorigenesis and plays a crucial role in sustaining Wnt-activated colon cancer stem cells. Somatic mutations of Mll1 in colon cancer are rare, but human colon carcinomas exhibited high expression of Mll1 that coincided with nuclear β-catenin. This suggests that the oncogenic Wnt/β-catenin signalling exploits the histone methyltransferase Mll1 to promote intestinal tumorigenesis and colon cancer stemness. Our data demonstrate that oncogenic Wnt-activated colon cancer cells strongly depend on Mll1. Accordingly, Mll1 represents an 'epigenetic vulnerability' [103] in Wnt-driven colon cancer. Interfering with Mll1 function can eliminate colon cancer stem cells, might further prevent differentiated tumor cells from acquiring stemness, and has potential as a rational treatment for Wnt-driven colon cancer. Human colon cancer cells with β-catenin gain-of-function (Ls174T) and APC loss-of-function mutations (DLD1) were equally sensitive to the knockdown of Mll1, indicating that patients with either mutation of the Wnt pathway would benefit from Mll1 inhibition.

Targeting Mll1 in colon cancer therapy will require a fine balancing, and a beneficial effect will depend on the precise dosing of Mll1 inhibition, maintaining a 'just-right' level of Mll1 function for the intestinal stem cells to thrive but eliminating the Mll1-addicted colon cancer stem cells. Our analyses indicated that the loss of Mll1 impacts the $\beta\text{-cat}^{GOF}$-mutant $Lgr5^{+}$ stem cells more

severely than the Lgr5^{+} stem cells at homeostasis. However, further preclinical studies *in vivo* are required to dissect the role of Mll1 in adult intestinal stem cells to anticipate potential drug toxicities and to determine whether we will be able to play on the Mll1 dependency of colon cancer stem cells without perturbing intestinal homeostasis. It further remains to be determined in detail whether the inhibition of Mll1 will have a beneficial effect in advanced colon cancer. We approached the role of Mll1 in tumor maintenance using a xenograft assay. However, the Mll1 knockdown efficiency varied, which rendered the assay impractical to conclusively demonstrate a beneficial effect of Mll1 inhibition in established intestinal tumors. An important follow-up study to help clarify these issues will be to treat intestinal tumors of β-cat^{GOF} mice with Mll1 inhibitors such as MI-2[147]. In our *in vitro* studies, MI-2 treatment resulted in death of human colon cancer cells and β-cat^{GOF} intestinal organoids, which might be partially attributed to an inhibition of Mll1 function. We did not observe apoptosis upon specific knockdown or genetic ablation of Mll1, though, indicating that the effect of MI-2 treatment on cell viability may rather be caused by interference with Mll2 and Menin functions[147, 247]. The MM-401 inhibitor holds promise to have a greater specificity for Mll1[148]. However, MM-401 and its derivatives particularly interfere with the methyltransferase activity of Mll1, which we found to be subsidiary for the role of Mll1 in sustaining colon cancer stemness. MM-401 targets the Mll1-Wdr5 interaction to prevent the assembly of the WRAD complex which is essential for methyltransferase activity[148]. It needs to be tested whether inhibition of the WRAD complex assembly by MM-401 also impairs Mll1 chromatin binding and has an effect in the Wnt-mutated colon cancer cells. A systemic application of Mll1 inhibitors is anticipated to cause severe side effects, in particular due to the crucial role of Mll1 in the hematopoietic system. A tumor-directed application of Mll1 inhibitors will thus be critical and ongoing technological advances in this field will profoundly increase the clinical value of Mll1 as a rational target in colon cancer therapy. As indicated by our studies in Ls174T cells that underwent a p53-dependent senescence in response to prolonged Mll1 depletion, p53-competent cancer cells might require a senolytic follow-up therapy to eradicate cancer cells that have become senescent due to Mll1-inhibiting therapy.

To sum up, our study reveals Mll1 as a critical factor in the epigenetic regulation of stem cell gene expression induced by oncogenic Wnt/β-catenin signalling. Mll1 sustains the Wnt-induced stemness of colon cancer cells and prevents cancer cell differentiation. Our data suggest targeting Mll1 as a powerful strategy to eliminate the stemness and plasticity of Wnt-driven colon cancer cells.

5 Materials and Methods

5.1 Mice.

All mice were bred in pathogen-free conditions, and care and use of animals were performed according to the European and national regulations, published in the Official Journal of the European Union L 276/33, September 22, 2010. All animal procedures were approved by the Landesamt für Gesundheit und Soziales (LaGeSo), Berlin (G0101/18). The transgenic mouse lines used in this study have been described: Lgr5-EGFP-IRES-Cre^{ERT2} [15], β-catenin$^{deltaEx3/+}$ [78], Gt(ROSA)26Sor^{tm1Sor} [189], Mll1^{flox} (Kmt2a^{tm1Afst}) [188], Mek1DD[221, 222]. Compound mutant mice were obtained by crossing with Lgr5-EGFP-IRES-Cre^{ERT2} mice as depicted in Figure 5.1.

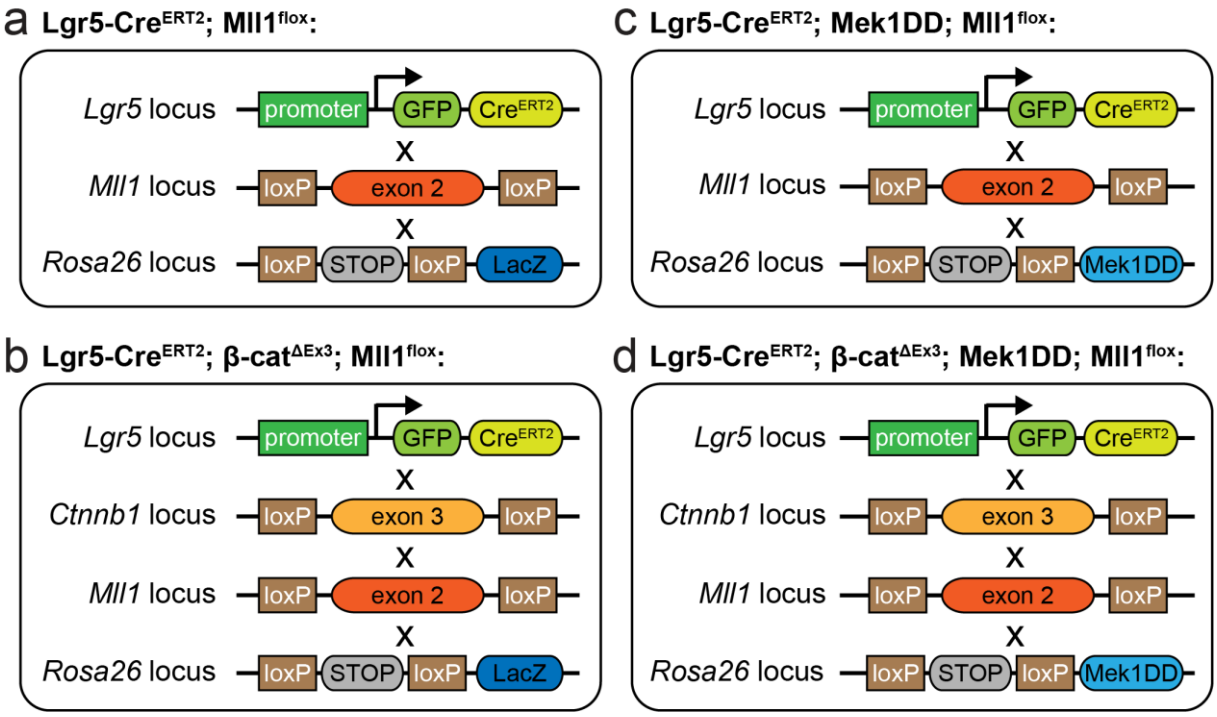

Figure 5.1: Genetically engineered mouse models.
a) Lgr5-Cre^{ERT2}; Mll1^{flox} mice express GFP and the tamoxifen-inducible Cre^{ERT2} under the control of the *Lgr5* promoter. Cre activity deletes the floxed exon 2 of the *Mll1* locus and removes a STOP cassette in the *Rosa26* locus, enabling LacZ expression. **b)** In Lgr5-Cre^{ERT2}; β-cat^{deltaEx3}; Mll1^{flox} mice, Lgr5-Cre activity deletes the floxed exon 3 of the *Ctnnb1* locus and the floxed exon 2 of the *Mll1* locus, and removes a STOP cassette in the *Rosa26* locus, enabling LacZ expression. **c)** In Lgr5-Cre^{ERT2}; Mek1DD; Mll1^{flox} mice, the Lgr5-Cre activity deletes the floxed exon 2 of the *Mll1* locus and removes a STOP cassette in the *Rosa26* locus, driving expression of a constitutively active gain-of-function variant of Mek1 (Mek1DD). **d)** In Lgr5-Cre^{ERT2}; β-cat^{deltaEx3}; Mek1DD; Mll1^{flox} mice, the Lgr5-Cre activity deletes the floxed exon 3 of the *Ctnnb1* locus and the floxed exon 2 of the *Mll1* locus and removes a STOP cassette in the *Rosa26* locus, driving expression of a constitutively active gain-of-function variant of Mek1 (Mek1DD).

Mutagenesis was induced in 4-6 weeks-old mice by intraperitoneal (i.p.) injections of tamoxifen (Sigma, 50mg/kg, diluted 1:10 in sunflower oil) on three consecutive days. Mice were analysed at indicated time points after the last tamoxifen injection. The mice were given i.p. injections of

BrdU (Millipore) at 2h before sacrifice, final concentration 50µg/g of body weight in PBS. Kaplan Meier plot for tumor incidence was calculated based on macroscopic observation of hyperplastic intestinal tissue. Both females and males were analysed.

For genotyping, ear biopsies were treated with 1µg proteinase K (Sigma) in lysis buffer (100mM Tris pH 8.5, 10mM EDTA, 0.2% SDS, 200mM NaCl) at 56°C. Lysates were diluted 1:10 in nuclease-free H_2O and genotyped by PCR, using Taq DNA polymerase (Invitrogen) and the following primer sequences:

Table 1: Primer sequences for genotyping.

primer	sequence (5'-3')
Lgr5-Cre_fwd	CACTGCATTCTAGTTGTGG
Lgr5-Cre_rev	CGGTGCCCGCAGCGAG
β-catenin^{deltaEx3}_fwd	AGAATCACGGTGACCTGGGTTAAA
β-catenin^{deltaEx3}_rev	CATTCATAAAGGACTTGGGAGGTGT
Mll1_fwd	CCTGCTGCCTGTGCTTGTAAA
Mll1_rev	GTAGAAACCTACTTCCCATGCC
Mek1DD_fwd	GTCAATGAGCCTCCTCCAAA
Mek1DD_rev	GCAATATGGTGGAAAATAAC
Rosa26_fwd	CCAGATGACTACCTATCCTC
Rosa26_rev	GAGCTGCAGTGGAGTAGGC
Rosa^{LacZ}_fwd	TCCCAACAGTTGCGCAGCCTGAATG
Rosa^{LacZ}_rev	ATATCCTGATCTTCCAGATAACTGCCG

For crypt-villus fractionations, the mouse small intestinal epithelium was fractionated into crypts and villi following the procedure for the preparation of intestinal organoids (compare 5.2, page 86). Fractions were passed through a 70µm cell strainer, separating the fractions in crypts in the flow-through and villi stuck on the filter. Villi were recovered from the filter by rinsing in ice-cold 0.1% BSA-PBS upside-down. Fractions were collected by centrifugation at 1000rpm for 5min and snap-frozen in liquid nitrogen.

The fluorescence-activated cell sorting (FACS) of Lgr5-GFP^{+} intestinal stem cells was performed by Neha Goveas in the lab of Francis Stewart at the Technical University Dresden. In brief, small intestinal crypts from Lgr5-EGFP-IRES-Cre^{ERT2} mice of the respective genotypes were enriched, and crypts were dissociated into single cells with TrypLE Express (Thermo Fisher Scientific) for 30min at 37°C. Dissociated cells were passed through a 70µm cell strainer and washed with 5% FBS/PBS. Cells were stained with APC-conjugated anti-326 (EpCAM) antibody (1:100 dilution, eBioscience, Cat no. 17-5791-80) and Alexa-Fluor 700 CD45 antibody (1:50 dilution, BD, Cat no. 560693) for 45min on ice. EpCAM labels epithelial cells, the cell

surface marker CD45 was used to exclude haematopoietic cells. The stained cells were collected by centrifugation and resuspended in SYTOX blue dead cell stain (1:20,000 dilution, Thermo Fisher Scientific). FACS sorting was performed on a FACS AriaTM III cell sorter (BD). RNA sequencing of isolated Lgr5-GFP^{+} intestinal stem cells from four independent mice per genotype was performed in collaboration with the Stewart lab (Technical University Dresden, Germany) as described in 5.12 (page 93).

5.2 Organoid culture.

Intestinal organoids were obtained as previously described[64]. Small intestines were dissected and villi were removed by gentle scraping with a glass coverslip. Intestines were cut into pieces of 5mm and dissociated in 8mM EDTA/PBS for 5min at RT followed by 20min incubation in ice-cold 2mM EDTA/PBS at 4°C. The epithelia were fractionated by shaking in ice-cold PBS. Crypt-enriched fractions were collected by centrifugation, washed once in ice-cold 0.1% BSA-PBS/HBSS (Gibco #14175-053) (1:1) and applied on a 70µm cell strainer to isolate the crypts and remove remaining villi and large debris. 250 crypts were seeded in 20µl of growth factor-reduced Matrigel (Corning #356231) and cultured in basic crypt medium (60/40 Advanced DMEM/F12 supplemented with N2 (Gibco) and B27 (Gibco), GlutaMax (Gibco), N-Acetylcysteine (Gibco) and Penicillin/Streptomycin (Invitrogen)) containing 50ng/ml murine EGF (Gibco), 100ng/ml murine Noggin (Peprotech) and 500ng/ml human R-spondin1 (Peprotech). Organoids were split every 3-4 days by mechanical disruption. Cre-mediated recombination was induced by addition of 800nM 4-hydroxy-tamoxifen (Sigma #94873) for 2 days. β-cat^{GOF} organoids were selected by R-spondin1 withdrawal. Analyses were performed starting from 7-10 days after mutagenesis. EdU incorporation was assayed with the Click-iT EdU Imaging kit (Invitrogen). Recombinant human BMP4 (Peprotech) was added for 24h in Noggin-free crypt medium supplemented with EGF and R-spondin1. For serial re-plating, β-cat^{GOF}; Mll1$^{-/-}$ organoids were dissociated into single cells by 5min incubation in TrypLE^{TM} (Gibco) at 37°C in a water bath, and 2,000 cells were seeded in 20µl of growth-factor reduced Matrigel and cultured in crypt medium supplemented with EGF, Noggin and R-spondin1.

5.3 Cell culture.

HEK293TN cells, DLD1 and Ls174T human colon cancer cell lines were cultured in 1xDMEM (Gibco) supplemented with 10% fetal bovine serum (FBS) and 1% Penicillin/Streptomycin (PenStrep) at 37°C, 90% H_2O, 5% CO_2. Cell line identity was confirmed by Multiplex human Cell line Authentication (MCA, Multiplexion). For non-adherent sphere culture, dishes were coated with 12mg/ml polyhema/95% EtOH (Sigma) over night at 55°C. Single cells were cultured in cancer stem cell (CSC) medium (DMEM/F12 (1:1) + GlutaMAX (Gibco), 1%PenStrep supplemented with N2, 10ng/ml human FGF (Gibco) and 10ng/ml human EGF (Peprotech)) for 4-5 days, dissociated with trypsin for 5min at 37°C, and re-plated in CSC

medium on polyhema-coated dishes. After 1 day of secondary sphere culture, spheres were harvested by centrifugation and processed for RNA/protein analyses. Gsk126[209] (ApexBio) was administered for 96h at 5µM. Recombinant human BMP4 (Peprotech, final concentration 500ng/ml) and recombinant human Noggin (Peprotech, final concentration 100ng/ml) were added for 48h. ICG-001[101], LF3[100] and MI-2[147] were administered for 48h at indicated concentrations.

5.4 Generation and cloning of shMLL1.

Doxycycline-inducible shRNA knockdown cell lines were generated by lentiviral transduction, using the doxycycline-inducible pInducer11 system established by Meerbrey et al. (2011)[201]. shRNA targeting MLL1 was designed with the optimized miR30a backbone (Fellmann et al. 2013[248]) and cloned into the pInducer11 vector (addgene #44363). To introduce restriction sites the shMLL1 was amplified in a PCR reaction using the following primers (5'-3': mirE Amp-fwd TGAACTCGAGAAGGTATATTGCTGTTGACAGTGAGCG; mirE Amp-rev TCTCGAATTC TAGCCCCTTGAAGTCCGAGGCAGTAGGC). The PCR product was purified with the PCR purification kit (Roche). Purified shMLL1-mirE Amp and the pInducer11 vector were digested with EcoRI and XhoI restriction enzymes (New England Biolabs) for 8h at 37°C to generate compatible overhangs. The digested shMLL1 insert was purified with the PCR purification kit (Roche). The cut pInducer11 vector was separated on a 1% agarose gel and the vector backbone was purified with the QIAgen gel purification kit (Qiagen). The shMLL1 insert was ligated into the pInducer11 vector for 3h at RT using the T4 DNA ligase (Promega). The ligation reaction was performed in a total volume of 15µl using 8µl shMLL1-mirE Amp PCR product and 30ng of the processed pInducer11 vector. Competent XL10 gold bacteria were transformed with the ligation product by incubation on ice for 45min followed by a heat shock at 42°C for 45sec in a water bath. Bacteria were cultured over night at 30°C on agar plates in the presence of 100µg/ml ampicillin. Successfully transformed bacteria possess ampicillin resistance and grow into clonal colonies. Colonies were picked and cultured over night at 30°C with gentle shaking in LB medium containing 100µg/ml ampicillin. Plasmid DNA was isolated using the QIAgen plasmid purification kit (Qiagen) and incorporation of the shMLL1 insert was checked in a restriction digest with XhoI and MluI (New England Biolabs). Sequence identity was verified using the Sanger sequencing service from Source Bioscience.

Table 2: Sequence shMLL1.

	sequence (5'-3')
shMLL1	TGCTGTTGACAGTGAGCGAAAGAAAGATTCTAAAAGTATATAGTGAAGCCACAGAT GTATATACTTTTAGAATCTTTCTTCTGCCTACTGCCTCGGA

5.5 Generation of lentiviral particles and lentiviral transduction.

For production of lentiviral particles, HEK293TN cells were co-transfected with 10µg psPAX2 (addgene #12260), 2.5µg pMD2.G (addgene #12259) and 10µg pInducer11-shMLL1 by transfection with polyethylenimine (PEI) (Sigma). Supernatants containing lentiviral particles were collected at 24h and 48h after transfection. For lentiviral transduction, the lentiviral particle-containing supernatant was mixed 1:1 with fresh growth medium containing 8µg/ml polybrene. Ls174T and DLD1 cells were transduced at 1000rpm for 1h at RT followed by over night incubation at 37°C. Transduced cells with high expression of shRNA were selected by FACS for GFP and tRFP[201], and cultured as single cell clones to establish shMLL1 Ls174T cell lines. Knockdown was induced by addition of doxycycline to the growth medium (LKT Laboratories D5897, final concentration 300ng/ml).

5.6 Serial re-plating and colony formation assay.

For serial re-plating assays, cells were seeded at a density of $0.5x10^6$ cells on 10cm-cell culture dishes. Upon passaging every 2-3 days, cells were trypsinized and resuspended in 10ml growth medium. Cell suspensions were diluted 1:2 in 0.4% Trypan Blue/PBS to distinguish viable and dead cells. Viable cells were counted manually and re-plated at a density of $0.5x10^6$ cells.

For colony formation assays, cells were counted with a cell counter (CASY). 500 cells were seeded per well of a 6-well tissue culture plate, and cultured for a period of 13 days. Inducible shMLL1 Ls174T cells were pre-treated with 300ng/ml doxycycline for 3 days and kept on doxycycline throughout the assay. Inhibitors at indicated concentrations were added upon plating, the medium was changed every other day. Cell colonies were stained with crystal violet and counted manually. The colony formation rate was further quantified by de-staining in 10% acetic acid and measuring the absorbance of the released dye with an iMark microplate reader (BioRad).

5.7 TCF/LEF luciferase reporter assay.

To assess the transcriptional activity of the β-catenin/TCF complex in control and shMLL1 Ls174T cells, cells were transiently transfected with 1µg of a reporter construct which encodes a *firefly* luciferase under the control of a TCF/LEF promoter element (TOPflash) and responds to canonical Wnt signalling by driving luciferase activity[206]. In parallel, control and shMLL1 Ls174T cells were transfected with a negative control plasmid (FOPflash). The FOPflash plasmid contains mutated TCF binding sites and is unable to respond to active Wnt signalling; it serves to control for non-specific effects of luciferase activity. All cells were co-transfected with 0.1µg of a constitutively active construct encoding *Renilla* luciferase (SV40 Renilla, addgene #27163). All transfections were performed in 12-well tissue culture plates, using

Lipofectamine™ 2000 (Invitrogen) and following the manufacturer's instructions. The composition of the transfection mix was as follows:

TOPflash or FOPflash	1 µg
SV40 Renilla	0.1 µg
Lipofectamine™ 2000	2 µl
OptiMEM (Gibco)	200 µl

The culture medium was changed at 24h after transfection and 3µM CHIR99021[207] (Axon #1386) and 50µM LF3[100] were added. The shMLL1 Ls174T cells were pre-treated with 300ng/ml doxycycline for 6 days prior to transfection and kept on doxycycline throughout the assay. At 48h after transfection, cells were washed once with PBS and lysed in Passive Lysis Buffer (Promega) for 10min at RT. Lysates were harvested by scraping, centrifuged for 1min at 14,000rpm and transferred into MicroWell Assay microplates (Nunc). Luciferase activity was measured with a Centro XS^3 LB960 microplate luminometer (Berthold technologies) with automated addition of *firefly* and *Renilla* substrate buffers (*firefly* luciferase buffer: 150mM HEPES, 8mM $MgSO_4$, 40mM DTT, 200µM EDTA, 1.06mM ATP pH 8 diluted 1:1 in H_2O and supplemented with 270µM CoA and 200µM luciferin; *Renilla* luciferase buffer: 30mM Na_4PPi, 15mM NaAc, 20mM CDTA, 800mM Na_2SO_4 pH 5.0 diluted 1:1 in H_2O and supplemented with 2.2µM coelenterazin and 50µM APMBT), each sample was measured in triplicate. *Firefly* activity was normalized to respective *Renilla* control, TOPflash values were calculated relative to FOPflash activity (TOP/FOP activity).

5.8 Xenografts.

For xenograft assays, $1x10^6$ cells in 200µl PBS were injected under the skin of nude mice, NMRI:nu/nu, female. The inducible shMLL1 Ls174T cell lines were pre-treated with 300ng/ml doxycycline for 4 days and mice were administered doxycycline in drinking water (2mg/ml doxycycline in 5g/l sucrose) from day -1 throughout the experiment. Mice inoculated with non-induced control cells were kept without doxycycline. Health condition, tumor size and mouse body weight were measured every other day. For the tumor maintenance xenograft, $1x10^6$ non-induced shMLL1 Ls174T cells were resuspended in 200µl PBS and injected under the skin of female NMRI:nu/nu mice. For ablation of MLL1, mice were administered doxycycline in drinking water (2mg/ml doxycycline in 5g/l sucrose) starting from day 8 after cell inoculation. Control mice were kept without doxycycline throughout the experiment. Health condition, tumor size and body weight were monitored throughout the experiment. All xenograft assays were performed with the Experimental Pharmacology and Oncology (EPO), Berlin-Buch.

5.9 Histology, immunofluorescence staining and analysis.

Analysis of naïve human colon cancer biopsies was approved by the ethic commission of the Friedrich-Alexander Universität Erlangen-Nürnberg (148_19 BC). Murine tissue was fixed in 4% formaldehyde/PBS over night at 4°C or for 3h at RT and transferred to 70% EtOH at 4°C. Tissue was dehydrated by sequential incubation in 70%, 80%, 90% and 100% EtOH for 1h each at RT, cleared in toluol and paraffin-embedded. Organoids were fixed in 4% formaldehyde/PBS for 1h at RT and embedded in 1.5% agarose-PBS prior to dehydration and paraffin embedding. 5-7µm sections were cut with a microtome (Microm HM355S) and placed on microscope slides (Menzel Glass, Superfrost Plus, Thermo Fisher). For H&E staining, tissue sections were incubated with hematoxylin solution for 1min, washed under running tab water for 5-10min and stained with eosin for 5min prior to dehydration and mounting with non-aqueous mounting medium. Hematoxylin stains nuclei blue, eosin stains cytoplasm and extracellular matrix in different shades of pink. Alcian blue solution (pH 2.5 in 3% acetic acid) was incubated for 30min to stain acidic polysaccharides and glycosaminoglycans, sections were washed under running tab water for 1min and counter-stained with nuclear fast red for 5min or hematoxylin for 30sec.

For immunostaining on paraffin sections, antigen retrieval was carried out by boiling in 10mM sodium citrate pH 6.0 or 1mM EDTA 20mM Tris pH 8.5 in a microwave oven at P100 and P40 as indicated in Table 3 (compare 5.13, page 96). For immunohistochemistry (IHC), sections were incubated in 4% H_2O_2/PBS for 5min prior to 1h incubation with blocking solution (0.1% Tween20, 5-10% horse serum, 1% BSA in PBS) followed by incubation of the primary antibody diluted in blocking solution over night at 4 °C. Fluorochrome-conjugated or HRP-coupled secondary antibodies and 4′,6-diamidino-2-phenylindole (DAPI) were incubated in blocking solution for 1-2h at RT. Immunohistochemistry was developed with the DAB chromogenic substrate (DAKO), dehydrated and mounted with non-aqueous mounting medium (Entellan). Cells for Mll1 immunofluorescence staining were cultured on chamber slides, fixed in 4% formaldehyde/PBS for 10min at RT, washed twice with PBS, permeabilized in 0.1% Triton-X100/PBS for 1min, treated with ice-cold methanol for 10min at -20°C and incubated in blocking solution (0.1% Tween20, 5% horse serum, PBS) for 1h at RT prior to incubation of primary antibodies over night at 4°C.

All antibodies used were validated by the manufacturers for immunostaining applications. Specificity of the Mll1 antibody (D6G8N, Cell Signaling Technology #14197) was confirmed by the absence of staining on Mll1-deficient tissue (see Figure 3.15c, page 42). Secondary antibody specificity was validated by lack of staining in the absence of targeted primary antibodies (see Supplementary Figure 2, page 115).

5.9.1 LacZ whole-mount staining.

Murine intestine was cut open longitudinally, fixed for 2h in ice-cold fixative (1% formaldehyde, 0.2% glutaraldehyde, 0.02% NP-40 in PBS), washed twice in PBS, incubated in staining solution (2mM $MgCl_2$, 5mM $K_3Fe(CN)_6$, 5mM $K_4Fe(CN)_6$, 0.01% NP-40, 0.01% sodium deoxycholate, 1mg/ml X-gal (Roth) in PBS) over night at RT protected from light, dehydrated and processed for paraffin embedding. 10µm paraffin sections of LacZ-stained tissue were counter-stained with nuclear fast red.

5.9.2 Senescence-associated β-galactosidase (SA-β-Gal) staining.

Cells were washed with PBS, fixed in 4% PFA/PBS for 5min at RT, washed twice with 0.1% BSA-PBS for 20min and stained with SA-β-Gal staining solution (40mM citric acid/sodium phosphate pH 6.0, 1mM $MgCl_2$, 1 mg/ml X-gal, 5mM $K_3Fe(CN)_6$, 5mM $K_4Fe(CN)_6$ in H_2O) for 3-5hrs or over night at 37°C without CO_2.

5.9.3 Light microscopy and data analysis.

Representative z-stacks were acquired with inverted laser scanning microscopes LSM710 and LSM700 using 405nm, 488nm, 561nm, and 633nm lasers and a PlanApochromat 40x NA 1.3 objective (Zeiss Jena, Germany) or a spinning disc confocal microscope CSU-W1 (Nikon/Andor) equipped with an iXON888 camera, using PlanApo 20x NA 0.75 and Apo LWD 40x NA 1.15 objectives of the advanced light microscopy (ALM) core facility at the MDC. Maximal intensity projections of z-stacks were performed with ImageJ. Mean fluorescence intensity in 3D reconstructed samples was quantified with Imaris 8 (Bitplane/Andor) software, using the surface module and selecting for nuclear fluorescence signal with a mask created in the DAPI channel. Mll1 staining intensity in the crypt cell populations was quantified with the measurement point tool in Imaris 8 and normalized to the mean staining intensity in the TA cell population. H&E and IHC stainings were imaged with an Axio Scope.A1 (Zeiss).

5.10 Chromatin immunoprecipitation.

Chromatin immunoprecipitation (ChIP) of histone modifications was performed from pInducer11-shMLL1 Ls174T lines induced with 300ng/ml doxycycline for 11 days, following the instructions of the iDEAL ChIP-seq kit for histones (Diagenode). In brief, cells were grown to 80% confluency, trypsinized for 3min at 37°C, collected by centrifugation in growth medium and resuspended in PBS for cell counting. Aliquots of $10x10^6$ cells per 500µl were fixed in 1% formaldehyde/PBS for 8min at RT and quenched by addition of glycine for 5min at RT. For ChIP of Mll1, Tcf4 and β-catenin, pInducer11-shMLL1 Ls174T and DLD1 cell lines were induced with 300ng/ml doxycycline for 6 days and 8 days, respectively, and chromatin was prepared using the ChIP-IT Express kit (Active Motif). Cells were grown to 80% confluency, trypsinized for 3min at 37°C, fixed in 1% formaldehyde-DMEM for 10min at RT and quenched

with glycine for 5min at RT. Chromatin was sheared with a Branson Sonifier 450 at 4°C: 3min shearing time, duty cycle 60, output control 6, sonicate 10x for Diagenode kit, 4x for Active Motif kit Ls174T cells, 2x for Active Motif kit DLD1 cells, 1min pause between each sonication round. Shearing efficiency was checked on a 1% agarose gel. 10 µg of sheared chromatin were used for ChIP anti-Mll1, -Tcf4, and -β-catenin. ChIP-qPCR analysis was performed in a total volume of 20µl SYBR green reaction mix (Roche Diagnostics) containing 0.25µM of forward and reverse primers each in a CFX96-C1000T thermal cycler (BioRad): 2min 50°C, 2min 95°C followed by 42 cycles of 15sec 95°C and 1min 60°C. Ct values of precipitated DNA were calculated relative to input DNA (% input). ChIP-qPCR primers were designed using H3K4 methylation profiles available in the UCSC genome browser (human reference genome GRCh37/hg19) and the Mll1 ChIP-seq UCSC genome browser data set from Active Motif (https://www.activemotif.com/catalog/details/61295/mll-hrx-antibody-pab). Primer sequences used for ChIP-qPCR are given in Supplementary Table 2 (page 117).

5.11 SDS-PAGE and Western blotting.

Organoids were harvested and washed once in ice-cold 0.1% BSA-PBS and rinsed once in ice-cold PBS, cells were washed twice in ice-cold PBS prior to lysis in ice-cold RIPA buffer (50mM Tris pH8.0, 150mM NaCl, 0.1% SDS, 1% NP40, 0.5% sodium deoxycholate) containing 1x protease inhibitors (cOmplete Mini EDTA-free, Roche). For analysis of protein phosphorylation, phosphatase inhibitor cocktails 2 and 3 (Sigma) were added. Snap-frozen tissue samples were grinded with mortar and pestle on dry ice and lysed in RIPA buffer. Lysates were sonicated to disrupt cell membranes and fragment genomic DNA. Protein concentration was determined using the Bio-Rad Protein Assay (Bio-Rad, #500-0006) and measuring absorbance at 595nm with an iMark microplate reader (BioRad) according to the Bradford method. Equal concentrations of total protein were diluted with ice-cold PBS and denatured by boiling at 95°C for 5min in 1x SDS loading buffer (3x buffer: 180mM Tris/HCl pH6.8, 6% SDS, 30% glycerol, 15% β-mercaptoethanol and 0.01% bromphenol blue). The whole cell protein extracts were separated by molecular weight on polyacrylamide gels (stacking gel: 125mM Tris/HCl pH6.8, 0.1% SDS, 3% acrylamide, 0.1% ammonium persulfate, 0.1% TEMED; separating gel: 375mM Tris/HCl pH8.8, 6-12% acrylamide, 10% glycerol, 0.1% SDS, 0.025% ammonium persulfate, 0.1% TEMED) via SDS-PAGE running at 20mA per gel for about 1h in electrophoresis buffer (25mM Tris, 20mM glycine, 2% SDS). Proteins were transferred to a methanol-activated nitrocellulose membrane via semidry transfer for 1h 15min at 90mA or wet transfer for 3h at 85V and 4°C. Transfer buffer for semi-dry transfer was composed of 25mM Tris, 192mM glycine and 20% methanol; for wet transfer of 25mM Tris, 191mM glycine, 0.01% SDS and 20% methanol. To detect specific proteins, membranes were blocked with 5% BSA or 5% skim milk in 0.1% Tween20/TBS and probed with primary antibodies diluted in blocking solution over night at 4°C. Blots were washed three times in

0.1% Tween20/TBS and HRP-conjugated secondary antibodies were incubated in blocking solution for 1h at RT. Western blots were developed with Western Lightning Plus ECL (Perkin Elmer) for 3min and imaged with a Vilber Lourmat imaging system FUSION SL-3.

5.12 RNA preparation for RT-PCR analysis and RNA sequencing.

Total RNA from cells, organoids and snap-frozen tissue was isolated by Trizol extraction (Invitrogen) or with the NucleoSpin RNA isolation kit (Macherey-Nagel). DNA contaminations were removed by DNase1 digestion (Invitrogen) in the presence of RNase inhibitor (RNase Out, Invitrogen) and RNA was purified by phenol/chloroform extraction. For quantitative reverse transcription (RT)-PCR, 5µg of total RNA were reverse transcribed with random hexamer primers (Invitrogen) and MMLV reverse transcriptase (Promega, 200U/µl). RT-PCR was performed in a total volume of 20µl SYBR green reaction mix (Roche Diagnostics) containing 0.25µM of forward and reverse primers each in a CFX96-C1000T thermal cycler (BioRad): 2min 50°C, 2min 95°C followed by 42 cycles of 15sec 95°C and 1min 60°C. All reactions were performed in duplicates. Expression of target genes in treated versus control samples was calculated relative to the endogenous reference *Gapdh*, using the ΔΔCt method. Primer sequences used for RT-PCR are listed in Supplementary Table 3 (page 118).

For RNA sequencing of human colon cancer cells, total RNA from shMLL1 Ls174T cells induced with 300ng/ml doxycycline for 3 days and non-induced parental cells was isolated with the NucleoSpin RNA isolation kit (Macherey-Nagel). RNA from three independent pairs of induced and non-induced shMLL1 Ls174T cell clones was sequenced on a NextSeq500 (Illumina). RNA-seq reads were quality-checked by FASTQC (v0.11.5) software. Sequencing reads were mapped to the human whole genome (hg38) using STAR aligner (v. 2.5.3a) and default parameters. Read counts for each gene (gencode v12) were extracted from the BAM file using featureCounts software (v. 1.5.1). Read counts from different biological groups were subjected to differential expression analysis using the DESeq2 R statistical package. Comparisons between shMLL1 and parental control cells were corrected by individual technical replicates (paired comparison). In order to avoid background signal/noise, genes with less than 10 reads over all samples were excluded before adjusting the p-value for multiple testing. Genes with adjusted p-value lower than 0.05 and absolute fold-change ($\log_{10}$) higher than 0.5 were considered differentially expressed. Gene expression profile comparison was done by GeneOverlap R package by overlapping lists of differentially expressed genes (MGI symbol) from different sources ('Clevers'[195], 'Soshnikova'[204], 'Batlle'[89]) with our own data. All conversions from Ensembl ID to MGI symbol and from human gene names to mouse gene names were done by biomaRt. Heatmap was generated using the heatmap.2 function from R. Gene set enrichment analysis (GSEA) was performed using the R/Bioconductor package DOSE[249]. Volcano plots were generated by a generic R X-Y plotting using the $\log_2$FoldChange versus the $\log_2$ adjusted p-values. RNA-seq data from shMLL1 Ls174T human colon cancer

cells are available in the ArrayExpress database (http://www.ebi.ac.uk/arrayexpress) under accession number E-MTAB-8152.

For RNA sequencing of Lgr5-GFP$^+$ mouse intestinal stem cells, 300 single cells were sorted into a PCR tube containing 2µl of nuclease-free H_2O with 0.2% Triton-X100 and 4U murine RNase Inhibitor (NEB), and stored at -80°C. RNA isolation and library preparation were performed based on the Smart-seq2 protocol[250]. In brief, RNA was denatured for 3min at 72°C in the presence of 2.4mM dNTP (Invitrogen), 240nM dT-primer and 4U RNase Inhibitor (NEB), and reverse transcribed using the Superscript II Reverse Transcriptase (Invitrogen). Single-stranded cDNA was amplified with the Kapa HiFi HotStart Readymix (Roche) and purified using Sera-Mag SpeedBeads (GE Healthcare). cDNA quality and concentration were determined with the Fragment Analyzer (Agilent). Sequencing was performed on a NextSeq500 (Illumina) with a sample sequencing depth of 30mio reads on average. RNA-seq reads were aligned to the mm10 transcriptome with GSNAP (version 2018-07-04) and a table of read counts per gene was created based on the overlap of the uniquely mapped reads with the Ensembl Gene annotation (version 92), using featureCounts (version 1.6.3). Read counts were further processed with the DESeq2 R package (version 1.22.2). Sample-to-sample correlation was computed by Euclidean distance between samples based on the normalized counts. Differential gene expression analysis was performed with DESeq2, for which a maximum of 10% false discoveries (10% FDR) was accepted. Volcano plots were generated by a generic R X-Y plotting using the $\log_2$FoldChange versus the $\log_2$ adjusted p-values. RNA-seq data from Lgr5-GFP$^+$ intestinal stem cells are available under the GEO accession GSE148394.

5.13 Antibodies.

The following antibodies were used in this study (dilutions given for immunostaining/Western Blot and ChIP if applicable):

anti-Mll1 (D6G8N, Cell Signaling Technology #14197, RRID:AB_2688010, 1:100/1:2000, 1:50 for ChIP), anti-hSet1 (Bethyl A300-289A, RRID:AB_263413, 1:2000), anti-H3K4me3 (Cell Signaling Technology #9727, RRID:AB_561095, 1:2000/1:10,000, 1:50 for ChIP), anti-H3K27me3 (Millipore #07-449, RRID:AB_310624, 1:1000, 5µg for ChIP), anti-H3K4me2 (Millipore #07-030, RRID:AB_11213050, 1:5000), anti-H3K4me1 (Millipore #07-436, RRID:AB_310614, 1:5000), anti-H3K9me3 (Abcam Cat# ab8898, RRID:AB_306848, 1:2000/1:10,000), anti-H3 (Abcam ab1791, RRID:AB_302613, 1:10,000), anti-p21 (Santa Cruz Biotechnology sc-6246, RRID:AB_628073, 1:100/1:1000), anti-p53 (Millipore MABE327, RRID:AB_11213651, 1:500, 3µg for ChIP), anti-cleaved Caspase-3 (Cell Signaling Technology #9661, RRID:AB_2341188, 1:400/1:2000), anti-E-cadherin (BD Biosciences #610181, RRID:AB_397580, 1:200), anti-Mmp7 (Santa Cruz Biotechnology sc-26680, RRID:AB_2144469, 1:100), anti-GFP (Abcam #ab6673, RRID:AB_305643, 1:500), anti-Ki67 (Thermo Fisher Scientific MA5-14520, RRID:AB_10979488, 1:300), anti-BrdU (Abcam ab6326, RRID:AB_305426, 1:100), anti-β-catenin (BD Biosciences #610153, RRID:AB_397554, 1:300/1:1000, 3µg for ChIP), anti-β-catenin (PAIII, self-made by Huelsken et al. (1994)[251], 1:1000), anti-TCF4 (Cell Signaling Technology #2569, RRID:AB_2199816, 1:50 for ChIP), anti-Lyz (Agilent A0099, RRID:AB_2341230, 1:500), anti-ITF (Santa Cruz Biotechnology sc-18272, RRID:AB_2287326, 1:300), anti-GATA6 (R and D Systems Cat# AF1700, RRID:AB_2108901, 1:100-1:500), anti-GATA4 (Santa Cruz Biotechnology sc-25310, RRID:AB_627667, 1:200), anti-phospho-Erk1/2 (Sigma-Aldrich M8159, RRID:AB_477245, 1:3000 for Western Blot), anti-phospho-Erk1/2 (Cell Signaling Technology #4370, RRID:AB_2315112, 1:200 for IHC) anti-Erk1/2 (Cell Signaling 9102, RRID:AB_330744, 1:1000), anti-phospho-Mek1/2 (Cell Signaling Technology 9154, RRID:AB_2138017, 1:1000), anti-Mek1/2 (Cell Signaling Technology 4694, RRID:AB_10695868, 1:1000), anti-alpha tubulin (Sigma-Aldrich #00020911, RRID:AB_10013740, 1:10,000) and anti-vinculin antibody (Sigma-Aldrich V9131, RRID:AB_477629, 1:5000).

For immunofluorescence and immunohistochemistry, cyanine-labelled secondary antibodies (Jackson ImmunoResearch) and HRP-conjugated polymer and DAB reagent (DAKO) were used. IgG control antibodies were rabbit monoclonal IgG isotype control (Cell Signaling Technology #3900, RRID:AB_1550038) and mouse monoclonal IgG isotype control (Santa Cruz Biotechnology sc-2025, RRID:AB_737182). The specificity of histone modification antibodies was confirmed by dot blotting against synthetic peptides carrying the modifications of interest (Diagenode).

Table 3: Antibodies for immunostainings.

primary antibody	manufacturer and catalogue number	dilution	retrieval, blocking, primary antibody incubation
mouse anti-β-catenin	BD Biosciences #610153	1:300	Tris/EDTA pH8.5 or citrate pH6 boiling 4min P100 13-18min P40, 10% horse serum 1% BSA PBS-T
rabbit anti-β-catenin (PAIII)	self-made (Huelsken et al. 1994[251])	1:1000	Tris/EDTA pH8.5 boiling 4min P100 15min P40, 10% horse serum 1% BSA PBS-T
rat anti-BrdU	Abcam ab6326	1:100	Tris/EDTA pH8.5 boiling 4min P100 13min P40, 10% horse serum 1% BSA PBS-T
rabbit anti-cleaved Caspase-3	Cell Signaling Technology #9661	1:400	Tris/EDTA pH8.5 boiling 4min P100 13min P40, 10% horse serum 1% BSA PBS-T
mouse anti-E-cadherin	BD Biosciences #610181	1:200	Tris/EDTA pH8.5 or citrate pH6 boiling 4min P100 13-18min P40, 10% horse serum 1% BSA PBS-T
goat anti-GFP	Abcam ab6673	1:500	Tris/EDTA pH8.5 or citrate pH6 boiling 4min P100 13-18min P40, 10% horse serum 1% BSA PBS-T
goat anti-GATA6	R and D Systems Cat# AF1700	1:100 (1:500)	Citrate pH6 boiling 4min P100 18min P40, 5% horse serum 1% BSA PBS-T
mouse anti-GATA4	Santa Cruz Biotechnology sc-25310	1:200	Citrate pH6 boiling 4min P100 18min P40, 10% horse serum 1% BSA PBS-T
rabbit anti-H3K4me3	Cell Signaling Technology #9727	1:2000	Tris/EDTA pH8.5 boiling 4min P100 15min P40, 10% horse serum 1% BSA PBS-T
rabbit anti-H3K9me3	Abcam ab8898	1:2000	Tris/EDTA pH8.5 boiling 4min P100 13min P40, 5% horse serum 1% BSA PBS-T
goat anti-ITF	Santa Cruz Biotechnology sc-18272	1:300	Citrate pH6 boiling 4min P100 18min P40, 10% horse serum 1% BSA PBS-T
rabbit anti-Ki67	Thermo Fisher Scientific MA5-14520	1:300	Tris/EDTA pH8.5 boiling 4min P100 13min P40, 10% horse serum 1% BSA PBS-T
rabbit anti-Lyz	Agilent A0099	1:500	Citrate pH6 boiling 4min P100 18min P40, 10% horse serum 1% BSA PBS-T
rabbit anti-Mll1	D6G8N, Cell Signaling Technology #14197	1:100	**for IF:** citrate pH6 boiling 4min P100 18min P40, 10min -20°C methanol permeabilization, 5% horse serum 1% BSA PBS-T **for IHC:** Tris/EDTA pH8.5 boiling 5min P100 18min P40, 8min ice-cold methanol, 10% horse serum 1% BSA PBS-T
goat anti-Mmp7	Santa Cruz Biotechnology sc-26680	1:100	Citrate pH6 boiling 4min P100 18min P40, 10% horse serum 1% BSA PBS-T
mouse anti-p21	Santa Cruz Biotechnology sc-6246	1:100	Tris/EDTA pH8.5 boiling 4min P100 13min P40, 5% horse serum 1% BSA PBS-T
rabbit anti-phospho-Erk1/2	Cell Signaling Technology #4370	1:200	Tris/EDTA pH8.5 boiling 5min P100 35min P40, 10% horse serum 1% BSA **T**BS-T

5.14 Quantification and Statistical analysis.

All data are presented as mean ± SD unless otherwise indicated. For normalization data were calculated relative to the average value of controls. Statistical details of the experiments can be found in the figure legends. Graphs and statistics were generated with GraphPad Prism software. Tests for normal distribution were performed with D'Agostino-Pearson and Shapiro-Wilk tests. Significance (p-value) was determined with Mann-Whitney test (two-tailed) or two-tailed Student's t test. No statistical method was used to estimate sample size. No specific randomization or blinding protocol was used. N indicates the numbers of independent biological replicates per experiment unless otherwise indicated. p-value ≤ 0.05 was considered statistically significant ($p \leq 0.05$ *, $p \leq 0.01$ **, $p \leq 0.001$ ***, $p \leq 0.0001$ ****).

6 List of Figures

7 List of Tables

8 Abbreviations

APC	adenomatous polyposis coli
Ascl2	Achaete scute complex-like 2
Atoh1	atonal homologue 1
β-cat^{GOF}	gain-of-function mutation in β-catenin (Ctnnb1)
Bmp	bone morphogenetic protein
BrdU	bromodeoxyuridine
BSA	bovine serum albumin
CBC	crypt base columnar cells
CBP	CREB-binding protein
cDNA	complementary DNA
ChIP	chromatin immunoprecipitation
CSC	cancer stem cell
ctr	control
DAPI	4',6-diamidino-2-phenylindole
DMEM	Dulbecco's modified eagle medium
DNA	deoxyribonucleic acid
dNTP	deoxynucleotide triphosphate
EDTA	ethylenediamine tetraacetic acid
EdU	5-ethynyl-2'-deoxyuridine
e.g.	*exempli gratia*, for example
eGFP	enhanced green fluorescent protein
Ezh2	enhancer of zeste homolog 2
FACS	fluorescence-activated cell sorting
FBS	fetal bovine serum
FGF	fibroblast growth factor
FSC	forward scatter
GAPDH	glyceraldehyde 3-phosphate dehydrogenase
GATA4/6	GATA binding protein 4/6
GFP	green fluorescent protein
GOF	gain-of-function
GSK3β	glycogen synthase kinase 3β
Hath1	human atonal homologue 1
H&E	hematoxylin and eosin
i.e.	*id est*, that is
IF	immunofluorescence
Igfbp4	insulin-like growth factor-binding protein 4
IHC	immunohistochemistry
i.p.	intraperitoneal
IRES	internal ribosome entry site
Lgr5	leucine-rich repeat-containing G-protein coupled receptor 5
MAPK	mitogen-activated protein kinase
Math1	mouse atonal homologue 1
Mek1	mitogen-activated protein kinase (Mapk) kinase 1
MLL	mixed lineage leukemia
mRNA	messenger ribonucleic acid
NP-40	tergitol-type NP-40
ns	not significant

Olfm4	Olfactomedin-4
PBS	phosphate-buffered saline
PcG	Polycomb Group
PCR	polymerase chain reaction
PEI	polyethylenimine
pH	*potentium hydrogenii*
PHD	plant homeodomain
polyhema	poly(2-hydroxyethyl methacrylate)
PRC1	polycomb repressive complex 1
PRC2	polycomb repressive complex 2
RNA	ribonucleic acid
RNA pol II	RNA polymerase II
RT	room temperature
RT-PCR	(quantitative) reverse transcription PCR
SD	standard deviation
SDS	sodium dodecyl sulfate
SDS-PAGE	sodium dodecyl sulfate-polyacrylamide gel electrophoresis
SET	Su(var3-9), E(z), Trx; catalytic domain of histone lysine methyltransferases
Smoc2	secreted modular calcium-binding matricellular protein-2
Spdef	SAM pointed domain containing ETS transcription factor
SSC	side scatter
TA cell	transit-amplifying cell
TA zone	transit-amplifying zone
TBS	Tris-buffered saline
TCF4	T-cell factor 4 (TCF7L2)
TEMED	N, N, N’, N’-tetra-methylethylenediamine
tRFP	turbo red fluorescent protein
Tris	2-amino-2(hydroxymethyl)-1, 3-propandiol
Trx	trithorax
TrxG	Trithorax Group
TSS	transcription start site
Tween	polyoxyethylenesorbitan monolaurate
utr	untreated/non-induced
Wdr5	WD40-repeat domain protein 5
Wnt	wingless / homologue of int-1
WRAD	complex of Wdr5, Rbbp5, Ash2l and Dpy30 at the SET domain of Mll enzymes

9 References

1. Siegel, R.L., Miller, K.D. & Jemal, A. Cancer statistics, 2019. *CA Cancer J Clin* **69**, 7-34 (2019).
2. Kinzler, K.W. & Vogelstein, B. Lessons from hereditary colorectal cancer. *Cell* **87**, 159-170 (1996).
3. Sottoriva, A. *et al.* A Big Bang model of human colorectal tumor growth. *Nat Genet* **47**, 209-216 (2015).
4. Druliner, B.R. *et al.* Molecular characterization of colorectal adenomas with and without malignancy reveals distinguishing genome, transcriptome and methylome alterations. *Sci Rep* **8**, 3161 (2018).
5. Cancer Genome Atlas, N. Comprehensive molecular characterization of human colon and rectal cancer. *Nature* **487**, 330-337 (2012).
6. Drost, J. *et al.* Sequential cancer mutations in cultured human intestinal stem cells. *Nature* **521**, 43-47 (2015).
7. Leporrier, J. *et al.* A population-based study of the incidence, management and prognosis of hepatic metastases from colorectal cancer. *Br J Surg* **93**, 465-474 (2006).
8. Hanahan, D. & Weinberg, R.A. Hallmarks of cancer: the next generation. *Cell* **144**, 646-674 (2011).
9. Weinstein, I.B. Cancer. Addiction to oncogenes--the Achilles heal of cancer. *Science* **297**, 63-64 (2002).
10. Clevers, H. The intestinal crypt, a prototype stem cell compartment. *Cell* **154**, 274-284 (2013).
11. Leedham, S.J. *et al.* A basal gradient of Wnt and stem-cell number influences regional tumour distribution in human and mouse intestinal tracts. *Gut* **62**, 83-93 (2013).
12. Christie, M. *et al.* Different APC genotypes in proximal and distal sporadic colorectal cancers suggest distinct WNT/beta-catenin signalling thresholds for tumourigenesis. *Oncogene* **32**, 4675-4682 (2013).
13. Barker, N. Adult intestinal stem cells: critical drivers of epithelial homeostasis and regeneration. *Nat Rev Mol Cell Biol* **15**, 19-33 (2014).
14. Cheng, H. & Leblond, C.P. Origin, differentiation and renewal of the four main epithelial cell types in the mouse small intestine. I. Columnar cell. *Am J Anat* **141**, 461-479 (1974).
15. Barker, N. *et al.* Identification of stem cells in small intestine and colon by marker gene Lgr5. *Nature* **449**, 1003-1007 (2007).
16. Fevr, T., Robine, S., Louvard, D. & Huelsken, J. Wnt/beta-catenin is essential for intestinal homeostasis and maintenance of intestinal stem cells. *Mol Cell Biol* **27**, 7551-7559 (2007).
17. Korinek, V. *et al.* Depletion of epithelial stem-cell compartments in the small intestine of mice lacking Tcf-4. *Nat Genet* **19**, 379-383 (1998).
18. Klaus, A. & Birchmeier, W. Wnt signalling and its impact on development and cancer. *Nat Rev Cancer* **8**, 387-398 (2008).
19. Rubinfeld, B. *et al.* Association of the APC gene product with beta-catenin. *Science* **262**, 1731-1734 (1993).
20. Munemitsu, S., Albert, I., Souza, B., Rubinfeld, B. & Polakis, P. Regulation of intracellular beta-catenin levels by the adenomatous polyposis coli (APC) tumor-suppressor protein. *Proc Natl Acad Sci U S A* **92**, 3046-3050 (1995).
21. Liu, C. *et al.* Control of beta-catenin phosphorylation/degradation by a dual-kinase mechanism. *Cell* **108**, 837-847 (2002).
22. Behrens, J. *et al.* Functional interaction of an axin homolog, conductin, with beta-catenin, APC, and GSK3beta. *Science* **280**, 596-599 (1998).
23. Aberle, H., Bauer, A., Stappert, J., Kispert, A. & Kemler, R. beta-catenin is a target for the ubiquitin-proteasome pathway. *EMBO J* **16**, 3797-3804 (1997).
24. Li, V.S. *et al.* Wnt signaling through inhibition of beta-catenin degradation in an intact Axin1 complex. *Cell* **149**, 1245-1256 (2012).

25. MacDonald, B.T., Tamai, K. & He, X. Wnt/beta-catenin signaling: components, mechanisms, and diseases. *Dev Cell* **17**, 9-26 (2009).
26. Behrens, J. *et al.* Functional interaction of beta-catenin with the transcription factor LEF-1. *Nature* **382**, 638-642 (1996).
27. van Es, J.H. *et al.* A critical role for the Wnt effector Tcf4 in adult intestinal homeostatic self-renewal. *Mol Cell Biol* **32**, 1918-1927 (2012).
28. Cavallo, R.A. *et al.* Drosophila Tcf and Groucho interact to repress Wingless signalling activity. *Nature* **395**, 604-608 (1998).
29. Hecht, A., Vleminckx, K., Stemmler, M.P., van Roy, F. & Kemler, R. The p300/CBP acetyltransferases function as transcriptional coactivators of beta-catenin in vertebrates. *EMBO J* **19**, 1839-1850 (2000).
30. Thompson, B., Townsley, F., Rosin-Arbesfeld, R., Musisi, H. & Bienz, M. A new nuclear component of the Wnt signalling pathway. *Nat Cell Biol* **4**, 367-373 (2002).
31. Kramps, T. *et al.* Wnt/wingless signaling requires BCL9/legless-mediated recruitment of pygopus to the nuclear beta-catenin-TCF complex. *Cell* **109**, 47-60 (2002).
32. Brembeck, F.H. *et al.* Essential role of BCL9-2 in the switch between beta-catenin's adhesive and transcriptional functions. *Genes Dev* **18**, 2225-2230 (2004).
33. Lustig, B. *et al.* Negative feedback loop of Wnt signaling through upregulation of conductin/axin2 in colorectal and liver tumors. *Mol Cell Biol* **22**, 1184-1193 (2002).
34. de Lau, W. *et al.* Lgr5 homologues associate with Wnt receptors and mediate R-spondin signalling. *Nature* **476**, 293-297 (2011).
35. Carmon, K.S., Gong, X., Lin, Q., Thomas, A. & Liu, Q. R-spondins function as ligands of the orphan receptors LGR4 and LGR5 to regulate Wnt/beta-catenin signaling. *Proc Natl Acad Sci U S A* **108**, 11452-11457 (2011).
36. Koo, B.K. *et al.* Tumour suppressor RNF43 is a stem-cell E3 ligase that induces endocytosis of Wnt receptors. *Nature* **488**, 665-669 (2012).
37. Hao, H.X. *et al.* ZNRF3 promotes Wnt receptor turnover in an R-spondin-sensitive manner. *Nature* **485**, 195-200 (2012).
38. Yan, K.S. *et al.* Non-equivalence of Wnt and R-spondin ligands during Lgr5(+) intestinal stem-cell self-renewal. *Nature* **545**, 238-242 (2017).
39. Andreu, P. *et al.* Crypt-restricted proliferation and commitment to the Paneth cell lineage following Apc loss in the mouse intestine. *Development* **132**, 1443-1451 (2005).
40. He, X.C. *et al.* BMP signaling inhibits intestinal stem cell self-renewal through suppression of Wnt-beta-catenin signaling. *Nat Genet* **36**, 1117-1121 (2004).
41. Tian, H. *et al.* Opposing activities of Notch and Wnt signaling regulate intestinal stem cells and gut homeostasis. *Cell Rep* **11**, 33-42 (2015).
42. Qi, Z. *et al.* BMP restricts stemness of intestinal Lgr5(+) stem cells by directly suppressing their signature genes. *Nat Commun* **8**, 13824 (2017).
43. Kosinski, C. *et al.* Gene expression patterns of human colon tops and basal crypts and BMP antagonists as intestinal stem cell niche factors. *Proc Natl Acad Sci U S A* **104**, 15418-15423 (2007).
44. Pellegrinet, L. *et al.* Dll1- and dll4-mediated notch signaling are required for homeostasis of intestinal stem cells. *Gastroenterology* **140**, 1230-1240 e1231-1237 (2011).
45. Marshman, E., Booth, C. & Potten, C.S. The intestinal epithelial stem cell. *Bioessays* **24**, 91-98 (2002).
46. Batlle, E. *et al.* Beta-catenin and TCF mediate cell positioning in the intestinal epithelium by controlling the expression of EphB/ephrinB. *Cell* **111**, 251-263 (2002).
47. Ireland, H., Houghton, C., Howard, L. & Winton, D.J. Cellular inheritance of a Cre-activated reporter gene to determine Paneth cell longevity in the murine small intestine. *Dev Dyn* **233**, 1332-1336 (2005).
48. Sato, T. *et al.* Paneth cells constitute the niche for Lgr5 stem cells in intestinal crypts. *Nature* **469**, 415-418 (2011).
49. Durand, A. *et al.* Functional intestinal stem cells after Paneth cell ablation induced by the loss of transcription factor Math1 (Atoh1). *Proc Natl Acad Sci U S A* **109**, 8965-8970 (2012).

50. Aoki, R. *et al.* Foxl1-expressing mesenchymal cells constitute the intestinal stem cell niche. *Cell Mol Gastroenterol Hepatol* **2**, 175-188 (2016).
51. Valenta, T. *et al.* Wnt Ligands Secreted by Subepithelial Mesenchymal Cells Are Essential for the Survival of Intestinal Stem Cells and Gut Homeostasis. *Cell Rep* **15**, 911-918 (2016).
52. Gregorieff, A. *et al.* Expression pattern of Wnt signaling components in the adult intestine. *Gastroenterology* **129**, 626-638 (2005).
53. Farin, H.F. *et al.* Visualization of a short-range Wnt gradient in the intestinal stem-cell niche. *Nature* **530**, 340-343 (2016).
54. Auclair, B.A., Benoit, Y.D., Rivard, N., Mishina, Y. & Perreault, N. Bone morphogenetic protein signaling is essential for terminal differentiation of the intestinal secretory cell lineage. *Gastroenterology* **133**, 887-896 (2007).
55. Fre, S. *et al.* Notch signals control the fate of immature progenitor cells in the intestine. *Nature* **435**, 964-968 (2005).
56. Yang, Q., Bermingham, N.A., Finegold, M.J. & Zoghbi, H.Y. Requirement of Math1 for secretory cell lineage commitment in the mouse intestine. *Science* **294**, 2155-2158 (2001).
57. van Es, J.H. *et al.* Notch/gamma-secretase inhibition turns proliferative cells in intestinal crypts and adenomas into goblet cells. *Nature* **435**, 959-963 (2005).
58. Shroyer, N.F. *et al.* Intestine-specific ablation of mouse atonal homolog 1 (Math1) reveals a role in cellular homeostasis. *Gastroenterology* **132**, 2478-2488 (2007).
59. Riccio, O. *et al.* Loss of intestinal crypt progenitor cells owing to inactivation of both Notch1 and Notch2 is accompanied by derepression of CDK inhibitors p27Kip1 and p57Kip2. *EMBO Rep* **9**, 377-383 (2008).
60. Stamataki, D. *et al.* Delta1 expression, cell cycle exit, and commitment to a specific secretory fate coincide within a few hours in the mouse intestinal stem cell system. *PLoS One* **6**, e24484 (2011).
61. Shroyer, N.F., Wallis, D., Venken, K.J., Bellen, H.J. & Zoghbi, H.Y. Gfi1 functions downstream of Math1 to control intestinal secretory cell subtype allocation and differentiation. *Genes Dev* **19**, 2412-2417 (2005).
62. Gregorieff, A. *et al.* The ets-domain transcription factor Spdef promotes maturation of goblet and paneth cells in the intestinal epithelium. *Gastroenterology* **137**, 1333-1345 e1331-1333 (2009).
63. Noah, T.K., Kazanjian, A., Whitsett, J. & Shroyer, N.F. SAM pointed domain ETS factor (SPDEF) regulates terminal differentiation and maturation of intestinal goblet cells. *Exp Cell Res* **316**, 452-465 (2010).
64. Heuberger, J. *et al.* Shp2/MAPK signaling controls goblet/paneth cell fate decisions in the intestine. *Proc Natl Acad Sci U S A* **111**, 3472-3477 (2014).
65. van Es, J.H. *et al.* Wnt signalling induces maturation of Paneth cells in intestinal crypts. *Nat Cell Biol* **7**, 381-386 (2005).
66. Sansom, O.J. *et al.* Loss of Apc in vivo immediately perturbs Wnt signaling, differentiation, and migration. *Genes Dev* **18**, 1385-1390 (2004).
67. de Sousa, E.M.F. & de Sauvage, F.J. Cellular Plasticity in Intestinal Homeostasis and Disease. *Cell Stem Cell* **24**, 54-64 (2019).
68. Tian, H. *et al.* A reserve stem cell population in small intestine renders Lgr5-positive cells dispensable. *Nature* **478**, 255-259 (2011).
69. Buczacki, S.J. *et al.* Intestinal label-retaining cells are secretory precursors expressing Lgr5. *Nature* **495**, 65-69 (2013).
70. Castillo-Azofeifa, D. *et al.* Atoh1(+) secretory progenitors possess renewal capacity independent of Lgr5(+) cells during colonic regeneration. *EMBO J* **38** (2019).
71. Ishibashi, F. *et al.* Contribution of ATOH1(+) Cells to the Homeostasis, Repair, and Tumorigenesis of the Colonic Epithelium. *Stem Cell Reports* **10**, 27-42 (2018).
72. Tetteh, P.W. *et al.* Replacement of Lost Lgr5-Positive Stem Cells through Plasticity of Their Enterocyte-Lineage Daughters. *Cell Stem Cell* **18**, 203-213 (2016).
73. Yu, S. *et al.* Paneth Cell Multipotency Induced by Notch Activation following Injury. *Cell Stem Cell* **23**, 46-59 e45 (2018).

74. Sato, T. *et al.* Single Lgr5 stem cells build crypt-villus structures in vitro without a mesenchymal niche. *Nature* **459**, 262-265 (2009).
75. Clevers, H. Modeling Development and Disease with Organoids. *Cell* **165**, 1586-1597 (2016).
76. van de Wetering, M. *et al.* Prospective derivation of a living organoid biobank of colorectal cancer patients. *Cell* **161**, 933-945 (2015).
77. Morin, P.J. *et al.* Activation of beta-catenin-Tcf signaling in colon cancer by mutations in beta-catenin or APC. *Science* **275**, 1787-1790 (1997).
78. Harada, N. *et al.* Intestinal polyposis in mice with a dominant stable mutation of the beta-catenin gene. *EMBO J* **18**, 5931-5942 (1999).
79. Barker, N. *et al.* Crypt stem cells as the cells-of-origin of intestinal cancer. *Nature* **457**, 608-611 (2009).
80. Preston, S.L. *et al.* Bottom-up histogenesis of colorectal adenomas: origin in the monocryptal adenoma and initial expansion by crypt fission. *Cancer Res* **63**, 3819-3825 (2003).
81. Shih, I.M. *et al.* Top-down morphogenesis of colorectal tumors. *Proc Natl Acad Sci U S A* **98**, 2640-2645 (2001).
82. Schwitalla, S. *et al.* Intestinal tumorigenesis initiated by dedifferentiation and acquisition of stem-cell-like properties. *Cell* **152**, 25-38 (2013).
83. Scholer-Dahirel, A. *et al.* Maintenance of adenomatous polyposis coli (APC)-mutant colorectal cancer is dependent on Wnt/beta-catenin signaling. *Proc Natl Acad Sci U S A* **108**, 17135-17140 (2011).
84. Dow, L.E. *et al.* Apc Restoration Promotes Cellular Differentiation and Reestablishes Crypt Homeostasis in Colorectal Cancer. *Cell* **161**, 1539-1552 (2015).
85. Fodde, R. & Brabletz, T. Wnt/beta-catenin signaling in cancer stemness and malignant behavior. *Curr Opin Cell Biol* **19**, 150-158 (2007).
86. Schepers, A.G. *et al.* Lineage tracing reveals Lgr5+ stem cell activity in mouse intestinal adenomas. *Science* **337**, 730-735 (2012).
87. Vermeulen, L. *et al.* Single-cell cloning of colon cancer stem cells reveals a multi-lineage differentiation capacity. *Proc Natl Acad Sci U S A* **105**, 13427-13432 (2008).
88. Vermeulen, L. *et al.* Wnt activity defines colon cancer stem cells and is regulated by the microenvironment. *Nat Cell Biol* **12**, 468-476 (2010).
89. Merlos-Suarez, A. *et al.* The intestinal stem cell signature identifies colorectal cancer stem cells and predicts disease relapse. *Cell Stem Cell* **8**, 511-524 (2011).
90. Martin, M.L. *et al.* Logarithmic expansion of LGR5(+) cells in human colorectal cancer. *Cell Signal* **42**, 97-105 (2018).
91. de Sousa e Melo, F. *et al.* A distinct role for Lgr5(+) stem cells in primary and metastatic colon cancer. *Nature* **543**, 676-680 (2017).
92. van der Flier, L.G. *et al.* Transcription factor achaete scute-like 2 controls intestinal stem cell fate. *Cell* **136**, 903-912 (2009).
93. Dalerba, P. *et al.* Phenotypic characterization of human colorectal cancer stem cells. *Proc Natl Acad Sci U S A* **104**, 10158-10163 (2007).
94. Shvab, A. *et al.* Induction of the intestinal stem cell signature gene SMOC-2 is required for L1-mediated colon cancer progression. *Oncogene* **35**, 549-557 (2016).
95. VanDussen, K.L. *et al.* Notch signaling modulates proliferation and differentiation of intestinal crypt base columnar stem cells. *Development* **139**, 488-497 (2012).
96. Liu, W. *et al.* Olfactomedin 4 deletion induces colon adenocarcinoma in Apc(Min/+) mice. *Oncogene* **35**, 5237-5247 (2016).
97. Batlle, E. & Clevers, H. Cancer stem cells revisited. *Nat Med* **23**, 1124-1134 (2017).
98. Dylla, S.J. *et al.* Colorectal cancer stem cells are enriched in xenogeneic tumors following chemotherapy. *PLoS One* **3**, e2428 (2008).
99. Shimokawa, M. *et al.* Visualization and targeting of LGR5(+) human colon cancer stem cells. *Nature* **545**, 187-192 (2017).
100. Fang, L. *et al.* A Small-Molecule Antagonist of the beta-Catenin/TCF4 Interaction Blocks the Self-Renewal of Cancer Stem Cells and Suppresses Tumorigenesis. *Cancer Res* **76**, 891-901 (2016).

101. Emami, K.H. *et al.* A small molecule inhibitor of beta-catenin/CREB-binding protein transcription [corrected]. *Proc Natl Acad Sci U S A* **101**, 12682-12687 (2004).
102. Kahn, M. Can we safely target the WNT pathway? *Nat Rev Drug Discov* **13**, 513-532 (2014).
103. Dawson, M.A. & Kouzarides, T. Cancer epigenetics: from mechanism to therapy. *Cell* **150**, 12-27 (2012).
104. Waddington, C.H. The epigenotype. 1942. *Int J Epidemiol* **41**, 10-13 (2012).
105. Shilatifard, A. The COMPASS family of histone H3K4 methylases: mechanisms of regulation in development and disease pathogenesis. *Annu Rev Biochem* **81**, 65-95 (2012).
106. Wohrle, S., Wallmen, B. & Hecht, A. Differential control of Wnt target genes involves epigenetic mechanisms and selective promoter occupancy by T-cell factors. *Mol Cell Biol* **27**, 8164-8177 (2007).
107. Van der Flier, L.G. *et al.* The Intestinal Wnt/TCF Signature. *Gastroenterology* **132**, 628-632 (2007).
108. Nakamura, Y., de Paiva Alves, E., Veenstra, G.J. & Hoppler, S. Tissue- and stage-specific Wnt target gene expression is controlled subsequent to beta-catenin recruitment to cis-regulatory modules. *Development* **143**, 1914-1925 (2016).
109. Teo, J.L., Ma, H., Nguyen, C., Lam, C. & Kahn, M. Specific inhibition of CBP/beta-catenin interaction rescues defects in neuronal differentiation caused by a presenilin-1 mutation. *Proc Natl Acad Sci U S A* **102**, 12171-12176 (2005).
110. Kouzarides, T. Chromatin modifications and their function. *Cell* **128**, 693-705 (2007).
111. Barski, A. *et al.* High-resolution profiling of histone methylations in the human genome. *Cell* **129**, 823-837 (2007).
112. Strahl, B.D. & Allis, C.D. The language of covalent histone modifications. *Nature* **403**, 41-45 (2000).
113. Zhang, Y. & Reinberg, D. Transcription regulation by histone methylation: interplay between different covalent modifications of the core histone tails. *Genes Dev* **15**, 2343-2360 (2001).
114. Jenuwein, T., Laible, G., Dorn, R. & Reuter, G. SET domain proteins modulate chromatin domains in eu- and heterochromatin. *Cell Mol Life Sci* **54**, 80-93 (1998).
115. Feng, Q. *et al.* Methylation of H3-lysine 79 is mediated by a new family of HMTases without a SET domain. *Curr Biol* **12**, 1052-1058 (2002).
116. Shi, Y. *et al.* Histone demethylation mediated by the nuclear amine oxidase homolog LSD1. *Cell* **119**, 941-953 (2004).
117. Bernstein, B.E. *et al.* Genomic maps and comparative analysis of histone modifications in human and mouse. *Cell* **120**, 169-181 (2005).
118. Heintzman, N.D. *et al.* Distinct and predictive chromatin signatures of transcriptional promoters and enhancers in the human genome. *Nat Genet* **39**, 311-318 (2007).
119. Wysocka, J. *et al.* A PHD finger of NURF couples histone H3 lysine 4 trimethylation with chromatin remodelling. *Nature* **442**, 86-90 (2006).
120. Vermeulen, M. *et al.* Selective anchoring of TFIID to nucleosomes by trimethylation of histone H3 lysine 4. *Cell* **131**, 58-69 (2007).
121. Santos-Rosa, H. *et al.* Active genes are tri-methylated at K4 of histone H3. *Nature* **419**, 407-411 (2002).
122. Hodl, M. & Basler, K. Transcription in the absence of histone H3.2 and H3K4 methylation. *Curr Biol* **22**, 2253-2257 (2012).
123. Howe, F.S., Fischl, H., Murray, S.C. & Mellor, J. Is H3K4me3 instructive for transcription activation? *Bioessays* **39**, 1-12 (2017).
124. Stein, A.B. *et al.* Loss of H3K4 methylation destabilizes gene expression patterns and physiological functions in adult murine cardiomyocytes. *J Clin Invest* **121**, 2641-2650 (2011).
125. Benayoun, B.A. *et al.* H3K4me3 breadth is linked to cell identity and transcriptional consistency. *Cell* **158**, 673-688 (2014).
126. Roguev, A. *et al.* The Saccharomyces cerevisiae Set1 complex includes an Ash2 homologue and methylates histone 3 lysine 4. *EMBO J* **20**, 7137-7148 (2001).

127. Mohan, M. *et al.* The COMPASS family of H3K4 methylases in Drosophila. *Mol Cell Biol* **31**, 4310-4318 (2011).
128. van Nuland, R. *et al.* Quantitative dissection and stoichiometry determination of the human SET1/MLL histone methyltransferase complexes. *Mol Cell Biol* **33**, 2067-2077 (2013).
129. Hu, D. *et al.* The MLL3/MLL4 branches of the COMPASS family function as major histone H3K4 monomethylases at enhancers. *Mol Cell Biol* **33**, 4745-4754 (2013).
130. Wu, M. *et al.* Molecular regulation of H3K4 trimethylation by Wdr82, a component of human Set1/COMPASS. *Mol Cell Biol* **28**, 7337-7344 (2008).
131. Ardehali, M.B. *et al.* Drosophila Set1 is the major histone H3 lysine 4 trimethyltransferase with role in transcription. *EMBO J* **30**, 2817-2828 (2011).
132. Rao, R.C. & Dou, Y. Hijacked in cancer: the KMT2 (MLL) family of methyltransferases. *Nat Rev Cancer* **15**, 334-346 (2015).
133. Zhang, Y. *et al.* Evolving Catalytic Properties of the MLL Family SET Domain. *Structure* **23**, 1921-1933 (2015).
134. Piunti, A. & Shilatifard, A. Epigenetic balance of gene expression by Polycomb and COMPASS families. *Science* **352**, aad9780 (2016).
135. Di Croce, L. & Helin, K. Transcriptional regulation by Polycomb group proteins. *Nat Struct Mol Biol* **20**, 1147-1155 (2013).
136. Wang, H. *et al.* Role of histone H2A ubiquitination in Polycomb silencing. *Nature* **431**, 873-878 (2004).
137. Ringrose, L. & Paro, R. Epigenetic regulation of cellular memory by the Polycomb and Trithorax group proteins. *Annu Rev Genet* **38**, 413-443 (2004).
138. Brand, M., Nakka, K., Zhu, J. & Dilworth, F.J. Polycomb/Trithorax Antagonism: Cellular Memory in Stem Cell Fate and Function. *Cell Stem Cell* **24**, 518-533 (2019).
139. Benard, A. *et al.* Histone trimethylation at H3K4, H3K9 and H4K20 correlates with patient survival and tumor recurrence in early-stage colon cancer. *BMC Cancer* **14**, 531 (2014).
140. Chiacchiera, F. *et al.* Polycomb Complex PRC1 Preserves Intestinal Stem Cell Identity by Sustaining Wnt/beta-Catenin Transcriptional Activity. *Cell Stem Cell* **18**, 91-103 (2016).
141. Salz, T. *et al.* hSETD1A regulates Wnt target genes and controls tumor growth of colorectal cancer cells. *Cancer Res* **74**, 775-786 (2014).
142. Ansari, K.I., Kasiri, S., Mishra, B.P. & Mandal, S.S. Mixed lineage leukaemia-4 regulates cell-cycle progression and cell viability and its depletion suppresses growth of xenografted tumour in vivo. *Br J Cancer* **107**, 315-324 (2012).
143. Natarajan, T.G. *et al.* Epigenetic regulator MLL2 shows altered expression in cancer cell lines and tumors from human breast and colon. *Cancer Cell Int* **10**, 13 (2010).
144. Krivtsov, A.V. & Armstrong, S.A. MLL translocations, histone modifications and leukaemia stem-cell development. *Nat Rev Cancer* **7**, 823-833 (2007).
145. Thiel, A.T. *et al.* MLL-AF9-induced leukemogenesis requires coexpression of the wild-type Mll allele. *Cancer Cell* **17**, 148-159 (2010).
146. Chen, Y. *et al.* MLL2, Not MLL1, Plays a Major Role in Sustaining MLL-Rearranged Acute Myeloid Leukemia. *Cancer Cell* **31**, 755-770 e756 (2017).
147. Grembecka, J. *et al.* Menin-MLL inhibitors reverse oncogenic activity of MLL fusion proteins in leukemia. *Nat Chem Biol* **8**, 277-284 (2012).
148. Cao, F. *et al.* Targeting MLL1 H3K4 methyltransferase activity in mixed-lineage leukemia. *Mol Cell* **53**, 247-261 (2014).
149. Grebien, F. *et al.* Pharmacological targeting of the Wdr5-MLL interaction in C/EBPalpha N-terminal leukemia. *Nat Chem Biol* **11**, 571-578 (2015).
150. Erfurth, F.E. *et al.* MLL protects CpG clusters from methylation within the Hoxa9 gene, maintaining transcript expression. *Proc Natl Acad Sci U S A* **105**, 7517-7522 (2008).
151. Cosgrove, M.S. & Patel, A. Mixed lineage leukemia: a structure-function perspective of the MLL1 protein. *FEBS J* **277**, 1832-1842 (2010).
152. Hsieh, J.J., Cheng, E.H. & Korsmeyer, S.J. Taspase1: a threonine aspartase required for cleavage of MLL and proper HOX gene expression. *Cell* **115**, 293-303 (2003).

153. Hsieh, J.J., Ernst, P., Erdjument-Bromage, H., Tempst, P. & Korsmeyer, S.J. Proteolytic cleavage of MLL generates a complex of N- and C-terminal fragments that confers protein stability and subnuclear localization. *Mol Cell Biol* **23**, 186-194 (2003).
154. Southall, S.M., Wong, P.S., Odho, Z., Roe, S.M. & Wilson, J.R. Structural basis for the requirement of additional factors for MLL1 SET domain activity and recognition of epigenetic marks. *Mol Cell* **33**, 181-191 (2009).
155. Yokoyama, A. *et al.* Leukemia proto-oncoprotein MLL forms a SET1-like histone methyltransferase complex with menin to regulate Hox gene expression. *Mol Cell Biol* **24**, 5639-5649 (2004).
156. Yokoyama, A. & Cleary, M.L. Menin critically links MLL proteins with LEDGF on cancer-associated target genes. *Cancer Cell* **14**, 36-46 (2008).
157. Artinger, E.L. *et al.* An MLL-dependent network sustains hematopoiesis. *Proc Natl Acad Sci U S A* **110**, 12000-12005 (2013).
158. Milne, T.A. *et al.* Menin and MLL cooperatively regulate expression of cyclin-dependent kinase inhibitors. *Proc Natl Acad Sci U S A* **102**, 749-754 (2005).
159. Dou, Y. *et al.* Physical association and coordinate function of the H3 K4 methyltransferase MLL1 and the H4 K16 acetyltransferase MOF. *Cell* **121**, 873-885 (2005).
160. Arai, M., Dyson, H.J. & Wright, P.E. Leu628 of the KIX domain of CBP is a key residue for the interaction with the MLL transactivation domain. *FEBS Lett* **584**, 4500-4504 (2010).
161. Sierra, J., Yoshida, T., Joazeiro, C.A. & Jones, K.A. The APC tumor suppressor counteracts beta-catenin activation and H3K4 methylation at Wnt target genes. *Genes Dev* **20**, 586-600 (2006).
162. Zhu, Q. *et al.* The Wnt-Driven Mll1 Epigenome Regulates Salivary Gland and Head and Neck Cancer. *Cell Rep* **26**, 415-428 e415 (2019).
163. Wang, P. *et al.* Global analysis of H3K4 methylation defines MLL family member targets and points to a role for MLL1-mediated H3K4 methylation in the regulation of transcriptional initiation by RNA polymerase II. *Mol Cell Biol* **29**, 6074-6085 (2009).
164. Wang, K.C. *et al.* A long noncoding RNA maintains active chromatin to coordinate homeotic gene expression. *Nature* **472**, 120-124 (2011).
165. Yu, B.D., Hess, J.L., Horning, S.E., Brown, G.A. & Korsmeyer, S.J. Altered Hox expression and segmental identity in Mll-mutant mice. *Nature* **378**, 505-508 (1995).
166. Yagi, H. *et al.* Growth disturbance in fetal liver hematopoiesis of Mll-mutant mice. *Blood* **92**, 108-117 (1998).
167. Ernst, P., Mabon, M., Davidson, A.J., Zon, L.I. & Korsmeyer, S.J. An Mll-dependent Hox program drives hematopoietic progenitor expansion. *Curr Biol* **14**, 2063-2069 (2004).
168. Yu, B.D., Hanson, R.D., Hess, J.L., Horning, S.E. & Korsmeyer, S.J. MLL, a mammalian trithorax-group gene, functions as a transcriptional maintenance factor in morphogenesis. *Proc Natl Acad Sci U S A* **95**, 10632-10636 (1998).
169. Jones, W.D. *et al.* De novo mutations in MLL cause Wiedemann-Steiner syndrome. *Am J Hum Genet* **91**, 358-364 (2012).
170. McMahon, K.A. *et al.* Mll has a critical role in fetal and adult hematopoietic stem cell self-renewal. *Cell Stem Cell* **1**, 338-345 (2007).
171. Jude, C.D. *et al.* Unique and independent roles for MLL in adult hematopoietic stem cells and progenitors. *Cell Stem Cell* **1**, 324-337 (2007).
172. Ernst, P. *et al.* Definitive hematopoiesis requires the mixed-lineage leukemia gene. *Dev Cell* **6**, 437-443 (2004).
173. Mishra, B.P. *et al.* The histone methyltransferase activity of MLL1 is dispensable for hematopoiesis and leukemogenesis. *Cell Rep* **7**, 1239-1247 (2014).
174. Lim, D.A. *et al.* Chromatin remodelling factor Mll1 is essential for neurogenesis from postnatal neural stem cells. *Nature* **458**, 529-533 (2009).
175. Kawabe, Y., Wang, Y.X., McKinnell, I.W., Bedford, M.T. & Rudnicki, M.A. Carm1 regulates Pax7 transcriptional activity through MLL1/2 recruitment during asymmetric satellite stem cell divisions. *Cell Stem Cell* **11**, 333-345 (2012).

176. Addicks, G.C. *et al.* MLL1 is required for PAX7 expression and satellite cell self-renewal in mice. *Nat Commun* **10**, 4256 (2019).
177. Weirich, S., Kudithipudi, S. & Jeltsch, A. Somatic cancer mutations in the MLL1 histone methyltransferase modulate its enzymatic activity and dependence on the WDR5/RBBP5/ASH2L complex. *Mol Oncol* **11**, 373-387 (2017).
178. Wend, P. *et al.* Wnt/beta-catenin signalling induces MLL to create epigenetic changes in salivary gland tumours. *EMBO J* **32**, 1977-1989 (2013).
179. Qiang, R. *et al.* MLL1 promotes cervical carcinoma cell tumorigenesis and metastasis through interaction with beta-catenin. *Onco Targets Ther* **9**, 6631-6640 (2016).
180. Gallo, M. *et al.* A tumorigenic MLL-homeobox network in human glioblastoma stem cells. *Cancer Res* **73**, 417-427 (2013).
181. Ansari, K.I., Kasiri, S. & Mandal, S.S. Histone methylase MLL1 has critical roles in tumor growth and angiogenesis and its knockdown suppresses tumor growth in vivo. *Oncogene* **32**, 3359-3370 (2013).
182. Zhang, C. *et al.* KMT2A promotes melanoma cell growth by targeting hTERT signaling pathway. *Cell Death Dis* **8**, e2940 (2017).
183. Zhu, J. *et al.* Gain-of-function p53 mutants co-opt chromatin pathways to drive cancer growth. *Nature* **525**, 206-211 (2015).
184. Malik, R. *et al.* Targeting the MLL complex in castration-resistant prostate cancer. *Nat Med* **21**, 344-352 (2015).
185. Crosnier, C., Stamataki, D. & Lewis, J. Organizing cell renewal in the intestine: stem cells, signals and combinatorial control. *Nat Rev Genet* **7**, 349-359 (2006).
186. Porter, E.M., Bevins, C.L., Ghosh, D. & Ganz, T. The multifaceted Paneth cell. *Cell Mol Life Sci* **59**, 156-170 (2002).
187. Russell, R.G., Lasorella, A., Dettin, L.E. & Iavarone, A. Id2 drives differentiation and suppresses tumor formation in the intestinal epithelium. *Cancer Res* **64**, 7220-7225 (2004).
188. Kranz, A. *et al.* An improved Flp deleter mouse in C57Bl/6 based on Flpo recombinase. *Genesis* **48**, 512-520 (2010).
189. Soriano, P. Generalized lacZ expression with the ROSA26 Cre reporter strain. *Nat Genet* **21**, 70-71 (1999).
190. Morita, H. *et al.* Neonatal lethality of LGR5 null mice is associated with ankyloglossia and gastrointestinal distension. *Mol Cell Biol* **24**, 9736-9743 (2004).
191. Schuijers, J., van der Flier, L.G., van Es, J. & Clevers, H. Robust cre-mediated recombination in small intestinal stem cells utilizing the olfm4 locus. *Stem Cell Reports* **3**, 234-241 (2014).
192. Jaks, V. *et al.* Lgr5 marks cycling, yet long-lived, hair follicle stem cells. *Nat Genet* **40**, 1291-1299 (2008).
193. Barker, N. *et al.* Lgr5(+ve) stem/progenitor cells contribute to nephron formation during kidney development. *Cell Rep* **2**, 540-552 (2012).
194. Barker, N. *et al.* Lgr5(+ve) stem cells drive self-renewal in the stomach and build long-lived gastric units in vitro. *Cell Stem Cell* **6**, 25-36 (2010).
195. Munoz, J. *et al.* The Lgr5 intestinal stem cell signature: robust expression of proposed quiescent '+4' cell markers. *EMBO J* **31**, 3079-3091 (2012).
196. Farrall, A.L. *et al.* Wnt and BMP signals control intestinal adenoma cell fates. *Int J Cancer* **131**, 2242-2252 (2012).
197. Haber, A.L. *et al.* A single-cell survey of the small intestinal epithelium. *Nature* **551**, 333-339 (2017).
198. Van der Sluis, M. *et al.* Muc2-deficient mice spontaneously develop colitis, indicating that MUC2 is critical for colonic protection. *Gastroenterology* **131**, 117-129 (2006).
199. Lo, Y.H. *et al.* Transcriptional Regulation by ATOH1 and its Target SPDEF in the Intestine. *Cell Mol Gastroenterol Hepatol* **3**, 51-71 (2017).
200. Berg, K.C.G. *et al.* Multi-omics of 34 colorectal cancer cell lines - a resource for biomedical studies. *Mol Cancer* **16**, 116 (2017).
201. Meerbrey, K.L. *et al.* The pINDUCER lentiviral toolkit for inducible RNA interference in vitro and in vivo. *Proc Natl Acad Sci U S A* **108**, 3665-3670 (2011).

202. Zuber, J. *et al.* Toolkit for evaluating genes required for proliferation and survival using tetracycline-regulated RNAi. *Nat Biotechnol* **29**, 79-83 (2011).
203. Whissell, G. *et al.* The transcription factor GATA6 enables self-renewal of colon adenoma stem cells by repressing BMP gene expression. *Nat Cell Biol* **16**, 695-707 (2014).
204. Nigmatullina, L. *et al.* Id2 controls specification of Lgr5(+) intestinal stem cell progenitors during gut development. *EMBO J* **36**, 869-885 (2017).
205. Blache, P. *et al.* SOX9 is an intestine crypt transcription factor, is regulated by the Wnt pathway, and represses the CDX2 and MUC2 genes. *J Cell Biol* **166**, 37-47 (2004).
206. Molenaar, M. *et al.* XTcf-3 transcription factor mediates beta-catenin-induced axis formation in Xenopus embryos. *Cell* **86**, 391-399 (1996).
207. Ring, D.B. *et al.* Selective glycogen synthase kinase 3 inhibitors potentiate insulin activation of glucose transport and utilization in vitro and in vivo. *Diabetes* **52**, 588-595 (2003).
208. Li, B.E., Gan, T., Meyerson, M., Rabbitts, T.H. & Ernst, P. Distinct pathways regulated by menin and by MLL1 in hematopoietic stem cells and developing B cells. *Blood* **122**, 2039-2046 (2013).
209. McCabe, M.T. *et al.* EZH2 inhibition as a therapeutic strategy for lymphoma with EZH2-activating mutations. *Nature* **492**, 108-112 (2012).
210. Chan, C.W. *et al.* Gastrointestinal differentiation marker Cytokeratin 20 is regulated by homeobox gene CDX1. *Proc Natl Acad Sci U S A* **106**, 1936-1941 (2009).
211. Bosse, T. *et al.* Gata4 is essential for the maintenance of jejunal-ileal identities in the adult mouse small intestine. *Mol Cell Biol* **26**, 9060-9070 (2006).
212. van de Wetering, M. *et al.* The beta-catenin/TCF-4 complex imposes a crypt progenitor phenotype on colorectal cancer cells. *Cell* **111**, 241-250 (2002).
213. Kretzschmar, M., Liu, F., Hata, A., Doody, J. & Massague, J. The TGF-beta family mediator Smad1 is phosphorylated directly and activated functionally by the BMP receptor kinase. *Genes Dev* **11**, 984-995 (1997).
214. Leverkoehne, I. & Gruber, A.D. The murine mCLCA3 (alias gob-5) protein is located in the mucin granule membranes of intestinal, respiratory, and uterine goblet cells. *J Histochem Cytochem* **50**, 829-838 (2002).
215. el-Deiry, W.S. *et al.* WAF1, a potential mediator of p53 tumor suppression. *Cell* **75**, 817-825 (1993).
216. Itahana, Y. *et al.* Histone modifications and p53 binding poise the p21 promoter for activation in human embryonic stem cells. *Sci Rep* **6**, 28112 (2016).
217. Stein, G.H., Drullinger, L.F., Soulard, A. & Dulic, V. Differential roles for cyclin-dependent kinase inhibitors p21 and p16 in the mechanisms of senescence and differentiation in human fibroblasts. *Mol Cell Biol* **19**, 2109-2117 (1999).
218. Uchida, R. *et al.* Epigenetic silencing of Lgr5 induces senescence of intestinal epithelial organoids during the process of aging. *NPJ Aging Mech Dis* **5**, 1 (2019).
219. Salama, R., Sadaie, M., Hoare, M. & Narita, M. Cellular senescence and its effector programs. *Genes Dev* **28**, 99-114 (2014).
220. Fernandez Larrosa, P.N. *et al.* RAC3 more than a nuclear receptor coactivator: a key inhibitor of senescence that is downregulated in aging. *Cell Death Dis* **6**, e1902 (2015).
221. Cowley, S., Paterson, H., Kemp, P. & Marshall, C.J. Activation of MAP kinase kinase is necessary and sufficient for PC12 differentiation and for transformation of NIH 3T3 cells. *Cell* **77**, 841-852 (1994).
222. Srinivasan, L. *et al.* PI3 kinase signals BCR-dependent mature B cell survival. *Cell* **139**, 573-586 (2009).
223. Snippert, H.J. *et al.* Intestinal crypt homeostasis results from neutral competition between symmetrically dividing Lgr5 stem cells. *Cell* **143**, 134-144 (2010).
224. Lopez-Garcia, C., Klein, A.M., Simons, B.D. & Winton, D.J. Intestinal stem cell replacement follows a pattern of neutral drift. *Science* **330**, 822-825 (2010).
225. Snippert, H.J., Schepers, A.G., van Es, J.H., Simons, B.D. & Clevers, H. Biased competition between Lgr5 intestinal stem cells driven by oncogenic mutation induces clonal expansion. *EMBO Rep* **15**, 62-69 (2014).

226. Vermeulen, L. *et al.* Defining stem cell dynamics in models of intestinal tumor initiation. *Science* **342**, 995-998 (2013).
227. Humphries, A. & Wright, N.A. Colonic crypt organization and tumorigenesis. *Nat Rev Cancer* **8**, 415-424 (2008).
228. Avgustinova, A. & Benitah, S.A. Epigenetic control of adult stem cell function. *Nat Rev Mol Cell Biol* **17**, 643-658 (2016).
229. Uchida, H. *et al.* Overexpression of leucine-rich repeat-containing G protein-coupled receptor 5 in colorectal cancer. *Cancer Sci* **101**, 1731-1737 (2010).
230. Rickels, R. *et al.* An Evolutionary Conserved Epigenetic Mark of Polycomb Response Elements Implemented by Trx/MLL/COMPASS. *Mol Cell* **63**, 318-328 (2016).
231. Jadhav, U. *et al.* Acquired Tissue-Specific Promoter Bivalency Is a Basis for PRC2 Necessity in Adult Cells. *Cell* **165**, 1389-1400 (2016).
232. Klymenko, T. & Muller, J. The histone methyltransferases Trithorax and Ash1 prevent transcriptional silencing by Polycomb group proteins. *EMBO Rep* **5**, 373-377 (2004).
233. Pasini, D. *et al.* Characterization of an antagonistic switch between histone H3 lysine 27 methylation and acetylation in the transcriptional regulation of Polycomb group target genes. *Nucleic Acids Res* **38**, 4958-4969 (2010).
234. Koppens, M.A. *et al.* Deletion of Polycomb Repressive Complex 2 From Mouse Intestine Causes Loss of Stem Cells. *Gastroenterology* **151**, 684-697 e612 (2016).
235. Campbell, S.A., McDonald, C.L., Krentz, N.A.J., Lynn, F.C. & Hoffman, B.G. TrxG Complex Catalytic and Non-catalytic Activity Play Distinct Roles in Pancreas Progenitor Specification and Differentiation. *Cell Rep* **28**, 1830-1844 e1836 (2019).
236. Delgado, R.N. *et al.* Maintenance of neural stem cell positional identity by mixed-lineage leukemia 1. *Science* **368**, 48-53 (2020).
237. Lan, Q. *et al.* FoxA transcription factor Fork head maintains the intestinal stem/progenitor cell identities in Drosophila. *Dev Biol* **433**, 324-343 (2018).
238. Ma, W. *et al.* The clinical significance of forkhead box protein A1 and its role in colorectal cancer. *Mol Med Rep* **14**, 2625-2631 (2016).
239. Beuling, E. *et al.* GATA factors regulate proliferation, differentiation, and gene expression in small intestine of mature mice. *Gastroenterology* **140**, 1219-1229 e1211-1212 (2011).
240. Bossuyt, W. *et al.* Atonal homolog 1 is a tumor suppressor gene. *PLoS Biol* **7**, e39 (2009).
241. Kohlnhofer, B.M., Thompson, C.A., Walker, E.M. & Battle, M.A. GATA4 regulates epithelial cell proliferation to control intestinal growth and development in mice. *Cell Mol Gastroenterol Hepatol* **2**, 189-209 (2016).
242. Rodriguez-Colman, M.J. *et al.* Interplay between metabolic identities in the intestinal crypt supports stem cell function. *Nature* **543**, 424-427 (2017).
243. Voloshanenko, O. *et al.* Wnt secretion is required to maintain high levels of Wnt activity in colon cancer cells. *Nat Commun* **4**, 2610 (2013).
244. Kabiri, Z. *et al.* Wnt signaling suppresses MAPK-driven proliferation of intestinal stem cells. *J Clin Invest* **128**, 3806-3812 (2018).
245. Yamashita, M. *et al.* Crucial role of MLL for the maintenance of memory T helper type 2 cell responses. *Immunity* **24**, 611-622 (2006).
246. Chiacchiera, F., Rossi, A., Jammula, S., Zanotti, M. & Pasini, D. PRC2 preserves intestinal progenitors and restricts secretory lineage commitment. *EMBO J* **35**, 2301-2314 (2016).
247. Chen, Y. *et al.* Distinct pathways affected by menin versus MLL1/MLL2 in MLL-rearranged acute myeloid leukemia. *Exp Hematol* **69**, 37-42 (2019).
248. Fellmann, C. *et al.* An optimized microRNA backbone for effective single-copy RNAi. *Cell Rep* **5**, 1704-1713 (2013).
249. Subramanian, A. *et al.* Gene set enrichment analysis: a knowledge-based approach for interpreting genome-wide expression profiles. *Proc Natl Acad Sci U S A* **102**, 15545-15550 (2005).
250. Picelli, S. *et al.* Smart-seq2 for sensitive full-length transcriptome profiling in single cells. *Nat Methods* **10**, 1096-1098 (2013).

251. Hulsken, J., Birchmeier, W. & Behrens, J. E-cadherin and APC compete for the interaction with beta-catenin and the cytoskeleton. *J Cell Biol* **127**, 2061-2069 (1994).
252. Garcia, M.I. *et al.* LGR5 deficiency deregulates Wnt signaling and leads to precocious Paneth cell differentiation in the fetal intestine. *Dev Biol* **331**, 58-67 (2009).

Supplementary Information

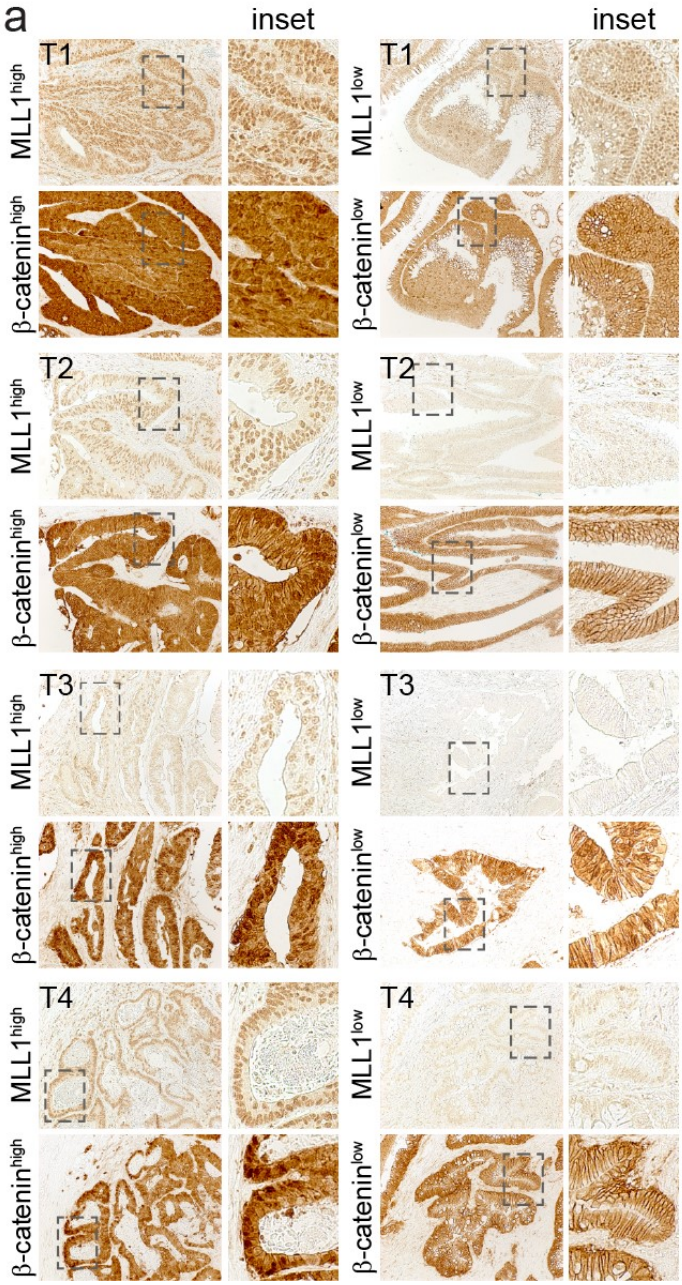

b

nuclear β-catenin	nuclear MLL1			
	weak	mod.	strong	total (n)
low	7	7	0	14
high	2	15	8	25
total (n)	8	22	9	39

Supplementary Figure 1: MLL1 expression in human colon carcinomas.
a) Representative immunohistochemistry stainings for MLL1 (upper panels) and β-catenin (lower panels) on colon cancer patient biopsies: tumor stages T1-T4, with high expression (left) and low expression (right) of MLL1 and β-catenin, insets show magnifications of indicated regions. **b)** Quantification of MLL1 expression in tumor sections with low and high β-catenin across tumor stages T0-T4, determined by immunohistochemistry analysis, n=39.

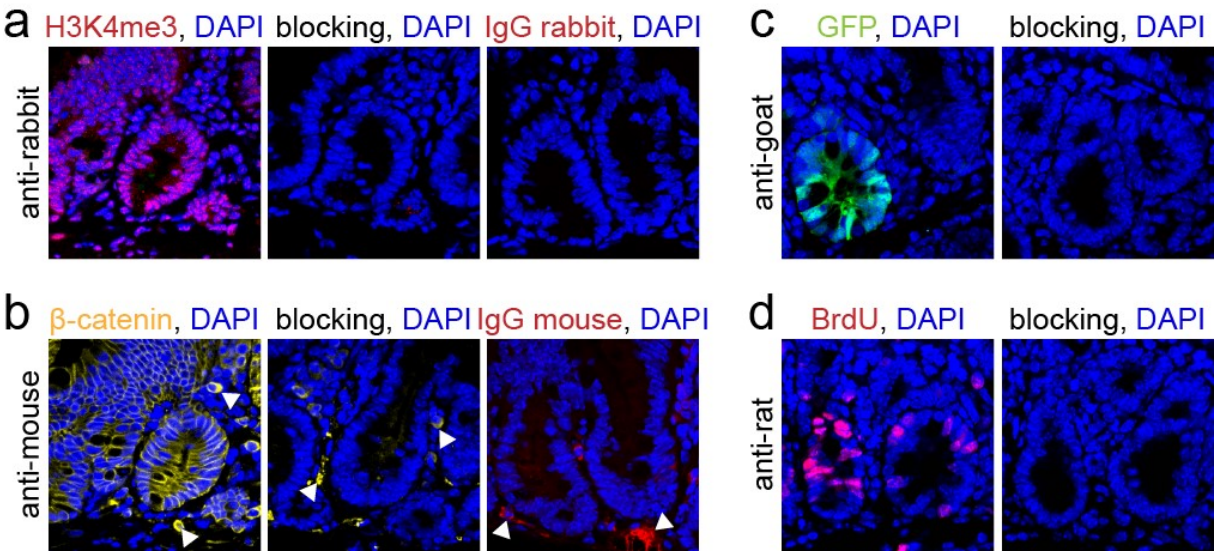

Supplementary Figure 2: Secondary antibody staining controls.
Immunostainings on sections of mouse small intestine to validate specificity of secondary antibodies used in this study: donkey anti-rabbit (**a**), donkey anti-mouse (**b**), donkey anti-goat (**c**), donkey anti-rat (**d**). Nuclei in blue (DAPI). Specific staining is detected in the presence of the primary antibodies rabbit anti-H3K4me3 (a), mouse anti-β-catenin (b), goat anti-GFP (c), rat anti-BrdU (d) (first panels), but is absent in serial control specimens incubated with blocking solution only (second panels) or control IgG (third panels in a, b). White arrowheads mark non-specific signal due to recognition of mouse immune cells by anti-mouse secondary antibody; the non-specific signal is well distinguishable from the specific staining in the epithelium (b, first panel) and does not interfere with our analyses.

Supplementary Table 1: MLL1-regulated colon cancer stem cell signature.

ARHGEF4	PLCG2	ISG20	TINAG
PRKD3	NFIA	SMPDL3A	A1CF
DYNC2H1	SULT1B1	FBP1	PPM1K
ISYNA1	RUNDC3B	IQGAP2	SLC28A2
SMOC2	BCL2L15	RBM43	FAM20B
CLIC4	CCL28	MERTK	CIB2
CLU	DDX60	PLA2G2A	RASSF10
IL17RD	AGMO	UBA7	VWA2
RASSF5	NPC1L1	SLC4A4	KLHL13
OLFM4	VAV3	PLAC8	IGFBP4
WWTR1	ELL2	SERPINB9	NRP1
SMAD5	RABGAP1L	FHDC1	TACC1
WDR35	AREG	UBE2L6	MDFIC
PRKACB	FHL2	KLF9	ABTB2
ENPP1	KCNJ2	SLC7A7	LGR5
FAM13A	TLR3	NEURL3	
IFITM2	B4GALT6	ALDH1L1	
TLR2	FILIP1L	MAML2	
SOAT1	AKR1B10	MYO1A	
SLCO3A1	CKB	CD14	
CACHD1	CCL20	TRIM31	
ADRA2A	XIAP	SULT1C2	
AK7	GPRIN3	RELB	
KRT23	ALDOB	SPCS3	
APCDD1	PLA2G16	ZC3H12A	
SNX10	TNFRSF11A	ST5	
POLI	CASP1	OSBPL6	
NME4	XK	ENC1	
TNFSF10	SNPH	SLC39A8	
ESRRG	CTSS	RNF128	
BLVRA	TFPI	CLDN12	
ACP5	MBNL2	ZC3H12D	
KLHL24	RNASE1	BIRC3	
AKAP7	SLC6A4	ACVR1C	
SLC5A9	SLC3A1	AMPD3	
BTG2	ZG16	SP1	
CTH	ADCY9	THRB	
THBS1	DUOXA2	TGFBI	
STARD13	MOCS1	DOCK11	

Supplementary Table 2: Primer sequences for ChIP-qPCR.

ChIP-qPCR primer	sequence (5'-3')
ASCL2 fwd	GATCCGCCAGCACTAGAGAC
ASCL2 rev	TGGCTTCGATTTCGCTCACT
AXIN2 fwd	ACTAAGAAGGGTAGGGGCTGAA
AXIN2 rev	CTCGAGGCTCTGGTCGGG
AXIN2_TCF4 fwd	GGCTTTCTTTGAAGCGGCTC
AXIN2_TCF4 rev	TAACCCCTCAGAGCGATGGA
GATA6 fwd	GGGTCGCTAGCCAGGTCA
GATA6 rev	AGGCAGACAATGAGAGCCGC
GATA6_Mll1 fwd	CACAAGCTCTCCGCATTGCC
GATA6_Mll1 rev	GCCCCAGAGAGAAATGCAACT
IGFBP4 fwd	GAAGGCAGGTACGTGGCAG
IGFBP4 rev	CACTGGGATTTCACCCTCGG
IGFBP4_Mll1 fwd	TGCACACACTGATGCACGG
IGFBP4_Mll1 rev	CACTCAGGAGGGAATTGGGA
LGR5 fwd	GAGGGGAAGGAAGGTTCGTC
LGR5 rev	CATTTCTCTGCGGGTCCAGA
LGR5_Mll1 fwd	CTACTTCGGGCACCATGGAC
LGR5_Mll1 rev	CTCAGCAACACACCAGACCT
LGR5_TCF4 fwd	GCAACCACAAACCCCGATTA
LGR5_TCF4 rev	CCCGGGGGAAGAGATGGTTA
MECOM fwd	GAAACCGACGGACAGAGACA
MECOM rev	TCCTTGTTCCTCCTGCGAAA
OLFM4 fwd	ACTCAGATTCCTGGGTGTCCT
OLFM4 rev	TGTCCTCTTAGCTGGAGCCG
OLFM4_Mll1 fwd	GGGAAGAAGGCAGAGGTCAC
OLFM4_Mll1 rev	CCTGAGCTTCTTGTGAGCCA
p21 -2282 fwd[216]	AGCAGGCTGTGGCTCTGATT
p21 -2282 rev[216]	CAAAATAGCCACCAGCCTCTTCT
SMOC2 fwd	CCTGTGGGGAACCAGGTCT
SMOC2 rev	CGGCTCACTTACGAGGGTC
SMOC2_Mll1 fwd	GACCTGGAGCTCAAGTGGTG
SMOC2_Mll1 rev	TCCTACCTGCTCCAGCCTC
TAL1 +70 fwd[141]	GTGGCCACAAAGCAAGGAAT
TAL1 +70 rev[141]	TCTCTGGAATCTCCAAGGCAA

Supplementary Table 3: Primer sequences for RT-PCR.

RT-PCR primer	species	sequence (5'-3')
ASCL2_fwd	human	GCGTGAAGCTGGTGAACTTG
ASCL2_rev	human	GGATGTACTCCACGGCTGAG
AXIN2_fwd	human	AACTGAAACTGGAGCTGGAAAGCC
AXIN2_rev	human	TTTGTGGGTCCTCTTCATAGCTGC
BMP4_fwd	human	TCTATGTGGACTTCAGCGATGTGG
BMP4_rev	human	AATTGACCAGGGTCTGCACAATGG
CD166_fwd	human	ACACGATGAGGCAGACGAGA
CD166_rev	human	AGTAGACGACACCAGCAACA
CD44_fwd	human	GGCTTTCAATAGCACCTTGC
CD44_rev	human	ACACCCCTGTGTTGTTTGCT
DEFA5_fwd	human	TCCCTCCTGCAGGTGACCCCA
DEFA5_rev	human	GTGGCTCTTGCCTGAGAACCTGA
GAPDH_fwd	human	AAGGTGAAGGTCGGAGTCAA
GAPDH_rev	human	AATGAAGGGGTCATTGATGG
GATA6_fwd	human	TGCCAACTGTCACACCACAA
GATA6_rev	human	CATAGCAAGTGGTCTGGGCA
IGFBP4_fwd	human	TTCCACCCCAAGCAGTGTCA
IGFBP4_rev	human	TCCAGAGCACAGGAGTAGCA
ITF_fwd[64]	human	ATCCAGAGCAGCTGTGCAAACAAC
ITF_rev[64]	human	TTTGCAGACAGGCCCACGTACTC
KRT20_fwd	human	CAGTGGTACGAAACCAACGC
KRT20_rev	human	CACACCGAGCATTTTGCAGT
LGR5_fwd	human	TGCTTACCAGTGCTGTGCATTTGG
LGR5_rev	human	TGCACTGAATGAAGGGCTTTCAGG
LRIG1_fwd	human	GGTGAGCCTGGCCTTATGTGAATA
LRIG1_rev	human	CACCACCATCCTGCACCTCC
LYZ_fwd[64]	human	GCCTAGCAAACTGGATGTGTTTGG
LYZ_rev[64]	human	TTTGCACAAGCTACAGCATCAGCG
MLL1 (KMT2A)_fwd	human, mouse	TGAGCTGCAGATGACTGGTTA
MLL1 (KMT2A)_rev	human, mouse	CCAGAGCATCAGAGGAGAGC
MLL2 (KMT2B)_fwd	human	ATCCCAGCGAGGTCGAG
MLL2 (KMT2B)_rev	human	GCCGGAGAAGTTCAGTCAGT
MLL3 (KMT2C)_fwd	human	CAAAGAACAATCTGCAGAAGAGGA
MLL3 (KMT2C)_rev	human	GGTTGGTTTCTCCATGGCAAG

MLL4 (KMT2D)_fwd	human	CCCTGAGTATCTGAAGGGCG
MLL4 (KMT2D)_rev	human	AGGGTATGGGGCCGTTTGTA
MUC2_fwd[64]	human	TTTGATGCCAGCATTTGCATCCCG
MUC2_rev[64]	human	TTGGCCGAGTACATGACAAATGTCCC
OLFM4_fwd	human	ATCATCTGCCTCTTCAGGCG
OLFM4_rev	human	CCCAGGTTTCTTCCAGGCAT
p21_fwd	human	AGTCAGTTCCTTGTGGAGCC
p21_rev	human	CATTAGCGCATCACAGTCGC
RAC3_fwd	human	CGAGAATGTTCGTGCCAAGTG
RAC3_rev	human	ACAGAGCCCACCAATCTCCC
SETD1A_fwd	human	GTCGAAGACCTCCAAGACCC
SETD1A_rev	human	ACCTCTTCCACCTCACCGTA
SETD1B_fwd	human	ACTCGTTGGGCATGGAAGAG
SETD1B_rev	human	GGCTCTGGAGACAGCAACAT
SMOC2_fwd	human	AAGCCCGGAAGGAGTTTCAG
SMOC2_rev	human	TGCGGCATCATCTGTTTTTCC
SOX9_fwd	human	AGTACCCGCACTTGCACAAC
SOX9_rev	human	CGTTCTTCACCGACTTCCTC
TCF1_fwd[141]	human	TCAGGGAAGCAGGAGCTG
TCF1_rev[141]	human	TTCTTGATGGTTGGCTTCTTG
TCF4_fwd[141]	human	ATGGAGGGCTCTTTAAGG
TCF4_rev[141]	human	AGGCGATAGTGGGTAATAC
Ascl2_fwd[64]	mouse	AAAGCTTGGTCCGGTTCTTCATCC
Ascl2_rev[64]	mouse	GCAGATGCTTAGCTTATTGCGTCC
Axin2_fwd	mouse	AGTCAGCAGAGGGACAGGAA
Axin2_rev	mouse	CTTCGTACATGGGGAGCACT
Bmp4_fwd	mouse	AGAAGAATAAGAACTGCCGTCGCC
Bmp4_rev	mouse	ATGGCATGGTTGGTTGAGTTGAGG
Cd44_fwd[64]	mouse	CACCTTGGCCACCACTCCTA
Cd44_rev[64]	mouse	TTGGATGTGAGATTGGGTCGAA
Gapdh_fwd[64]	mouse	AAATGGTGAAGGTCGGTGTGAACG
Gapdh_rev[64]	mouse	TGATGACAAGCTTCCCATTCTCGG
Gata4_fwd	mouse	AAACGGAAGCCCAAGAACCT
Gata4_rev	mouse	ACACAGTACTGAATGTCTGGGA
Gob5_fwd[64]	mouse	TGAAATTGTGCTGCTGACCGATGG
Gob5_rev[64]	mouse	TGCTGCGAAAGCATCAACAAGACC

Itf_fwd	mouse	TGGGATAGCTGCAGATTACGTTGG
Itf_rev	mouse	TTTGAAGCACCAGGGCACATTTGG
Lgr5_fwd[252]	mouse	CCTACTCGAAGACTTACCCAGT
Lgr5_rev[252]	mouse	GCATTGGGGTGAATGATAGCA
Lyz_fwd[64]	mouse	GCAGCCATACAATGTGCAAAGAGG
Lyz_rev[64]	mouse	TTTGCCCTGTTTCTGCTGAAGTCC
Mll2_fwd	mouse	GATGGTTCCTCAGACCTACTG
Mll2_rev	mouse	CTCCACACTGAAGCCATCATC
Mll3_fwd	mouse	CAGAGGAGCACATTGAAGTGG
Mll3_rev	mouse	GGCTTTTCTCCACAACTTGGC
Mll4_fwd	mouse	CTGTGCCAGATCAGAACCGAA
Mll4_rev	mouse	CTGAGATGACTTGGAGTGCAC
Mmp7_fwd	mouse	AGGAGTGAACTTCCTGTTTGCTGC
Mmp7_rev	mouse	TTCTGAATGCCTGCAATGTCGTCC
Muc2_fwd[64]	mouse	TGTGATGCCAATGACAAGGTGTCC
Muc2_rev[64]	mouse	ACCACAATGTTGATGCCAGACTCG
Olfm4_fwd[64]	mouse	TTGGGTTACCAAGCAGTACAAGCC
Olfm4_rev[64]	mouse	TCTCATTGTGATGCCTAGGTTGCC
Setd1a_fwd	mouse	GTTTGCCATGGAACCCATTGC
Setd1a_rev	mouse	GTGCAGCAGTGGTTGATGAAC
Setd1b_fwd	mouse	CTGTTGGTGAGCTGGATGCTA
Setd1b_rev	mouse	CTGGAGTAAGCTGTGTCTTGG
Smoc2_fwd[64]	mouse	CATAGGACCGCGGAGCAGTT
Smoc2_rev[64]	mouse	AGGCTGCAGTCTCTGTCTTTG
Spdef_fwd[64]	mouse	AACATGTATCCCGACGATAGCAGC
Spdef_rev[64]	mouse	TCAATATCTTTCAGGACCTCGCCC

Publications

Grinat J, Heuberger J et al. 2020: The epigenetic regulator Mll1 is required for Wnt-driven intestinal tumorigenesis and cancer stemness, *submitted*

Heuberger J, **Grinat J** et al. 2020: Mll1 and Yap confer oncogenic activity in intestinal cancer: a signaling cascade, *in preparation*

Talks

EU-LIFE Annual Scientific Meeting on “Signalling & Gene Regulation in Health & Disease” 2019, Babraham Institute, Cambridge, United Kingdom

5th TRR81 Symposium on “Chromatin Changes in Differentiation and Malignancies” 2019, Bad Nauheim, Germany

MDC-FMP PhD retreat 2019, Joachimsthal, Germany

EMBO Workshop 2018 “Epigenomics and epitranscriptomics in cell fate choice”, Capri, Italy

Young Scientists in Cancer Research Symposium 2017, Molekulares Krebsforschungszentrum (MKFZ), Charité Medical School Berlin, Germany

Poster Presentations

“in Cancer“ Conference 2019, Molekulares Krebsforschungszentrum (MKFZ), Charité Medical School Berlin, Germany

“in Cancer“ Conference 2017, Molekulares Krebsforschungszentrum (MKFZ), Charité Medical School Berlin, Germany

International PhD Student Cancer Conference (IPSCC) 2017, MDC Berlin, Germany

EMBO Conference “Chromatin and Epigenetics” 2017, EMBL Heidelberg, Germany

Acknowledgements

Thank you to everyone who accompanied and supported me in the exciting time of my PhD.

I would like to express my deep gratitude to Prof. Dr. Walter Birchmeier for taking me as a PhD student in his lab, competently matching me to the colon subgroup headed by ‘a postdoc from Marburg’ and entrusting us with an amazing project.
The challenges you put in my way helped me grow stronger.

I would like to acknowledge the members of my PhD committee, Prof. Dr. Ana Pombo and PD Dr. Frederik Damm, for their conscientiousness and constructive comments.

A giant thank you to Dr. Julian Heuberger, the greatest PhD supervisor I could ever imagine. Thank you for your caring supervision, your brilliant ideas and creativeness, for your support and valuable advice, your kindness and your guidance. Thank you for sharing your expertise and passing your scientific spirit in numerous intense and constructive discussions.
I will never forget the wonderful and inspiring time we have spent together.
The lab was not the same after you had left.
Thank you for taking me under your wing and bringing out the best in me.

Thank you to Frauke Kosel for her reliable technical support and perfection.
I very much enjoyed working next to you and will gladly remember the good times we had in our small colon subgroup.

Thank you to all members of the Birchmeier lab for their support and the nice time.
I would further like to acknowledge Marcel Harrig for the reliable and thorough caretaking in the animal facility.

Thank you to my family and friends.

Special thanks to my beloved sister for being my partner in craziness.
You are the best of all!

A big thank you to my parents for their moral support, their wisdom and advice.
Thank you for believing in me.

Declaration

Erklärung

Hiermit erkläre ich, die vorliegende Dissertation selbstständig und nur unter Verwendung der angegebenen Hilfen und Hilfsmittel angefertigt zu haben. Ich habe mich anderwärts nicht um einen Doktorgrad beworben und besitze keinen entsprechenden Doktorgrad. Ich erkläre, dass ich die Dissertation oder Teile davon nicht bereits bei einer anderen wissenschaftlichen Einrichtung eingereicht habe und dass sie dort weder angenommen noch abgelehnt wurde.
Ich erkläre die Kenntnisnahme der dem Verfahren zugrundeliegenden Promotionsordnung der Lebenswissenschaftlichen Fakultät der Humboldt-Universität zu Berlin vom 05. März 2015.
Weiterhin erkläre ich, dass keine Zusammenarbeit mit gewerblichen Promotionsberaterinnen/ Promotionsberatern stattgefunden hat und dass die Grundsätze der Humboldt-Universität zu Berlin zur Sicherung guter wissenschaftlicher Praxis eingehalten wurden.

Declaration

I hereby declare that I completed the doctoral thesis independently based on the stated resources and aids. I have not applied for a doctoral degree elsewhere and do not have a corresponding doctoral degree. I have not submitted the doctoral thesis, or parts of it, to another academic institution and the thesis has not been accepted or rejected.
I declare that I have acknowledged the Doctoral Degree Regulations which underlie the procedure of the Faculty of Life Sciences of Humboldt-Universität zu Berlin, as amended on 5th March 2015. Furthermore, I declare that no collaboration with commercial doctoral degree supervisors took place, and that the principles of Humboldt-Universität zu Berlin for ensuring good academic practice were abided by.

Berlin, April 2020